MECHANISMS FOR EXTRACELLULAR MATRIX-DEPENDENT BLOOD-BRAIN BARRIER DYSFUNCTION

by

Brian Adam Hoettels

A dissertation

submitted in partial fulfillment

of the requirements for the degree of

Doctor of Philosophy in Biomolecular Sciences

Boise State University

December 2021

BOISE STATE UNIVERSITY GRADUATE COLLEGE

DEFENSE COMMITTEE AND FINAL READING APPROVALS

of the dissertation submitted by

Brian Adam Hoettels

Dissertation Title: Mechanisms for Extracellular Matrix-dependent Blood-Brain Barrier Dysfunction

Date of Final Oral Examination: 04 November 2021

The following individuals read and discussed the dissertation submitted by student Brian Adam Hoettels, and they evaluated the student's presentation and response to questions during the final oral examination. They found that the student passed the final oral examination.

Richard Beard Jr., Ph.D.	Chair, Supervisory Committee
Daniel Fologea, Ph.D.	Member, Supervisory Committee
Lisa Warner, Ph.D.	Member, Supervisory Committee

The final reading approval of the dissertation was granted by Richard Beard, Jr., Ph.D., Chair of the Supervisory Committee. The dissertation was approved by the Graduate College.

DEDICATION

To my mother who believed in me when I didn't and who still shows up higher on Google Scholar. Life is less vibrant without you.

ACKNOWLEDGMENTS

Although written in 1623, the message of John Donne's meditation 17 ("No man is an island") is just as relevant today. Throughout my five years at BSU, I have been supported by many inside the lab and out. *First*, I would like to thank my mentor Rich Beard for taking a chance on me when I first applied to his lab as a volunteer, then as a Ph.D. student. *Second*, I would like to thank my committee members Lisa Warner and Daniel Fologea for agreeing to sit on my Supervisory Committee. *Third*, I would like to thank the other members of the Beard MVP lab for their assistance with animal and cell culture experiments. This includes Travis Wertz, Kristina Chapman, Desiree Self, Sacora Sanders, Jessica McAllister, Emily Lawrence, Colton Brodock, Heidi Henderson, Ofeira Faapouli, Steven Pilarski, Alex Lanza, Erica Korbel, and Nilufar Ali. *Fourth*, I would like to thank the current and former staff of the BRC – Tracy Yarnell, Rhiannon Wood, Barb Gibben, Diane Smith, Laura Bond, Cindy Keller-Peck, and Shin Pu – and Beth Gee from the BMOL program for all their advice, both professional and personal. *Fifth*, I have been fortunate to receive funding from multiple entities. This includes Teaching and Research Assistantships from the BMOL program, Research Assistantships from Rich's grants, travel funding from the BMOL program, the BRC, and Rich's grants, and research funding from Sigma Xi. *Finally*, to my partner-in crime, Travis, without all your support, this Ph.D. would not have been possible.

ABSTRACT

Dysfunction of the blood vessels that form the blood-brain barrier (BBB) is observed across various neurological disorders, including multiple sclerosis (MS). As barrier loss culminates in neuronal dysfunction and degeneration, a better understanding of the mechanisms underlying BBB dysfunction is needed.

Tight junctions are multiprotein complexes maintained by the endothelial cells lining the inner blood vessel wall to seal the intercellular space, and their disruption impairs BBB function. *In my first chapter*, I focus on how tight junctions are altered in CNS inflammatory demyelinating diseases (CNS-IDDs) like MS as BBB dysfunction is one of the earliest known stages in their disease progression. Literature searches were conducted for relevant studies involving three prominent tight junction protein families, namely the claudins, tight junction-associated MARVEL proteins (TAMPs), and angulins. As few studies analyzed patient tissues, additional literature searches were conducted for relevant cell culture and animal models. Particular attention is paid to studies involving pharmacological interventions or genetic manipulations as tight junctions are increasingly being recognized as possible therapeutic targets for preserving or restoring BBB function and, in turn, CNS homeostasis.

In my second chapter, I explore how the molecular composition of the vascular basement membrane (BM) can influence barrier function. Under healthy conditions, the vascular BM surrounding the endothelium fosters BBB function through cell-extracellular matrix (ECM) protein interactions that promote the tight junction protein claudin-5. During

inflammation, however, the molecular composition of the BM is perturbed. Recently, the ECM proteins collagen type I and decorin, both of which are typically absent from the BM, were observed surrounding vessels in the lesions of MS patients. As their roles in inflammation are poorly understood, I investigated whether they can influence barrier function or claudin-5 expression. Using a mouse model of inflammatory encephalomyelitis, I found that decorin is present within the BM during early disease when the onset of BBB dysfunction occurs. In complement, I conducted cell culture studies with mouse BBB endothelial cells, overall finding an inverse relationship between decorin and barrier function or claudin-5. Similar cell culture studies using collagen type I revealed a similar inverse relationship between it and barrier function or claudin-5.

Overall, this work suggests that 1) tight junction proteins may be a viable therapeutic target in restoring BBB dysfunction and 2) inflammation-associated alterations to the vascular BM may contribute to BBB dysfunction by suppressing the tight junction protein claudin-5.

TABLE OF CONTENTS

LIST OF TABLES

LIST OF FIGURES

LIST OF ABBREVIATIONS

CNS-IDD	Central Nervous System-Inflammatory Demyelinating Disease
MS	Multiple Sclerosis
NMOSD	Neuromyelitis Optica Spectrum Disorder
ADEM	Acute Disseminated Encephalomyelitis
BBB	Blood-Brain Barrier
RR-MS	Relapsing-remitting Multiple Sclerosis
SP-MS	Secondary Progressive Multiple Sclerosis
PP-MS	Primary Progressive Multiple Sclerosis
PR-MS	Progressive-relapsing Multiple Sclerosis
NMO	Neuromyelitis Optica
AQP4	Aquaporin-4
AHLE	Acute Hemorrhagic Leukoencephalomyelitis
NVU	Neurovascular Unit
EC	Endothelial Cell
BBB-EC	Blood-Brain Barrier Endothelial Cell
TAMP	Tight Junction-associated MARVEL Protein
ECL	Extracellular Loop
IL	Intracellular Loop
PDZ	Postsynaptic Density Protein 95/Discs Large1/Zonula Occludens-1
ZO-1	Zonula-Occludens-1

Da	Dalton
kDa	kiloDalton
FITC	Fluorescein Isothiocyanate
NaFluor	Sodium Fluorescein
CLDN5	Claudin-5
MarvelD2	MARVEL Domain-containing Protein 2
MarvelD2	MARVEL Domain-containing Protein 3
MARVEL	MAL & Related Proteins for Vesicle Trafficking & Membrane Link
OCEL	Occludin/ELL
HIV	Human Immunodeficiency Virus
VEGF	Vascular Endothelial Growth Factor
IG	Immunoglobulin
LSR	Lipolysis-stimulated Lipoprotein Receptor
ILDR1	Immunoglobulin-like Domain-containing Receptor 1
ILDR2	Immunoglobulin-like Domain-containing Receptor 2
EAE	Experimental Autoimmune Encephalomyelitis
E-NMOSD	Experimental Neuromyelitis Optica Spectrum Disorder
TMEV	Theiler's Murine Encephalomyelitis Virus
PRISMA	Preferred Reporting Items for Systematic & Meta-analyses
WoS	Web of Science
CNS-EC	Central Nervous System Endothelial Cell
WM	White Matter

GM	Grey Matter
NAWM	Normal-appearing White Matter
MA	Microarray Analysis
qPCR	Quantitative Polymerase Chain Reaction
NAGM	Normal-appearing Grey Matter
hCMEC/D3	Human Cortical Microvessel Endothelial Cell (Clone D3)
TY	Human Brain Microvascular Endothelial Cell (Clone TY)
TEER	Transendothelial Electrical Resistance
MMP	Matrix Metalloproteinase
TNF-α	Tumor Necrosis Factor Alpha
IFN-γ	Interferon Gamma
IL-17	Interleukin-17
S1PR	Sphingosine 1-Phosphate Receptor
FDA	Food and Drug Administration
VDR	Vitamin D Receptor
LETM	Longitudinally Extensive Transverse Myelitis
NMO-IgG	Neuromyelitis Optica Immunoglobulin
AECA	Anti-Endothelial Cell Antibody
GRP78	Glucose-regulated Protein 78
TGF-β	Transforming Growth Factor Beta
IL-6	Interleukin-6
TPE	Therapeutic Plasma Exchange
CD4	Cluster of Differentiation 4

TCR	T Cell Receptor
MOG	Myelin Oligodendrocyte Glycoprotein
MOG_{35-55}	Myelin Oligodendrocyte Glycoprotein (residues 35-55)
VEGF-A	Vascular Endothelial Growth Factor-A
CD31	Cluster of Differentiation 31
d.p.o.	Days post-onset
d.p.i.	Days post-induction
TYMP	Thymidine Phosphorylase
eNOS	Endothelial Nitric Oxide Synthase
CD45	Cluster of Differentiation 45
2DLR	2-deoxy-L-ribose
Nrf2	Nuclear Factor Erythroid 2–related Factor 2
IFN-β	Interferon Beta
MSC	Mesenchymal Stem Cell
NF-κB	Nuclear Factor Kappa B
B1R	Bradykinin Receptor B1
KO	Knockout
WT	Wild-type
IRGM1	Immunity-related GTPase Family M Protein 1
KNCK2	Potassium Channel Subfamily K Member 2
NG2	Neuron-Glial Antigen 2
LXRα	Liver X Receptor Alpha
ASM	Acid Sphingomyelinase

IFNγR	Interferon Gamma Receptor
LR	Leptin Receptor
ITGB4	Integrin Beta 4
CCL2	C-C Motif Chemokine Ligand 2
EC^{KO}	Endothelial-restricted Knockout
AC^{KO}	Astrocyte-restricted Knockout
IκBα	Nuclear factor of kappa light polypeptide gene enhancer in B-cells inhibitor, alpha
eGFP	Enhanced Green Fluorescent Protein
IV-2PM	Intravital Two-photon Microscopy
LacZ	Beta-Galactosidase
MOG_{1-125}	Myelin Oligodendrocyte Glycoprotein (residues 1-125)
DA	Dark Agouti
CCL	C-C Motif Chemokine Ligand
PVG	Piebald Virol Glaxo
Av1	Major Histocompatibility Complex Haplotype Av1
SCH	Spinal Cord Homogenate
MBP	Myelin Basic Protein
CBA	Cross of Bagg Albino with Dark Brown Agouti
iNOS	Inducible Nitric Oxide Synthase
SJL	Swiss Jim Lambert
PLP	Proteolipid Protein
$PLP_{139-151}$	Proteolipid Protein (residues 139-151)

CMH	Chronic Mild Hypoxia
PKC-β	Protein Kinase C-Beta Isoform
SD	Sprague Dawley
AOD	Average Optical Density
BBG	Brilliant Blue G
P2X7R	Purinergic Receptor P2X 7
AVPR	Arginine Vasopressin Receptor
TCR-1640	T Cell Receptor 1640
MOG_{92-106}	Myelin Oligodendrocyte Glycoprotein (residues 92-106)
PMN	Polymorphonuclear
RNA	Ribonucleic Acid
PIFS	Peptide-induced Fatal Syndrome
CD8	Cluster of Differentiation 8
VP2	Viral Capsid Protein 2
$VP2_{121-130}$	Viral Capsid Protein 2 (residues 121-130)
Hpp	Hours post-peptide
GR-1	Granulocyte Receptor-1
Ly6G	Lymphocyte antigen 6 complex locus G6D
NRP-1	Neuropilin-1
VEGFR2	Vascular Endothelial Growth Factor 2
PRF1	Perforin-1
OL	Oligodendrocyte
HRP	Horseradish Peroxidase

EB	Evans Blue
TBI	Traumatic Brain Injury
BM	Basement Membrane
$[\alpha1(IV)]_2\alpha2(IV)$	Collagen Type IV trimer composed of two alpha 1 and one alpha 2 subunits
COL4A1	Collagen Type IV, Alpha 1
COL4A2	Collagen Type IV, Alpha 2
SLRP	Small Leucine-rich Proteoglycan
MCAO	Middle Cerebral Artery Occlusion
COL1A1	Collagen Type I, Alpha 1
COL1A2	Collagen Type I, Alpha 2
DCN	Decorin
ITGA1	Integrin Subunit Alpha 1
ITGA2	Integrin Subunit Alpha 2
Ai14	Mice carrying the *Gt(ROSA)26Sor*$^{tm14(CAG-tdTomato)Hze}$ allele
Dcn-floxed	Mice carrying the *Dcn*$^{tm1.1Debi}$ allele
Bgn-floxed	Mice carrying the *Bgn*$^{tm1.1Debi}$ allele
Tie2-Cre	Mice carrying the *Tg(Tek-cre/ERT2)1Arnd* transgene
Slco1c1-Cre	Mice carrying the *Tg(Slco1c1-iCre/ERT2)1Mrks* transgene
i.p.	intraperitoneally
d.p.i.	days post-induction
CS	Clinical Score
PBS	Phosphate-buffered saline

TCA	Trichloroacetic Acid
Ex.	Excitation
Em.	Emission
TL	Tomato lectin
PFA	Paraformaldehyde
BSA	Bovine Serum Albumin
AF488	AlexFluor 488
HBSS	Hanks Buffered Salt Solution
HEPES	2-[4-(2-hydroxyethyl)piperazin-1-yl]ethanesulfonic acid
DMEM	Dulbecco's Modified Eagle's Medium
d.p.s.	Days post-seeding
FBS	Fetal Bovine Serum
MEM	Modified Eagle's Medium
IL-12	Interleukin-12
CM	Conditioned Media
C8-D1A	Immortalized Mouse Astrocyte line
ETcA-CM	Conditioned Media from Astrocytes with Effector T cells
NTcA-CM	Conditioned Media from Astrocytes with Naïve T cells
PMN-ETcA-CM	Conditioned Media from PMNs exposed to ETcA-CM
PMN-NTcA-CM	Conditioned Media from PMNs exposed to NTcA-CM
Actb	Beta Actin
TAT-HA2	Fusogenic peptide from influenza hemagglutinin (HA2) with a cell-penetrating peptide tag from HIV (TAT)

TAT-Cre	Recombinant Cre recombinase (Cre) with a cell-penetrating peptide tag from HIV (TAT)
RFP	Red Fluorescent Protein
GFP	Green Fluorescent Protein
ECIS-TEER	Electric Cell-Substrate Impedance Sensing-Transendothelial Electrical Resistance
P_{app}	Apparent Permeability Coefficient
MFT	Multiple Frequency per Time
Hz	Hertz
kHz	kiloHertz
R_b	Cell-Cell Adhesion Parameter for ECIS-TEER Modeling
α	Cell-Matrix Adhesion Parameter for ECIS-TEER Modeling
C_m	Cell Membrane Capacitance Parameter for ECIS-TEER Modeling
MV	Microvessel
ICW	In-cell Western
NIR	Near-infrared
bEnd.3	Mouse Brain Microvascular Endothelial Line
MP	Methylprednisolone
DMAQ-B1	Demethylasterriquinone B1
siRNA	Small interfering RNA
Floxed	Flanked by loxP
$\alpha_1\beta_1$	Integrin dimer composed of alpha 1 and beta 1 subunits
$\alpha_2\beta_1$	Integrin dimer composed of alpha 2 and beta 1 subunits

RNA-Seq	RNA-Sequencing
$\alpha_3\beta_1$	Integrin dimer composed of alpha 3 and beta 1 subunits
$\alpha_6\beta_1$	Integrin dimer composed of alpha 6 and beta 1 subunits
$\alpha_4\beta_1$	Integrin dimer composed of alpha 4 and beta 1 subunits
$\alpha_5\beta_1$	Integrin dimer composed of alpha 5 and beta 1 subunits
$\alpha_1\beta_1\gamma_1$	Laminin trimer composed of alpha 1, beta 1, and gamma 1 subunits
ILK	Integrin-linked Kinase
PINCH	Particularly Interesting New Cysteine-Histidine-rich Protein
IPP	ILK-PINCH-Parvin Complex
LMVEC	Lung Microvascular Endothelial Cell
HUVEC	Human Umbilical Vein Endothelial Cell
FoxO1	Forkhead box Protein O1
SMI	Small Molecule Inhibitor
ATP	Adenosine Triphosphate
BAEC	Bovine Aortic Endothelial Cell
RBE.4	Rat Brain Microvascular Endothelial Cell Line
cAMP	Cyclic Adenosine Monophosphate
PKA	Protein Kinase A
DMVEC	Dermal Microvascular Endothelial Cell
GEF	Guanine Exchange Factor
EPAC	Exchange Protein Directly Activated by cAMP
C/EBP-α	CCAAT/enhancer-binding protein alpha

RhoA	Ras homologue family member A
ROCK	Rho-associated Kinase
SFK	Src Family of Kinases
VE-CAD	Vascular endothelial cadherin
PP2	pan-SFK inhibitor
LRR	Leucine-rich repeat
GAG	Glycosaminoglycan
F3	Recombinant mini-collagen
Ang	Angiopoietin
Ang2-EC^{KI}	Endothelial-restricted Knockin of Angiopoeitin-2
cEND	Mouse Cerebral Microvascular Endothelial Cell line
TB	*Tie2-Cre* x *Bgn*-floxed Mice
TD	*Tie2-Cre* x *Dcn*-floxed Mice
TBD	*Tie2-Cre* x *Bgn*-floxed x *Dcn*-floxed Mice
SB	*Slco1c1-Cre* x *Bgn*-floxed Mice
SD	*Slco1c1-Cre* x *Dcn*-floxed Mice
SBD	*Slco1c1-Cre* x *Bgn*-floxed x *Dcn*-floxed Mice

CHAPTER ONE: BLOOD-BRAIN BARRIER DYSFUNCTION & TIGHT JUNCTION DYSREGULATION IN CNS INFLAMMATORY DEMYELINATING DISEASES AND THEIR MODELS – A LITERATURE REVIEW.

CNS Inflammatory Demyelinating Diseases (CNS-IDDs)

CNS-IDDs are a diverse group of diseases that include multiple sclerosis (MS), neuromyelitis optica spectrum disorder (NMOSD), and acute disseminated encephalomyelitis (ADEM).[1,2] Despite their differences, all share the pathological hallmarks of inflammatory demyelination[1,2] and compromise of the blood-brain barrier (BBB).[3,4] Due to their idiopathic nature, therapeutic strategies historically have relied on immunomodulatory or immunosuppressive drugs.[5,6] However, the contribution of vascular dysfunction to the pathogenesis of CNS-IDDs and other neurological disorders now suggests the vasculature as a viable therapeutic target.[7] Thus, a better understanding of the mechanisms governing BBB function and dysfunction in CNS-IDDs may uncover new treatment strategies applicable to patients suffering neurological disorders as a whole.

Multiple Sclerosis

Patients with MS primarily suffer lesions within the brain and spinal cord.[8] Leakage of plasma proteins like fibrinogen is variably observed across the life of the lesions, including prior to the onset of demyelination.[9,10] Although its underlying etiology remains unknown, MS involves innate and adaptive immune responses against the myelin sheath.[11]

There are four main clinical forms of MS (Figure 1.1). Relapsing-remitting MS (RR-MS), affecting ~80% of patients, has episodes of relapse interspersed by stable remission (Figure 1.1A).[12] Within 15 years, half of these patients will transition to secondary-progressive MS (SP-MS), experiencing a gradual worsening of neurological function independent of relapse (Figure 1.1B).[13] Primary-progressive MS (PP-MS), affecting ~10-15% of patients, involves the gradual worsening of neurological function from the initial crossing above clinical threshold (Figure 1.1C).[14] Finally, for ~5% of patients, progressive-relapsing (PR-MS), distinguishes itself from PP-MS with clear superimposed relapses throughout the progressive disease course (Figure 1.1D).[12,14]

Additionally, there are several rare variants. First, acute MS (Marburg's disease) follows a fulminant disease course, with rapid deterioration of health and death generally within 12-18 months post-diagnosis.[15,16] Next, concentric sclerosis (Balo's disease) is distinguished by lesions containing concentric rings of demyelination separated by rings of preserved myelin.[15,16] Finally, tumefactive sclerosis presents as large tumor-like lesions that can cause mass effect and edema.[15,16]

Neuromyelitis Optica Spectrum Disorder

Originally thought to be a variant of MS, NMOSD is now classified separately.[17] Patients with classic NMO (Devic's disease) primarily suffer lesions within the optic nerve or spinal cord, and are seropositive for pathogenic antibodies against the astrocyte water channel protein aquaporin-4 (AQP4).[18,19] Vascular leakage is observed primarily during the early stages of lesion evolution when active astrocyte lysis is happening.[20] As this precedes oligodendrocyte dysfunction and death, classic NMO likely reflects a primary astrocytopathy that triggers secondary demyelination.[21] Revisions to the original diagnostic

criteria have led to an expanded term, NMOSD, which recognizes that patients may also exhibit lesions in the brain or brainstem, and may be seronegative for AQP4 but otherwise fulfill the diagnostic criteria.[19] Disease generally follows a relapsing-remitting course (Figure 1.2A), with optic neuritis more prevalent during early disease and transverse myelitis more prevalent during late disease.[22]

Acute Disseminated Encephalomyelitis

Patients with ADEM primarily suffer lesions within the brain or spinal cord.[4,23] Although it can occur at any age, ADEM predominantly is observed in children or young adults following viral infection.[4,23] With rare exception, classic ADEM follows a monophasic disease course with subsequent full recovery (Figure 1.2.B).[4,23] However, acute hemorrhagic leukoencephalomyelitis (AHLE) is a proposed rare variant that is fulminant and is hallmarked by cerebral microhemorrhages.[4] Although its etiology is not fully understood, it is hypothesized that molecular mimicry between pathogen and myelin proteins or bystander activation of virus-specific immune cells may be responsible.[4,23]

The Blood-brain Barrier in Neurovascular Unit Homeostasis

Neuronal activity is metabolically and energetically costly.[24] Despite the adult human brain representing only 2% of the total body weight, it accounts for nearly 20% of total energy consumption.[25] To meet these needs, local neuronal activity is tightly coupled to local blood flow which is regulated by vascular cells (endothelial cells, vascular smooth muscle cells, pericytes) that work in tandem with glial cells (astrocytes, microglia, and oligodendrocytes).[24,25] Collectively, these cells form the neurovascular unit (NVU) as shown in Figure 1.3.

The Endothelium Forms the *de facto* BBB

The interior blood vessel surface is lined by a single layer of endothelial cells (ECs).[26,27] At the microvessel level, BBB-ECs are surrounded by pericytes and astrocytic end-feet processes, plus a vascular basement membrane that provides structural support and serves as a conduit for soluble factor signaling or cell-matrix protein interactions (Figure 1.3).[27] As it the endothelium that provides the physical and metabolic barrier properties of the vessel, it is the *de facto* BBB.

Tight Junctions Confer Barrier Properties to the Endothelium

To fulfill their barrier functions, BBB-ECs maintain multi-protein complexes called tight junctions at cell-cell contacts to seal shut the intercellular space.[28] This physical restriction of paracellular transport, in turn, contributes to metabolic barrier functionality by ensuring that transcellular transport is the primary route for exchange.[29]

Tight junctions are formed by a branching network of transmembrane proteins that act in homophilic or heterophilic fashion within the same cell membrane and across to the opposing membrane.[28] In turn, scaffolding proteins couple the transmembrane proteins to the cytoskeleton for stability and establishment of signaling hubs.[30] Although the molecular composition of tight junctions in BBB-ECs is still under investigation, three families of integral proteins known to play key roles in barrier function and its regulation are the claudin, tight junction-associated MARVEL protein (TAMP), and angulin families.[30,31]

The Claudin Family

Claudins are tetraspan proteins (Figure 1.5) that fulfill barrier- or pore-forming functions at bicellular junctions (Figures 1.4 & 1.5), with 27 putative members across humans and rodents.[32] Structurally, claudins contain a short intracellular N-terminal tail,

two extracellular loops (ECLs), a short intracellular loop (IL), and an intracellular C-terminal tail.[32] The first ECL contains a conserved W-GLW-C-C signature motif and can confer ion selectivity depending on whether charged amino acids are present, while the second ECL mediates *trans*-interactions.[32] For most members, the C-terminus contains a Postsynaptic Density Protein 95/Discs Large 1/Zonula Occludens-1 (PDZ)-binding motif (Y-V) which is recognized by PDZ domain-containing scaffolding proteins like zonula occludens-1 (ZO-1), thereby allowing coupling to the cytoskeleton.[32] Additionally, C-terminal tails frequently contain phosphorylation, palmitoylation, and ubiquitination sites for trafficking and regulation under healthy or disease conditions.[32]

Historically, claudin-5 has been considered the predominant barrier-forming member in BBB-ECs.[28] Its knockdown in immortalized human BBB-ECs increases their permeability to small- or medium-sized tracers like Lucifer Yellow (457 Dalton (Da)) or 4 kiloDalton (kDa) fluorescein isothiocyanate (FITC)-conjugated dextran, but not large tracers like 70 kDa FITC-dextran, and delays recovery of barrier integrity following osmotic disruption with mannitol.[33] Similarly, we have demonstrated that its knockdown in primary mouse BBB-ECs increases their permeability to sodium fluorescein (NaFluor; 376 Da).[34] On the organismal level, *Cldn5*-deficient mice die within 10 hours of birth and suffer selective leakage of small molecules up to 800 Da in size,[35] while persistent endothelial-restricted knockdown in adult mice results in schizophrenia-like behavior, vascular leakage of serum proteins (fibrinogen; ~340 kDa), and complete mortality.[36] In humans, deletion of 22q11.2, within which *CLDN5* is located, is one of the strongest known genetic risk factors for schizophrenia,[37] especially for patients that also possess a single nucleotide polymorphism (rs10314) within the 3' untranslated region of *CLDN5* that

impairs its translation.[36] In light of the above, claudin-5 has been described as an essential gatekeeper for BBB function and CNS homeostasis.[38]

Besides claudin-5, several other family members have been reported, including claudins 1, 3, 11, and 12.[28,39,40] However, actual member representation is still not settled. Several transcriptional profiling studies have screened purified human or rodent brain microvessels.[39,41,42] Member presence and relative abundance varied, with isolation technique appearing to have a significant effect (Appendix A). Furthermore, cross-reactivity of antibodies is a known issue in the field due to the limited regions available for binding and the generally conserved nature of the sequences in the available regions.[43] Early studies that reported claudin-1 was enriched at tight junctions in human and mouse BBB-ECs used an antibody that subsequently was shown to be cross-reactive with claudin-3.[44] Since then, claudin-1 generally has been reported absent or weakly present within the cytoplasm, rather than at the tight junctions under homeostatic conditions.[39,45,46] Similarly, two recent studies have demonstrated that commercial antibodies against claudin-3 or claudin-12 can still localize to the tight junctions of the respective knockout animal.[47,48] Thus, more research is sorely needed to confirm which claudins are present in BBB-ECs.

The TAMP Family

TAMPs are tetraspan proteins (Figure 1.5) that share minimal homology with claudins and that fulfill modulatory roles in barrier function.[28,49] The TAMP family is comprised of three members: occludin, tricellulin (gene name: *MarvelD2*), and MarvelD3.[49] Unlike claudins, TAMPs exhibit preferential localization at cell-cell contacts.[49,50] Under non-pathological conditions, occludin is enriched at bicellular junctions, tricellulin at tricellular junctions, and MarvelD3 at both (Figures 1.4 & 1.5).[49,50]

TAMPs possess two ECLs, a short IL, and intracellular tails.[49,51] Additionally, all three possess a MAL & Related Proteins for Vesicle Trafficking & Membrane Link (MARVEL) domain which spans across all four transmembrane domains.[49,51] However, only occludin and tricellulin possess an Occludin/ELL (OCEL) domain in their C-termini.[52] For both, this domain is involved in trafficking to the tight junctions.[31,52] Additionally, for occludin, it serves as a binding site for scaffolding proteins and is necessary for internalization.[52]

Although all members are predicted to be phospho-proteins, to date, the role of phosphorylation has only been explored with occludin.[53] Increased tyrosine phosphorylation is observed in primary human BBB-ECs experiencing oxidative stress[54–56] and in the brain microvessels of patients suffering from encephalopathy due to human immunodeficiency virus (HIV) infection.[57,58] Separately, increased serine phosphorylation promotes its removal from the bicellular junctions and its interaction with the E3 ubiquitin ligase Itch for subsequent degradation in bovine retinal ECs following stimulation with vascular endothelial growth factor (VEGF).[59]

Finally, multiple splice variants in humans and rodents for each of the members have been reported.[49,60–62] However, no studies have yet explored which variants are expressed in BBB-ECs under healthy or pathological conditions, nor their relative contributions to barrier function.

The Angulin Family

Unlike the other two families, angulins are single-pass proteins with extracellular N-terminal tails containing immunoglobulin (IgG)-like domains (Figure 1.5).[31] The angulin family is comprised of three members: lipolysis-stimulated lipoprotein receptor

(LSR), and immunoglobulin-like domain-containing receptors 1 and 2 (ILDR1 and ILDR2).[31] All three are enriched at tricellular junctions where they participate in central sealing element formation (Figure 1.4).[31]

There is limited information regarding the expression or function of angulins in BBB-ECs. Currently, only LSR has been reported to be expressed *in vivo*.[63,64] Its knockout is embryonically lethal in mice.[64] At E14.5, when the BBB should be functional, knockout embryos suffer leakage of Sulfo-NHS-Biotin (443 Da) but do not have altered bicellular junctions, suggesting leakage is occurring via the tricellular junctions.[64] As for the remaining two members, a recent study that performed transcriptional analysis of primary mouse BBB-ECs reported that *Ildr2*, but not *Ild1*, is additionally expressed.[65] However, no functional characterization was performed.

Inter- and Intra-Family Interactions

Tight junctions rely on the transmembrane and scaffolding proteins present to act in concert. At bicellular junctions, claudins form an initial network of loose strands that confers basic barrier functionality to the cell.[66] However, incorporation of proteins like occludin is required for the formation of branching strands between the lateral strands to yield a continuous, anastomosing network.[66] Similarly, at tricellular junctions, although angulins form the initial central sealing element, recruitment of proteins like tricellulin is required to couple the bicellular junctions to the central sealing element.[66] Under this framework, it is readily apparent that disruptions to any of these families will likely negatively impact the others. However, intra-family interactions also exist.

Claudin Interactions. Sladojevic *et al.* reported that claudin-1 upregulation and its incorporation into the tight junctions was associated with claudin-5 loss and BBB

dysfunction in patients with chronic stroke and an animal model of chronic stroke.[46] Furthermore, claudin-1 overexpression disrupted the *cis*- and *trans*-interactions of claudin-5 and increased permeability to inulin in an immortalized mouse BBB-EC line.[46] Similarly, Berndt *et al.* reported claudin-5 knockdown led to claudin-1 upregulation, while claudin-11 overexpression led to the formation of short, alternating claudin-5^{+} or claudin-11^{+} strands at the cell borders.[39]

TAMP Interactions. Studies that modeled hereditary forms of deafness due to loss-of-function mutations in *Ocln* or *MarvelD2* have repeatedly demonstrated that loss of one results in the redistribution of the other at the cost of barrier integrity and cellular degeneration.[49,67–69] However, these interactions have not been investigated in BBB-ECs.

Angulin Interactions. The interplay amongst angulins is the least understood of the three families. Based on studies that focused on the gut epithelium, kidney epithelium, or cochlear hair cells, loss of one can be partially compensated by the others.[70,71] As with the TAMPs, interactions in BBB-ECs have not been reported.

Rationale for Systematic Literature Search

Given the close connection between tight junctions and BBB function, the expression and localization patterns of tight junction proteins are commonly chosen as surrogate markers for barrier dysfunction in CNS-IDDs and other CNS disorders. Unfortunately, an all-too-common trend is to assess a single protein at a single stage of disease. While this strategy may work well from a publication perspective, it has left the field disjointed, with findings spread across scores of articles. Moreover, it too easily allows for the oversimplification of the results to simple binary perspectives as to whether tight junctions are disrupted or barrier function compromised. Consequently, this has left

it challenging to understand the dynamics of tight junction protein expression and localization across the disease course.

To address this outstanding defect, I have conducted a systematic literature search for studies characterizing the claudin, TAMP, and angulin families in patients with CNS-IDDs. To support these findings, I have additionally conducted searches for human-derived CNS-EC culture models and commonly used animal models of CNS-IDDs, namely, experimental autoimmune encephalomyelitis (EAE), experimental NMOSD (E-NMOSD), Theiler's murine encephalomyelitis virus (TMEV), and cuprizone.

Methodology

Literature Search Strategy

Searches were conducted following the preferred reporting items for systematic reviews and meta-analyses (PRISMA) guidelines.[72] The Web of Science platform (WoS; Clarivate Analysis) was chosen for its ability to simultaneously search across multiple databases, including Science Citation Index Expanded and MEDLINE. Databases were queried from their inception through March 1st, 2021.

Briefly, the 'OR' operator was used to generate data sets for each family member. To avoid missing relevant results that did not mention the families in the title or abstract, additional searches were performed using a wildcard approach ("tight junction*"). Then, the 'OR' operator was used to unify the individual data sets. Analogously, the 'OR' operator was used to generate data sets for each disease or model and then to unify them. Finally, the 'AND' operator was used to restrict the unified tight junction data set with the unified disease and model data set, yielding 657 unique results (Figure 1.8). For the complete search strategies used, see Appendix B.

Inclusion Criteria

Results were independently screened by two individuals for peer-reviewed studies with full-text availability in the English language. Additionally, conference abstracts and review articles were examined to identify relevant publications not found by the database searches (Figure 1.6). This yielded an additional thirteen studies (Figure 1.8).

Studies were assessed for inclusion on four points: 1) analysis specific to one or more of the queried diseases or models, 2) analysis specific to one or more of the queried families, 3) analysis specific to the endothelial blood-CNS barriers in patient tissues or human-derived CNS-EC cultures involving patient serum or IgG, and 4) an assessment about the member in the disease or model, rather than its usage as a cell marker (Figure 1.7). Ultimately, sixty-six studies fulfilling all four points were included for qualitative synthesis (Figures 1.9-11, 1.13-14, 1.16-25, Appendices C-F). However, forty studies failing only the third point are summarized in Appendices C-F. Disagreements between reviewers were resolved through discussion until consensus was achieved.

Summary of Literature Search

CNS-IDD Patient Samples

First, of the fifty-nine MS studies identified, plus two not found by WoS, forty-three were excluded as they did not meet the second eligibility point. Of the remaining eighteen studies, eight met all four points (Figures 1.9 & 1.10, Appendix C), seven met all points except the third (Appendix C), and three were excluded as the members were used solely as CNS-EC[73,74] or myelin markers.[75] Next, of the two NMOSD studies identified, one met all four points (Figure 1.13, Appendix C) and one met all points except the third

(Appendix C). Finally, one ADEM study was identified, but was excluded as it did not meet the second point.

Human CNS-EC Culture Models

First, of the eight MS studies identified, plus one not found by WoS, six met all four points (Figure 1.11, Appendix D), and the remaining three met all points except the third (Appendix D). Next, of the four NMOSD studies identified, plus one not found by WoS, four met all four points (Figure 1.14, Appendix D), while the remaining study met all points except the third (Appendix D). Finally, no studies for ADEM were found.

Animal Models

First, of the 116 EAE studies identified, plus two not found by WoS, forty-eight were excluded as they did not meet the second eligibility point. Of the remaining sixty-eight studies, forty-six met all four points (Figures 1.16-1.22, Appendix E), twenty met all points except the third (Appendix E), and two were excluded as the members were used solely as CNS-EC markers.[76,77] Next, of the two E-NMOSD studies identified, one was excluded as it did not meet the second point. The remaining study met all four points (Figure 1.23, Appendix F). Third, of the six TMEV studies identified, one was excluded as it did not meet the second point. The remaining five studies met all four points (Figure 1.24, Appendix F). Finally, of the four cuprizone studies identified, plus one not found by WoS, three were excluded as they did not meet the second eligibility point. Of the remaining two studies, one met all four points (Figure 1.25, Appendix F), while the other met all points except the third (Appendix F).

Alterations in Patients with MS

MS Lesions Staging

White matter (WM) lesions are temporally classified into pre-active, active, or chronic stages based on the presence or absence of two key pathological figures – activated microglia/macrophages and demyelination (Figure 1.9A).[78,79] Conversely, grey matter (GM) lesions are spatially classified as one of four types (Figure 1.10A).[80]

WM Lesions

Pre-active Lesions. Activated microglial clusters with variable other pathology but without demyelination have been termed pre-reactive lesions (Figure 1.9A – *left*).[81] However, not all clusters evolve into active lesions, nor are they unique to MS.[81]

From a mixed patient group, Horssen *et al.* selected a subset based on their high incidence of activated clusters.[82] These clusters were distant from microvessels and lacked astrogliosis, fibrinogen leakage, or T cell presence.[82] Claudin-5 was present in cross-sectional views of vessels, but no comparisons with normal-appearing WM (NAWM) or control donors were performed.[82] Next, in a group of patients primarily with SP-MS, Plumb *et al.* reported that areas with clusters had a greater proportion of abnormal tight junctions compared to NAWM based on the proportion of vessels with altered occludin or ZO-1 staining.[83] Additionally, the authors noted the presence of leukocytes around the vessels with disrupted tight junctions.[83] Finally, in a study of patients with RR- or SP-MS, Alvarez *et al.* observed disruption and loss of claudin-5 and occludin in areas with activated clusters that also exhibited astrogliosis, plasma protein leakage, and sparse lymphocytic infiltrates.[9]

Active Lesions. Active lesions are dense with activated macrophages and microglia variably laden with myelin degradation products (Figure 1.9A – *middle*).[78,79] Active lesions

are most common in patients with limited disease duration or RR-MS, and decrease in prevalence over time.[84]

In a group of patients primarily with SP-MS, Plumb *et al.* reported that occludin was disrupted or lost in lesional vessels.[83] Furthermore, these disturbances were prominent in regions with macrophage clusters, leukocytic infiltrates, or fibrinogen leakage.[83] When the authors tallied the number of vessels with altered occludin or ZO-1 staining, they found a high proportion of abnormal tight junctions regardless of how many lipid-laden cells were present, or the degree of their activation.[83] Separately, Wosik *et al.* measured a decreased peak fluorescence intensity and strand thickness for occludin in lesional vessels compared to NAWM from a group of MS patients whose clinical forms were not provided.[85]

Chronic Lesions. Lesions without active demyelination and lack microglia or macrophages except at the rim are termed chronic active, while lesions generally lacking cells are considered inactive (Figure 1.9A – *right*).[78,79] Both are most common in patients with prolonged disease duration or progressive MS, and increase in prevalence over time.[84]

In a group of patients primarily with progressive MS, van Horssen *et al.* reported that vessels in inactive lesions were sporadically negative for claudin-5.[86] Separately, Cunnea *et al.* measured gene expression in brain microvessels isolated from patients with progressive forms of MS.[87] The authors initially found an increase in occludin for chronic active lesions versus NAWM using microarray analysis (MA).[87] Subsequent validation by quantitative polymerase chain reaction (qPCR), however, measured a decrease in occludin for chronic active or inactive lesions versus NAWM.[87]

GM Lesions

Based on early studies using post-mortem samples, it was thought that demyelination in cortical lesions occurs by different mechanisms based on a general absence of observable inflammation.[88,89] Consequently, a spatial classification system was established instead (Figure 1.10A).[88,89] However, follow-up studies that included patient biopsies have since shown that inflammation and barrier dysfunction are present in cortical lesions, albeit mostly during early MS.[88,89] Interestingly, the presence of meningeal inflammation is topographically associated with cortical lesion presence, suggesting that the meninges may act as a backdoor for entry into the cortical tissues.[89]

In a study using post-mortem tissues from a patient group diagnosed primarily with progressive MS, van Horssen *et al.* observed that fibrinogen and IgG were still luminally confined in pure GM lesions or the GM portion of mixed GM-WM lesions.[86] In line, the vessels in pure GM lesions and adjacent normal-appearing GM (NAGM) were comparably reactive for claudin-5.[86]

Studies with Partial Staging

In a group of patients with RR-MS, Musolino *et al.* reported disruption and loss of claudin-5 in the vessels of demyelinated WM lesions, but additional staging information was not available.[90] Separately, Uchida *et al.* noted a disruption and loss of claudin-11 in frontal lobe brain and spinal cord vessels from patients whose clinical forms were not provided.[40] As a further complication, the analysis considered the entire tissue section and did not distinguish between matter types or lesion presence.

Summary

Across the eight studies that included patient tissues, only bicellular tight junction proteins (claudin-5, claudin-11, and occludin) have been characterized.

For WM lesions, studies suggest that bicellular tight junction disruption and barrier dysfunction precedes demyelination and variably persists throughout the life of the lesion. Conversely, for GM lesions, despite visible demyelination, bicellular tight junctions and barrier function do not appear disturbed compared to NAGM. However, given the findings of the more recent biopsy tissue-based studies, the results of this post-mortem tissue-based study likely reflect late MS and may not be indicative of what occurs in cortical lesions during early MS. Therefore, follow-up studies with cortical lesions exhibiting active inflammation are needed before conclusions about tight junction disruption or the viability of their therapeutic targeting can be made.

Alterations in Cell Culture Models of MS

Cell Lines Used in Studies

All studies used the hCMEC/D3[91] or TY series[92–94] of brain endothelial cell lines.

Serum- or IgG-induced Alterations

Shimizu *et al.* reported that the serum of patients who fulfilled the 2010 revised McDonald diagnostic criteria during the acute phase of disease had no impact on total claudin-5 or occludin protein, or transendothelial electrical resistance (TEER).[95] Similarly, Tasaki *et al.* found no difference in total claudin-5 protein, nor TEER, using serum from a comparable patient group.[96] Conversely, Shimizu *et al.* measured a loss of total claudin-5 protein and TEER using serum from patients with SP-MS or RR-MS during relapse, but not from patients with RR-MS in remission.[97] However, a loss of total occludin protein

was only detected with serum from patients with SP-MS.[97] The loss of total claudin-5 protein and TEER followed incubation with IgG isolated from the serum of patients with SP-MS, but not the IgG from either RR-MS group.[97] However, no patient IgG altered total occludin protein.[97] Finally, Sheikh *et al.* measured a decreased mean intensity fluorescence for occludin using the serum of patients with RR-MS by flow cytometry.[98] This was accompanied by decreased TEER and increased permeability to 70 kDa FITC-Dextran.[98]

Interventions

Inhibition of matrix metalloproteinases (MMPs) or proinflammatory cytokines. Using serum from patients who fulfilled the 2010 revised McDonald diagnostic criteria during the acute phase of disease, Tasaki *et al.* found no alteration in total claudin-5 protein or TEER using GM6001, a pan-MMP inhibitor.[96] Conversely, Shimizu *et al.* identified a rescue in total claudin-5 protein and TEER, but not total occludin protein, using GM6001 with serum from patients with RR-MS during relapse.[97] GM6001 was ineffective for rescue of either protein with serum from patients with SP-MS.[97] The authors also found a rescue in total claudin-5 protein and TEER using an anti-VEGF antibody, but not antibodies against tumor necrosis factor alpha (TNF-α), interferon gamma (IFN-γ), or interleukin 17 (IL-17), with serum from patients with RR-MS during relapse.[97] However, total occludin protein was unaltered with any antibody for serum from patients with RR-MS during relapse, and all of the antibodies were ineffective for either protein with serum from patients with SP-MS.[97] Notably, patient MMP and VEGF serum concentrations were comparable to control donors, suggesting autocrine MMP & VEGF secretion.[97]

Sphingosine 1-Phosphate Receptor (S1PR) Modulation. Fingolimod is a Food and Drug Administration (FDA)-approved S1PR modulator for patients with RR-MS.[99]

Nishihara *et al.* found a rescue for total claudin-5 protein and TEER with serum from patients with SP-MS or RR-MS following monolayer pre-treatment with fingolimod.[100] However, no rescue was found for total occludin protein with any of the patient sera.[100] Additionally, a rescue for claudin-5 gene expression was measured.[100] In this case, however, all patient groups were considered as a single disease group.

Vitamin D Receptor (VDR) Agonism. Takahashi *et al.* found a rescue for total claudin-5 protein with serum from patients with RR-MS during relapse, but not RR-MS in remission or SP-MS, following monolayer pre-treatment with Vitamin D_3.[101]

Summary

Across the six studies that used human-derived BBB-EC cultures with patient serum or IgG, only bicellular junction proteins (claudin-5 and occludin) have been characterized.

Incubation with patient serum, but not IgG, generally led to the loss of bicellular tight junction proteins and barrier dysfunction. These findings are supported by studies that incubated mouse- or rat-derived EC cultures with patient serum and reported suppression of claudin-5 and occludin expression on the mRNA and protein levels (Appendix D). However, the results of mixed cell culture models can be difficult to interpret, especially given the known differences in human and rodent immunology.[102] Nevertheless, successful therapies will likely require consideration of patient type and pro-inflammatory autocrine signaling in CNS-ECs.

Alterations in Patients with NMOSD

NMOSD Lesion Staging

Historically, six lesion types have been described based in NMOSD on their pathology.[103] However, this classification system could not infer lesion progression or how the types related to each other. Just this year, Takai *et al.* proposed the first temporal staging system which is focused on astrocyte morphology (Figure 1.12).[104]

At their earliest stages, lesions exhibit active astrocyte lysis, perivascular complement deposition, oligodendrocyte damage, and inflammatory cuffs.[21,104] Following astrocyte depletion, activated macrophages and microglia remain.[21,104] Over time, astrocyte repopulation and partial oligodendrocyte regeneration occurs, although astrocytes remain reactive and form characteristic honeycomb-like gliotic scarring.[21,104]

Alterations in Patient Lesions

In a group of patients with NMOSD, Winkler *et al.* reported that claudin-5 was present in cross-sectional views of lesions with completed astrocyte loss, demyelination, and primarily activated macrophages and microglia, but without fibrinogen leakage.[20] Although the serostatus of the patients was not known, all patients fulfilled at least two core NMOSD characteristics.[20] Lesions were located within the hippocampus, basal ganglia, or spinal cord, and the proportion of claudin-5^{+} lesional or perilesional vessels did not differ from control donors.[20] Additionally, the authors noted that claudin-3 and occludin were present in transverse sections from a single spinal cord lesion with partial astrocyte repopulation and were comparable to control donors.[20]

Summary

Only a single study that included patient samples was identified. In it, only bicellular tight junction proteins (claudin-3, claudin-5, and occludin) were characterized.

Barrier dysfunction is most prominent during active astrocyte lysis. However, all lesions assessed for tight junction disruption already had completed astrocyte lysis and generally lacked markers of recent vascular leakage. Thus, the finding that bicellular tight junction protein presence in patient lesions was comparable to control donor tissues is not unexpected. Follow-up studies involving early lesions with active astrocyte lysis are needed before conclusions about tight junction disruption or the viability of their therapeutic targeting can be made.

Alterations in Cell Cultures of NMOSD

Cell Lines Used in Studies

All studies used the TY08 brain endothelial cell line.[92]

Serum- or IgG-induced Alterations

Shimizu *et al.* reported a loss of total claudin-5 protein and TEER, but not total occludin protein, with serum from patients with NMO during the acute phase of disease.[95] Similarly, Tasaki *et al.* observed a loss of total claudin-5 protein and TEER, plus increased permeability to NaFluor, with serum from patients with NMOSD during the acute phase of disease.[96] Patients were diagnosed with definitive NMO or longitudinally extensive transverse myelitis (LETM).[96] However, no loss in total claudin-5 protein was detected using serum from patients in remission.[96]

Tasaki *et al.* also reported no changes in total claudin-5 protein, TEER, or permeability to NaFluor with IgG from NMOSD patients during the acute phase of

disease.[96] Similarly, using a transwell co-culture system with astrocytes, Takeshita *et al.* found that pooled NMO-IgG was insufficient to alter claudin-5 localization or permeability to 10 kDa FITC-dextran when the astrocytes did not express AQP4.[105] Conversely, Shimizu *et al.* reported a disruption and loss of claudin-5 with pooled NMO-IgG.[106] In this case, however, the authors identified an anti-endothelial cell antibody (AECA) against glucose-regulated protein 78 (GRP78).[106] Incubation with patient-derived recombinant antibodies was sufficient to replicate claudin-5 loss and barrier hyperpermeability.[106]

Interventions

Inhibition of MMPs. Tasaki *et al.* reported a rescue for total claudin-5 protein and TEER using GM6001 or inhibitors specific to MMPs 2 or 9 with sera from patients with NMOSD during the acute phase of disease.[96] The inhibitors likely targeted endothelial-derived MMPs as patient sera did not have elevated levels compared to controls.[96]

Inhibition of proinflammatory cytokines. Shimizu *et al.* found a rescue in total claudin-5 protein and gene expression using serum from patients with NMO during the acute phase of disease with an anti-VEGF antibody, but not antibodies against IFN-γ, TNF-α, transforming growth factor beta (TGF-β), interleukin-6 (IL-6), or IL-17.[97] While a rescue for occludin gene expression was observed using the anti-IL-17 antibody, no alteration on the total protein level was detected.[97] In line, TEER was rescued with the anti-VEGF antibody, but not the anti-IL-17 antibody.[97] The anti-VEGF antibody likely targeted endothelial VEGF as patient serum did not have elevated levels compared to controls.[97]

Depletion of humoral factors. Shimizu *et al.* found a rescue in total claudin-5 protein and TEER comparing the serum from two patients with NMO after therapeutic plasma exchange (TPE) against their serum before TPE.[95] Separately, the authors incubated

patient serum for 30 or 150 minutes with astrocyte cultures overexpressing AQP4.[95] Although depletion of anti-AQP4 antibodies not achieved until the second time point, increased total claudin-5 protein and TEER was achieved with serum from either time point.[95] Taken together, depletion of humoral factors other than pathogenic AQP4 antibodies was likely responsible for the rescue.[95]

Summary

Across the four studies that used human-derived BBB-EC cultures with patient serum or IgG, only bicellular tight junction proteins (claudin-5 and occludin) have been characterized.

Like the studies with MS sera, incubation with patient serum generally resulted in loss of bicellular tight junction proteins and barrier dysfunction regardless of classic NMO versus expanded NMOSD diagnosis. Patient IgG generally had no impact unless co-cultures with AQP4-expressing astrocytes were used, underscoring the relationship between local pathology and barrier dysfunction. Notably, a sub-set of patients with NMOSD additionally appear to possess pathogenic AECAs capable of triggering tight junction disruption and barrier compromise. Thus, successful therapies will likely require consideration of pathogenic antibodies besides those against AQP4, plus pro-inflammatory autocrine signaling in CNS-ECs.

Alterations in EAE Models

Background

In the classic EAE model, animals are immunized with CNS tissue homogenates or myelin protein-derived peptides to produce a $CD4^+$ T cell-driven disease.[107,108] This manifests as an initial period without observable neurological deficit followed by

ascending flaccid paralysis, although the kinetics and resolution are antigen- and strain-dependent.[107,108] Broadly speaking, models can be classified as chronic, relapsing-remitting, or monophasic based on the observed disease course (Figure 1.15). Additionally, to circumvent the initial induction phase responsible for T cell priming, transgenic mice that express myelin-reactive T cell receptors (TCRs) or adoptive transfer of primed $CD4^+$ T cells into naïve animals is frequently performed.[107,108]

MOG_{35-55} Peptide-based Models

Immunization of C57BL/6 mice with a peptide corresponding to residues 33-55 of myelin oligodendrocyte glycoprotein (MOG_{35-55}) yields a chronic disease course.[107,108]

Alterations in the Base Disease State

Pre-onset Stage. Paul *et al.* reported no apparent disruption of claudin-5 in thoraco-lumbar spinal cord capillaries or venules, despite focal IgG deposition, about halfway between induction and onset.[109] In two subsequent studies, however, the authors noted its disruption in venules with infiltrates close to onset.[110,111] Separately, we have demonstrated a loss of claudin-5 in isolated brain microvessels from animals with barrier dysfunction close to onset.[34] Additionally, we measured a lowered claudin-5 density at the tight junctions and loss of total claudin-5 protein in microvessel homogenates.[34]

Onset-to-Early Stages. Argaw *et al.* reported disruption and loss of claudin-5 in lumbar spinal cord vessels with barrier dysfunction at onset.[112] Similarly, at the early stage, the authors noted disruption and loss of claudin-5 and occludin in vessels with barrier dysfunction, or those near strong VEGF-A staining.[112] In line, Paul *et al.* observed the disruption and loss of claudin-5 in thoraco-lumbar spinal cord venules with infiltrates.[109] Moreover, claudin-5 density at the tight junctions was lower at the early stage than at the

pre-onset stage.[109] In the brain, Errede *et al.* noted worsened disruption and loss of claudin-5 in the cortical and subcortical vessels of animals with more severe disability than those with milder disability.[113] Disruption and loss of occludin in cortical vessels was only apparent in mice with severe disability.[113] Conversely, Welser *et al.* did not measure a difference in the ratio of claudin-5^+ per $CD31^+$ reactive area in the medulla oblongata.[114]

Peak Stage. Niu *et al.* noted a loss of occludin in spinal cord vessels.[115] Similarly, Li *et al.* observed a disruption and loss of claudin-5 and occludin in spinal cord vessels,[116] while Wang *et al.* demonstrated the disruption and loss of claudin-5 in lumbar spinal cord vessels and brain vessels.[117] Separately, Welser *et al.* measured a decreased ratio of claudin-5^+ per $CD31^+$ reactive area for the medulla oblongata,[114] while Bittner *et al.* reported no changes for claudin-5 gene expression from isolated brain microvessels across two separate experiments, but a loss of occludin mRNA for one of the two.[118] Finally, Uchida *et al.* noted disruption and loss of claudin-11 in brain and spinal cord vessels.[40]

Late Stage. Argaw *et al.* observed disruption and loss of claudin-5 and occludin in lumbar spinal cord vessels with fibrinogen or albumin leakage.[112] In line, Paul *et al.* reported disruption and loss of claudin-5 in thoraco-lumbar spinal cord venules, but not capillaries, with infiltrates.[110] Furthermore, claudin-5 density at the tight junctions was decreased in the venules, but not the capillaries.[110] Likewise, Zhang *et al.* noted a loss of claudin-5 in lumbar spinal cord vessels,[119] while Bénardais *et al.* tallied fewer claudin-5+ spinal cord vessels per field of view.[120] Separately, Errede *et al.* observed worsened disruption and loss of claudin-5 and occludin in cortical vessels from animals with more severe disability versus those with milder disability.[113] Likewise, Eilam *et al.* reported disruption and loss of claudin-5 in cortical vessels.[121]

Estimated Staging. Sohet *et al.* reported a loss of LSR reactivity in spinal cord vessels with infiltrates and IgG leakage at 4 days post-onset (*d.p.o.*), suggesting early staging.[64] Chapouly *et al.* reported disruption and loss of claudin-5 in lumbar spinal cord vessels of animals with paraparesis or paraplegia at 15-18 days post-induction (*d.p.i.*), suggesting early-to-peak staging.[122] Additionally, claudin-5 presence negatively correlated with VEGF and thymidine phosphorylase (TYMP) presence.[122] Separately, Becker *et al.* observed disruption and loss of claudin-5 in the spinal cord vessels of animals with no provided clinical scores or staging,[123] while Mora *et al.* measured a decrease in claudin-5 gene expression from isolated spinal cord microvessels at 13 *d.p.i.*, suggesting onset-to-early staging.[124] Separately, Alt *et al.* measured a decrease of claudin-11 and occludin gene expression in brain microvessels from animals at 12 *d.p.i.* with limp tails, suggesting onset-to-early staging.[125] Finally, Ferrara *et al.* and Girolamo *et al.* both observed disruption and loss of claudin-5 and occludin reactivity in cortical vessels.[126,127] Staging was not explicitly defined in either study, but related experiments suggest late or peak staging, respectively.

Interventions

Inhibition of astrocyte signaling. Argaw *et al.* noted VEGF upregulation in the astrocytes of diseased mice.[128] The authors inhibited endothelial nitric oxide synthase (eNOS) activity, a downstream target, with cavtratin following onset of disability.[128] The treatment group at peak exhibited a rescue in claudin-5 and fibrinogen leakage in lumbar spinal cord vessels, plus lessened disability, demyelination, and $CD45^+$ infiltration.[128] Similarly, Chapouly *et al.* noted VEGF and TYMP upregulation in the astrocytes of diseased mice.[122] The authors inhibited eNOS activity, TYMP activity, or both, with cavtratin, 2-deoxy-L-ribose (2DLR), or both, following onset of disability.[122] All treatment

groups at peak exhibited a rescue in claudin-5 and fibrinogen leakage in lumbar spinal cord vessels, plus lessened disability, demyelination, and $CD45^+$ infiltration.[122]

Promotion of the Nrf2 antioxidant pathway. Bénardais *et al.* administered dimethyl fumarate, an FDA-approved fumaric acid ester for patients with RR-MS,[129] starting at induction.[120] Although the treatment group exhibited lessened disability at a late stage, there was no rescue in the proportion of claudin-5^+ spinal cord vessels.[120] Conversely, Li *et al.* administered sulforaphane, an isocyanate found in cruciferous vegetables, starting at induction.[116] The treatment group at peak exhibited a rescue in claudin-5 and occludin and barrier dysfunction in spinal cord vessels, plus lessened demyelination and smaller infiltrates.[116] Similarly, Niu *et al.* administered naringenin, a flavonoid found in citrus fruits, starting at four weeks pre-induction.[115] The treatment group at peak exhibited a rescue of occludin and barrier dysfunction in spinal cord vessels.[115]

Immunomodulators. Hou *et al.* administered minocycline, interferon beta (IFN-β)-secreting mesenchymal stem cells (MSCs), or both, following onset of disability.[130] All treatment groups exhibited a rescue of occludin in lumbar spinal cord vessels at a late stage, plus lessened disability and barrier dysfunction. Separately, Eilam *et al.* administered glatiramer acetate, an FDA-approved synthetic peptide mixture for patients with RR-MS,[131] before peak disability.[121] The treatment group at a late stage exhibited a rescue of claudin-5 in cortical vessels, plus lessened disability and greater pericyte coverage.[121]

Inhibition of NF-κB signaling. Zhang *et al.* administered tetramethylpyrazine (TMP) or IKK-16, following onset of disability.[119] Both treatment groups exhibited a rescue of claudin-5 in lumbar spinal cord vessels at a late stage, plus diminished astrogliosis, demyelination, and barrier dysfunction.[119]

Inhibition of Glutamate Signaling. Bittner *et al.* measured a rescue of occludin mRNA, but unaltered claudin-5 mRNA, at peak disability in brain microvessels isolated from animals administered riluzole either at induction or following onset of disability, although it was unclear which of the two intervention strategies was reported.[118]

Non-Claudin-involved Genetic Manipulations

Bradykinin receptor B1 (B1R). Göbel *et al.* observed strong B1R upregulation in vessels within lesions of MS patients whose form was not provided.[132] The authors reported a rescue for occludin gene expression, but for claudin-5, in brain microvessels isolated at peak from knockout (KO) animals, along with lessened disability.[132]

Immunity-related GTPase family M protein 1 (IRGM1). Wang *et al.* observed strong IRGM1 upregulation in multiple cell types, including astrocytes, in wild-type (WT) diseased animals.[117] KO animals at peak exhibited a rescue for claudin-5 in brain and spinal cord vessels, plus lessened disability, astrocyte swelling, or infiltrates.[117]

Potassium channel subfamily K member 2 (KNCK2). Bittner *et al.* observed loss of KNCK2 in vessels within lesions of MS patients whose form was not provided.[118] KO animals exhibited no difference in claudin-5 or occludin gene expression, nor in barrier dysfunction, but suffered worsened disability.[118] Additionally, in spinal cord vessels from lesions whose staging was not defined, but likely also at peak, there was no difference in occludin intensity for KO animals.[118]

Neuron-glial antigen 2 (NG2). Ferrara *et al.* observed strong NG2 upregulation in pericytes and splenocytes of WT diseased animals.[126] KO animals exhibited a rescue for claudin-5 and occludin in cortical vessels, plus lessened disability or barrier dysfunction, at an unclear staging, but likely at a late stage.[126] Additionally, using bone marrow

chimeras, the authors reported worsened disruption and loss of claudin-5 and occludin in the cortical vessels of WT recipients than KO recipients at a late stage, regardless of donor genotype.[126] However, recipients of WT bone marrow exhibited worsened disability and demyelination than recipients of KO bone marrow.[126] Separately, Girolamo *et al.* observed strong NG2 presence in pericytes and oligodendrocyte precursor cells of diseased WT animals.[127] In line, KO animals exhibited a rescue for claudin-5 and occludin in cortical vessels, plus diminished barrier dysfunction, for KO animals whose staging was not defined, but likely at peak.[126]

Liver X receptor alpha (LXRα). Wouters *et al.* initially observed barrier dysfunction, loss of claudin-5, and elevated monocyte migration in LXRα-knockdown hCMEC/D3 cells.[133] Similarly, KO animals exhibited a lower claudin-5+ area in the brain at post-peak.[133]

Acid sphingomyelinase (ASM). Becker *et al.* reported a rescue in claudin-5 in spinal cord vessels of KO animals at a non-specified stage.[123] Additionally, KO animals exhibited lessened disability, infiltrate presence, and barrier dysfunction.[123]

Interferon Gamma Receptor (IFNγR). Ni *et al.* reported worsened loss of claudin-5 in the cerebellar vessels of KO animals at peak.[134] KO animals exhibited worsened disability, greater infiltrate presence in the spinal cord and cerebellum, and atypical behavior like head tilting or ataxia.[134] However, endothelial-restricted expression of IFNγR rescued claudin-5 at peak compared to KO animals, and animals exhibited lessened infiltrate presence in the cerebellum or atypical behavior.[134]

Leptin receptor (LR). Ouyang *et al.* observed an initial rise, then loss, for LR gene expression in cortical and spinal cord vessels isolated from diseased WT animals over the

disease course.[135] KO animals exhibited a rescue at peak for occludin gene expression, but not for claudins 1, 2, 3, or 5, in spinal cord vessels, plus lessened disability and infiltrate presence in the spine.[135]

Integrin beta 4 (ITGB4). Welser *et al.* observed strong upregulation of ITGB4 in medulla oblongata vessels of diseased WT animals over the disease course.[114] KO animals at peak exhibited a worsened loss of claudin-5, plus aggravated disability, barrier dysfunction, and infiltrate presence.[114]

C-C Motif Chemokine Ligand 2 (CCL2). Paul *et al.* observed strong upregulation of CCL2 in spinal cord ECs and astrocytes of diseased wild-type animals at 16 *d.p.i.*[109] Endothelial-restricted or astrocyte-restricted knockout (EC^{KO} and AC^{KO}, respectively) animals exhibited a rescue in claudin-5 density at the tight junctions in the spinal cord venules at 9 or 16 *d.p.i.* compared to their WT counterparts at the same time points.[109] Density remained unchanged between the two time points in the EC^{KO} animals, but decreased in the AC^{KO} animals.[109] However, disability was not reported until 20 *d.p.i.* in the EC^{KO} animals and 14 *d.p.i.* in the AC^{KO} animals compared to 11 *d.p.i.* for their WT counter parts, complicating direct comparison by stage.[109]

Vascular endothelial growth Factor A (VEGF-A). Argaw *et al.* observed a strong upregulation of VEGF-A in spinal cord astrocytes of diseased wild-type animals.[128] AC^{KO} animals exhibited a rescue for claudin-5 in spinal cord vessels at peak, plus lessened disability, barrier dysfunction, demyelination, or infiltrate presence.[128]

Dominant-negative mutant of NF-κB inhibitor alpha (IκBα). Brambilla *et al.* reported no rescue for claudin-5 in thoracic spinal cord vessels from diseased animals with astrocyte-restricted expression of a dominant-negative mutant of IκBα post-peak or at a

late stage.[136] However, dominant-negative animals exhibited lessened peak-to-late disability, which was associated with improved remyelination processes.[136]

Claudin-involved Genetic Manipulations

Claudin-1. Pfeiffer *et al.* generated an animal with inducible expression of claudin-1 in endothelial cells under the control of doxycycline.[45] Although only 30% induction was achieved in brain vessels, this was sufficient to ameliorate disability at a late stage, but not during peak disease.[45] Additionally, while knockin animals had a comparable number of inflammatory cuffs, claudin-1^+ cuffs exhibited lessened barrier dysfunction.[45]

Claudin-5. Paul *et al.* generated an animal with constitutive expression of an eGFP-claudin-5 fusion protein in endothelial cells.[111] The authors observed disruption of eGFP-claudin-5 in thoraco-lumbar spinal cord venules with infiltrates close to onset.[111] Using the same animal line, Lutz *et al.* employed intravital two-photon microscopy (IV-2PM) to observe eGFP-claudin-5 in lumbar spinal cord venules.[137] At pre-onset, early, or peak, the authors observed disruption of eGFP-claudin-5^+ tight junctions in venules with fibrinogen leakage.[137] Furthermore, the authors found rapid remodeling of eGFP-claudin-5^+ tight junctions at all three stages, while non-continuous, or tortuous eGFP-claudin5^+ patterns were observed only in animals exhibiting disability.[137] Additionally, the authors crossed the eGFP-claudin-5 knockin line with a caveolin-1 knockout line.[137] The absence of caveolin-1, however, did not alter the proportion of eGFP-claudin-5^+ tight junctions with protrusions, gaps, or tortuosity close to onset.[137]

Claudin-12. Castro Dias *et al.* generated an animal whose open reading frame (ORF) was replaced with a beta-galactosidase (LacZ) reporter cassette.[48] Complete KO

animals followed a comparable disease course to their WT counterparts, and no difference in severity of barrier dysfunction was noted between the two.[48]

MOG$_{1-125}$ Peptide-based Models

Immunization of rats with a peptide corresponding to residues of 1-125 of MOG (MOG$_{1-125}$) yields a variable disease course depending on the strain.[138] Generally, it is either chronic or relapsing-remitting.[138]

Adzemovic *et al.* generated a congenic DA rat that carries the *Eae18b* locus, which contains CCLs 1, 2, 7, 11, and 12, from the EAE-resistant PVG.av1 rat line.[139] The congenic DA line exhibited a rescue in occludin shortly post-onset, plus diminished *Ccl11* gene upregulation in spinal cord homogenates (SCH).[139]

MBP Peptide- or Full-length Protein-based Models

Immunization of rodents with full-length myelin basic protein (MBP) or MBP-derived peptides yields a disease course that is monophasic and generally reaches remission, although demyelination is generally limited in rats.[108]

Using Lewis rats, Morgan *et al.* observed disruption and loss of claudin-5 and occludin in lumbar spinal cord vessels with infiltrates at peak.[140] Separately, using wild-type or inducible nitric oxide synthase (iNOS) knockout CBA mice, Ninkovic *et al.* observed a comparable loss of occludin in forebrain sections at a late stage between genotypes.[141] Additionally, administration of agmatine to WT or KO animals starting at induction resulted in a comparable rescue in occludin reactivity at a late stage between genotypes compared to their vehicle-control counterparts.[141]

$PLP_{139-151}$ Peptide-based Models

Immunization of SJL mice with residues 139-151 of proteolipid protein ($PLP_{139-151}$) yields a disease course that is relapsing-remitting in nature.[107,108]

Halder *et al.* noted a disruption and loss of occludin in lumbar spinal cord vessels at peak.[142] However, the authors found a partial rescue in occludin for diseased animals exposed to chronic mild hypoxia (CMH – 10% oxygen) starting at induction.[142] This was accompanied by lessened disability, demyelination, or barrier dysfunction.[142] In a subsequent study, the authors noted a disruption and loss of occludin at peak and remission.[143] Intervention with CMH following onset of disability failed to rescue occludin at peak, but did rescue it at three separate time points during remission.[143] This was paralleled by lessened disability, demyelination, or barrier dysfunction during remission, but not at peak.[143] Separately, Lanz *et al.* administered LY317615, a protein kinase C-beta (PKC-β) inhibitor to animals at unclear time point (possibly at peak), and the treatment group exhibited a rescue of claudin-5 in spinal cord vessels.[144]

SCH-based Models

Immunization of rodents with syngeneic or guinea pig SCH yields a variable disease course depending on the strain and sex.[138] Generally, it is either monophasic or relapsing-remitting.[138]

Using syngeneic SCH in SJL mice, Wolburg *et al.* observed loss of claudin-1 and claudin-3 in brain vessels near infiltrates in paraplegic mice.[44] While claudin-5 and occludin were still detectable in the vessels, the authors noted that altered vessel morphology precluded assessment of subcellular localization.[44] Using SD rats, Huang *et al.* noted a worsened disruption and loss of claudin-5 in cerebellar vessels of diseased

animals with severe disability versus those with mild disability.[145] The authors found a rescue in claudin-5 at peak in animals administered ImKTx88, a voltage-gated potassium channel blocker, starting at induction or post-onset of disability.[145] This was accompanied by lessened disability, demyelination, and barrier dysfunction.[145]

Using guinea pig SCH, Shou *et al.* noted a loss of claudin-5 in brain vessels of diseased Wistar rats at onset, peak, and late stages.[146] The average optical density (AOD) for claudin-5 decreased between onset and peak, with a modest increase by the late stage.[146] In line, Yang *et al.* observed a loss of claudin-5 and occludin in brain vessels of Lewis rats at peak. The authors found a rescue for both proteins**,** plus barrier dysfunction, at peak for animals administered Tanshinone IIA, an immunomodulatory diterpenoid, at two separate dosages.[147] There was a greater increase for both proteins at the higher dosage.[147] Separately, Grygorowicz *et al.* reported the loss of total claudin-5 protein in brain microvessels isolated from the GM of diseased Lewis rats at four times points before onset of disability, plus at peak disability.[148] A similar trend was noted for claudin-5 reactivity.[148] Additionally, when the authors administered Brilliant Blue G (BBG), a purinergic receptor P2X 7 (P2X7R) antagonist, starting at induction, they found a rescue in total claudin-5 protein, although onset of disease was delayed in the treatment group, complicating direct comparison of stages.[148] Finally, Viñuela-Berni *et al.* reported a loss in total claudin-5 protein in brain and spinal cord vessels isolated from diseased Lewis rats at peak.[149] When the authors administered Conivaptan, an arginine vasopressin receptor (AVPR) antagonist, starting at induction, they found an intermediate rescue in total claudin-5 protein.[149] This was accompanied by lessened disability and barrier dysfunction.[149]

Transgenic EAE Models

TCR-1640 mice carry a TCR specific to residues 92-106 of MOG (MOG_{92-106}).[9] On an SJL background, this yields a disease course that is spontaneous, although in females it is generally relapsing-remitting, while in males it generally is chronic.[9]

Alvarez *et al.* considered the relationship between local pathology and barrier dysfunction in TCR-1640 animals prior to onset.[9] The authors noted disruption and loss of occludin in cerebellar vessels in areas with astrogliosis and macrophage infiltrates.[9] There was a specific and progressive loss in pixel intensity for occludin, but not claudin-3 or claudin-5, over the time points selected.[9]

Summary

Of all the queried diseases or models, the EAE model accounts for the majority of studies found and included for synthesis. In line, the greatest number of members were identified, with six claudins (1, 2, 3, 5, 11, & 12), one TAMP (occludin), and one angulin (LSR). It is also the only model that has assessed tricellular junction proteins (LSR).

Most studies focused on the post-onset stages of diseases, where tight junction disruption and barrier dysfunction are expected. However, several induction- and transgenic-based models have considered the pre-onset timeframe. In the MOG_{35-55} model, claudin-5-containing tight junctions appear intact in spinal cord microvessels halfway between induction and onset,[110] but by 1-2 days pre-onset, they are disrupted.[109,111] Using this model, we recently demonstrated barrier dysfunction and decreased claudin-5 density at tight junctions in brain microvessels isolated from animals close to onset.[34] Similarly, total claudin-5 protein was diminished in brain microvessels isolated from Lewis rats induced with guinea pig spinal cord at several times pre-onset.[148] Most interesting,

however, are the findings from the TCR-1640 model, where barrier dysfunction and tight junction alterations are observed weeks before observable neurological deficit.[9] Taken together, it is clear that BBB compromise is an early event in disease progression.

Many therapeutic interventions have been tested with the EAE model. Most studies that reported successful rescue of neurologic function also reported rescues in barrier function and tight junction expression. For instance, Eilam *et al.* reported that administration of the FDA-approved drug glatiramer acetate rescued disability and claudin-5 expression.[121] This outcome is most likely due to the immunomodulatory properties of glatiramer acetate rather than direct targeting of the BBB.[150] However, it is worth pointing out that other FDA-approved drugs, including glucocorticoids,[151] S1PR agonists,[152] and IFN-β,[153] have been demonstrated to promote BBB-EC function and tight junction protein expression. Thus, therapeutic strategies that target the CNS vasculature directly could prove valuable in treating patients with CNS-IDDs.[7]

Finally, genetic manipulations involving the claudin family in EAE have shed light on the contributions of its members in health and disease. Endothelial-restricted claudin-1 overexpression rescued disease and vascular leakage during the chronic stage of the MOG_{35-55} model,[45] suggesting that promotion of claudins could be a viable therapeutic target. Endothelial-restricted expression of a eGFP-CLDN5 fusion protein identified that its localization and turnover dynamics at the tight junctions is altered pre-onset in the MOG_{35-55} model,[74] suggesting that tight junction remodeling is an early regulatory mechanism in disease progression. Lastly, global claudin-12 knockout mice exhibited a comparable disease course in the MOG_{35-55} model, and LacZ reporter mice suggest that

claudin-12, in fact, is mostly expressed in other CNS cells than BBB-ECs, calling into question whether it plays a role in barrier function.[48]

Alterations in Experimental NMOSD Models

Background

Animal models follow one of three approaches, each partially recapitulating NMOSD pathology. EAE-induced animals can be administered pathogenic IgG without or without complement, adoptive transfer of AQP4-specific T cells and injection of pathogenic IgG into animals can be performed, or animals can be directly co-injected into the CNS with complement and pathogenic IgG.[154] Of the three, the last has become the preferred choice as it eliminates the complications of an EAE-based background.[154]

Alterations in Recombinant AQP4-IgG-Complement-based Models

Winkler *et al.* intracortically injected recombinant AQP4-IgG and complement into Lewis rats (Figure 1.23).[20] Onset of neutrophil infiltration, astrocyte loss, and barrier dysfunction occurred by 6 hours post-injection.[20] At this point, the authors reported a lowered proportion of occludin$^+$ vessels compared to animals administered a control antibody.[20] By 10 and 24 hours post-injection, occludin was generally absent, and did not fully return until 6 days post-injection.[20] Conversely, the proportion of claudin-3$^+$ or claudin-5$^+$ vessels was unchanged over the same duration.[20]

Interventions

Immune cell depletion. Winkler *et al.* depleted ~90% of circulating neutrophils, T cells, and B cells by administration of a rabbit anti-polymorphonuclear (PMN) antiserum before and after disease induction.[20] This rescued the proportion of occludin$^+$ vessels at 6 hours post-injection, along with astrocyte loss and barrier dysfunction.[20] The proportion of

claudin-3^+ or claudin-5^+ vessels, however, was unaltered with respect to disease or intervention.[20]

Summary

Only a single study that involved an E-NMOSD model was identified. In it, only bicellular tight junction proteins (claudin-3, claudin-5, and occludin) were characterized.

Like NMOSD, barrier dysfunction in the E-NMOSD model was most prominent during active astrocyte lysis. During this timeframe, immunoreactivity for occludin, but not claudins 3 or 5, was lost. From this, the authors concluded that occludin was selectively affected in the E-NMOSD model and that its loss was the sole factor for barrier dysfunction in the model. However, in light the study by Lutz *et al.* that demonstrated that claudin turnover at the tight junctions is altered under pathological conditions using IV-2PM,[137] caution must be exercised when correlating bicellular tight junction protein presence with unaltered regulation or contribution to barrier dysfunction.

Alterations in TMEV Models

Background

TMEV is an RNA virus from the *Picornaviridae* family that is injected intracranially into susceptible mouse lines.[155,156] The classic model follows a biphasic disease course that culminates in chronic spinal cord demyelination,[155,156] while the peptide-induced fatal syndrome (PIFS) model resembles AHLE.[157] PIFS exploits $CD8^+$ T cells that are specific for a peptide from the VP2 capsid protein ($VP2_{121-130}$).[158,159] Intravenous injection of the peptide at peak CNS expansion leads to rapid astrogliosis and neuron-derived VEGF secretion, followed by barrier dysfunction, microhemorrhages, demyelination, and death within 24-72 hours (Figure 1.24).[160]

Alterations in PIFS-based Models

Astrogliosis and barrier dysfunction peak at 4 and 12 hours post-peptide injection (*h.p.p.*), respectively.[159] At these time points, Suidan *et al*. found a decrease in total occludin protein, but unaltered total claudin-5 protein, in isolated brain microvessels.[159] By 24 *h.p.p.*, there was a partial recovery in total occludin protein and an increase in total claudin-5 protein.[159] Separately, Johnson *et al.* and Willenbring *et al.* noted disruption and loss of both proteins in areas with extensive barrier dysfunction at 12 and 24 *h.p.p.*[161,162]

Interventions

Immune cell depletion. Johnson *et al.* found that depletion of $CD8^+$ T cells with antibodies against granulocyte receptor 1 (GR-1) preserved claudin-5 and occludin localization at the tight junctions and minimizes barrier dysfunction.[161] However, depletion of neutrophils with antibodies against lymphocyte antigen 6 complex locus G6D (Ly6G) failed to rescue tight junction disruption or barrier dysfunction.[161]

Inhibition of VEGF signaling. Suidan *et al.* observed VEGF upregulation in the neurons of diseased animals.[163] The authors administered a peptide-based antagonist for neuropilin-1 (NRP-1), a co-receptor for VEGF receptor 2 (VEGFR2), before and after injection of the $VP2_{121\text{-}130}$ peptide.[163] The treatment group exhibited a rescue of total occludin protein in isolated brain microvessels and barrier dysfunction.[163]

Genetic Manipulations

Perforin-1 (Prf1). Suidan *et al.* reported that total claudin-5 and occludin protein are preserved in isolated brain microvessels of homozygous KO mice.[159] In line, Willenbring *et al.* observed no apparent disruption of claudin-5 in homozygous KO mice and minimal barrier dysfunction.[162] Conversely, the authors reported an intermediate

phenotype for hemizygous KO mice as modest disruption of claudin-5 and fibrinogen leakage were observed.[162] Finally, Johnson *et al.* demonstrated that adoptive transfer of perforin-competent $CD8^+$ T cells into KO mice restores susceptibility to PIFS, as evidenced by disruption of claudin-5 and occludin, barrier dysfunction, and astrogliosis.[164]

Summary

Across the five studies with the PIFS model, only bicellular tight junction proteins (claudin-5 and occludin) have been characterized.

The PIFS model is unique amongst animal models as it yields a fulminant disease course that is marked by microhemorrhaging. However, patients with MS[165] or NMOSD[166] generally do not exhibit cerebral microbleeding. Thus, the findings of the PIFS model are likely most relevant for patients with AHLE, for which no literature exists with respect to blood-brain barrier dysfunction (past the obvious occurrence of microbleeds) or tight junctions. Early PIFS-based studies identified losses of occludin, but not claudin-5 protein, in isolated microvessels.[159] However, this total protein approach failed to identify that alterations were primarily occurring at the level of subcellular localization.[161,162] This underscores the point that the expression level of tight junction proteins alone does not necessarily correlate with barrier function under pathological conditions. Rather, their subcellular localization is as critical, if not more, for maintaining barrier function.

As the PIFS model is $CD8^+$ T cell-mediated, the interventions and genetic manipulations reported may also have translational importance for other $CD8^+$ T cell-mediated CNS diseases like Susac syndrome which is an autoimmune disease directed against the endothelium, with microhemorrhaging driven by release of cytotoxic molecules like Granzyme B and perforin.[167] Regardless, like the other models, the PIFS model

underscores the close connection between local pathology and BBB dysfunction, as well as highlighting that preservation of BBB function as a valid strategy in CNS-IDDs.

Alterations in Cuprizone Models

Background

The cuprizone model is a toxic demyelination model that involves the administration of the toxin at low concentrations in the animal's chow.[168,169] In acute demyelination models, cuprizone is administered for 5-6 weeks, then withdrawn, allowing for re-myelination (Figure 1.25).[168,169] However, continued intoxication past this timeframe permanently impairs re-myelination capability.[168,169] Although the exact mechanisms are poorly understood, it is well-established that cuprizone intoxication results in preferential oligodendrocyte (OL) dysfunction and apoptosis.[168,169] Thus, demyelination in this model likely reflects a primary oligodendropathy with secondary demyelination.[168,169]

Early permeability studies using horseradish peroxidase (HRP) demonstrated luminal restriction, suggesting that the blood-brain barrier was intact.[170,171] However, several recent studies now challenge this assessment. Berghoff *et al.* demonstrated increased extravasation of Evans Blue (EB) and NaFluor after only five days of feeding, with preferential leakage of both observed in the corpus callosum compared to the cortex.[172] In the same study, the authors observed leakage of 70 kDa FITC-Dextran into the corpus callosum following five weeks of feeding,[172] while in two separate studies, they identified leakage of EB in the corpus callosum within the same timeframe.[172,173] In line, Shelestak *et al.* observed increased EB permeability after three, seven, or fourteen days of feeding.[174] Taken together, it is clear that barrier dysfunction is not only present in the cuprizone model but that it occurs before demyelination and persists during demyelination.

Alterations in Cuprizone-based Models

Berghoff *et al.* reported the disruption and loss of occludin in corpus callosum vessels following five weeks of administration.[172] Demyelination, astrogliosis, and activated microglia were prominent, with few mature OLs left. Furthermore, leakage of 70 kDa FITC-dextran was present, while tight junction disruption was evident by electron microscopy.[172] However, no significant alteration of occludin was observed in cortical vessels.[172] Moreover, pathology in the cortex was mild compared to the corpus callosum.[172] Taken together, the authors concluded that the loss of occludin and barrier dysfunction was due to local pathology rather than any potential toxicity to the endothelium.[172]

Summary

Only a single study with the cuprizone model was identified. In it, only bicellular tight junction proteins (occludin) were characterized.

As with the preceding models, the severity of barrier dysfunction and bicellular tight junction disruption was closely associated with the severity of local pathology. These findings are supported by reported decreases in claudin-5 and occludin gene expression and total protein expression in corpus callosum homogenates (Appendix F). However, it must be kept in mind that such experimental approaches prevent direct attribution of the changes to the BBB-ECs. Nevertheless, this underscores that global assessments of barrier function or tight junction expression may fail to identify pathological changes when they occur in a spatiotemporal-dependent manner.

Discussion

Following the completion of my systematic literature search, I have identified and summarized the known alterations of the claudin, TAMP, and angulin families at the endothelial blood-CNS barriers in patients with CNS-IDDs and their models (Figures 1.9-11, 1.13-14, 1.16-26, Appendices C-F). For completeness, I have also summarized relevant studies whose analyses were non-CNS-EC-specific (Appendices C-F).

Eight MS studies covered most clinical forms (RR-MS, SP-MS, and PP-MS), plus one rare variant (Acute MS). Across these studies, only claudin-5, claudin-11, and occludin have been characterized (Figures 1.9 & 1.10). Additionally, one study for NMOSD characterizing claudin-3, claudin-5, and occludin was identified (Figure 1.13), but no studies were found for ADEM (Figure 1.26).

In support, eight studies that incubated human BBB-ECs with the sera or IgG from patients with MS or NMOSD were identified (Figures 1.11 & 1.14), but none were found for ADEM (Figure 1.26). Across these studies, only claudin-5 and occludin were analyzed. As for animal models, EAE was the predominant model, with forty-six studies identified (Figures 1.14-1.22). In contrast, five TMEV studies (Figure 1.23) and a single study each for experimental NMOSD or cuprizone were found (Figures 1.24 & 1.25). Across all four models, claudins 1, 3, 5, 11, and 12, occludin, and LSR have been characterized.

Barrier Dysfunction & Tight Junction Disruption Are Early Events

Overall, the literature points to a close connection between the severity of local pathology and barrier dysfunction or tight junction disruption, both of which occur early in CNS-IDD lesion progression.

In NMOSD, lesions rapidly evolve from a state of active astrocyte lysis, prominent pathology, and barrier dysfunction to a state of completed astrocyte depletion, diminished pathology, and restoration of barrier integrity, followed by slow astrocyte repopulation and oligodendrocyte regeneration.[20,104] In parallel, the proportion of claudin-5^+ vessels from lesions with already completed astrocyte depletion were comparable to control donors, while the reactivity of claudin-3 and occludin in vessels from a single lesion with partial astrocyte repopulation was comparable to control donors.[20] Unfortunately, lesions with active astrocyte lysis have yet to be studied. While intracortical injection of recombinant AQP4-IgG and complement into Lewis rats resulted in the preferential loss of occludin during active astrocyte loss,[20] analysis of patient lesions is needed for confirmation.

In MS, barrier dysfunction is detected in pre-active lesions with activated microglia and macrophages, astrogliosis, and sparse lymphocyte infiltrates,[9] but not activated microglial clusters alone.[82] In parallel, focal disruption of claudin-5 or occludin is observed in pre-lesional vessels near activated microglia and macrophages, astrogliosis, and lymphocytic infiltrates,[9,83] but not activated microglial clusters alone.[82] Similarly, barrier dysfunction and fragmented occludin in the TCR-1640 model is noted following macrophage activation and astrogliosis, but before strong lymphocyte infiltration.[9]

An Incomplete Landscape

Bicellular Junctions. As mentioned in the introduction, claudin family representation is not yet settled. Given that the claudin family forms the backbone of bicellular tight junctions and confers the barrier- and pore-forming properties to the BBB endothelium, solving which members are present under homeostatic or pathological conditions is an important hurdle that must be overcome. Without this information,

researchers considering the claudins as therapeutic targets to modulate barrier function may inadvertently trigger disruptive claudin-claudin interactions. For example, the findings by Pfeiffer *et al.* would suggest that promoting claudin-1 expression in patients with CNS-IDDs could limit barrier dysfunction.[45] However, the more recent findings by Sladojevic *et al.* strongly argue against this approach since claudin-1 overexpression disrupts the constitutive *cis*- and *trans*-interactions of claudin-5.[46]

Tricellular Junctions. The molecular composition and ultra-structure of tricellular junctions are less defined than for bicellular tight junctions.[31] No patient studies have considered their alterations, nor their relative contribution to barrier dysfunction (Figure 1.26). However, one study that used the MOG_{35-55} model reported that LSR was lost at 4 days post-onset in areas of inflammation.[64] While this provides evidence for tricellular tight junction disruption in CNS-IDDs, it remains unknown whether their alterations parallel those of the bicellular tight junctions or follow a different course.

Future Considerations

As mentioned in the rationale, tight junction proteins are commonly used as surrogate markers for barrier integrity and could be therapeutically targeted to rescue barrier dysfunction in patients. However, researchers must keep in mind two recently developed concepts in the field when assessing the tight junctions.

First, barrier dysfunction does not require complete tight junction dismantlement. Rather, changes to the stability and density of the proteins at the cell-cell contacts can be sufficient. In primary human BBB-ECs, barrier function improved in tandem with increased stability of claudin-5 and occludin in membrane fractions following administration of lithium chloride,[175] but worsened with loss of occludin in lipid raft

fractions after exposure to lipid raft-disrupting drugs.[85] In EAE, transgenic eGFP-claudin-5 mice exhibit rapid turnover of the fusion protein in spinal cord venules,[137] while wild-type mice exhibit diminished claudin-5 density in thoraco-lumbar spinal cord venules[109,110] or isolated brain microvessels.[34] In patients with MS, occludin^{+} strands are thinned[85] or focally disrupted.[83] Thus, researchers must be careful to not assume that the tight junctions and barrier function are preserved without considering the possibility of altered stability or density in a disease state or following administration of pharmacologic agents.

Second, endothelial heterogeneity exists along the arteriovenous axis, by CNS region, and by matter type.[176] Analysis frequently is performed on thin tissue sections and from a cross-sectional profile, limiting the conclusions that can be made. Using 3D contour-based quantification, Paul *et al.* measured claudin-5 density at the tight junctions of mouse spinal cord capillaries and venules in 60 µm-thick sections.[110] Density was inversely related to vessel diameter in healthy animals, while a selective loss of density occurred in post-capillary venules of EAE-induced animals, with contiguous capillaries often unaffected.[110] Thus, where possible, researchers should sample thicker tissue sections and employ image reconstruction techniques or longitudinal profiling of vessels, plus report the anatomical locations, vessel types, and matter types analyzed.

Limitations

During the early stages of planning, I observed on multiple occasions that the title or abstract of relevant studies did not always specify which tight junction proteins were analyzed. Consequently, relevant studies were not being identified by the WoS platform. To address this, I 1) performed additional searches for studies that generically referenced the tight junctions, 2) screened all results, even those that initially appeared not relevant,

and 3) examined conference abstracts and reviews, then followed up with the corresponding authors. As this identified thirteen additional results not found by WoS, four of which were included in the qualitative synthesis, I believe my methodology ensured that the as many relevant studies as possible were found.

Nevertheless, I apologize in advance to any authors whose works I missed – your exclusion does not reflect on the quality of your science, but rather the current limitations faced when conducting literature searches.

Chapter One Figures

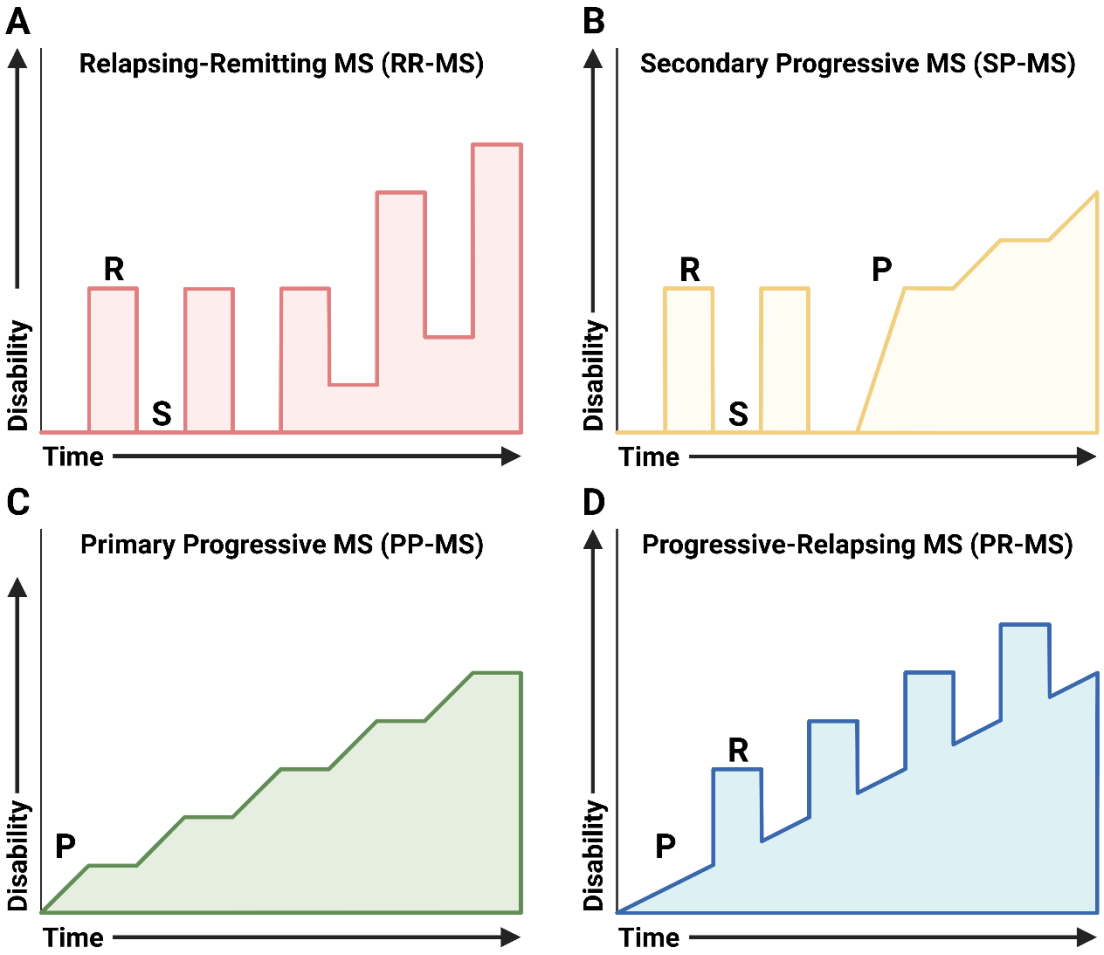

Figure 1.1. Disease Courses of MS.

Disease in patients with MS follows one of four courses based on clinical form. **A**. Patients with RR-MS experience episodes of relapse (**R**) that are separated with periods of stable remission (**S**). **B**. Patients with SP-MS are RR-MS patients who have transitioned to a progressive (**P**) disease course. **C**. Patients with PP-MS suffer progressive disability from onset. **D**. Patients with PR-MS follow a similar course to PP-MS, but also experience episodes of relapse. Created with BioRender.com.

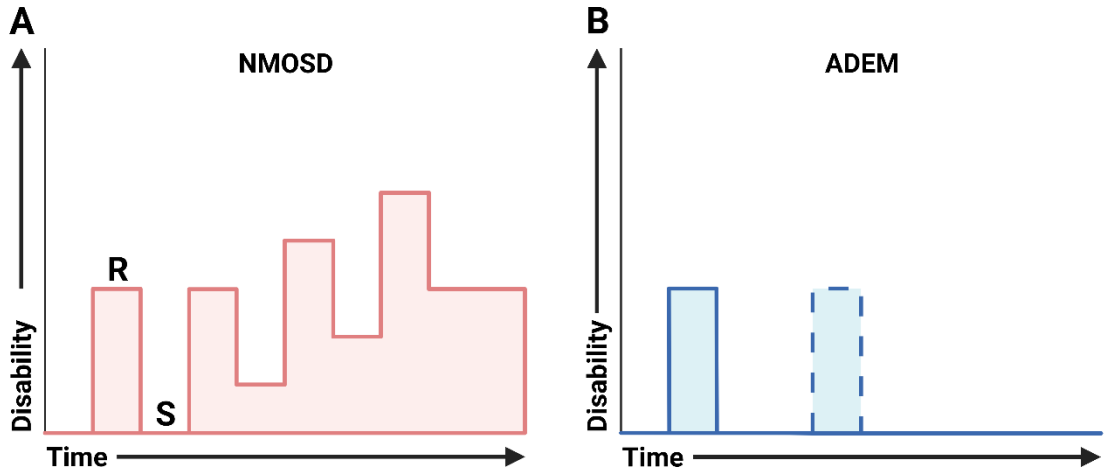

Figure 1.2. Disease Courses of NMOSD & ADEM.

A. Patients with NMOSD generally follow a course similar to RR-MS, with episodes of relapse (**R**) that are separated with periods of stable remission (**S**). **B.** Most patients with ADEM will only ever experience a single episode (*solid line*). In rare cases, additional episodes may occur (*dotted line*). Created with BioRender.com.

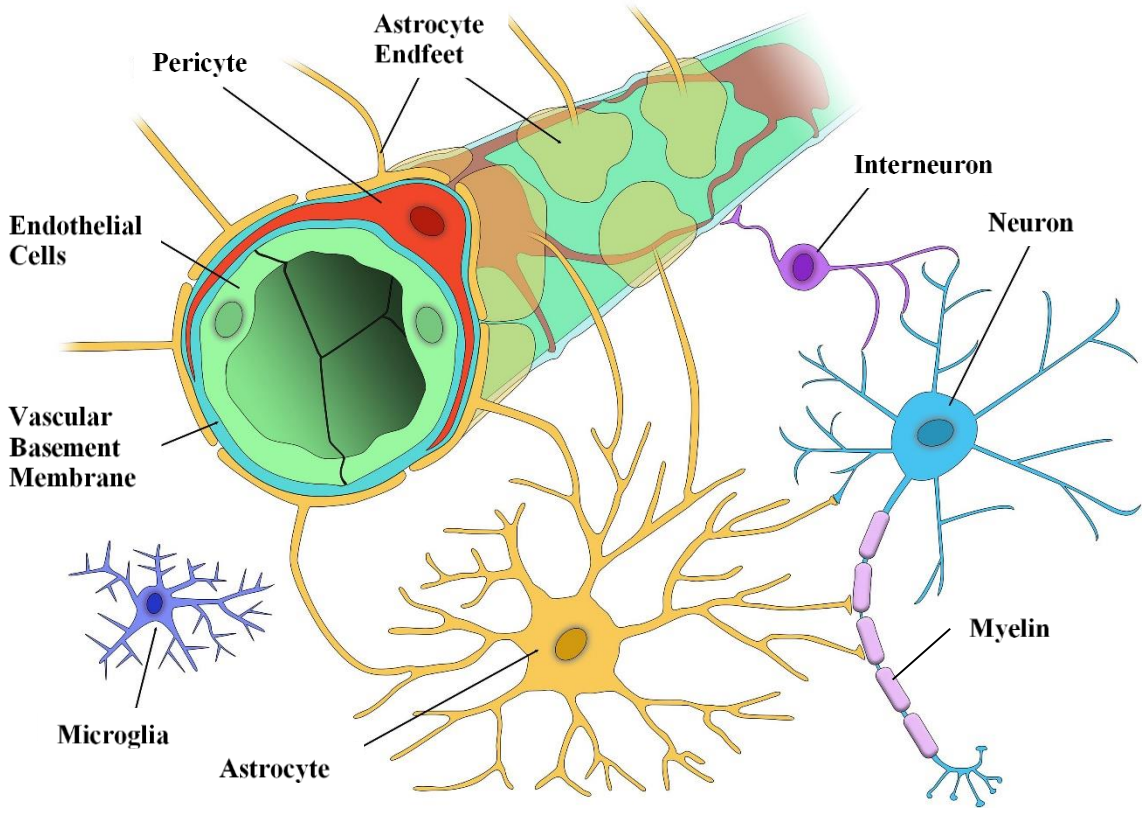

Figure 1.3. The BBB in Relationship to the NVU.

Endothelial cells (*green*) line the interior of the microvessels that serve the other NVU members. At the level of the capillary and post-capillary venule, the endothelium is immediately surrounded by pericytes (*red*) which are situated within a vascular basement membrane (*cyan*). In turn, they are enveloped by the endfoot processes of astrocytes (*yellow*) that acts as intermediaries between neurons (*light blue*) and the microvessels to couple blood flow with neuronal activity. Additionally, astrocytes interact with oligodendrocytes (*not shown*) to maintain the myelin sheath (*pink*), while interneurons (*purple*) innervate the microvessel as another mechanism to regulate blood flow. Finally, microglia (*dark blue*) are the primary resident innate immune cells within the CNS. Figure minimally adapted from Brown *et al.*[177] in Frontiers in Cellular Neuroscience (2019, Vol. 30) under a Creative Commons License (CC-BY).

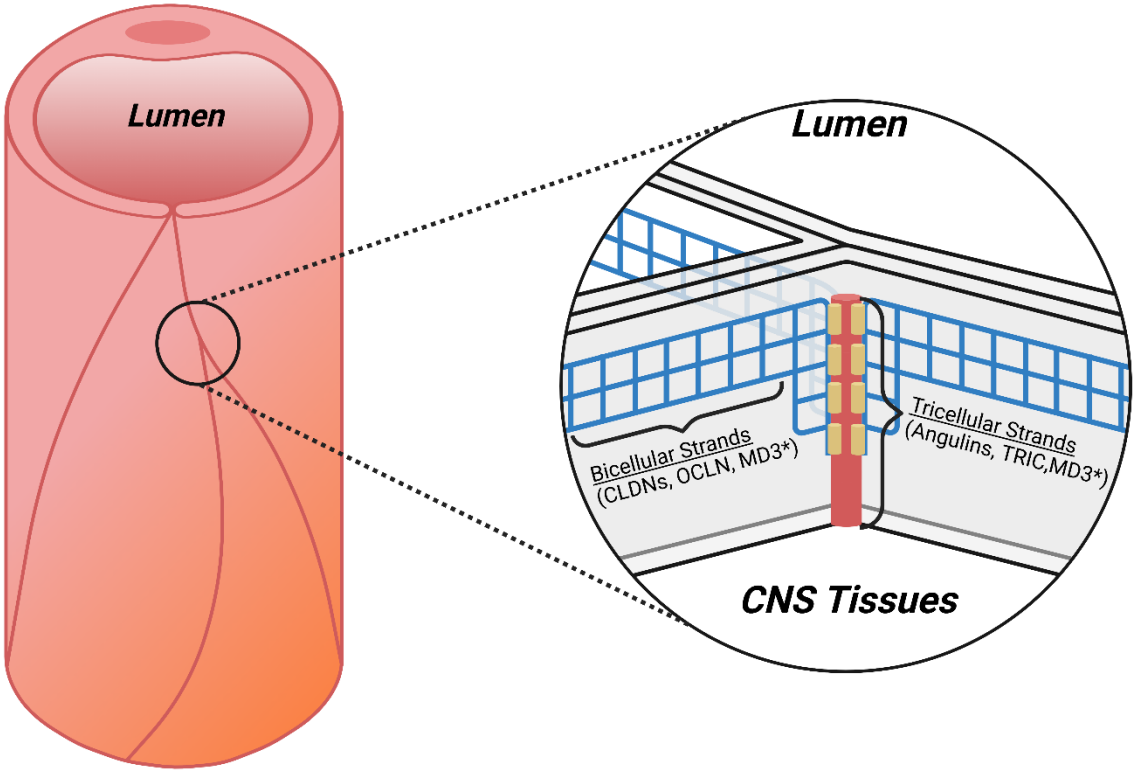

Figure 1.4. Bicellular and Tricellular Junction Ultrastructure & Composition.

Bicellular tight junctions (*blue*) are established between two neighboring endothelial cells. When viewed by freeze-fraction electron microscopy, a continuous, anastomosing network is observed. These tight junctions are composed of a claudin-based backbone that is regulated by members of the TAMP family. Tricellular tight junctions (*red*, *yellow*) are established at the meeting point of three adjacent endothelial cells. The angulin family forms the central sealing element (*red*) which connects to the bicellular strands via members of the TAMP family (*yellow*). Created with BioRender.com.

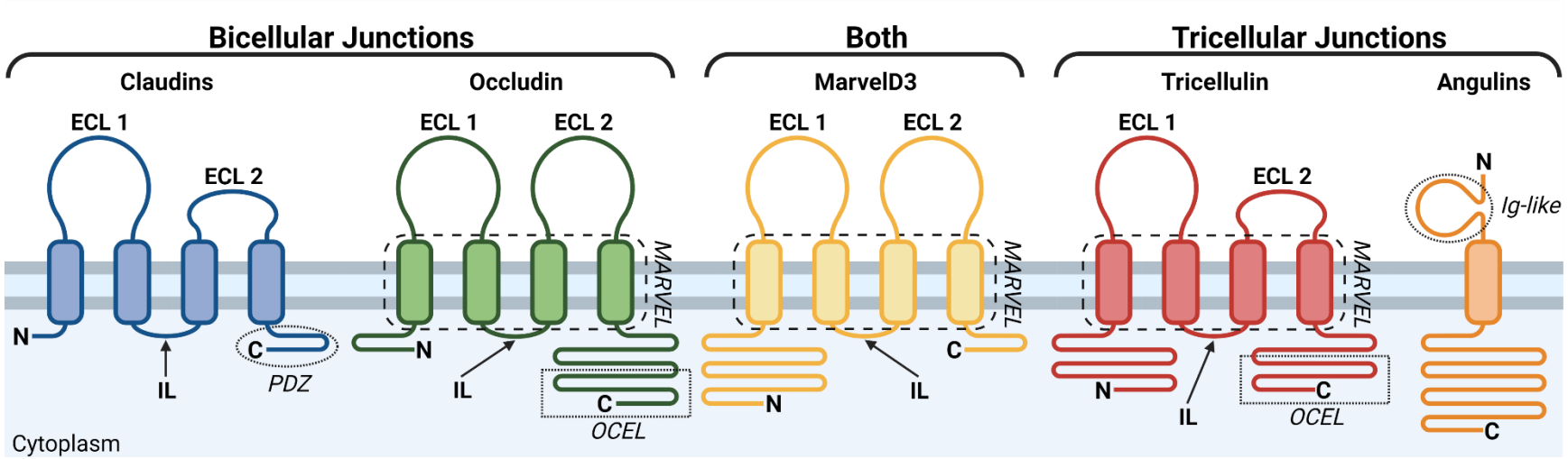

Figure 1.5. Protein Structure of the Claudin, TAMP, and Angulin Families.

Claudins (*blue*) are enriched at bicellular junctions. They have a short N-terminal tail (**N**), two extracellular loops (**ECLs**), a short intracellular loop (**IL**), and a C-terminal tail (**C**). Most possess a binding motif (**PDZ**) for coupling to scaffolding proteins. TAMPs – occludin (*green*), tricellulin (*red*), and MarvelD3 (*yellow*) – are enriched at bicellular, tricellular, or both types of junctions, respectively. Although all contain a similar transmembrane-helix architecture (**MARVEL** domain), they differ in size of their tails. Moreover, only occludin and tricellulin share a regulatory occludin/ELL domain (**OCEL**). Angulins are enriched at tricellular junctions, but information about their structure is limited. Thus far, it has been reported that their extracellular tail contains an immunoglobulin-like (**Ig-like**) domain. Created with BioRender.com.

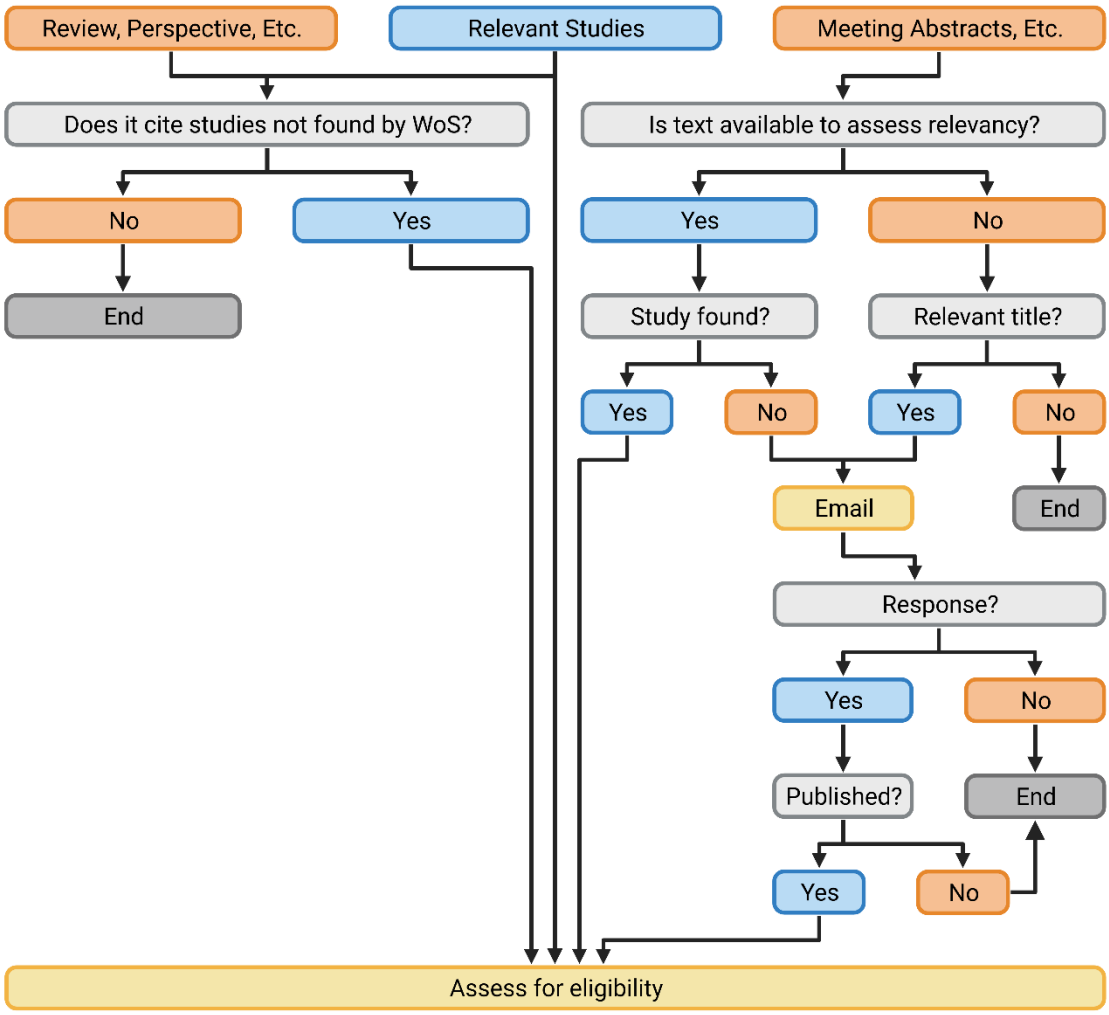

Figure 1.6. Flow Diagram Depicting the Initial Screening Process.

To identify relevant studies not found by database searches through the WoS platform, non-primary articles like reviews and meeting abstracts were also screened. Created with BioRender.com.

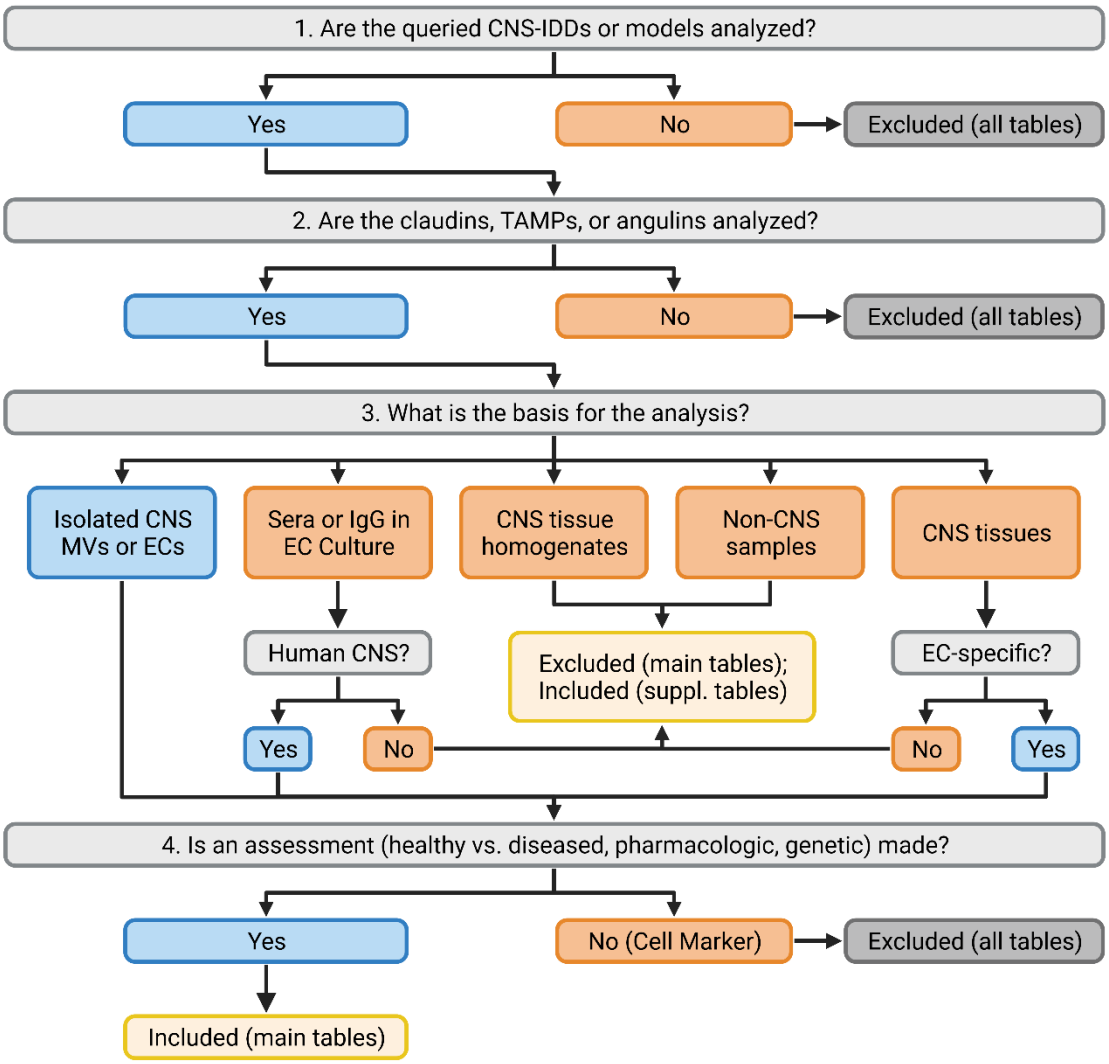

Figure 1.7. Flow Diagram Depicting the Inclusion Process.

To identify relevant studies, results were assessed for eligibility on four specific points. Studies that passed all four points were included for qualitative synthesis. For completeness, however, studies that passed all points except the third are summarized in Appendices C-F. Created with BioRender.com.

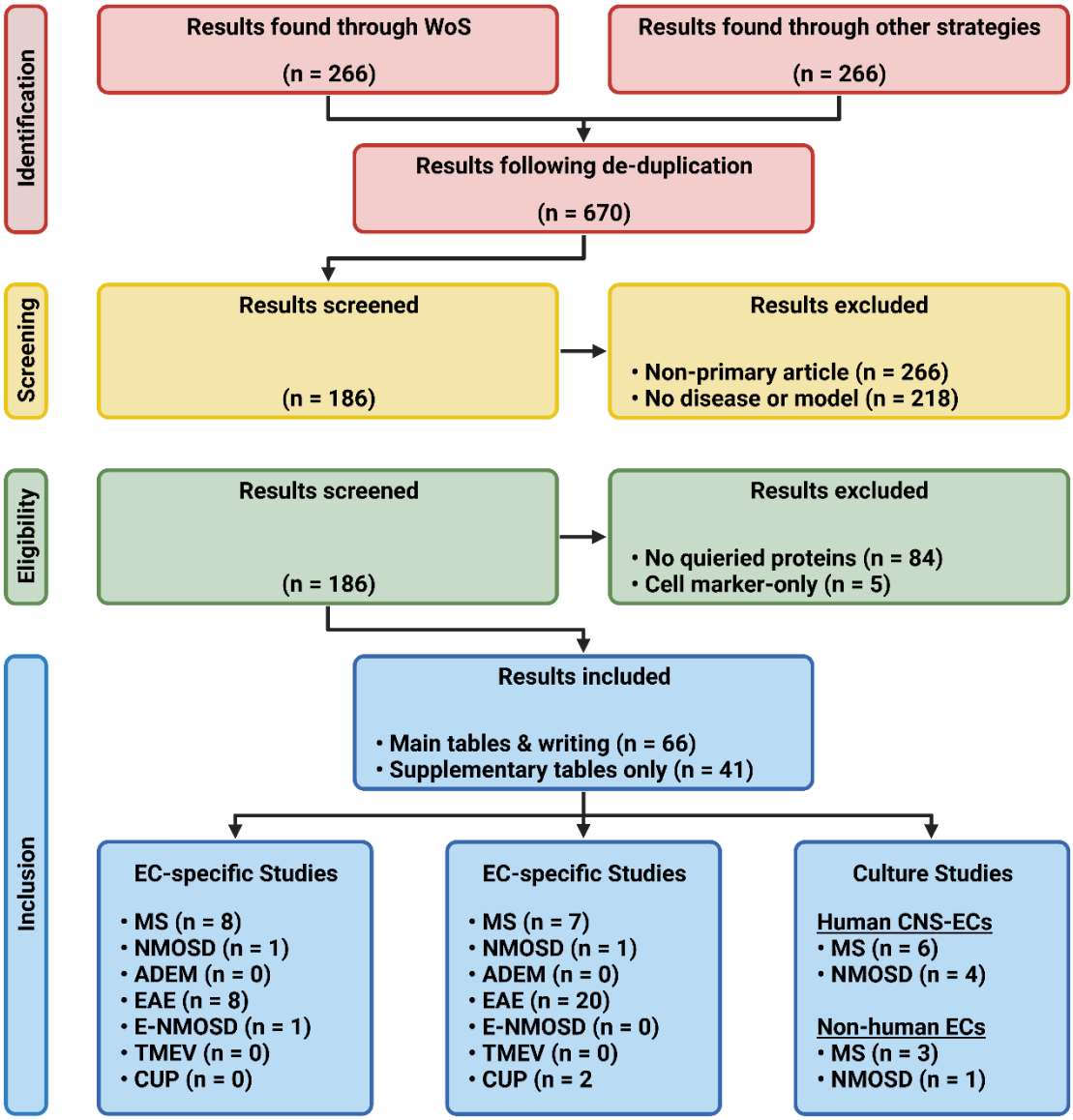

Figure 1.8. PRISMA Flow Diagram.

A graphic summary for the number of studies that were ultimately included or excluded for the claudin, TAMP, and angulin families in three CNS-IDDs (MS, NMOSD, and ADEM) and four animal models (EAE, E-NMOSD, TMEV, and cuprizone). **Note:** no studies involving ADEM were found. Additionally, studies often included more than one disease or model. This means that the total number of studies included (n = 98) does not equal the sum of the studies listed across all tables (n = 107). Created with BioRender.com.

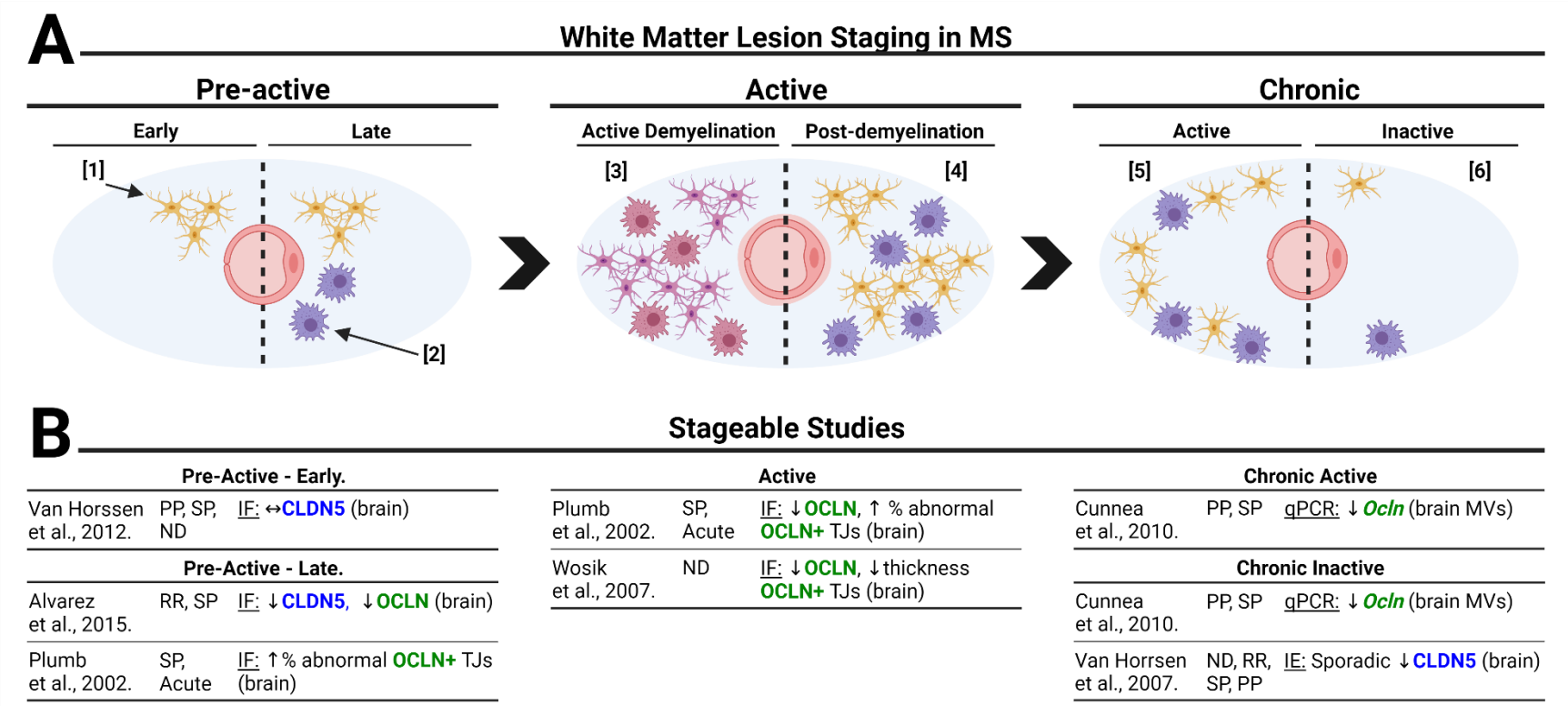

Figure 1.9. Alterations in Stageable MS White Matter Lesions.

A. At their earliest stages, lesions contain activated microglial clusters **[1]**. As the lesion evolves, macrophages are recruited **[2]**. During active demyelination, microglia and macrophages are laden with myelin debris **[3]** and remain following cessation of demyelination **[4]**. With time, microglia and macrophages are lost, radiating outwards from the center **[5-6]**. **B.** Summary of studies whose findings could be staged within the framework presented in **A.** of this figure. ND: Clinical form not available. IF: Immunofluorescence-based immunohistochemistry (IHC). qPCR: Quantitative polymerase chain reaction. IE: Immunoenzyme-based IHC. Created with BioRender.com.

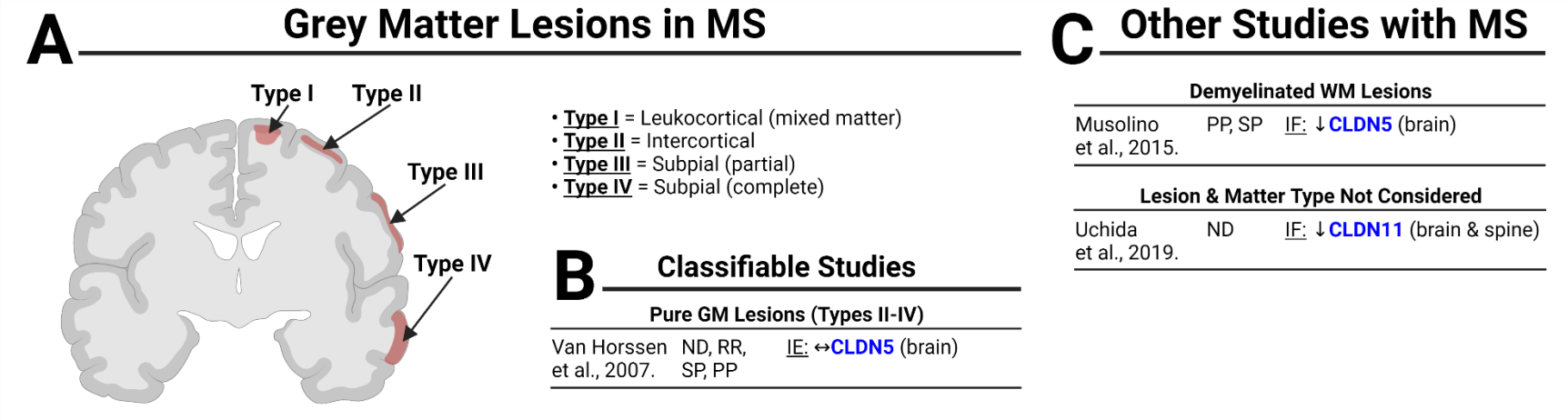

Figure 1.10. Alterations in Stageable MS Grey Matter Lesions or Non-stageable MS Lesions.

A. Grey matter lesions are classified based on their location within the cortical tissues (Types I-IV). Only type I lesions involve the adjacent white matter; all others (II-IV) are purely within the grey matter. **B.** Summary of studies whose findings could be staged within the frameworks presented in **A.** of this figure. ND: Clinical form not available. IE: Immunoenzyme-based immunohistochemistry (IHC). **C.** Summary of studies whose findings could not be staged within the frameworks presented in **A.** of this or the preceding figure. ND: Clinical form not available. IF: Immunofluorescent-based IHC. Created with BioRender.com.

A

Patient Serum & Immortalized Human BBB-ECs			
Shimizu et al., 2012.	MS	Barrier: ↔TEER	WB: ↔**CLDN5**, ↔**OCLN**
Tasaki et al., 2014.	MS	Barrier: ↔TEER	WB: ↔**CLDN5**
Shimizu et al., 2014.	RR-R RR-S SP	Barrier: ↓TEER Barrier: ↔TEER Barrier: ↓TEER	↓**CLDN5**, ↔**OCLN** WB: ↔**CLDN5**, ↔**OCLN** ↓**CLDN5**, ↓**OCLN**
Sheikh et al., 2020.	RR	Barrier: ↓TEER, ↑ 70 kDa Dex	FC: ↓**OCLN**

B

Patient IgG & Immortalized Human BBB-ECs			
Shimizu et al., 2014.	RR-R RR-S SP	↔TEER Barrier: ↔TEER ↓TEER	↔**CLDN5**, ↔**OCLN** WB: ↔**CLDN5**, ↔**OCLN** ↓**CLDN5**, ↔**OCLN**

C

Pharmacologic Interventions with Patient Serum & Immortalized Human BBB-ECs				
MMP Inhibition (GM6001)	Tasaki et al., 2014	MS	Barrier: ↔TEER, ↔NaFl	WB: ↔**CLDN5**
	Shimizu et al., 2014	RR-R	Barrier: ↑TEER	WB: ↑**CLDN5**, ↔**OCLN**
		SP		WB: ↔**CLDN5**, ↔**OCLN**
Neutralizing Abs (TNF-α, IFN-γ, IL-17, VEGF)	Shimizu et al., 2014	RR-R	Barrier: ↑TEER (α-VEGF)	WB: ↑**CLDN5**, ↔**OCLN** (α-VEGF) WB: ↔**CLDN5**, ↔**OCLN** (Others)
		SP		WB: ↔**CLDN5**, ↔**OCLN** (All)
VDR Agonism (Vitamin D_3)	Takahashi et al., 2017	RR-R RR-S SP		WB: ↑**CLDN5** WB: ↔**CLDN5** WB: ↔**CLDN5**
S1PR Agonism (FTY720P)	Nishihara et al., 2015	RR-R RR-S SP	↑TEER Barrier: ↔TEER ↑TEER	WB: ↑**CLDN5**, ↔**OCLN** WB: ↑**CLDN5**, ↔**OCLN** WB: ↑**CLDN5**, ↔**OCLN**
		All		qPCR: ↑***Cldn5***

Figure 1.11. Alterations in Human-derived CNS-EC Culture Models of MS.

A. Summary of studies involving patient sera. MS: Patients fulfilled the 2010 revised McDonald diagnostic criteria but lacked a clinical form. RR-R: Patients with RR-MS during a relapse. RR-S: Patients with RR-MS during a stable phase. TEER: Transendothelial electrical resistance. Dex: Dextran. WB: Western blot. FC: Flow cytometry. **B.** Summary of studies involving patient IgG. **C.** Summary of studies involving pharmacologic interventions and patient sera. MMP: Matrix metalloproteinase. Ab: Antibody. TNF-α: Tumor necrosis factor alpha. IFN-γ: Interferon gamma. IL-17: Interleukin-17. VEGF: Vascular endothelial growth factor. VDR: Vitamin D receptor. S1PR: Sphingosine 1-phosphate receptor. All: All three patient groups were treated as a single disease group for comparison. Created with BioRender.com

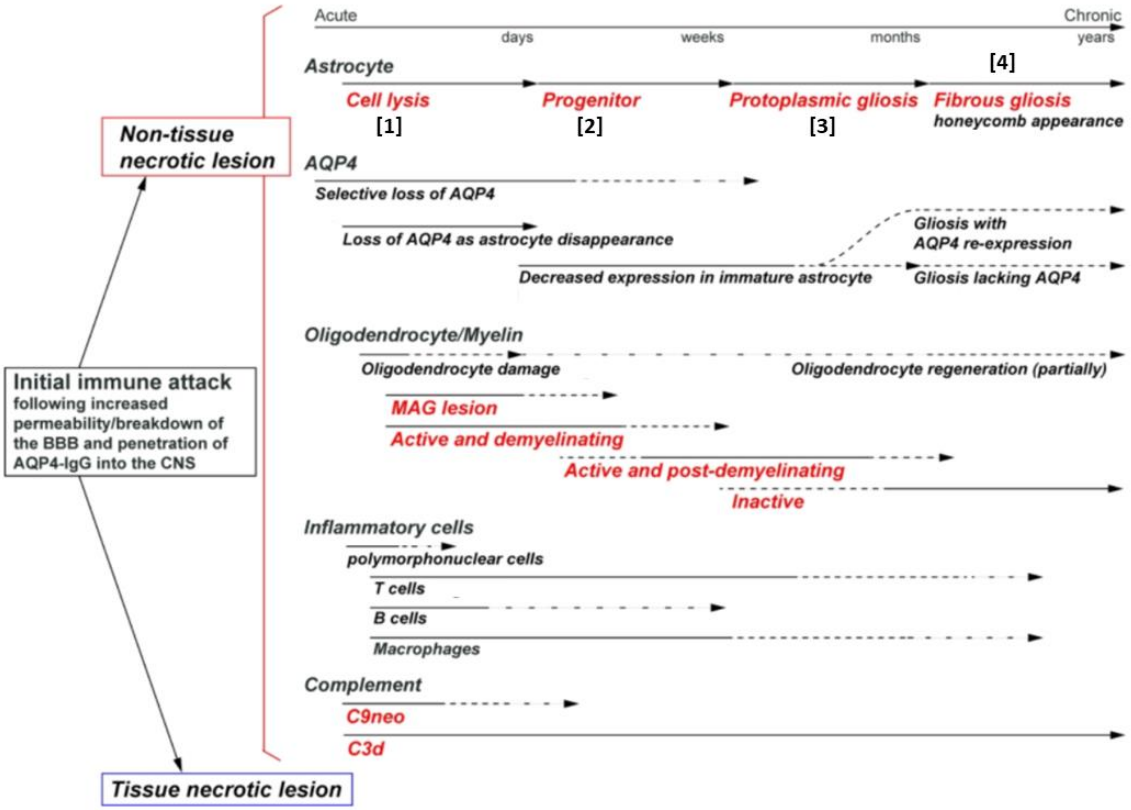

Figure 1.12. Temporal Staging of NMOSD Lesions according to Takai.

Based on histopathological analysis of autopsy tissues from eight patients who were seropositive for AQP4-IgG, Takai et al. developed a temporal staging system for NMOSD lesions centered around astrocyte morphology. Following initial complement-mediated astrocyte lysis [1], astrocyte progenitor cells are recruited to replace the lost cells [2]. However, these new astrocytes eventually turn gliotic [3], and form scars that exhibit a distinctive honeycomb-like appearance [4]. Figure minimally adapted from "Staging of Astrocytopathy and Complement Activation in Neuromyelitis Optica Spectrum Disorders" by Takai et al.104 in Brain (2021, Vol. 144, Issue 8) with permission from Oxford University Press.

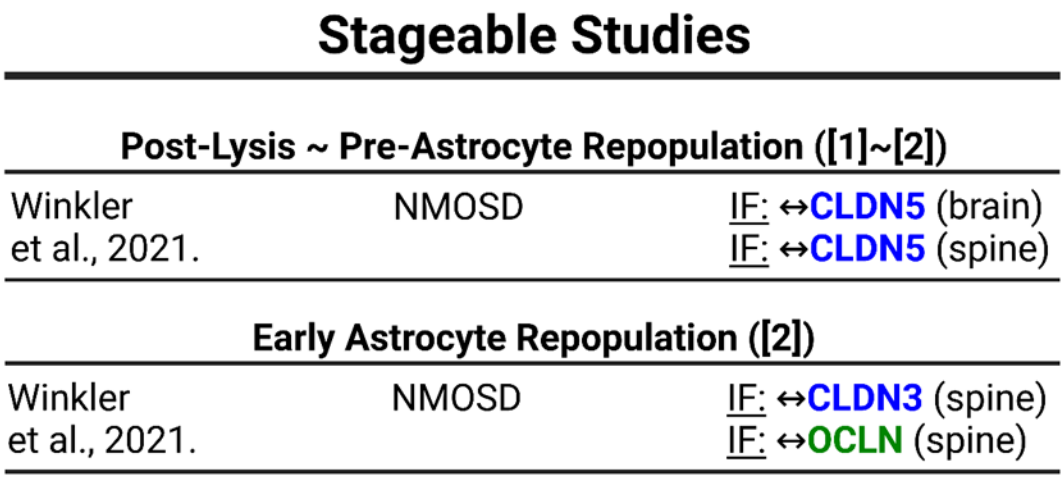

Figure 1.13. Alterations in NMOSD Lesions.

Summary of studies whose findings could be staged within the framework presented in **Figure 1.12.** **Note:** The estimated staging for the two lesion types described in Winkler *et al.* is provided in parentheses based on the histopathological description of the astrocyte presence and morphology. IF: Immunofluorescence-based immunohistochemistry. Created with BioRender.com.

A Patient Serum & Immortalized Human BBB-ECs

Shimizu et al., 2012.	NMO-A	Barrier: ↓TEER	WB: ↓**CLDN5**, ↔**OCLN**
Tasaki et al., 2014.	NMOSD-A	Barrier: ↓TEER, ↑ NaFl	WB: ↓**CLDN5**
	NMOSD-S	Barrier: ↔TEER, ↔ NaFl	WB: ↔**CLDN5**

B Patient IgG/rAb & Immortalized Human BBB-ECs (Mono-culture)

Tasaki et al., 2014.	NMOSD-A (IgG)	Barrier: ↔TEER, ↔ NaFl	WB: ↔**CLDN5**
Shimizu et al., 2017.	NMO-IgG		IF: ↓**CLDN5**
	NMO-rAb	Barrier: ↑10 kDa Dex.	IF: ↓**CLDN5**

C Patient IgG & Immortalized Human BBB-ECs (Co-culture with ACs)

Takeshita et al., 2017.	NMO	Barrier: ↓ 10 kDa Dex. (AQP4- ACs)	IF: ↑**CLDN5** (AQP4- ACs)

D Interventions with Patient Serum & Immortalized Human BBB-ECs

Plasma Exchange	Shimizu et al., 2012	NMO-A	Barrier: ↑TEER	WB: ↑**CLDN5**
Neutralizing Abs (TNF-α, IFN-γ, IL-6, IL-17, VEGF, TGF-β)	Shimizu et al., 2012	NMO-A	Barrier: ↑TEER (α-VEGF)	WB: ↑**CLDN5**, ↔**OCLN** (α-VEGF) qPCR: ↑***Cldn5***, ↔***Ocln*** (α-VEGF)
			Barrier: ↔TEER (α-IL-17)	WB: ↔**CLDN5**, ↔**OCLN** (α-IL-17) qPCR: ↔***Cldn5***, ↑***Ocln*** (α-IL-17)
				qPCR: ↔***Cldn5***, ↔***Ocln*** (others)
Ab Depletion (Pre-incubation of serum with ACs)	Shimizu et al., 2012	NMO-A	Barrier: ↑TEER	WB: ↑**CLDN5**
MMP Inhibition (Multiple, including GM6001)	Tasaki et al., 2012	NMOSD-A	Barrier: ↑TEER, ↑NaFl (all)	WB: ↑**CLDN5** (all)

Figure 1.14. Alterations in Human CNS-EC Culture Models of NMOSD.

A. Summary of studies involving patient sera. NMO-A: Patients with NMO during an acute phase (relapse). NMOSD-A: Patients with NMOSD during an acute phase (relapse). NMOSD-S: Patients with NMOSD during a stable phase. TEER: Transendothelial electrical resistance. NaFl: Sodium fluorescein. WB: Western blot. **B.** Summary of studies involving mono-cultures incubated with patient antibodies. IgG: Immunoglobulin. rAb: Recombinant antibody. Dex: Dextran. IF: Immunofluorescence-based immunohistochemistry. **C.** Summary of studies involving co-cultures incubated with patient IgG. AC: Astrocyte. AQP4: Aquaporin-4. **D.** Summary of studies involving therapeutic interventions with patient sera. TNF-α: Tumor necrosis factor alpha. IFN-γ: Interferon gamma. IL-6: Interleukin-6. IL-17: Interleukin-17. VEGF: Vascular endothelial growth factor. TGF-β: Transforming growth factor beta. MMP: Matrix metalloproteinase. qPCR: Quantitative polymerase chain reaction. Created with BioRender.com.

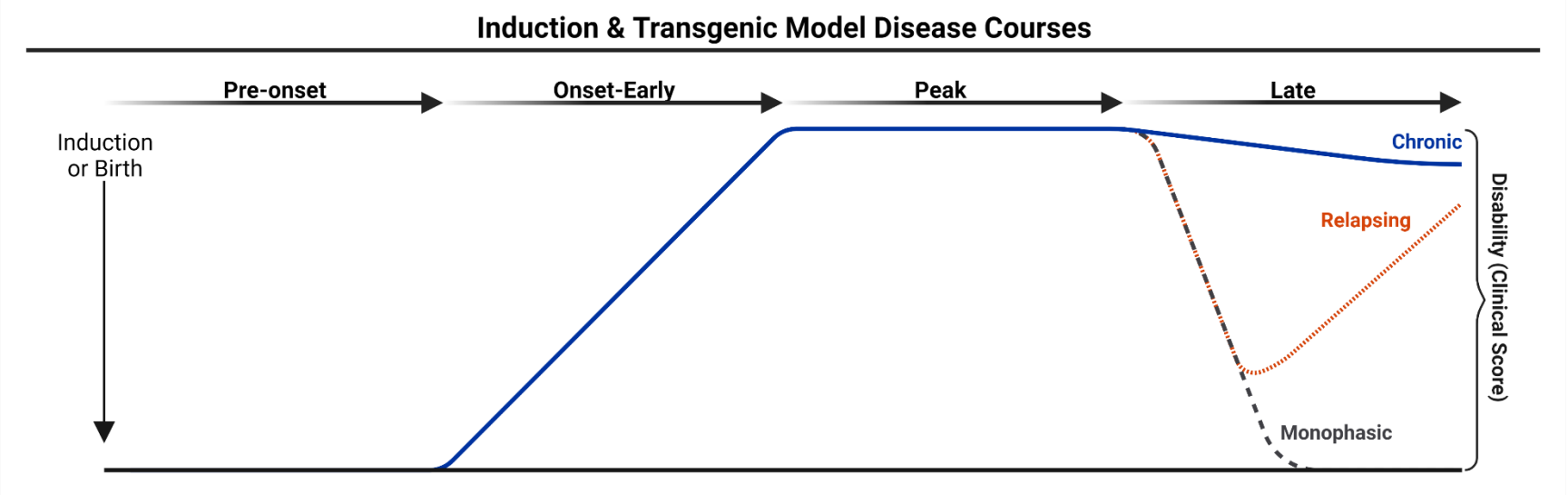

Figure 1.15. Disease Courses in EAE.

Depending on the antigens or transgenic lines used for EAE, one of three disease courses is generally observed. If animals only experience one episode before entering remission, the model is monophasic (*grey* – dashed line). If the animals experience multiple episodes with periods of partial or full remission separating them, the model is relapsing-remitting (*orange* – dotted line). If the animals experience one episode that plateaus and doesn't enter remission, the model is chronic (*blue* – solid line). Created with BioRender.com.

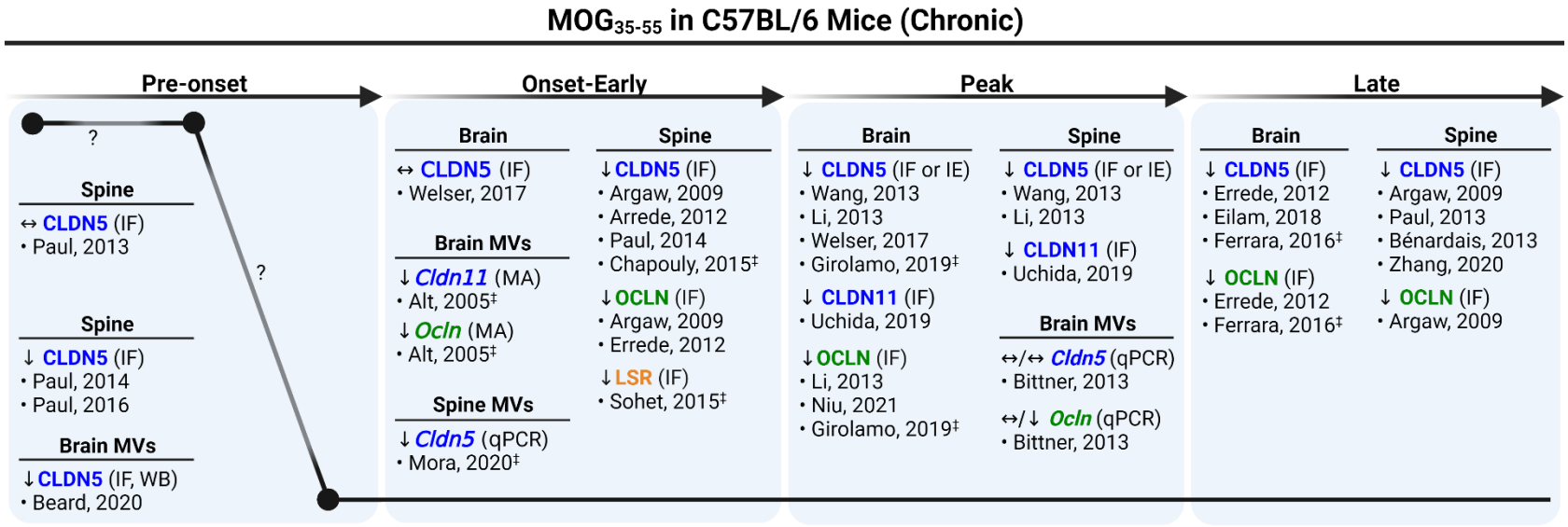

Figure 1.16. Alterations in MOG_{35-55}-based EAE Model (Base Disease).

Summary of studies that employed the MOG_{35-55}-based EAE model (chronic in nature) and whose findings could be classified within the framework presented in **Figure 1.15.** Studies whose staging was estimated is denoted by a double dagger (‡). The super-imposed trend line (*black*) reflects the kinetics of tight junction protein disturbance. Points in the disease course lacking information are denoted by a question mark (?). IF: Immunofluorescence-based immunohistochemistry (IHC). MV: Microvessel. WB: Western blot. MA: Microarray analysis. qPCR: Quantitative polymerase chain reaction. IE: Immunoenzyme-based IHC. Created with BioRender.com.

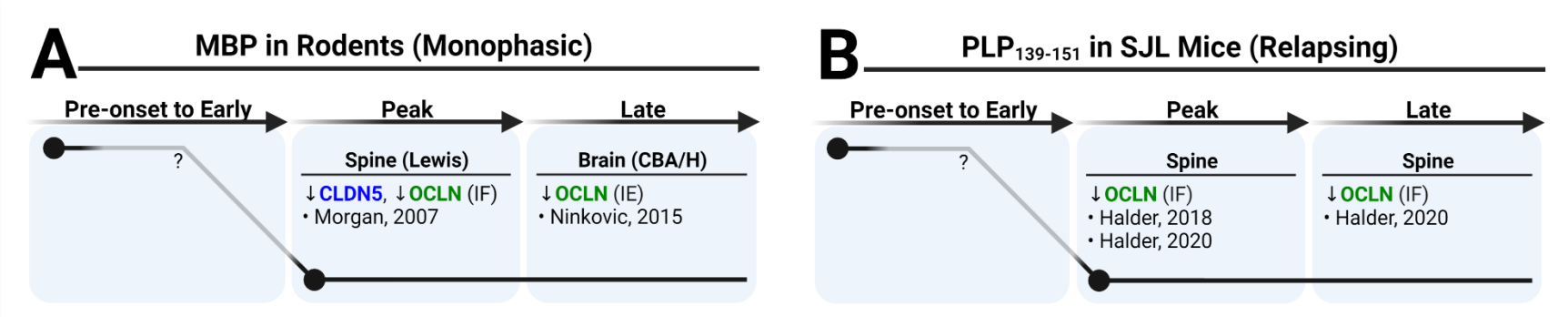

Figure 1.17. Alterations in MBP- & $PLP_{139-151}$-based EAE Models (Base Disease).

A. Summary of studies that employed the MBP-based EAE model (monophasic in nature) and whose findings could be classified within the framework presented in **Figure 1.15.** The super-imposed trend line (*black*) reflects the kinetics of tight junction protein disturbance. Points in the disease course lacking information are denoted by a question mark (?). IF: Immunofluorescence-based immunohistochemistry (IHC). IE: Immunoenzyme-based IHC. **B.** Summary of studies that employed the PLP139-151-based EAE model (relapsing-remitting in nature) and whose findings could be classified within the framework presented in **Figure 1.15.** Created with BioRender.com

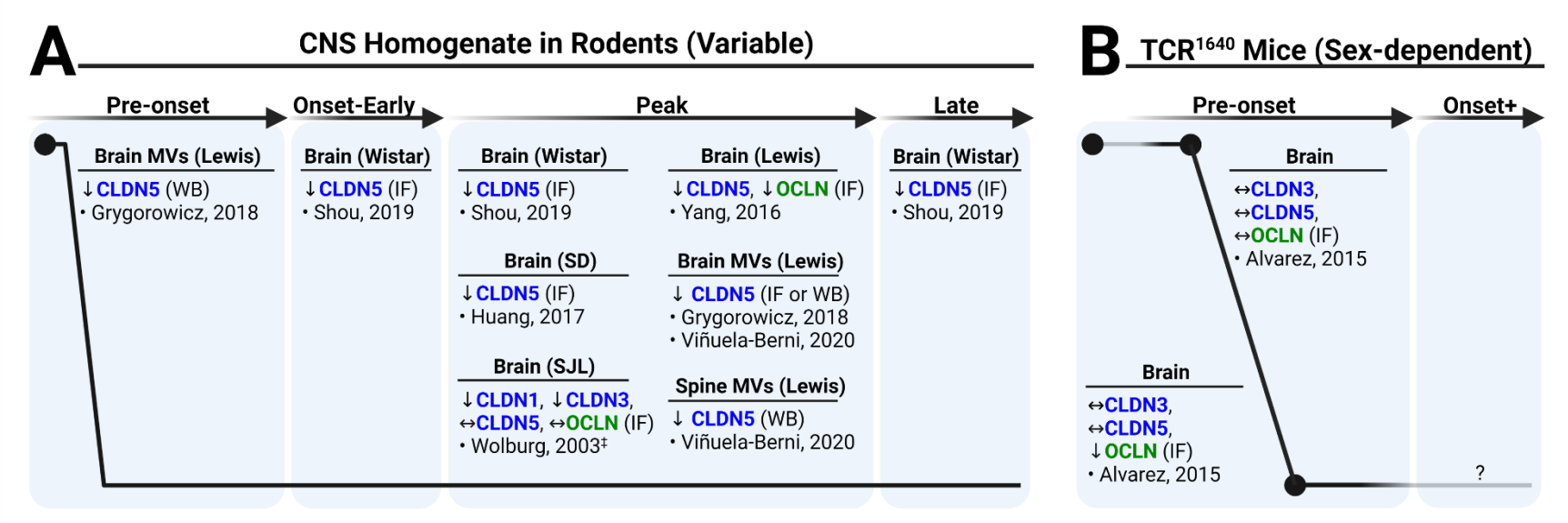

Figure 1.18. Alterations in CNS Homogenate- and Transgenic-based EAE Models (Base Disease).

A. Summary of studies that used syngeneic or guinea pig CNS homogenates (variable disease courses) and whose findings could be classified within the framework presented in **Figure 1.15.** Studies whose staging was estimated is denoted by a double dagger (‡). The super-imposed trend line (*black*) reflects the kinetics of tight junction protein disturbance. WB: Western blot. IF: Immunofluorescence-based immunohistochemistry. MV: Microvessel. **B.** Summary of studies that employed the TCR^{1640}-based EAE model (chronic in males, relapsing-remitting in females) and whose findings could be classified within the framework presented in **Figure 1.15.** Points in the disease course lacking information are denoted by a question mark (?). Created with BioRender.com.

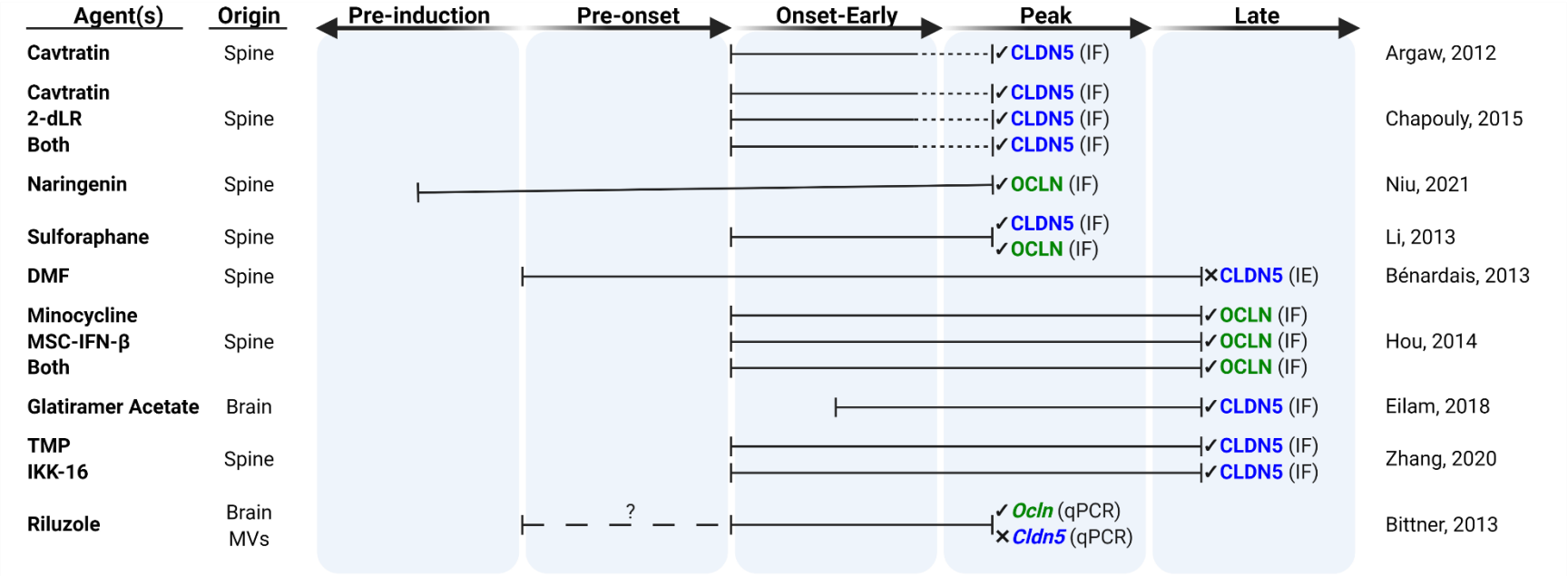

Figure 1.19. Interventions in MOG_{35-55}-based EAE Models.

Summary of studies that assessed intervention strategies using the MOG_{35-55}-based EAE model and whose findings could be classified within the framework presented in **Figure 1.15.** Intervention duration is represented by a black line, with solid portions reflecting continual administration and dotted portions reflecting no administration. Rescues in tight junction proteins are denoted by a check mark (✓) and non-rescues by a cross-mark (✕). Studies with ambiguous language describing the start or end dates of intervention are denoted by a question mark (?). 2-dLR: 2-deoxy-L-ribose. DMF: Dimethyl fumarate. MSC-IFN-β: Interferon beta-secreting mesenchymal stem cells. TMP: Tetramethylpyrazine. MV: Microvessel. IF: Immunofluorescence-based immunohistochemistry (IHC). qPCR: Quantitative polymerase chain reaction. IE: Immunoenzyme-based IHC. Created with BioRender.com.

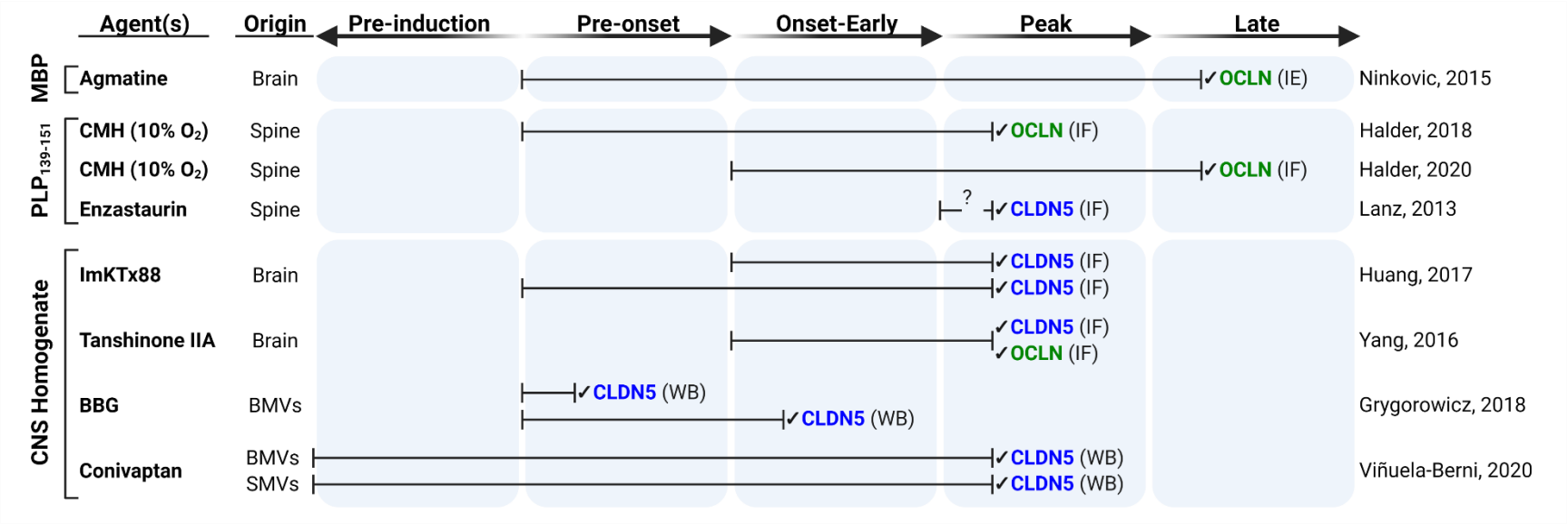

Figure 1.20. Interventions in Other Antigen-based EAE Models.

Summary of studies that assessed intervention strategies using MBP-, $PLP_{139-151}$-, or CNS homogenate-based EAE model and whose findings could be classified within the framework presented in **Figure 1.15.** Intervention duration is represented by a black line. Rescues in tight junction proteins are denoted by a check mark (✓) and non-rescues by a cross-mark (✗). Studies with ambiguous language describing the start or end dates of intervention are denoted by a question mark (?). CMH: Chronic mild hypoxia. BBG: Brilliant Blue G. BMV: Brain microvessel. SMV: Spinal microvessel. IF: Immunofluorescence-based immunohistochemistry (IHC). IE: Immunoenzyme-based IHC. WB: Western blot. Created with BioRender.com.

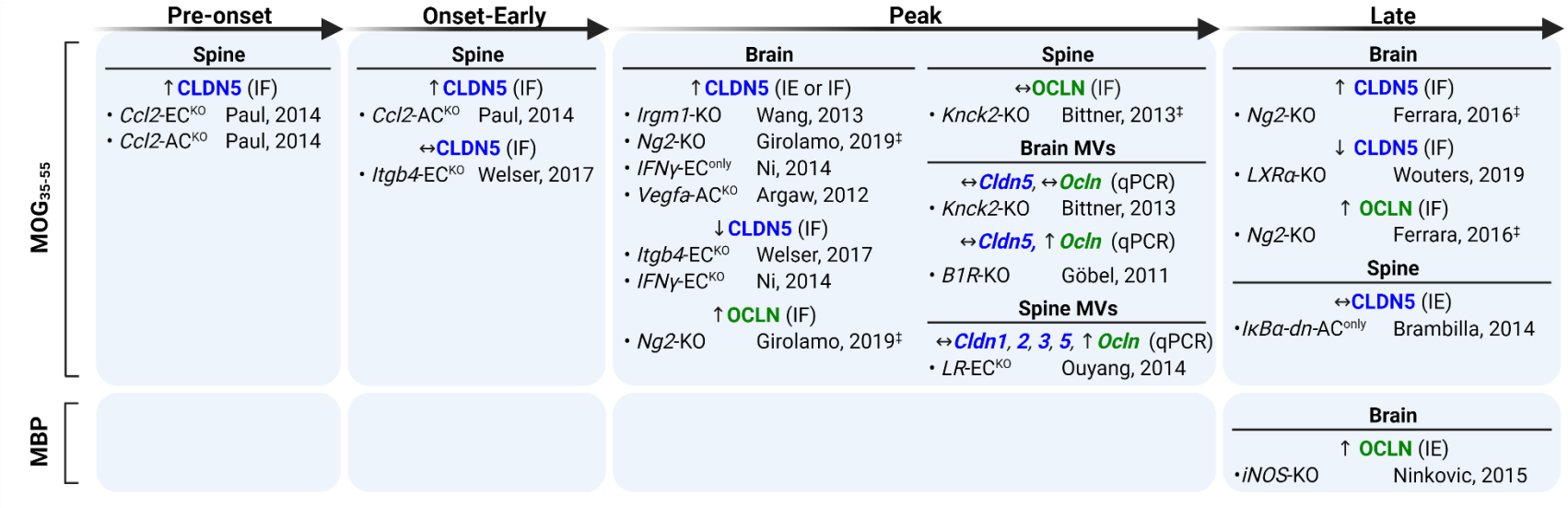

Figure 1.21. Non-Claudin-involved Genetic Manipulations in Antigen-based EAE Models.

Summary of studies that assessed transgenic animals using MOG_{35-55}- or MBP-based EAE models and whose findings could be classified within the framework presented in **Figure 1.15.** Studies whose staging was estimated is denoted by a double dagger (‡). CCL2: Chemokine (C-C motif) ligand 2. EC^{KO}: Endothelial-restricted knockout. AC^{KO}: Astrocyte-restricted knockout. ITGB4: Integrin beta 4. IRGM1: Immunity-related GTPase family M protein 1. KO: Knockout. NG2: Neuron-glial antigen 2. IFN-γ: Interferon gamma. EC^{only}: Endothelial-restricted expression. VEGFA: Vascular endothelial growth factor-A. KNCK2: Potassium channel subfamily K member 2. B1R: Bradykinin B1 receptor. LR: Leptin receptor. LXRα: Liver X receptor alpha. IκBα-dn: Dominant-negative mutant for nuclear factor of kappa light polypeptide gene enhancer in B-cells inhibitor, alpha. AC^{only}: Astrocyte-restricted expression. iNOS: Inducible nitric oxide synthase. MV: Microvessel. IF: Immunofluorescence-based immunohistochemistry (IHC). IE: Immunoenzyme-based IHC. qPCR: Quantitative polymerase chain reaction. Created with BioRender.com.

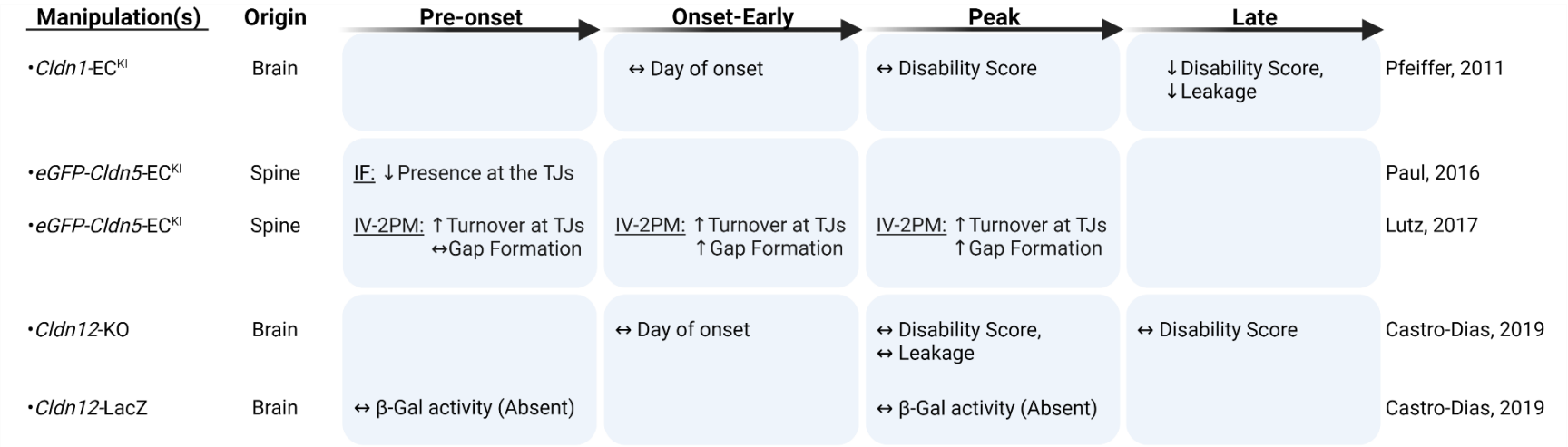

Figure 1.22. Claudin-involved Genetic Manipulations in MOG_{35-55}-based EAE Models.

Summary of studies that assessed transgenic animals using MOG_{35-55}- based EAE models and whose findings could be classified within the framework presented in **Figure 1.15.** EC^{KI}: Endothelial-restricted knockin. eGFP: Enhanced green fluorescent protein. KO: Knockout. LacZ: β-Galactosidase reporter cassette that replaced the encoding exon of claudin-12. IF: Immunofluorescence-based immunohistochemistry. TJ: Tight junction. IV-2PM: Intravital two-photon microscopy. β-Gal: Beta-galactosidase. Created with BioRender.com.

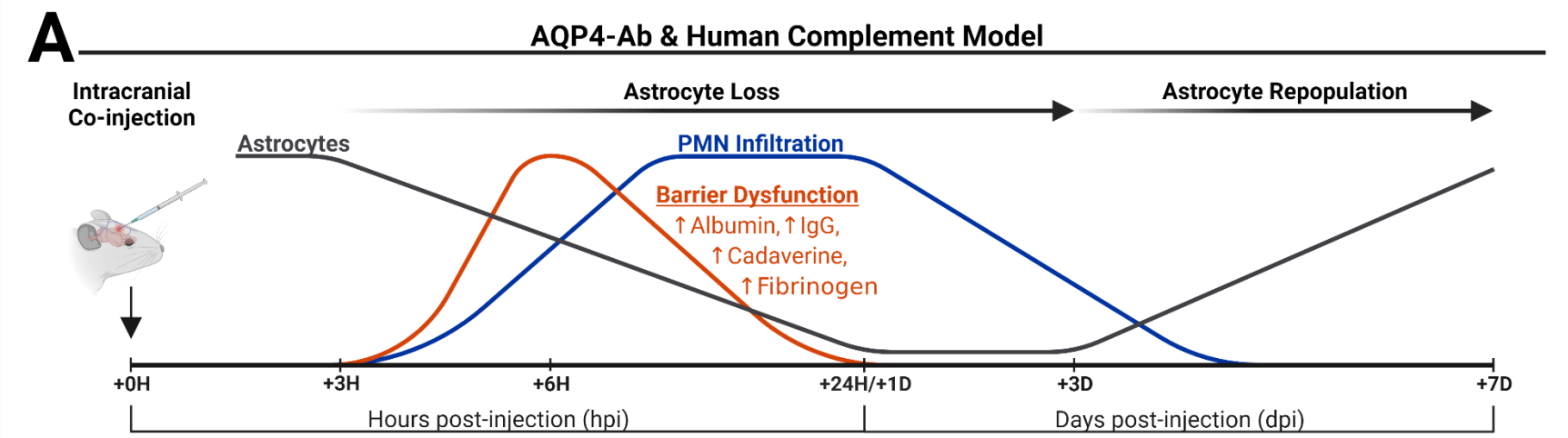

B Classifiable Studies

Wild-type Lewis Rats		
Winkler et al., 2021	6-24 hpi	IF: ↓**OCLN** (brain)
	3-6 dpi	IF: ↑**OCLN** (brain)
	6 hpi - 6 dpi	IF: ↔**CLDN3**, ↔**CLDN5** (brain)

Interventions in Wild-type Lewis Rats			
Winkler et al., 2021	Immune Cell Depletion (α-PMN antiserum -18 & +0 hpi)	6 hpi	IF: ↓**OCLN** (brain)
			IF: ↔**CLDN3**, ↔**CLDN5** (brain)

Figure 1.23. Alterations in E-NMOSD Models.

A. In this model, Lewis rats are intracranially co-injected with a recombinant AQP4 antibody and human-derived complement. This yields a disease course marked by rapid astrocyte loss (*grey*), BBB dysfunction (*red*), and neutrophil infiltration (*blue*), followed by barrier restoration and astrocyte repopulation. AQP4: Aquaporin-4. Ab: Antibody. IgG: Immunoglobulin. **B.** Summary of studies whose findings could be classified within the framework presented in **A.** IF: Immunofluorescence-based immunohistochemistry. PMN: Polymorphonuclear. Created with BioRender.com.

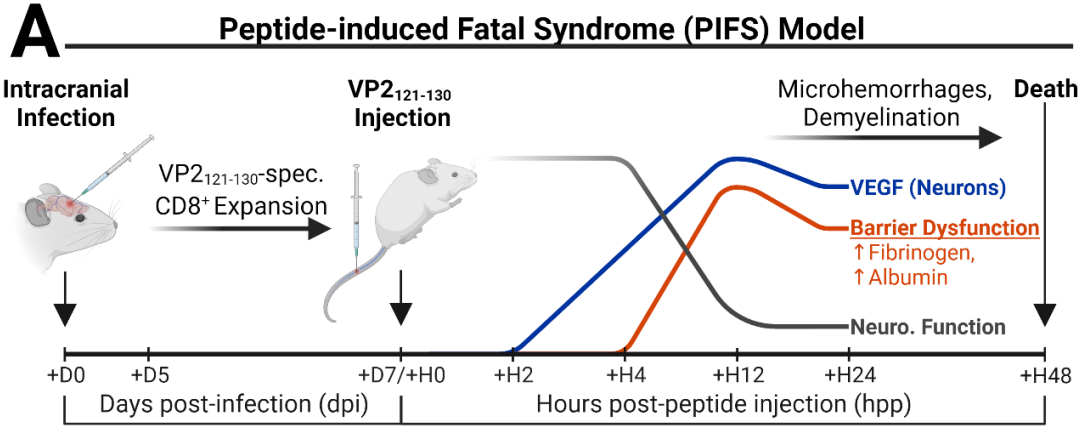

B Classifiable Studies

Wild-type C57BL/6 Mice		
Suidan et al., 2008.	0-12 hpp	WB: ↔**CLDN5**, ↓**OCLN** (brain microvessels)
	24 hpp	WB: ↑**CLDN5**, ↑**OCLN** (brain microvessels)
Johnson et al., 2012.	24 hpp	IF: ↓**CLDN5**, ↓**OCLN** (brain)
Willenbring et al., 2016.	12 hpp	IF: ↓**CLDN5** (brain)

C Classifiable Studies

Perforin-knockout C57BL/6 Mice			
Suidan et al., 2008.	Full KO	24 hpp	WB: ↔**CLDN5**, ↔**OCLN** (brain microvessels)
Johnson et al., 2014.	CD8+ Transfer WT →Full KO	24 hpp	IF: ↓**CLDN5**, ↓**OCLN** (brain)
Willenbring et al., 2016.	Partial KO, Full KO	12 hpp	IF: ↑**CLDN5** (brain) (Full KO > Partial KO)

Pharmacologic Interventions in Wild-type C57BL/6 Mice			
Suidan et al., 2010.	NRP-1 Inhibitior (-0.5, +3, +6, & +9 hpp)	12 hpp	WB: ↑**OCLN** (brain microvessels)
Johnson et al., 2012.	Neutrophil Depletion (α-Ly6G Ab 5-7 dpi)	24 hpp	IF: ↔**CLDN5**, ↔**OCLN** (brain)
	CD8+ Depletion (α-GR-1 Ab 5-7 dpi)	24 hpp	IF: ↑**CLDN5**, ↑**OCLN** (brain)

Figure 1.24. Alterations in TMEV Models.

A. In this model, C57Bl/6 mice are intracranially infected with TMEV, then injected with a peptide for the immunodominant epitope of a viral protein ($VP2_{121-130}$) during peak $CD8^+$ T cell expansion. This yields a fulminant disease marked by microhemorrhaging and loss of neurologic function (*grey*). BBB dysfunction (*red*) closely follows secretion of vascular endothelial growth factor (VEGF) from neurons. **B, C.** Summary of studies whose findings could be classified within the framework presented in **A.** for base disease (**B**), genetic manipulations (**C** – *left*), or pharmacologic interventions (**C** – *right*). WB: Western blot. IF: Immunofluorescence-based IHC. WT: Wild-type. KO: Knockout. NRP-1: Neuropilin-1. Ly6G: Lymphocyte antigen 6 complex locus G6D. GR-1: granulocyte receptor-1 antigen. Created with BioRender.com.

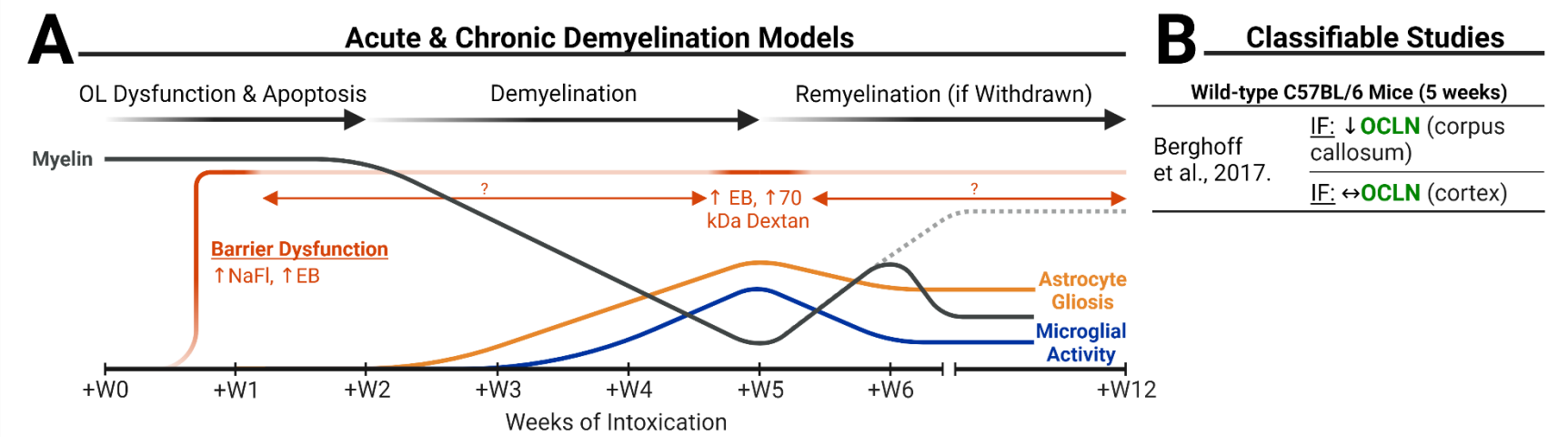

Figure 1.25. Alterations in Cuprizone Models.

A. Persistent intoxication of C57BL/6 mice with cuprizone results in oligodendrocyte (OL) dysfunction and death over the first two weeks. This is followed by progressive demyelination (*grey*) that reaches its lowest point in the corpus callosum at ~5 weeks. In acute models, cuprizone administration is halted, allowing remyelination to occur (*grey* – dotted line), while in chronic models, continued intoxication results in abortive remyelination (*grey* – solid line). Concurrent with these changes, BBB dysfunction (*red*) in the model has been demonstrated prior to detectable demyelination and at peak demyelination in the corpus callosum. Furthermore, BBB dysfunction is preferentially observed in areas with pathology such as astrocyte and microglial gliosis (*yellow* and *blue*, respectively), suggesting a close relationship between local pathology and barrier dysfunction. NaFl: Sodium Fluorescein. EB: Evans Blue. **B.** Summary of studies whose findings could be classified within the framework presented in **A.** IF: Immunofluorescent-based immunohistochemistry. Created with BioRender.com.

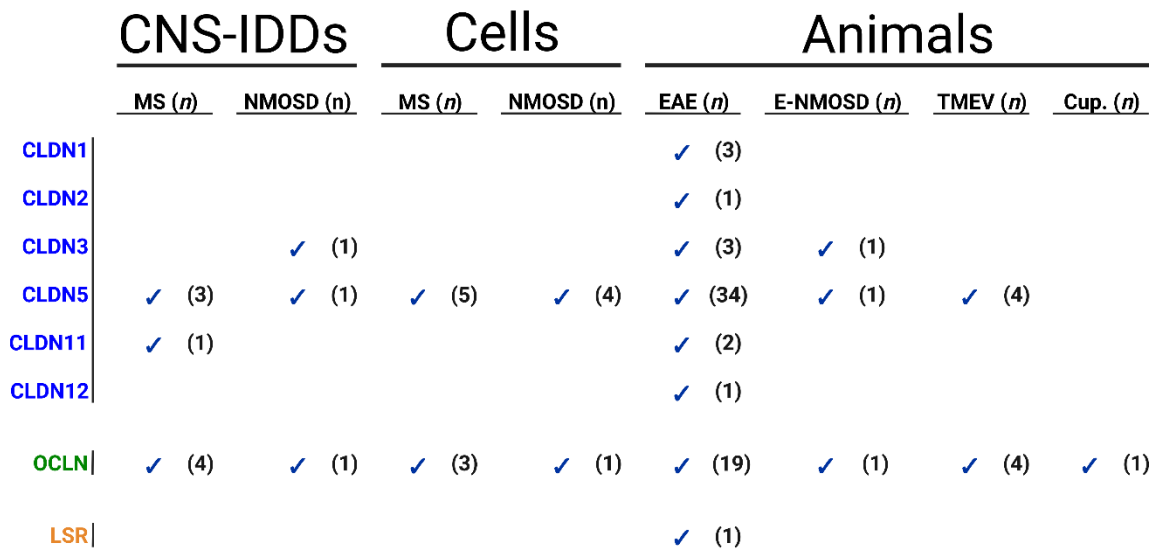

Figure 1.26. Summary of Studies Identified for Each Tight Junction Family.

Across the three families, six members of the claudin family (1, 2, 3, 5, 11, & 12), one member of the TAMP family (occludin), and one member of the angulin family (LSR) have been characterized in one or more of the CNS-IDDs or their models. For comparison purposes, the number of studies found for each member is listed in parentheses. Created with BioRender.com.

CHAPTER TWO: INFLAMMATION-ASSOCIATED ALTERATIONS TO THE VASCULAR BASEMENT MEMBRANE IMPAIR BLOOD-BRAIN BARRIER FUNCTION AND SUPPRESS CLAUDIN-5 EXPRESSION.

The Blood-Brain Barrier in Health & Disease

The blood-brain barrier (BBB) serves as a physical and metabolic interface between the peripheral circulation and the nervous tissues.[27] To fulfill these functions, microvessels are lined with endothelial cells (ECs) that restrict paracellular transport with multiprotein complexes called tight junctions.[178] However, their dysregulation is a common hallmark in neurodegenerative disorders like multiple sclerosis (MS)[38,179] and Alzheimer's disease,[180,181] insults to the CNS like ischemic stroke[46,182] and traumatic brain injury (TBI),[183,184] and psychiatric disorders like schizophrenia and major depression.[36,185] As BBB dysfunction compromises neurovascular unit (NVU) homeostasis,[29,38] a better understanding of the mechanisms that regulate BBB function is needed.

Claudin-5 in Blood-Brain Barrier & Neurologic Function

Tight junctions are formed by a branching network of transmembrane proteins that act in homophilic or heterophilic fashion within the same cell membrane and across to the opposing membrane.[30] The claudin family of tetraspan proteins form the backbone of tight junctions at bicellular contacts to provide either barrier- or pore-forming properties.[32] Of the 27 members across humans and rodents, claudin-5 is the dominant barrier-forming member in BBB-ECs.[28] Although its loss is not embryonically lethal in mice, deficient

animals perish within 10 hours of birth and suffer size-selective leakage of small molecules.[35] Similarly, knockdown of claudin-5 in adult mice results in BBB leakage, schizophrenia-like behavior, and mortality within 40 days.[36] Saliently, its loss in areas with barrier dysfunction is frequently observed in neurological disorders and their respective animal models.[38] Taken together, it is clear that claudin-5 is a gatekeeper of BBB and neurologic function that could serve as a therapeutic target to modulate or promote barrier function.[38] However, the regulatory mechanisms that govern claudin-5 expression and localization, especially under pathological conditions, are still under investigation.

The Vascular Basement Membrane in Health

Besides providing structural support, the vascular basement membrane (BM) contributes to the regulation of barrier function and tight junctions by acting as a conduit for 'outside-in' signaling via soluble factors and cell-matrix protein interactions.[186] The vascular BM primarily consists of collagen type IV, laminins, and a select number of other glycoproteins.[186–188] Among these, the contributions of collagen type IV, specifically the $[\alpha1(IV)]_2\alpha2(IV)$ trimer, to barrier integrity are the most well-characterized. Loss-of-function studies in rodents for *Col4a1* or *Col4a2* result in embryonic lethality, vascular defects, or intracerebral hemorrhage, comparable to human patients with cerebral small vessel disease due to *COL4A1* mutations.[189] Furthermore, these contributions are integrin β_1-dependent as its blockade in primary mouse BBB-ECs impairs barrier function and claudin-5 expression, while endothelial-restricted β_1-knockout animals or wild-type animals injected with a blocking antibody suffer vascular leakage.[190,191] Taken together, these studies suggest that disruption of endothelial-collagen type IV interactions is likely to be anti-BBB in nature.

The Vascular Basement Membrane in Disease

Alterations to the vascular BM are commonly observed in CNS diseases, including MS.[186,192] Besides secretion of proteases to degrade the constitutive BM, deposition of proteins normally absent from the BM occurs.[186] For example, in the active and chronic demyelinated white matter (WM) lesions of patients with MS, deposits of various fibril-forming collagens and members of the small leucine-rich proteoglycan (SLRP) family were observed.[193] Moreover, their strongest presence was around vessels within the core of the lesion and in areas of immune cell infiltration.[193] Recently, collagen type I and the class I SLRP decorin were identified as part of a core BBB dysfunction module of differentially expressed genes shared across four mouse disease models, including experimental autoimmune encephalomyelitis (EAE; Figure 2.1 & 2.2).[194] As with the MS lesions, deposits of both were detected.[194] However, the purpose of their deposition during disease is unclear given the differing pathologies underlying each of these four models. Moreover, how BM composition may influence endothelial function, especially under pathological conditions, is a poorly addressed topic in the literature.

Rationale for Study

Although most research involving MS and its animal models have focused on BBB dysfunction and tight junction disruption during the active stages of disease, both are, in fact, early events in their progression. Pre-active WM lesions from patients with MS or transgenic mice carrying T cell receptors against their myelin (TCR-1640) suffer BBB dysfunction and their vessels exhibit aberrant tight junctions before onset of demyelination (see Chapter One for more detail).[9] In line, we recently showed that loss of BBB integrity

and claudin-5 density at the tight junctions of isolated brain microvessels occurs before observable neurological deficit in EAE-induced mice (Figures J.1A & J.1B).[34]

Given the close connection between collagen type IV, BBB function, and claudin-5, deposition of BM proteins like collagen type I or decorin during inflammation could contribute to barrier dysfunction and claudin-5 loss by interfering with already established cell-matrix interactions or forming new ones. However, no studies have considered their expression patterns during the pre-active stages of disease.[193,194] Moreover, only two early studies for collagen type I[195,196] and no studies for decorin have even considered their possible influence on BBB-EC barrier function.

As less is known about decorin, in this dissertation I first investigate 1) its expression pattern in EAE-induced mice at the pre-onset stages of disease, 2) whether its presence in constructed basement membranes impacts the gene expression of claudin-5 and barrier function using primary mouse BBB-EC monolayers, and 3) whether its gene silencing may be beneficial. Additionally, I share preliminary data I've collected for collagen type I using similar approaches to those for decorin.

Methodology

Reagents, Primers, Antibodies, and Software

Complete listings for each are provided in Appendix G.

RNA-Seq Analysis

For the data presented in Figures 2.1 and 2.2, a recent bulk RNA-Seq data set that identified differently expressed genes in CNS-ECs common to four animal models of disease across active stages of disease (acute, sub-acute, and chronic) was used.[194] Namely, the kainic acid model of epilepsy, MOG_{35-55}-based EAE, middle cerebral artery occlusion

(MCAO) model of stroke, and focal cortical impact model of pediatric TBI were compared. This data set was queried for expression of collagen type I (*Col1a1* and *Col1a2*) and decorin (*Dcn*), and heat maps were created using the provided $\log_2$-transformed fold changes with respect to controls.

For the data presented in Appendix I, two bulk RNA-Seq data sets for various cell types isolated from mouse[197] or human cortices,[198] a bulk RNA-Seq data set for mouse brain and peripheral endothelial cell types,[199] a single-cell RNA-Seq data set for various cell types isolate from mouse whole brains,[200] and a single-cell RNA-Seq data for brain endothelial cells types isolated from mouse whole brains[199] were used. Data sets were queried for expression of α1 or α2 integrins (*Itga1* and *Itga2*, respectively) using the publicly accessible web portals created by the authors. The URL and data of accession for each data set are listed in the respective figure legend.

Animal Use

Wild-type C57BL/6J mice and fluorescent Cre reporter mice on a C57BL/6J background (*Ai14*; Stock No: 007914) were purchased from Jackson Laboratory (US). *Dcn*-floxed (*Dcn*$^{tm1.1Debi}$; MGI: 6119511) and *Bgn*-floxed (*Bgn*$^{tm1.1Debi}$; MGI: 6119512) mice on a C57BL/6 background were a kind gift from Dr. David E. Birk (University of South Florida, US). The two single floxed lines were crossed to achieve a dual *Dcn*-floxed x *Bgn*-floxed line. Pan-endothelial inducible Cre mice (*Tg(Tek-cre/ERT2)1Arnd*; MGI: 2450312) were purchased from the European Mouse Mutant Archive (EMMA, Germany), while BBB-EC-restricted inducible Cre mice (*Tg(Slco1c1-iCre/ERT2)1Mrks*; MGI: 5301361) were a kind gift from Dr. Markus Schwaninger (University of Lübeck, Germany). To generate inducible pan-endothelial or BBB-EC-restricted knockout lines,

the *Dcn*-, *Bgn*-, or dual *Dcn*-floxed *x Bgn*-floxed lines were crossed with the respective inducible Cre lines. All experimental mice were genotyped by Transnetyx (US).

Animals were maintained under a 12-hour light-dark schedule with food and water *ad libitum*. All experiments were approved by the Institutional Animal Care and Use Committees (IACUC) at University of South Florida or Boise State University and were performed in accordance with the Guide for the Care and Use of Laboratory Animals. All experiments have been reported in compliance with ARRIVE guidelines.

Induction of Active EAE

Active MOG_{35-55}-based EAE was induced in wild-type C57BL/6J mice as we have previously described.[34] Briefly, animals were immunized with MOG_{35-55} peptide suspended in complete Freund's adjuvant using a commercially available kit according to manufacturer's instructions (Hooke Labs, US). Pertussis toxin (80 ng/animal) was administered intraperitoneally (*i.p.*) on days 0 and 1 post-induction. At 8 days post-induction (*d.p.i.*), animals were scored from 0.0 to 5.0 according to the rubric established by Hooke Laboratories (Appendix H). Animals lacking a clinical score (CS) were harvested. As a healthy control group, non-induced animals were harvested in tandem with the diseased animals.

Analysis of BBB Integrity *in vivo*

The small fluorescent tracer sodium fluorescein (NaFluor; 376 Da) was used as we have previously described.[34] Briefly, animals were injected *i.p.* at 5 µL per gram body weight with a 10% NaFluor solution prepared in saline. After allowing the tracer sufficient time to circulate (2 hours), animals were anesthetized with isoflurane, their blood collected via cardiac puncture, and then flushed with Ringer's lactate solution. Following

decapitation, whole brains were excised, and the meninges and pial vessels removed. The remaining tissue was weighed, and then homogenized in 1 mL of phosphate-buffered saline (PBS). Homogenates were centrifuged at 12,000 x g for 15 minutes at 4°C, and the supernatant collected. Next, a freshly prepared 20% trichloroacetic acid (TCA) solution was used for protein precipitation. Brain supernatants were directly diluted 10-fold with TCA, while blood sera were first diluted 10-fold with PBS, then diluted 10-fold with TCA. Following incubation overnight at 4°C, supernatants and sera were centrifuged at 12,000 x g for 15 minutes at 4°C. Samples were then diluted with equal volumes of 50 mM borate buffer, pH 10. Finally, sample fluorescence was measured (Ex./Em. = 480/538 nm) and compared against standard curves of fluorescein prepared in solutions containing 10% TCA and 25 mM borate buffer, pH 10. The ratio of brain-to-serum concentrations was normalized to brain weight, then fold-change was calculated with respect to controls.

Tomato Lectin Staining

Demarcation of the brain vasculature was achieved using a tomato-derived lectin (TL; *Lycopersicon esculentum* agglutinin) that preferentially labels the endothelium.[201] Briefly, animals were anesthetized with isoflurane, then transcardially injected with 50 µL of a 1 mg/1 mL solution containing a commercially prepared TL conjugated with DyLight 649 (Vector Laboratories, US). After allowing the lectin sufficient time to circulate (3 minutes), animals were flushed with normal saline solution. Following decapitation, whole brains were excised, and the meninges and pial vessels removed.

Immunohistochemistry

Brains were post-fixed by immersion in a 2% paraformaldehyde (PFA) solution overnight at 4°C. They were then washed three times with PBS, embedded in low-melting

point agarose, and cut into 100 µm thick sections. For the data presented in Figures 2.5 and 2.6, slices were permeabilized with 0.5% Triton X-100, then blocked with 10% donkey serum. Free-floating sections were incubated with an AF488-conjugated anti-decorin antibody (1:50) overnight at 4°C. Sections were washed six times with PBS (hour-long washes), mounted with Vectashield on PFTE-coated microscope slides, and coverslipped. For the data presented in Figure 2.26, slices were directly mounted with Vectashield on PFTE-coated microscope slides and coverslipped. Prepared slides were examined with a Zeiss LSM 510 Meta inverted confocal microscope (Zeiss, Germany) using the 488, 543, or 633 nm laser lines and appropriate filter settings. Confocal images were analyzed using the ZEN imaging software (Zeiss, Germany).

Primary Mouse BBB-EC Isolation

Based on a publication by Watson *et al.* that described the isolation of primary rat brain or spinal cord ECs,[202] we devised a six-part protocol for the isolation of primary mouse BBB-ECs from 7-to-10 day-old pups using a combination of density centrifugation, enzymatic digestion, and positive selection (for an explanatory graphic, see Figure 2.6). To cover the surface of a T25 flask, 8-10 pups per isolation were required.

First, pups were euthanized by cervical dislocation, then decapitated. Whole brains were excised, and the meninges and pial vessels removed with a tissue. *Second*, the remaining tissue was homogenized (7-10 strokes with a loose-fitting 40 mL Dounce homogenizer) in 25 mL of chilled isolation buffer containing Hanks Buffered Salt Solution (HBSS) supplemented with 10 mM HEPES and 0.1% BSA. The homogenate was centrifuged at 4°C for 5 minutes at 500 x g, then the supernatant discarded. *Third*, the pellet was suspended in warmed digestion buffer containing Dulbecco's Modified Eagle's

Medium (DMEM) supplemented with collagenase/dispase and DNAse I at 2 mg/mL and 20 µg/mL, respectively, then slowly rotated for 30 minutes at 37°C using a tube rotator. The mixture was centrifuged at 4°C for 5 minutes at 400 x g, then the supernatant discarded. ***Fourth***, the pellet was suspended in a warmed separation buffer containing 22% BSA prepared in HBSS, centrifuged at 4°C for 7 minutes at 3000 x g, and the supernatant discarded. The pellet was then washed with DMEM prior to centrifugation at 4°C for 5 minutes at 500 x g. ***Fifth***, the pellet was suspended in warmed digestion buffer and slowly rotated for 25 minutes at 37°C using a tube rotator. The mixture was centrifuged at 37°C for 5 minutes at 500 x g, then the supernatant discarded. The pellet was then washed with DMEM prior to centrifugation at 37°C for 5 minutes at 500 x g. ***Sixth***, the pellet was suspended in warmed complete mouse endothelial cell medium (Cellbiologics, US) and seeded into T25 flasks coated with collagen type I (1 µg/cm^2). For the first three days post-seeding (*d.p.s.*), wells were rinsed with HBSS prior to the addition of fresh complete mouse endothelial cell medium supplemented with 3 µM puromycin. Daily media changes were continued with puromycin-containing media until ready for passaging (5-7 *d.p.s.*).

T Cell Activation

Fresh spleen and lymph node cells isolated from wild-type C57BL/6J mice induced with MOG_{35-55}-based EAE were purchased from Hooke Laboratories (US), then activated according to the provider's instructions. Briefly, cells were pooled and suspended at a final concentration of ~3.5 million cells per mL in RPMI 1640 media supplemented with 10% HEPES, 10% fetal bovine serum (FBS), 2 mM L-glutamine, 1X penicillin-streptomycin solution, 1X MEM non-essential amino acids solution, 1 mM sodium pyruvate, and 55 µM 2-mercaptoethanol. Next, MOG_{35-55} peptide, recombinant mouse interleukin-12 (IL-12),

and anti-mouse IFN-γ antibodies were added to a final concentration of 20 µg/mL, 20 ng/mL, and 10 µg mL, respectively. Cells were cultured for 72 hours before being pelleted via centrifugation for 10 minutes at 300 x g for determination of cell count. As controls, fresh spleen and lymph node cells isolated from naïve mice were also purchased from Hooke Laboratories (US).

Generation of Conditioned Media

Conditioned media (CM) from astrocytes, T cells, and neutrophils (PMNs) were created via sequential co-culture steps (for an explanatory graphic, see Figure 2.7). The spontaneously immortalized mouse astrocyte line C8-D1A was maintained in DMEM supplemented with 10% FBS, and 1X penicillin-streptomycin. Cells were cultured in 12-well plates, then activated T cells were added to the wells (50,000 each) for 24 hours. As a control, cells isolated from naïve mice were also used. The conditioned media from both groups (ETcA-CM and NTcA-CM, respectively) was collected and centrifuged at 10,000 x g for 10 minutes to remove any cellular debris. In turn, 50,000 naïve neutrophils isolated from the bone marrow of wild-type C57BL/6J mice using positive selection columns (Miltenyi Biotec) were exposed to the ETcA-CM or NTcA-CM for 6 hours. The conditioned media from both groups (PMN-ETcA-CM and PMN-NTcA-CM, respectively) was collected and centrifuged at 10,000 x g for 10 minutes to remove any cellular debris. All conditioned media were kept at -80°C until ready for usage in experiments.

RNA Isolation & Analysis

RNA was isolated from BBB-ECs and analyzed as previously described.[34] Briefly, cells were lysed using RNAzol RT (Molecular Research Center, US) according to manufacturer's instructions, then total RNA was isolated according to manufacturer's

instructions, including the optional step involving 4-bromoanisole. Sample quantity and purity were assessed using 260/280 and 260/230 absorbance ratios. Reverse transcription was completed with the iScript cDNA Synthesis kit according to manufacturer's instructions (Bio-Rad, US) using 500 ng total RNA per 20 µL reaction. Quantitative polymerase chain reaction (qPCR) was performed using SsoAdvanced Universal SYBR® Green Supermix and PrimePCR™ PCR primers for mouse *Cldn5* or *Dcn* according to manufacturer's instructions (Bio-Rad, US) using a LightCycler 96 instrument (Roche, Switzerland). Relative quantification of target gene expression was calculated through the $2^{-\Delta\Delta Cq}$ method using *Actb* as the reference gene.

TAT-Cre-mediated Recombination in BBB-ECs

To efficiently recombine floxed genes in primary mouse BBB-ECs, we adapted a cell-penetrating peptide-based Cre recombinase-delivery system devised by Wadia *et al*. (Figure 2.12).[203] Primary mouse BBB-ECs isolated from *Ai14* mice were cultured in black, clear-bottom 96-well plates coated with collagen type IV (10 µg/cm^2). Following maturation (5-7 *d.p.s.*), empirical testing with varying concentrations of TAT-HA2 and TAT-Cre identified that a single hour of incubation with serum-free media (Cellbiologics, US) containing 5 µM TAT-HA2 and 50 U/cm^2 TAT-Cre was most optimal with respect to recombination efficiency when assessed 48 hours later (see next section).

Live-cell imaging & Immunocytochemistry

For the data presented in Figure 2.13, media was exchanged with an equivalent volume of Live Cell Imaging Solution (Invitrogen, US), then monolayers were visualized with an EVOS FL Auto Imaging System equipped with a red fluorescent protein (RFP)-based filter set. For the data presented in Figure 2.14, monolayers were first fixed with a

4% PFA solution for 10 minutes, rinsed with PBS, permeabilized with a 0.1% Triton-X 100 solution for 10 minutes, rinsed with PBS, and blocked with 10% donkey serum for an hour at room temperature. Following overnight incubation with an AF488-conjugated anti-claudin-5 antibody (1:200 dilution) at 4°C, monolayers were washed five times with PBS supplemented with 0.1% TWEEN-20 (5 minutes each). Following a rinse with PBS, Live Cell Imaging Solution was added and monolayers were visualized with an EVOS FL Auto Imaging System equipped with green fluorescent protein (GFP)- and RFP-based filter sets.

Barrier Function Assessment

Barrier function of primary mouse BBB-ECs was assessed using permeability assays or electric cell-substrate impedance sensing-transendothelial electrical resistance (ECIS-TEER). The principles of each are shown in Figures 2.10 and 2.15, respectively.

Permeability Assays. Primary wild-type mouse BBB-ECs were seeded in 24-well transwell inserts coated with collagen type I, collagen type IV, decorin, or various combinations of each (10 μg/cm^2). Following maturation (5-7 *d.p.s.*), NaFluor was added at a final concentration of 0.5 mg/mL to the upper chamber. After allowing the tracer sufficient time to circulate (~30 minutes), aliquots were taken from the upper (luminal) and lower (abluminal) chambers. Next, samples were processed in an analogous fashion to the brain homogenate and blood sera to determine the tracer concentration in each sample. Finally, the apparent permeability coefficient (P_{app}) was calculated using the equation $P_{app} = \frac{[Ab]}{t} * \frac{1}{SA} * \frac{Vol_{Ab}}{[Lum]}$ where $[Ab]$ is the abluminal concentration, t is the time elapsed, SA is the surface area of the insert membrane, Vol_{Ab} is the volume of the abluminal chamber, and $[Lum]$ is the luminal concentration.

ECIS-TEER assays. For the data presented in Figures 2.18 and 2.19, primary wild-type mouse BBB-ECs were seeded at confluence into 8W10E+ PET arrays coated with collagen type I or collagen type IV (10 μg/cm^2). Following maturation (5-7 *d.p.s.*), data was collected by a 16-well ECIS Zθ station (Applied Biophysics, US) using the multiple frequency per time (MFT) option to collect readings from 62.5 Hertz to 64 kiloHertz (kHz). ECIS software was then used to derive the parameters R_b, α, and C_m (for their definitions, see Figure 2.15) using a cell-free well as a reference. For the data presented in Figure 2.16, *Dcn*-floxed BBB-ECs were cultured 5-7 *d.p.s.*, incubated with serum-free mouse endothelial cell medium (Cellbiologics, US) containing 5 μM TAT-HA2 with or without 50 U/cm^2 TAT-Cre for one hour, and then allowed to recover for 48 hours prior to incubation with 30% ETcA-CM for 24 hours. Readings were collected at a single frequency (4 kHz) to monitor barrier integrity.[204]

Tamoxifen-induced Cre-mediated Recombination *in vivo*

A 20 mg/mL solution of tamoxifen was prepared in a 10% ethanol-90% corn oil mixture. Animals were injected *i.p.* at 50 mg per kg body weight every 12 hours for five consecutive days, then allowed to recover at least fourteen days. For the data presented in Figure 2.25, animals were then induced with active EAE and scored as described above. For the data presented in Figure 2.26, animals were then anesthetized with isoflurane and processed for TL staining and confocal microscopy as described above.

Genomic DNA Isolation & Analysis

Brain microvessel (MV)-enriched pellets were isolated from mice as previously described.[34] Briefly, animals were anesthetized with isoflurane, transcardially perfused with saline until clear, and then decapitated. Whole brains were excised, the meninges and

pial vessels removed with a tissue, and the remaining tissue cut midsagittal with a sterile razor. The right hemisphere of each animal was homogenized (7-10 strokes with a loose-fitting 40 mL Dounce homogenizer) in PBS. The homogenate was mixed 1:1 with a 36% dextran (~71 kDa) solution prepared in DMEM supplemented with 2% FBS, then centrifuged at room temperature for 10 minutes at 10,000 x g. The supernatant was discarded, and the remaining MV-enriched pellets were immediately processed using a Phire Tissue Direct PCR kit according to manufacturer's instructions (ThermoFisher Scientific, US). PCR was completed using primers and thermocycling protocols provided by Dr. Birk for biglycan excision (Appendix G). Reaction products were then resolved on a 2% agarose gel containing ethidium bromide (2.5 µL/50 mL agarose) and visualized using a ChemiDoc Imaging System (Bio-Rad, US).

In-Cell Western Assay

To identify compounds that may promote claudin-5 expression in BBB-ECs, an in-cell western (ICW) protocol was designed using near-infrared (NIR) dyes (for an explanatory graphic, see Figure 2.28).[205,206] Immortalized mouse BBB-ECs (bEnd.3) were cultured in black, clear-bottom 96-well plates coated with collagen type IV (10 µg/cm^2). Monolayers were allowed to partially mature (2 days), then were administered methylprednisolone (MP; 10 µg/mL) with or without demethylasterriquinone B1 (DMAQ-B1; 5 µM), or a vehicle control. Twenty-four hours later, cells were fixed with a 4% PFA solution for 10 minutes, rinsed with PBS, permeabilized with a 0.1% Triton-X 100 solution for 10 minutes, rinsed with PBS, and blocked with a commercial blocking buffer for 30 minutes (LI-COR, US). Monolayers were incubated overnight with an anti-claudin-5 antibody overnight (1:200), washed five times with PBS supplemented with 0.1%

TWEEN-20 (5 minutes each), incubated for an hour at room temperature with an IRDye® 800CW-conjugated donkey anti-mouse antibody (1:1000) and CellTag™ 700 Stain (1:1000), and washed five times with PBS supplemented with 0.1% TWEEN-20 (5 minutes each). Following removal of all liquid from the well, plates were imaged using an Odyssey CLx (LI-COR, US) with a focus offset of 4 mm, 169 µm resolution, and intensities for the 700 and 800 nm channels set to auto. For quantification, the ICW analysis tool for Image Studio software was used according to developer's instructions (LI-COR, US). Briefly, a circular region of interest was drawn for each well. Next, the claudin-5 signals (800 nm channel) of each well were normalized to the CellTag signal (700 nm) and background subtraction was performed using wells incubated only with the IRDye® 800CW secondary antibody. Finally, the normalized and corrected claudin-5 signals were divided by the surface area of the 96-well plate (0.32 cm^2) to calculate the claudin-5 signal per square centimeter of cells.

Statistical Analysis

All statistical analyses were performed with Prism (GraphPad Software, Inc.). α was set at 0.05 a *priori* for statistical significance. No specific blinding was performed in these studies.

Results

Decorin is Deposited into the Vascular BM During the Pre-Onset Stage of EAE

Thus far, studies involving decorin deposition into the vascular BM during MS or EAE have not considered the early stages of disease.[193,194] Therefore, we induced MOG_{35-55}-based EAE in wild-type C57BL/6J mice and sacrificed them at 8 days post-induction

(*d.p.i.*) – a time point at which we've previously shown BBB dysfunction and claudin-5 loss without observable neurological deficit (Figures J.1A & J.1B).[34]

As an initial step, we confirmed BBB dysfunction using a sodium fluorescein (NaFluor) extravasation assay. As shown in Figure 2.3, compared to animals not induced with EAE, diseased animals exhibited significantly increased leakage into their brain (n = 6 for each group; $p < 0.05$, unpaired Student's *t*-test). Separately, we examined the brains of diseased animals for decorin expression via confocal microscopy. Intense deposits of decorin were observed along the length of cerebellar vessels of diseased animals (Figure 2.4 – *right*). Indeed, the deposits were sufficiently prevalent that micrographs of the 488 nm channel alone were sufficient to demarcate the microvessels without the need of the tomato lectin (TL) stain (Figure 2.4 – *top-right*). Furthermore, cross-sectional profiles of cerebellar microvessels revealed the decorin deposits to be immediately abluminal or overlapping with TL stain (Figure 2.5). Conversely, in the brains of non-induced animals only a few minor puncta were observed (Figure 2.4 – *left*).

Taken together, these data indicate that decorin deposition into the vascular BM starts prior to the onset of observable neurological deficit in EAE-induced animals exhibiting BBB dysfunction.

<u>Conditioned Media Induce Decorin & Suppress Claudin-5 in primary mouse BBB-ECs</u>

A veritable laundry list of chemokines and cytokines are involved in MS or EAE.[207–210] Rather than exhaustively screening every possible combination to identify those which may be sufficient to induce decorin expression, we chose to generate disease-relevant conditioned media. As a first step, immortalized mouse astrocytes were incubated with activated T cells isolated from wild-type C57BL/6J mice induced with MOG_{35-55}-

based EAE to mimic the known cross-talk between astrocytes and T cells in MS and EAE.[211,212] This yielded a conditioned medium termed ETcA-CM (Figure 2.7A – *left*). In turn, naïve mouse neutrophils (PMNs) isolated from the bone marrow were added to ETcA-CM to mimic the neutrophil activation and degranulation observed in MS and EAE.[213,214] This yielded a conditioned medium termed PMN-ETcA-CM (Figure 2.7A – *right*). For control conditioned media, naïve T cells isolated from non-induced mice were used instead. This yielded NTcA-CM and PMN-NTcA-CM, respectively (Figure 2.7B).

Exposure of wild-type primary BBB-ECs to control conditioned media did not significantly alter claudin-5 or decorin gene expression at 24 hours (Figure 2.8 – *purple* and *blue*; $p > 0.05$, one-way ANOVA with post-hoc Tukey's for both). Conversely, exposure to PMN-ETcA-CM led to strong induction of decorin (Figure 2.8A – *orange*; $p < 0.05$, one-way ANOVA with post-hoc Tukey's) and loss of claudin-5 (Figure 2.8B – *orange*; $p < 0.05$, one-way ANOVA with post-hoc Tukey's). Finally, exposure to ETcA-CM led an intermediate induction of decorin which was significantly greater than the control conditioned media but less than the PMN-ETcA-CM (Figure 2.8A - *red*; $p < 0.05$, one-way ANOVA with post-hoc Tukey's), while a non-significant decrease in claudin-5 was measured (Figure 2.8B – *red*; $p > 0.05$, one-way ANOVA with post-hoc Tukey's).

As the PMN-ETcA-CM yielded the strongest response for decorin and claudin-5, we conducted a time-course to better understand their gene expression patterns. Decorin was significantly elevated at 3 and 6 hours, and further increased at 12 hours (Figure 2.9A; $p < 0.05$, one-way ANOVA with post-hoc Tukey's). A mirror opposite trend was observed for claudin-5, with its lowest levels at 12 hours (Figure 2.9B; $p < 0.05$, one-way ANOVA with post-hoc Tukey's).

Taken together, these data indicate that conditioned media created using astrocytes, activated T cells, and neutrophils are sufficient to induce decorin and suppress claudin-5 gene expression in wild-type primary mouse BBB-ECs. Furthermore, elevated decorin gene expression is associated with lower claudin-5 gene expression.

Decorin Impairs Barrier Function & Claudin-5 Gene Expression

To more closely investigate this inverse relationship, wild-type primary mouse BBB-ECs were cultured in wells coated with collagen type IV, decorin, both, or neither. Monolayers cultured on collagen type IV had higher levels of claudin-5 compared to those on decorin or plastic (Figure 2.11A – *columns 1-3*; $p < 0.05$, one-way ANOVA with post-hoc Tukey's). Interestingly, monolayers cultured on decorin exhibited a downwards trend compared to those on plastic, albeit non-significant (Figure 2.11A – *columns 1 & 2*; $p > 0.05$, one-way ANOVA with post-hoc Tukey's). Finally, the additional presence of decorin impaired the pro-claudin-5 effects of collagen type IV (Figure 2.11A – columns 3 & 4; $p < 0.05$, one-way ANOVA with post-hoc Tukey's).

To determine whether barrier function was impacted, NaFluor permeability assays were conducted (for an explanatory graphic, see Figure 2.10) with wild-type primary mouse BBB-ECs cultured in transwell inserts coated with collagen type IV, decorin, both, or neither. Monolayers cultured on collagen type IV exhibited lower permeability compared to those on decorin or plastic (Figure 2.11B – *columns 1-3*; $p < 0.05$, one-way ANOVA with post-hoc Tukey's). Moreover, monolayers on decorin exhibited higher permeability than those on plastic (Figure 2.11B – *columns 1 & 2*; $p < 0.05$, one-way ANOVA with post-hoc Tukey's). Finally, the additional presence of decorin impaired the

pro-barrier effects of collagen type IV (Figure 2.11B – *columns 3 & 4*; $p < 0.05$, one-way ANOVA with post-hoc Tukey's).

Taken together, these data indicate that the decorin not only counteracts the beneficial effects of collagen type IV on claudin-5 gene expression and barrier function, but also appears to be a worse substrate than plastic alone.

Loss of Decorin Partially Rescues Barrier Dysfunction & Claudin-5 Gene Expression

Given the seemingly deleterious role of decorin, we wanted to investigate whether its silencing could be beneficial. However, it is challenging to efficiently silence genes in primary BBB-ECs using methods like small interfering RNA (siRNA). Therefore, we adapted a cell-penetrating peptide-based Cre recombinase-delivery system developed by Wadia *et al*.[203] Recombination of genes flanked by loxP (*floxed*) sites is achieved by a recombinant Cre enzyme fused with the protein transduction domain (PTD) of the HIV-1 TAT protein (TAT-Cre). Additionally, to promote endosomal escape, a fusogenic peptide consisting of the N-terminal portion of influenza hemagglutinin with the same PTD sequence from TAT is used.

To optimize recombination efficiency, we isolated primary mouse BBB-ECs from Cre reporter mice (*Ai14;* Figure 2.12A) and allowed them to mature. Subsequently, they were incubated in serum-free media containing various concentrations of TAT-Cre and TAT-HA2. Cells were allowed to recover, then visualized using live-cell imaging. Ultimately, a concentration of 5 μM TAT-HA2 and 50 U/cm^2 of TAT-Cre was chosen as it yielded in a high proportion of TdTomato-expressing cells (Figure 2.13 – *right*). Furthermore, fixed cells still exhibited circumferential staining of claudin-5 when

visualized with an epifluorescent microscope (Figure 2.14 – *right*), suggesting minimal perturbation to the tight junctions.

With this method, decorin gene ablation was performed in primary mouse BBB-ECs isolated from *Dcn*-floxed mice (Figure 2.16) prior to their incubation with PMN-ETcA-CM. To assess changes in barrier integrity in real-time, we employed an electric cell-substrate impedance sensing system to measure the transendothelial electrical resistance of the monolayers (ECIS-TEER; for an explanatory graphic, see Figure 2.15). Compared to non-recombined monolayers (Figure 2.16A – *grey*), loss of resistance was less severe in recombined monolayers (Figure 2.16A – *orange*). At sixteen hours, when both groups reached their lowest point in resistance, knockout monolayers had a significant rescue in resistance (Figure 2.16B; $p < 0.05$, unpaired Student's *t*-test).

Taken together, these indicate that loss of decorin expression can have a positive outcome on barrier function under proinflammatory conditions.

Collagen Type I Does Not Foster Barrier Function or Claudin-5 Gene Expression

Only a handful of early studies have considered how collagen type may influence endothelial function or tight junctions.[195,196,215] To continue where they left off, wild-type primary mouse BBB-ECs were cultured in wells coated with collagen type IV or type I. Monolayers cultured on collagen type IV had higher levels of claudin-5 gene expression compared to those on collagen type I (Figure 2.17A; $p < 0.05$, unpaired Student's *t*-test). Next, to determine whether barrier function was impacted, NaFluor permeability assays and ECIS-TEER experiments were conducted. Wild-type primary mouse BBB-ECs cultured in transwell inserts coated with collagen type IV had lower permeability compared to those on collagen type I (Figure 2.17B; $p < 0.05$, unpaired Student's *t*-test). Similarly,

monolayers cultured in arrays coated with collagen type IV (Figure 2.18 – *blue*) exhibited higher resistances than those on collagen type I (Figure 2.18 – *orange*). Furthermore, collection of readings across a wide range of frequencies (62.5 Hz to 64 kHz) allowed for modeling of the parameters R_b (cell-cell adhesion) and α (cell-substrate adhesion) by the ECIS software (for their definitions, see Figure 2.15). Monolayers cultured on collagen type IV had overall higher R_b and α values (Figures 2.19A & B – *blue*) compared to those culture on collagen type I (Figures 2.19A & B – orange).

Taken together, these preliminary data suggest that collagen type I is sub-optimal compared to collagen type IV with respect to claudin-5 gene expression and barrier function. Additionally, diminished cell-cell and cell-substrate adhesions are both observed for monolayers cultured on collagen type I.

Discussion

When it was first discovered, the BM was considered a static structure that merely provided structural support for the tissues it served.[186,216] However, it is now understood that the biochemical and biophysical characteristics of the BM can influence the cellular processes of the adjacent tissues, including the endothelium.[186,216]

Importance of Molecular Composition

Endothelial cells anchor themselves to the BM by establishing focal adhesions rich in integrin dimers that recognize and bind the collagen type IV and laminin networks.[217,218] In turn, cytoplasmic scaffolding proteins couple the integrin dimers to the cytoskeletal network and form regulatory hubs.[217,218] Thus, changes in the molecular composition can modulate intracellular signaling in an “outside-in” manner.

Collagen Type IV. Taken together, my studies (Figures 2.11, 2.17-19) strongly suggest that collagen type IV fosters barrier function and tight junction expression in BBB-ECs. Collagens are recognized by several integrin dimers, including $\alpha_1\beta_1$ and $\alpha_2\beta_1$.[219] The $\alpha_1\beta_1$ dimer preferentially binds collagen type IV over type I, and *vice versa* for $\alpha_2\beta_1$ dimer.[219] While no studies have systematically compared their expression in BBB-ECs, three bulk RNA-Seq data sets and two single-cell RNA-Seq data set all suggest α_1 to be the main isoform under basal conditions (Appendix I).

Two separate studies have demonstrated that blockade of β_1 integrin with a monoclonal antibody (clone: Ha2/5) for 24 hours suppresses claudin-5 and impairs barrier function in primary mouse BBB-EC monolayers cultured on collagen type IV (Figure 2.20A).[190,191] Strictly speaking, integrins that bind laminin isoforms ($\alpha_3\beta_1$, $\alpha_6\beta_1$) or fibronectin ($\alpha_4\beta_1$, $\alpha_5\beta_1$) also contain the β_1 isoform.[220] While the antibody was unlikely to block endothelial-fibronectin interactions given that both dimers are poorly expressed in endothelial cells not actively undergoing angiogenesis,[220] it cannot be excluded the possibility that the antibody may have additionally targeted laminin-binding integrins. In fact, one of the studies also cultured cells on laminin 111 ($\alpha_1\beta_1\gamma_1$ isoform) under the same conditions and observed similar reductions in claudin-5.[191] Regardless, it is clear that β_1-containing integrin dimers are important for mediating endothelial-matrix protein interactions and are needed for claudin-5 expression and barrier integrity.

Unfortunately, little is known about the downstream signaling. Izawa *et al.* reporting that knocking down integrin-linked kinase (ILK), which associates with the cytoplasmic tail of β1 integrins,[221,222] suppresses total claudin-5 expression (Figure 2.20B).[191] Despite its name, ILK is a putative pseudo-kinase that instead exerts its effects

primarily by acting as an adapter protein for ILK-particularly interesting new cysteine-histidine-rich protein (PINCH)-parvin (IPP) complexes that couple integrins to the actin cytoskeleton for stability and recruit signaling proteins to the adhesion sites.[221,222] Decreased activity of the kinase Akt was observed following adenovirus-mediated Cre recombination in primary lung microvascular endothelial cells (LMVECs) isolated from *Ilk*-floxed mice, with co-transduction of a wild-type ILK construct restoring activity.[223] A similar loss in Akt activity was reported in human umbilical vein endothelial cells (HUVECs) following siRNA-mediated silencing of *ILK* as well as in the retinal endothelium of endothelial-restricted inducible *Ilk*-knockout mice.[224] We and others have shown that Akt phosphorylates the transcription factor forkhead box protein O1 (FoxO1) to prevent its nuclear accumulation and formation of a transcriptional repressor complex at the claudin-5 promoter with other transcription factors, including beta-catenin (β-catenin).[34,225,226] As such, it is possible that the decreases in total claudin-5 expression reported by Izawa *et al.* is in part due to diminished Akt activity (Figure 2.20B). In support, Yau *et al.* reported that administration of QLT-0254, a small molecule inhibitor (SMI) against ILK, was associated with decreased Akt activity and decreased FoxO1 phosphorylation in an orthotopic pancreatic tumor mouse model.[227] The efficacy of the SMI may be explained by the requirement of ILK for ATP binding as part of its coordinating with PINCH and parvin.[228]

Future studies that are needed include: 1) using α isoform-specific blocking antibodies are needed to isolate the contribution of collagen-binding integrins and 2) studies investigating the downstream targets of IPP complex signaling are needed to clarify the connection between ILK and claudin-5.

Collagen Type I. Taken together, my preliminary data for collagen type I (Figures 2.17-19) strongly suggest that collagen type I is a sub-optimal substrate for BBB-ECs compared to collagen type IV. Previously, several early studies have considered collagen type I with respect to barrier function or tight junction proteins. First, Tagami *et al.* showed that bovine aortic endothelial cells (BAECs) co-cultured with primary rat astrocytes exhibited lower leakage of horseradish peroxidase and fewer plasmalemmal vesicles when cultured on collagen type IV versus collagen type I.[195] Next, Savettieri *et al.* found that rat immortalized BBB-ECs (RBE.4) cultured on collagen type IV had higher levels of gene expression for the tight junction protein occludin compared to those on type I.[229] Finally, Tilling *et al.* demonstrated that primary porcine BBB-ECs cultured on rat tail collagen, which primarily is comprised of collagen type I, exhibited lower TEER values compared to those on type IV.[196]

While several downstream intracellular signaling pathways have been identified across various endothelial cell types, none have directly been connected to claudin-5 expression. Consequently, interferences between studies are required. First, Whelan *et al.* demonstrated that engagement of $\alpha_1\beta_1$ or $\alpha_2\beta_1$ dimers by collagen type I suppresses cyclic adenosine monophosphate (cAMP) levels and protein kinase A (PKA) activity in primary human dermal microvascular endothelial cells (DMVECs).[230] As cAMP levels and PKA activity are positively associated with barrier function and claudin-5 expression in primary porcine BBB-ECs,[231] collagen type I could impair both by suppressing cAMP- or PKA-dependent pathways (Figure 2.21A). This may include an axis recently described by Kakogiannos *et al.* involving the guanine nucleotide exchange factor (GEF) exchange protein directly activated by cAMP (EPAC) that promotes claudin-5 expression through

the binding of the transcriptional factor CCAAT/enhancer-binding protein α (C/EBP-α) to the claudin-5 promoter.[232] Alternatively, Lee *et al.* have reported that FoxO1 is a substrate for PKA and that knock down or inhibition of PKA was associated with enhanced FoxO1 activity in human aortic endothelial cells (HAECs).[233]

Next, Liu *et al.* demonstrated that stimulation of the small GTPase Ras homologue family member A (RhoA) and the kinase Src is β_1 integrin-dependent in primary human DMVECs cultured on collagen type I (Figure 2.21B).[234] In primary human BBB-ECs, administration of lysophosphatidic acid, a known activator of RhoA, triggered the phosphorylation of claudin-5 via Rho-associated kinase (ROCK), which was closely followed by loss of barrier integrity in immortalized mouse BBB-ECs (bEnd.3).[58] As such, collagen type I could directly modulate claudin-5 through posttranslational modification. Alternatively, the Src family of kinases (SFKs) negatively regulate the adherens junction protein vascular endothelial-cadherin (VE-CAD; gene: *Cdh5*) which sequesters β-catenin to the cell-cell contacts.[235] Thus, collagen type I could trigger the destabilization of VE-CAD which, in turn, liberates β-catenin. In support of this, Liu *et al.* noted that inhibition of Src using a pan-SFK inhibitor (PP2) or through transduction of a dominant-negative construct preserved VE-CAD presence at the cell-cell contacts.[234]

Finally, González-Santiago reported a suppression of ILK kinase activity in a β_1 integrin-dependent manner for primary HUVECs cultured on collagen type I compared to collagen type IV (Figure 2.21C).[236] As ILK is a putative pseudo-kinase, these results likely reflect partial co-purification of kinases that associate with ILK or IPP complexes.[237,238] Indeed, recombinant ILK expressed in bacteria or endogenous ILK subjected to multiple rounds of purification does not exhibit kinase activity.[237,238] If interpreted through the lens

of a co-immunoprecipitation assay, collagen type I may disrupt the interaction of ILK or IPP complexes with undetermined adhesion-associated kinases. Thus, as with the findings by Izawa *et al.* involving knockdown of *Ilk*,[191] Akt activity may be impaired, in turn allowing nuclear accumulation of FoxO1 at the claudin-5 promoter.

Future studies that are needed include: 1) using α isoform-specific blocking antibodies are needed to isolate the contribution of collagen-binding integrins, 2) investigating the relative occupancy of activating or repressing transcription factors at the claudin-5 promoter to determine whether collagen types differentially regulate expression at the level of transcription, and 3) characterizing the phosphorylation profile of claudin-5 to determine whether collagen types differentially regulate stability at the tight junctions.

Decorin. Taken together, my data for decorin (Figures 2.11 & 2.16) strongly suggest that decorin not only is a sub-optimal substrate for BBB-ECs to collagen type IV, but it can also interfere with BBB-EC-collagen type IV interactions and its silencing under pro-inflammatory conditions can partially rescue barrier dysfunction.

Originally named for its ability to "decorate" collagen strands, decorin was originally ascribed a regulatory role in collagen fibrillogenesis.[239] The protein core adopts a banana-like tertiary structure with twelve leucine-rich repeats (LRRs) providing a concave surface of parallel β-sheets (Figure 2.22) that interact with collagen fibrils.[240] However, to regulate their diameter and orientation, decorin additionally requires the covalent attachment of a sulfated glycosaminoglycan (GAG) chain close to its N-terminus (Ser34).[241] Given the deposition of fibril-forming collagens during inflammation,[193,194] it is straightforward to speculate that decorin may be secreted to combat any untoward fibrosis. In support of this, multiple groups have reported successful suppression or

dissolution of fibrotic scars in rodents subjected to spinal cord injury models following administration of recombinant decorin to the injury site.[242]

To complicate matters, however, it is now understood that decorin can play stimulatory or inhibitory roles in the interconnected processes of wound repair, angiogenesis, tumorigenesis, and autophagy, all in a highly context-specific manner.[243–245] In fact, as of 2016, decorin has been demonstrated to interact with at least 69 proteins, including integrins, growth factors, cytokines, and receptor tyrosine kinases.[244] Among these, the most notable are $\alpha_2\beta_1$, transforming growth-factor beta (TGF-β), tumor necrosis factor-alpha (TNF-α), and vascular endothelial growth factor receptors (VEGFRs). Under acellular conditions, decorin interacts with the ectodomain of $\alpha_2\beta_1$, but not $\alpha_1\beta_1$, via its GAG chain and can modulate the interactions of $\alpha_2\beta_1$ with a recombinant mini-collagen (FC3).[246] These interactions were allosteric as decorin did not interact with FC3 or the collagen-binding region of $\alpha_2\beta_1$.[246] As for the others, dysregulated TGF-β-, TNF-α-, and VEGF-dependent signaling are all observed in MS.[247–249] Moreover, all can impair barrier function and claudin-5 expression in cultured BBB-ECs.[112,250,251] From this perspective, decorin could play a protective or damaging role in BBB function depending on which proteins it interacts with and at what point in the disease course.

Decorin is a known transcriptional target of FoxO1 in primary HUVECs and primary bovine LMVECs when angiopoietin (Ang)-Tie receptor signaling is altered.[252,253] Under healthy conditions, pericyte- and astrocyte-derived Ang-1 binds to endothelial Tie2 receptors which promotes Akt-dependent phosphorylation of FoxO1 (Figure 2.23A).[252–257] Additionally, basal expression of Ang-2 by endothelial cells promotes Tie2 signaling in the presence of the orphan receptor Tie1.[258] During inflammation, however, the

ectodomain of Tie1 is cleaved and Ang-2 expression increases, shifting it to an antagonistic role (Figure 2.23B).[258–261] Interestingly, Ang-2 itself is a transcriptional target of FoxO1, suggesting a positive feedback loop between it and FoxO1 during inflammation.[256]

Recently, Li *et al.* reported that Ang-2 is upregulated in EAE.[261] Moreover, mice with endothelial-restricted overexpression of Ang-2 (*Ang2*-EC^{KI}) suffered worsened disease and barrier dysfunction, while prophylactic blockade of Ang-2 in wild-type mice ameliorated disease and minimized barrier leakage.[261] Separately, Gurnik *et al.* reported that the brain microvessels isolated from *Ang2*-EC^{KI} mice had lower total claudin-5 protein.[260] In line, Blecharz *et al.* reported that blockade of Ang-2 rescued barrier function and claudin-5 gene expression in immortalized mouse BBB-ECs (cEND) incubated with sera from patients with Moyamoya disease.[262] Thus, altered Ang-Tie signaling during inflammation may concurrently promote decorin and suppress claudin-5 through FoxO1.

Future studies that are needed include: 1) using decorin with or without its GAG chain to isolate the contribution of each, 2) using substrates containing decorin and collagen type I to determine whether the additional presence of decorin modulates the response by BBB-ECs to collagen type I, and 3) using Ang-2 or FoxO1-specific inhibitors to probe whether they are involved in decorin deposition during inflammation.

Conclusion

In this dissertation, I have explored how deposition of inflammation-associated proteins into the vascular BM may contribute to BBB dysfunction or claudin-5 expression. Specifically, I focused on the proteins decorin and collagen type I, both of which are observed in MS and EAE during active disease.[193,194] I analyzed the brains of mice induced with EAE at the pre-onset stage and observed decorin in the BM of mice already suffering

BBB dysfunction. Additionally, I conducted cell culture studies using primary mouse BBB-ECs, overall finding an inverse relationship between decorin or collagen type I with barrier function or claudin-5. Taken together, this work suggests that inflammation-associated alterations to the BM occur early in the disease progression and can contribute to BBB dysfunction by suppressing expression of tight junction proteins like claudin-5.

Future Directions of Our Lab

Evaluating SLRP-knockout *in vivo*

Given the results using our cell culture model (Figure 2.16), we plan to test whether silencing decorin rescues BBB dysfunction *in vivo*. At the beginning of this project, we acquired *Dcn*-floxed mice (a kind gift from Dr. David Birk, University of Florida) and pan-endothelial-restricted Cre (*Tie2-Cre*) mice. However, a complicating factor when assessing decorin *in vivo* is that another class I SLRP, biglycan, can functionally compensate for its loss under certain circumstances.[263] Therefore, we additionally acquired *Bgn*-floxed mice from Dr. Birk with the goal of creating a three experimental lines: *Tie2-Cre* x *Bgn*-floxed (TB), *Tie2-Cre* x *Dcn*-floxed (TD), and *Tie2-Cre* x *Bgn*-floxed x *Dcn*-floxed (TBD).

Over the course of breeding, we isolated primary mouse BBB-ECs from Cre-negative littermates and incubated them with PMN-ETcA-CM following recombination with our TAT-Cre-based strategy (note: the data presented in Figures 2.16 & 24 are from the same experiment). Although each knockout group initially had different tracing profiles over the first 8 hours, all three plateaued to a comparable level by 16 hours (Figure 2.24D; $p > 0.05$, one-way ANOVA with post-hoc Tukey's). For all three, a significant rescue in barrier dysfunction was found compared to *Dcn*-floxed monolayers incubated with TAT-HA2 only as a control (Figures 2.24A-C; $p < 0.05$ for each, one-way ANOVA with post-

hoc Tukey's). Strictly speaking, the *Dcn*-floxed allele was not completely fixed at the time of this experiment in the BD line, meaning that these monolayers still carried a single wild-type allele. Regardless, complete ablation of biglycan and hemizygous ablation of decorin was sufficient to ameliorate barrier dysfunction.

Because biglycan is carried on the X chromosome,[264] we achieved the TB line before the others. Following twice daily injection of tamoxifen for five consecutive days, a cohort of TB mice and their Cre-negative littermates were allowed to recover for 14 days, then were induced with EAE. To our surprise, the disease course for both groups was comparable over 31 *d.p.i.* (Figure 2.25). Concerned that we may not be achieving efficient recombination *in vivo*, we crossed *Tie2-Cre* mice with *Ai14* mice (TA). Offspring with the TA genotype were injected with tamoxifen, allowed to recover, then had their brains harvested for analysis by confocal microscopy. As shown in Figure 2.26, only a small number of TL-stained vessels (*red*) exhibited TdTomato expression (*green*) in the cerebellum, suggesting poor recombination efficiency.

To circumvent this, we started our breeding over with a *Slco1c1-Cre* line (a kind gift from Dr. Markus Schwaninger, University of Lübeck, Germany) as its expression is primarily restricted to BBB-ECs.[265] Again, we achieved the *Slco1c1-Cre* x *Bgn*-floxed line (SB) before the *Slco1c1-Cre* x *Dcn*-floxed (SD) or *Slco1c1-Cre* x Bgn-floxed x Dcn-floxed (SBD). To compare recombination efficiency, we injected SB, TB, or Cre-negative littermates with tamoxifen, allowed them to recover, then isolated their brain mi7rovessels for analysis by PCR and agarose gel electrophoresis. As shown in Figure 2.27, products for the floxed allele were observed for all three lines. However, a product for the excised allele was only observed in the SB mice, suggesting that our tamoxifen regimen was not at

fault for the poor recombination in TB mice. As cohorts of SB, SD, and SBD mice become available, studies with EAE will be conducted to determine whether SLRP-knockout alters the disease course, BBB dysfunction, or claudin-5 expression.

Therapeutic Targeting of Tight Junctions to Rescue Barrier Function

Given their importance in barrier integrity, preservation or restoration of tight junctions for diseases in which BBB dysfunction occurs could be a viable strategy.[38] Strictly speaking, several FDA-approved disease-modifying drugs already have known pro-barrier or pro-tight junction properties. For example, glucocorticoids (GCs) can promote endothelial barrier function through transactivation of claudin-5 and occludin gene expression in human and bovine retinal ECs[266,267] or in mouse BBB-ECs.[268,269] Moreover, their administration undoes pro-inflammatory cytokine-induced suppression of claudin-5 or occludin in mouse BBB-ECs.[269,270] However, their long-term administration is not ideal for chronic diseases like MS as it elevates a patient's risk for infection or for other diseases like osteoporosis and cardiovascular disease.[271,272] Similarly, sphingosine 1-phosphate receptor (S1PR) modulators like fingolimod promote barrier function and claudin-5 gene expression in human BBB-ECs, including those exposed to the sera from patients with RR-MS during relapse (Figure 1.11). As with GCs, unfortunately, administration of S1PR modulators is associated with increased risks of infection.[273] Furthermore, they are contraindicated for patients with pre-existing cardiovascular conditions.[274] Thus, the identification of alternative compounds is warranted.

We recently demonstrated the utility of the selective insulin receptor (IR) agonist demethylasterriquinone B1 (DMAQ-B1) to rescue BBB dysfunction close to the onset of disease in EAE.[34] A single dose of DMAQ-B1 (5 mg/kg) via oral-gavage at 7 days post-

induction minimized the extravasation of NaFluor and EB, plus preserved total claudin-5 protein levels in the brain homogenates of treated animals (Figures J.7E-H).[34] Complementary cell culture studies using primary mouse BBB-ECs revealed that DMAQ-B1 dose-dependently promoted claudin-5 expression (Figure J.4D) and barrier function (Figures J.6A-C). Also, morphometric assessment of claudin-5 in DMAQ-B1-treated cells using Imaris software showed increased claudin-5 density at the tight junctions (Figure J.5). Taken together, these data suggest that promotion of claudin-5 via IR agonism during inflammation can preserve BBB function.

As its name suggests, DMAQ-B1 is a quinone derivative.[275,276] Unfortunately, quinones are non-ideal backbones for drug molecules as long-term they are cytotoxic.[277] To facilitate the identification of other potentially beneficial compounds, we have optimized an in-cell Western (ICW) assay for claudin-5 using a 96-well format (for an explanatory graphic, see Figure 2.28). As a proof-of-principle, we seeded immortalized mouse BBB-ECs (bEnd.3) at confluence into wells coated with collagen type IV. However, monolayers were administered methylprednisolone (MP; 10 µg/mL) with or without DMAQ-B1 (5 µM) when they were still only partially mature (2 *d.p.s.*) to ensure that their claudin-5 expression would not be maximal. As shown in Figure 2.29B, administration of MP significantly increased claudin-5 ($p < 0.05$, one-way ANOVA with post-hoc Tukey's). In turn, the additional presence of DMAQ-B1 further increased claudin-5 and was significantly greater than MP alone ($p < 0.05$, one-way ANOVA with post-hoc Tukey's). With this assay established, our lab will be able screens compounds across multiple concentrations or combinations in a more rapid manner than traditional formats.

Chapter Two Figures

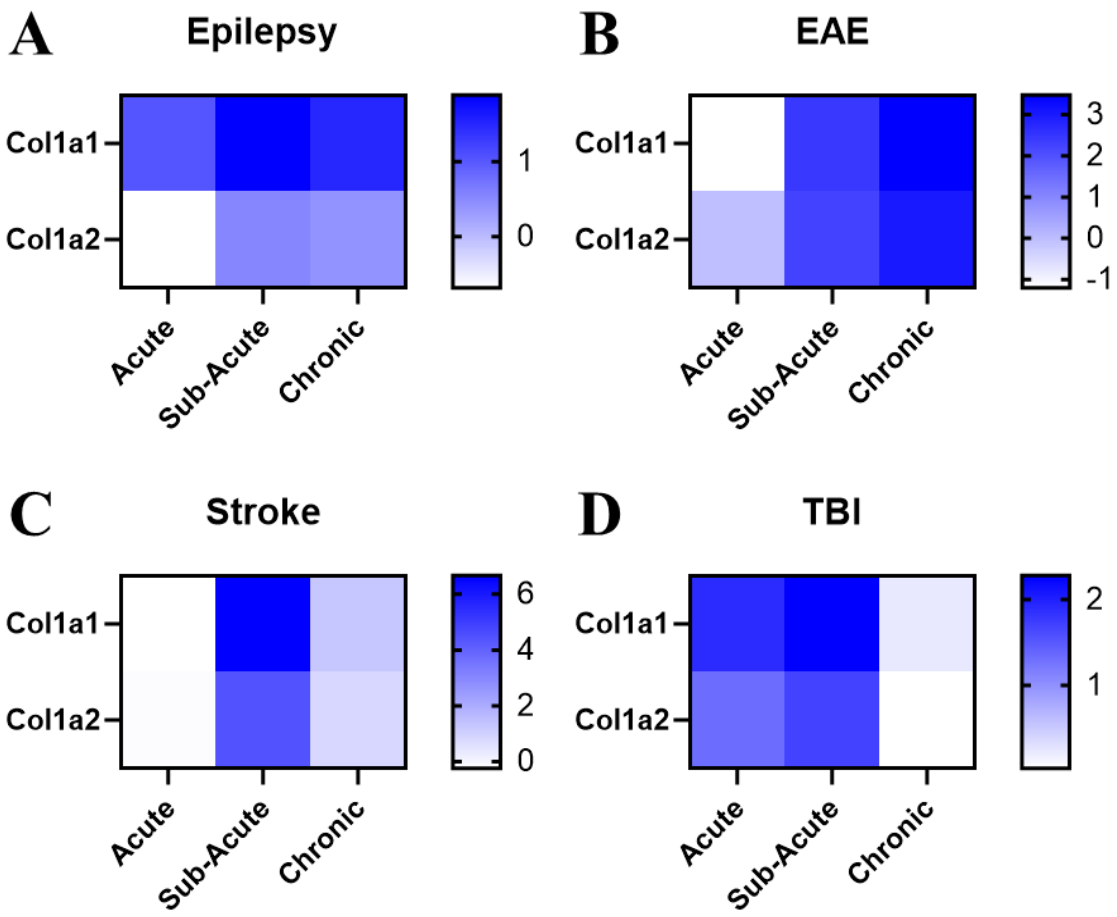

Figure 2.1. Collagen Type I Gene Expression is Upregulated in CNS Disease.

A publicly available RNA-Seq data set that identified differently expressed genes in CNS-ECs common to four animal models across their disease course was queried for expression of collagen type I (*Col1a1* & *Col1a2*).[194] A heat map for each model was created, with the scale reflecting the $\log_2$-transformed fold-change with respect to the control. **A.** Kainic acid model of epilepsy. **B.** MOG_{35-55}-based EAE. **C.** Middle cerebral artery occlusion model of stroke. **D.** Controlled focal cortical impact model of pediatric traumatic brain injury.

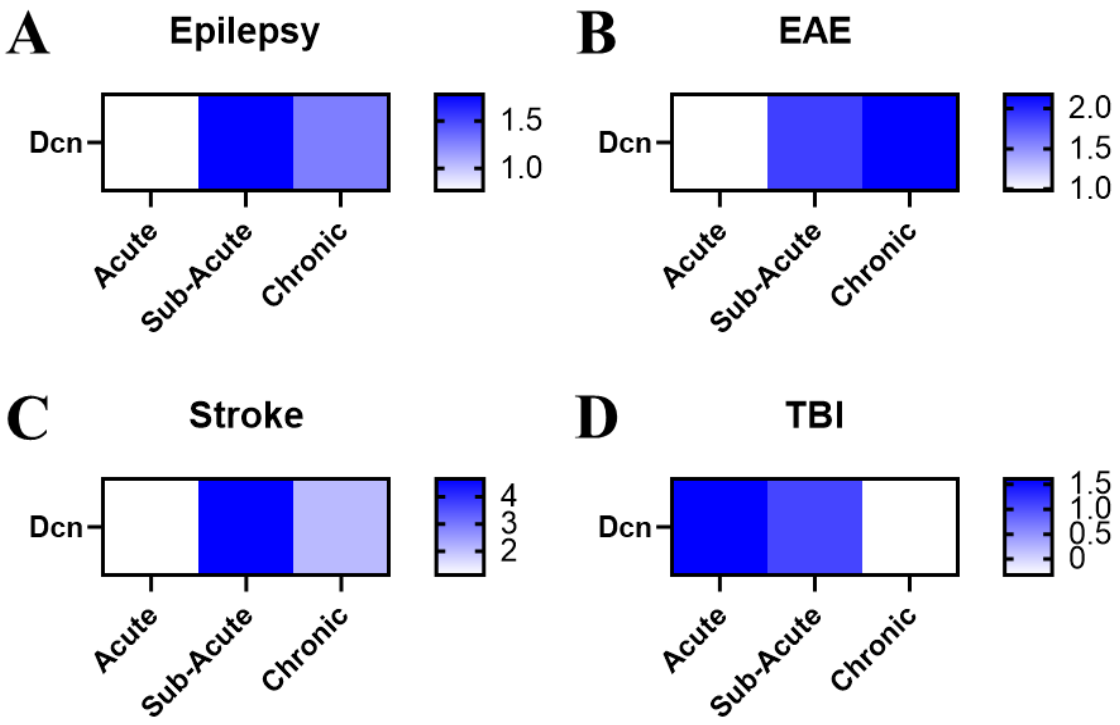

Figure 2.2. Decorin Gene Expression is Upregulated in CNS Disease.

A publicly available RNA-Seq data set that identified differently expressed genes in CNS-ECs common to four animal models across their disease course was queried for expression of decorin (*Dcn*).[194] A heat map for each model was created, with the scale reflecting the $\log_2$-transformed fold-change with respect to the control. **A.** Kainic acid model of epilepsy. **B.** MOG_{35-55}-based EAE. **C.** Middle cerebral artery occlusion model of stroke. **D.** Controlled focal cortical impact model of pediatric traumatic brain injury.

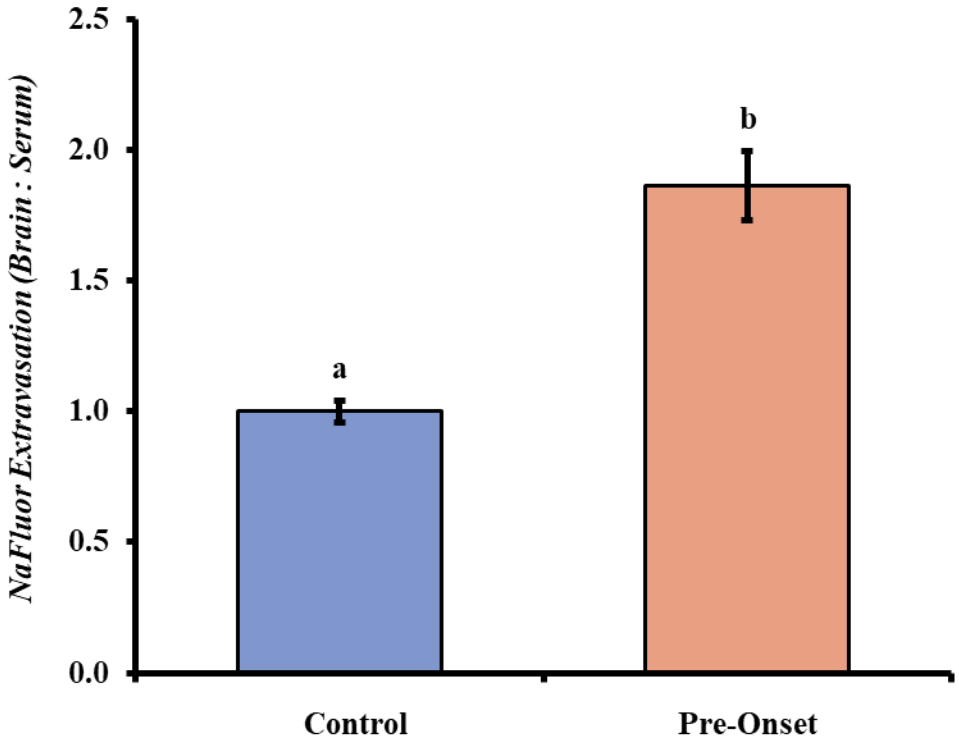

Figure 2.3. BBB Integrity is Compromised Before Onset in EAE.

Wild-type C57BL/6 mice (n = 6) were induced with active MOG_{35-55}-based EAE. 8 days post-induction, animals lacking clinical scores were injected *i.p.* with sodium fluorescein (**NaFluor**). Two hours later, animals were sacrificed, tracer concentrations in their brain homogenates and blood sera were determined, and the ratio of the brain concentration to the serum concentration was calculated. As controls, animals not induced with EAE (n = 6) were treated in the same manner. Error bars represent the standard deviation of the mean. Groups marked with different letters are statistically different from each other ($p < 0.05$, Student's *t*-test).

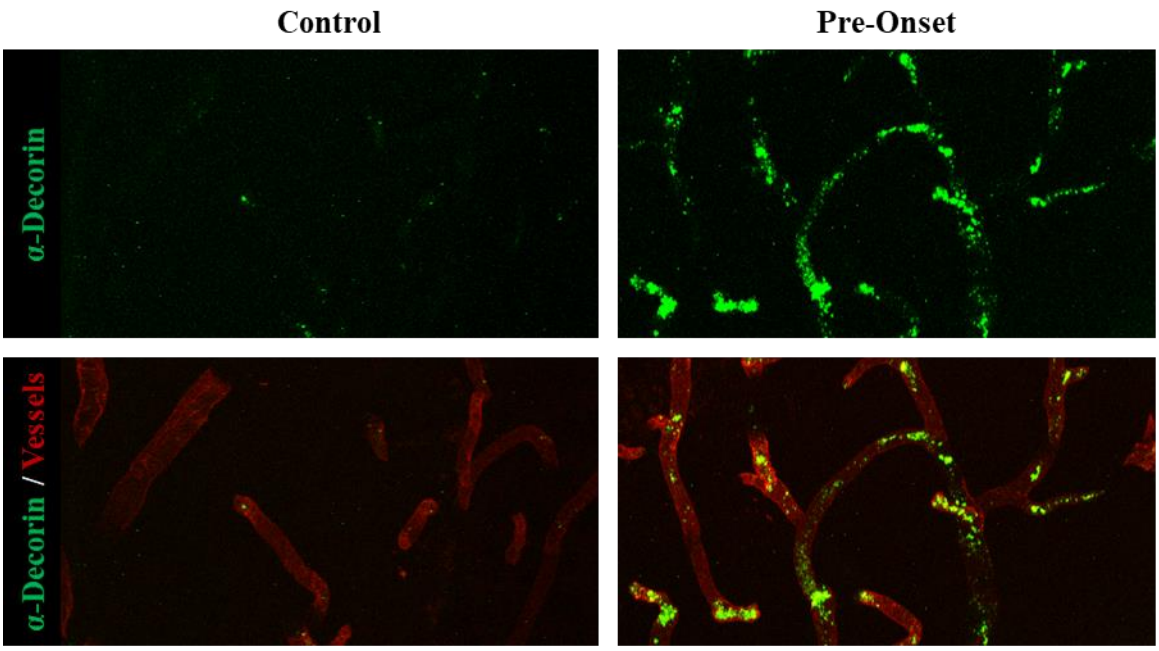

Figure 2.4. Decorin is Deposited Before Onset in EAE.

Wild-type C57BL/6 mice (n = 6) were induced with active MOG_{35-55}-based EAE. 8 days post-induction, animals lacking clinical scores were anesthetized and injected *t.c.* with TL-DyLight 649 to label the endothelium (*red*). Animals were then flushed, decapitated, and their brains processed for immunolabeling with an antibody against decorin conjugated with AF488 (*green*). As controls, animals not induced with EAE (n = 6) were treated in the same manner. A representative micrograph for each group is shown above.

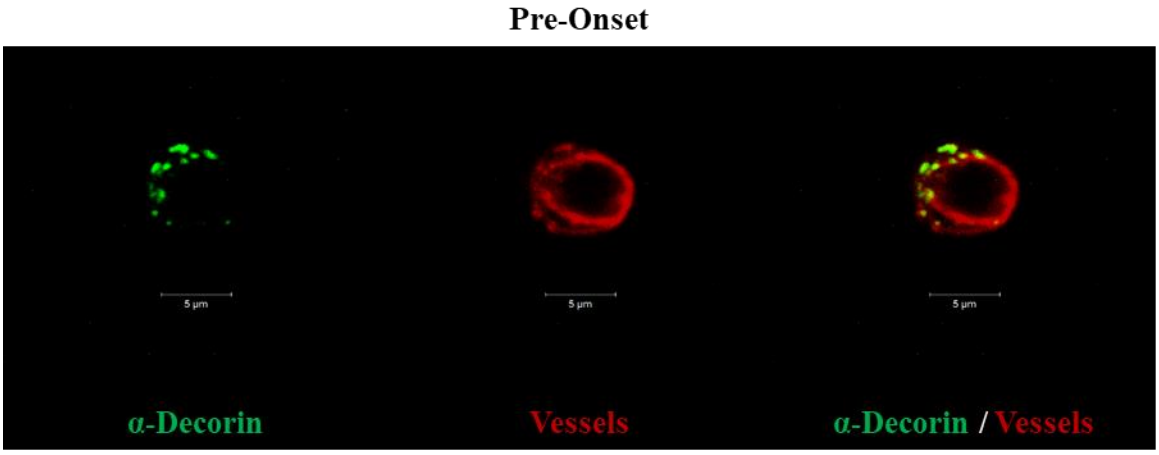

Figure 2.5. Decorin is Deposited at the Pre-Onset Stage of EAE.

Wild-type C57BL/6 mice (n = 6) were induced with active MOG_{35-55}-based EAE. 8 days post-induction, animals lacking clinical scores were anesthetized and injected *t.c.* with TL-DyLight 649 to label the endothelium (*red*). Animals were then flushed, decapitated, and their brains processed for immunolabeling with an antibody against decorin conjugated with AF488 (*green*). Scale bar = 5 µm.

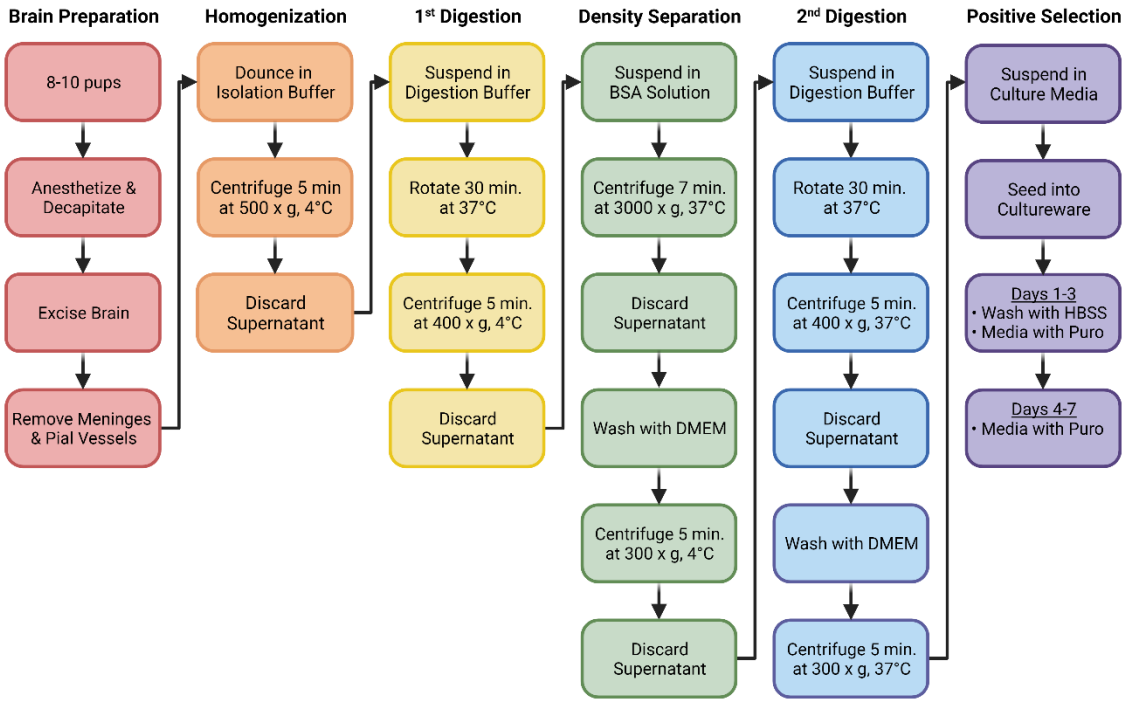

Figure 2.6. Primary Mouse BBB-EC Isolation Protocol.

A six-part protocol was devised and optimized to isolate primary mouse BBB-ECs from 7–10-day-old pups. Created with BioRender.com.

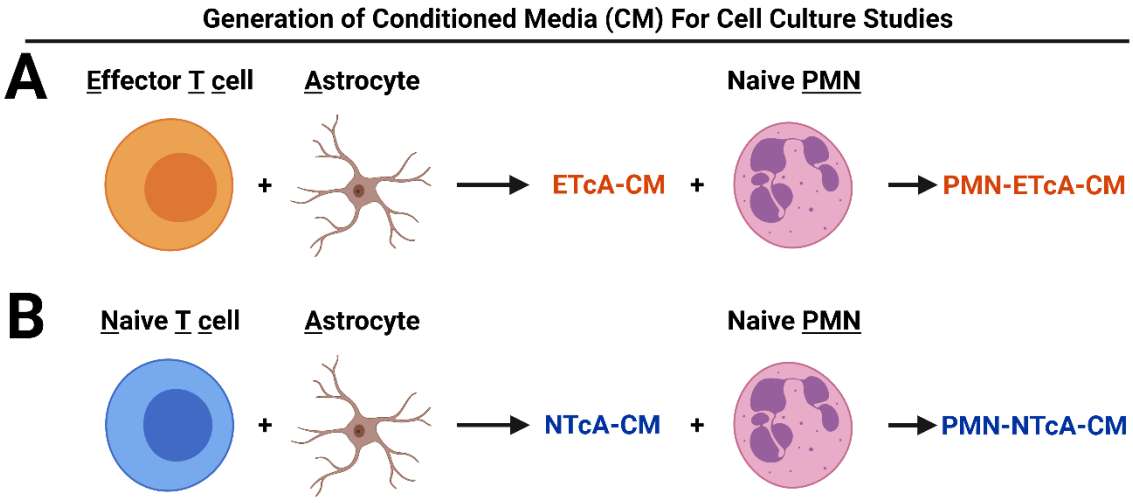

Figure 2.7. Experimental Design for Generating Conditioned Media.

A. Lymphocytes isolated from wild-type C57BL/6 mice induced with MOG_{35-55}-based EAE were pooled and activated in the presence of MOG_{35-55} peptide, IL-12, and an anti-IFN-γ antibody. Incubation of these cells with astrocytes yielded conditioned media (**CM**) termed **ETcA-CM**. In turn, incubation of naïve neutrophils (**PMN**) with this media yielded a second media termed **PMN-ETcA-CM**. **B.** Control CM were generated using lymphocytes isolated from animals not induced with EAE (**naïve**). Incubation of these cells with astrocytes yielded media termed **NTcA-CM**. In turn, incubation of naïve PMNs with this media yielded a second media termed PMN-NTcA-CM. Created with BioRender.com.

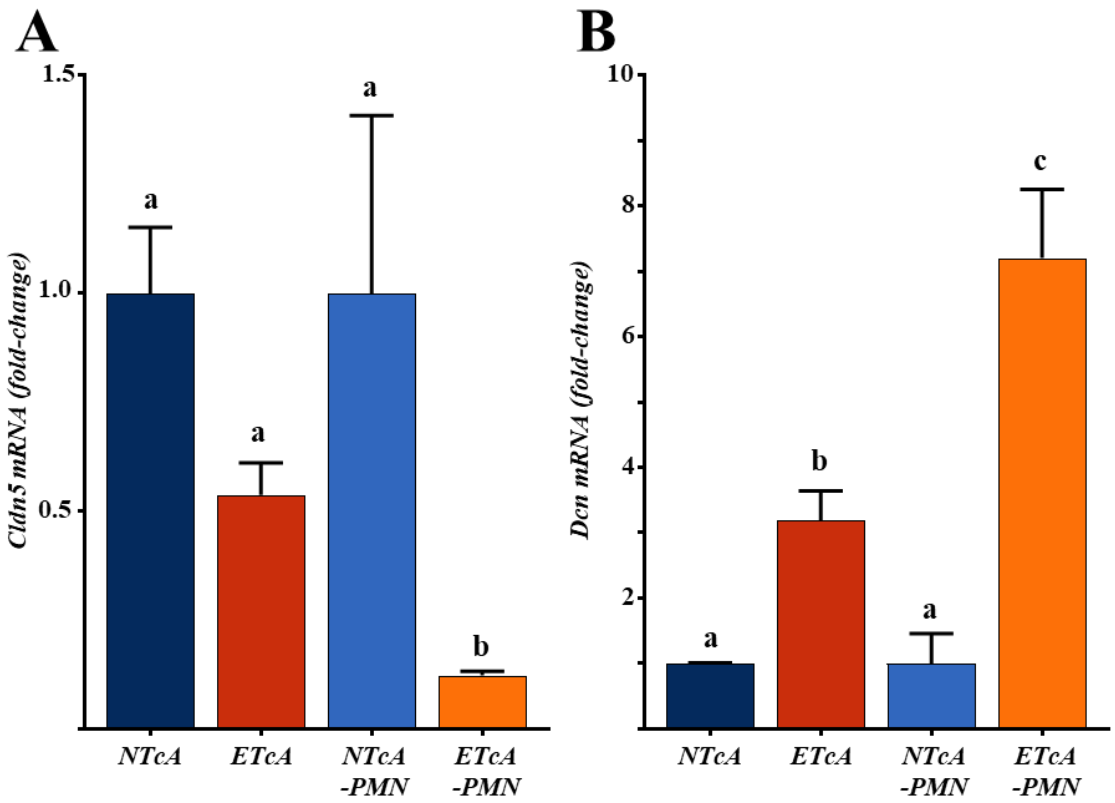

Figure 2.8. CM-induced Alterations in *Cldn5* & *Dcn* Expression.

Wild-type primary BBB-ECs were incubated with one of four conditioned media: Naïve T cell-Astrocyte (NTcA – *purple*), Effector T cell-Astrocyte (ETcA – *red*), Neutrophil-Naïve T cell-Astrocyte (PMN-NTcA – *blue*), or Neutrophil-Effector T cell-Astrocyte (PMN-NTcA – *orange*). 24 hours later, cells were lysed and assessed for expression of *Cldn5* (**A**) or *Dcn* (**B**). For the reference gene, *Actb* was used. Technical duplicates were performed for each group (n = 2 wells each), and then $2^{-\Delta\Delta Cq}$ values were calculated with the NTcA group arbitrarily set as the control group. Error bars represent the standard deviation of the mean. Groups marked with different letters are statistically different from each other ($p < 0.05$, one-way ANOVA with post-hoc Tukey's test).

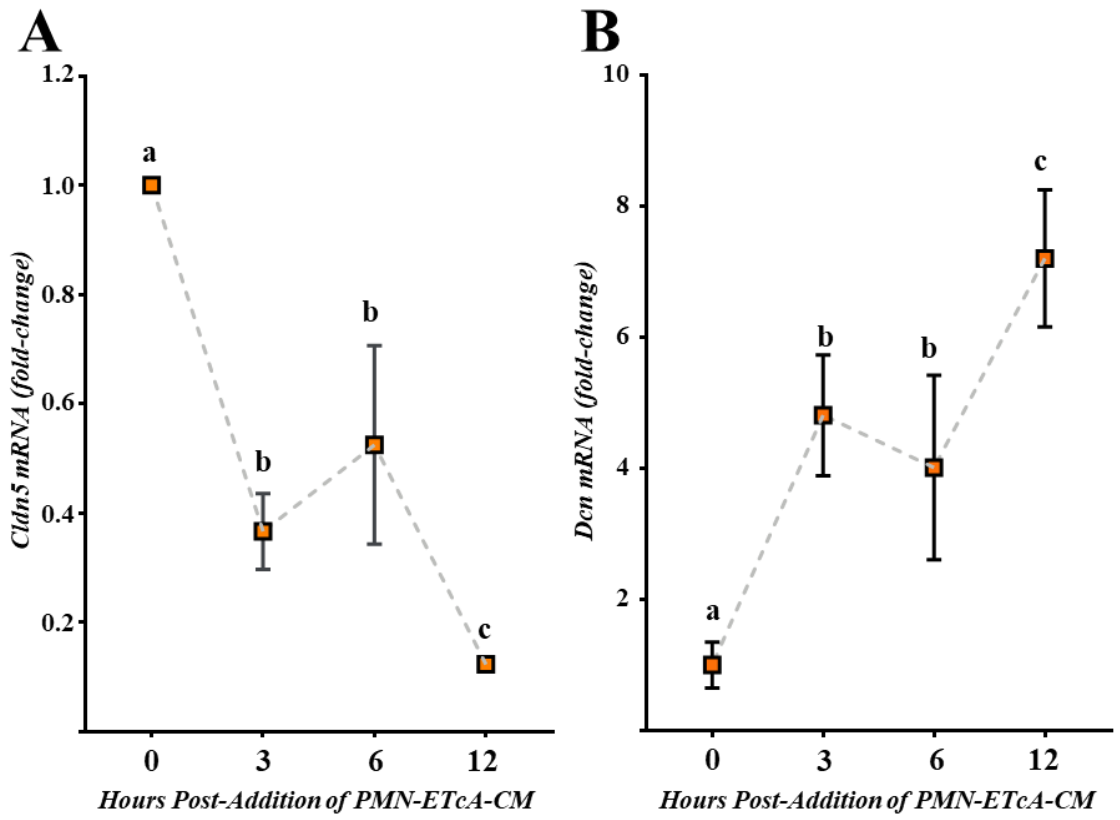

Figure 2.9. CM-induced Alterations in *Cldn5* & *Dcn* Expression.

Wild-type primary BBB-ECs were incubated with PMN-ETcA-CM for 0, 3, 6, or 12 hours. Cells were lysed and assessed for expression of *Cldn5* (**A**) or *Dcn* (**B**). For the reference gene, *Actb* was used. Technical duplicates were performed for each group (n = 2 wells each), and then $2^{-\Delta\Delta Cq}$ values were calculated with the zero-hour group arbitrarily set as the control group. Error bars represent the standard deviation of the mean. Groups marked with different letters are statistically different from each other ($p < 0.05$, one-way ANOVA with post-hoc Tukey's test).

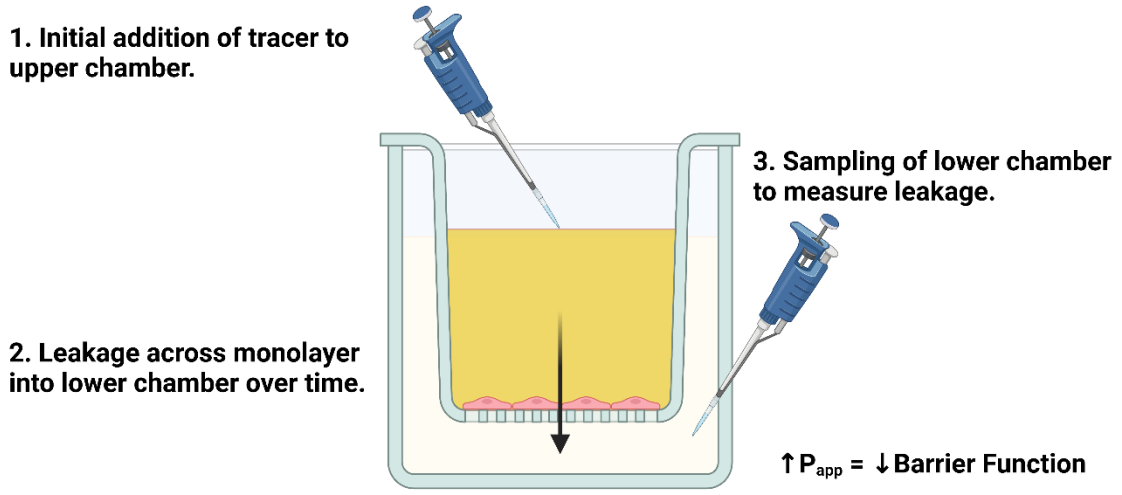

Figure 2.10. Principle of Permeability Assay for Modeling Barrier Function.

1. A known concentration of a tracer, such as sodium fluorescein, is added to the upper chamber of the transwell insert, upon which a cell monolayer has formed. **2.** The tracer is allowed to pass across the monolayer. **3.** Sampling of the lower chamber to determine tracer concentration and, in turn, calculation of the apparent permeability coefficient (higher coefficients reflect lower barrier function). Created with BioRender.com.

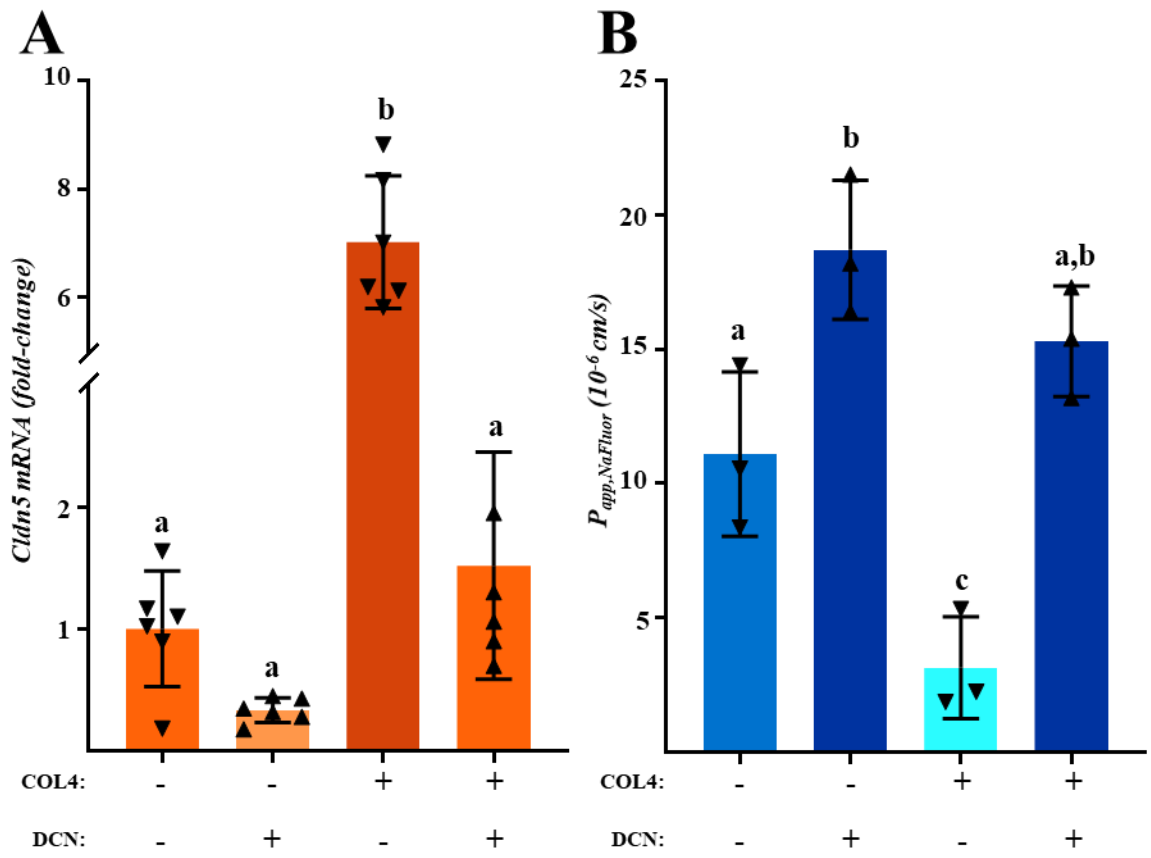

Figure 2.11. Modulation of Barrier Function by Decorin.

B. Mouse BBB-ECs were seeded at confluence into wells coated with decorin (DCN), collagen type IV (COL4), both, or neither. Following maturation, cells were lysed and assessed for expression of *Cldn5* or *Actb* as a reference gene. Technical duplicates were performed for each group (n = 3 wells each), and then $2^{-\Delta\Delta Cq}$ values were calculated with the no-substrate group arbitrarily set as the control group. Error bars represent the standard deviation of the mean. Groups marked with different letters are statistically different from each other ($p < 0.05$, Student's *t*-test). **B.** Mouse BBB-ECs were seeded at confluence into transwell inserts coated with decorin (DCN), collagen type IV (COL4), both, or neither. Following maturation, the apparent permeability coefficient (P_{app}) for the small solute tracer sodium fluorescein (NaFluor) was used to assess barrier permeability for each group (n = 3 inserts each). Error bars represent the standard deviation of the mean. Groups marked with different letters are statistically different from each other ($p < 0.05$, Student's *t*-test).

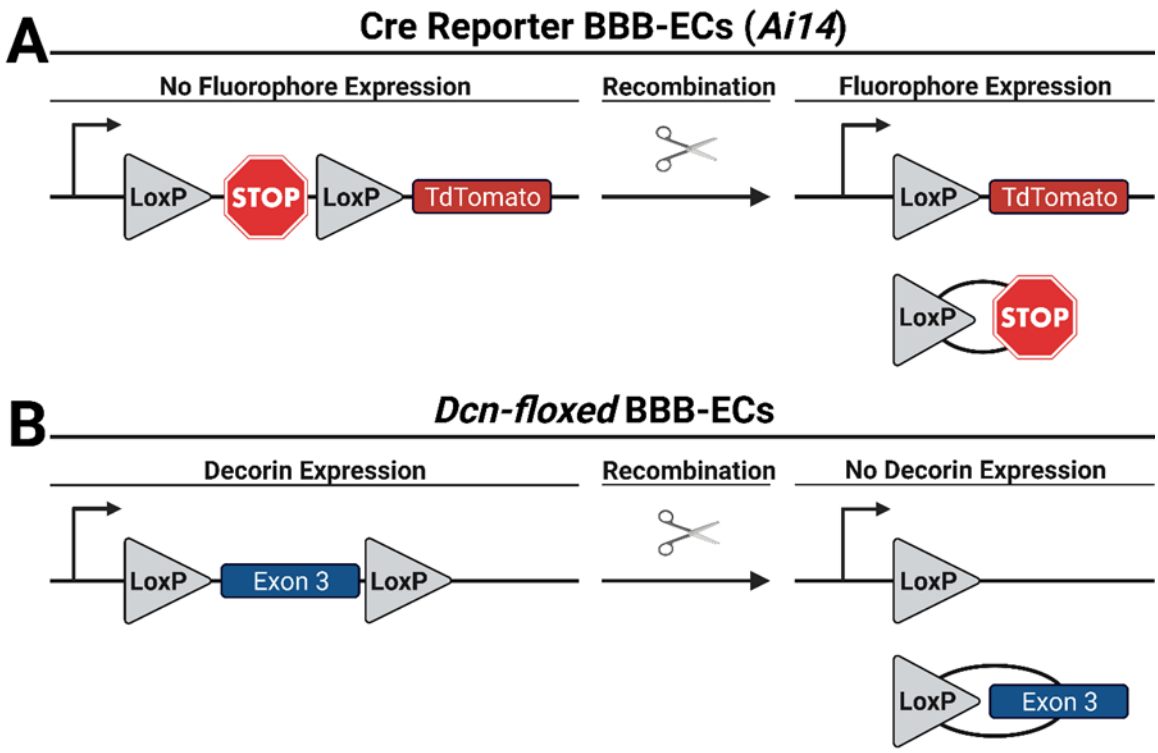

Figure 2.12. Principle of Cre-mediated Recombination.

A. The Cre reporter line *Ai14* carries a cassette containing a loxP-Stop-LoxP (LSL) sequence upstream of an open reading frame for the fluorophore TdTomato. Prior to recombination, the LSL sequence prevents transcription of TdTomato. In the presence of Cre, however, the stop sequence and one of the loxP sites are excised, permitting transcription of TdTomato. **B.** The *Dcn-floxed* line harbors loxP sites immediately upstream and downstream of exon 3. In the presence of Cre, the exon and one of the loxP sites are excised, thereby ablating decorin expression. Created with BioRender.com.

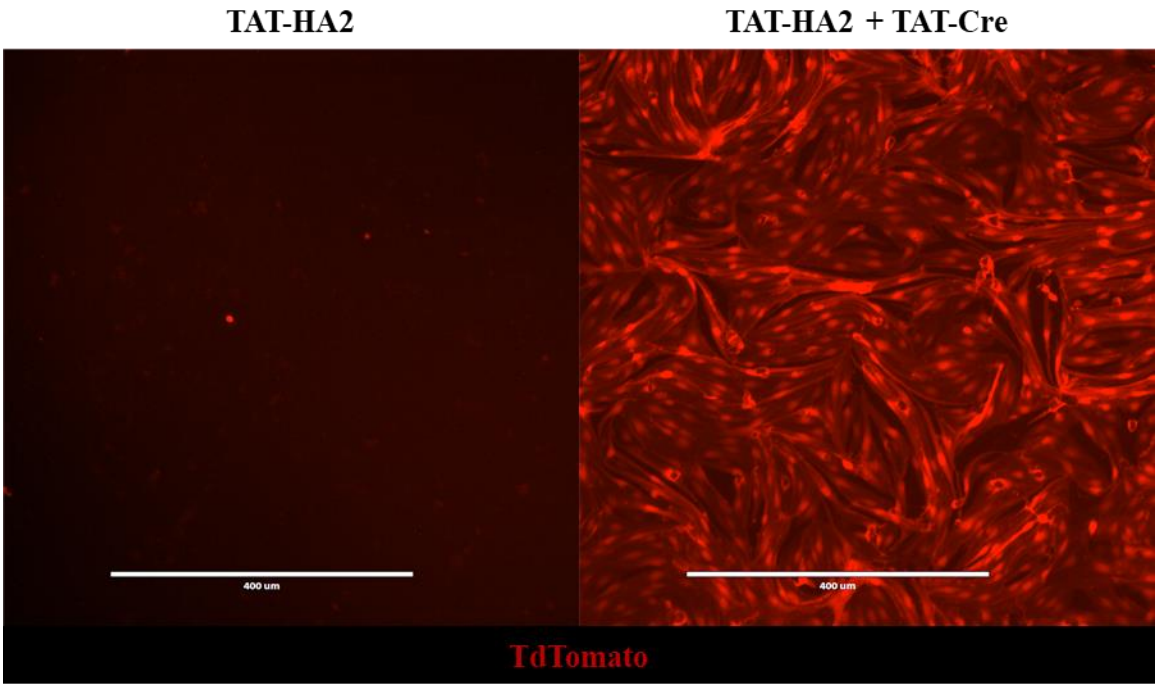

Figure 2.13. TAT-HA2 + TAT-Cre Efficiently Recombines *Floxed* Genes.

Mouse BBB-ECs isolated from *Ai14* mice were seeded at confluence onto glass-bottom wells coated with collagen type IV. Following maturation, monolayers were incubated for an hour with 5 µM TAT-HA2 in serum-free media alone (*left*) or additionally with 50 U/cm^2 TAT-Cre (*right*). Following a media change and 48 hours of recovery, monolayers were visualized with an epifluorescent microscope. **Note:** the dark spaces in the TdTomato channel (*right*) reflect non-recombined cells rather than holes in the monolayer (see Figure 2.15). Scale bar = 400 µm.

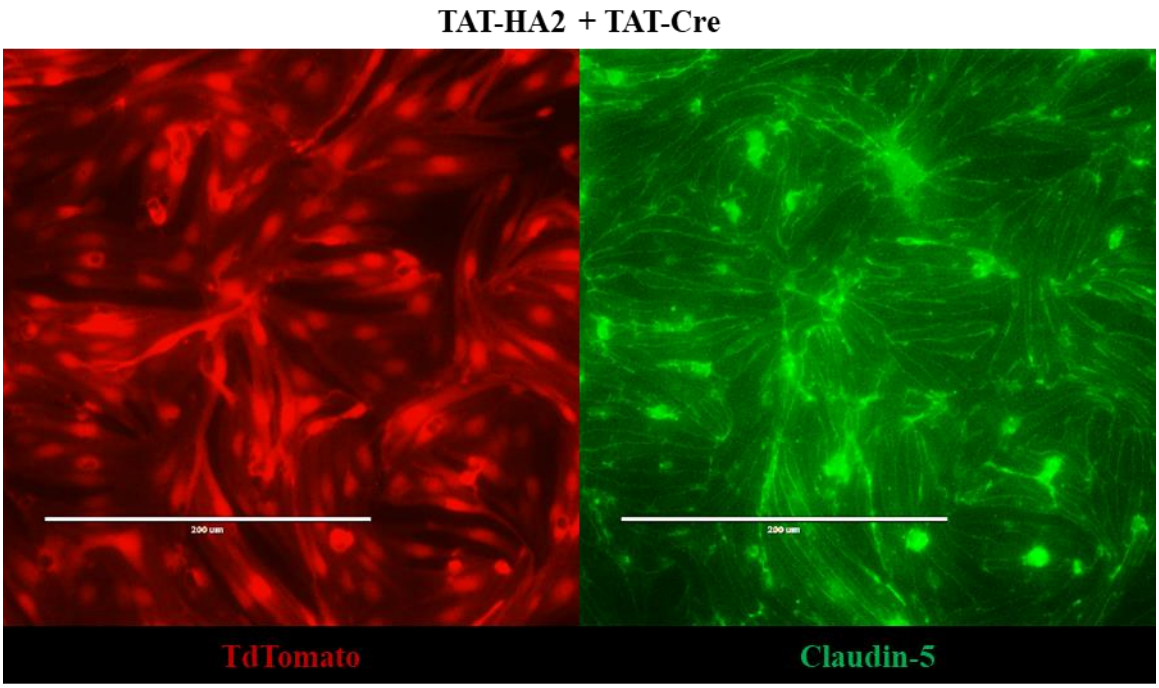

Figure 2.14. Claudin-5 is Present at the Tight Junctions of Recombined Cells.

Mouse BBB-ECs isolated from *Ai14* mice were seeded at confluence onto glass-bottom wells coated with collagen type IV. Following maturation, monolayers were incubated for an hour with 5 µM TAT-HA2 and 50 U/cm^2 TAT-Cre in serum-free media. Following a media change and 48 hours of recovery, monolayers were fixed and immunolabeled for claudin-5 expression. Monolayers were visualized with an epifluorescent microscope. **Note:** the dark spaces in the TdTomato channel (*left*) reflect non-recombined cells rather than holes in the monolayer as demonstrated by the continuous staining in the claudin-5 channel (*right*). Scale bar = 200 µm.

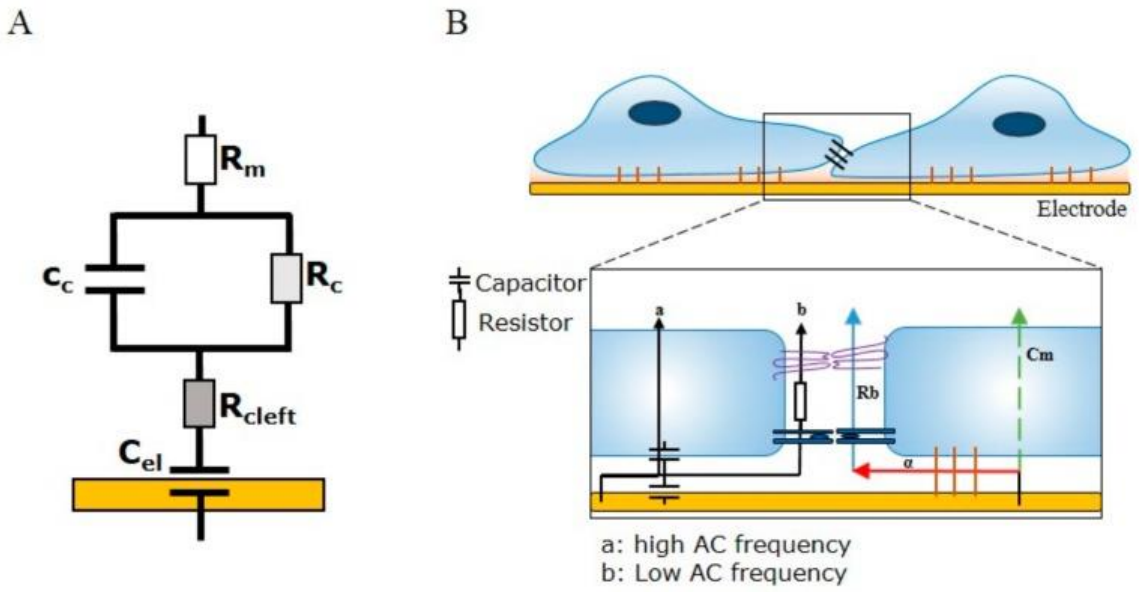

Figure 2.15. Principle of ECIS-TEER for Modeling Barrier Function.

A. Circuit diagram illustrating the relevant parameters for modeling ECIS-TEER. From top to bottom, this includes the resistance of the media ($\mathbf{R_m}$), the capacitance of the cell membrane ($\mathbf{C_c}$), the resistance of the cell ($\mathbf{R_c}$), the resistance of the basal cleft ($\mathbf{R_{cleft}}$), and the capacitance of the gold electrode ($\mathbf{C_{el}}$). **B.** The relative contributions of tight junctions ($\mathbf{R_b}$), cell-substrate interactions ($\boldsymbol{\alpha}$), and cell membrane composition ($\mathbf{C_m}$) can be modeled by varying the alternating current (**AC**) frequency. In general, lower frequencies like 4000 Hertz (Hz) are appropriate for assessing changes in $\mathbf{R_b}$ as current preferentially flows via paracellular pathways rather than via transcellular pathways. Figure minimally adapted from Robilliard *et al.*[278] in Biosensors (2018, Vol. 8, Issue 3) under a Creative Commons License (CC-BY).

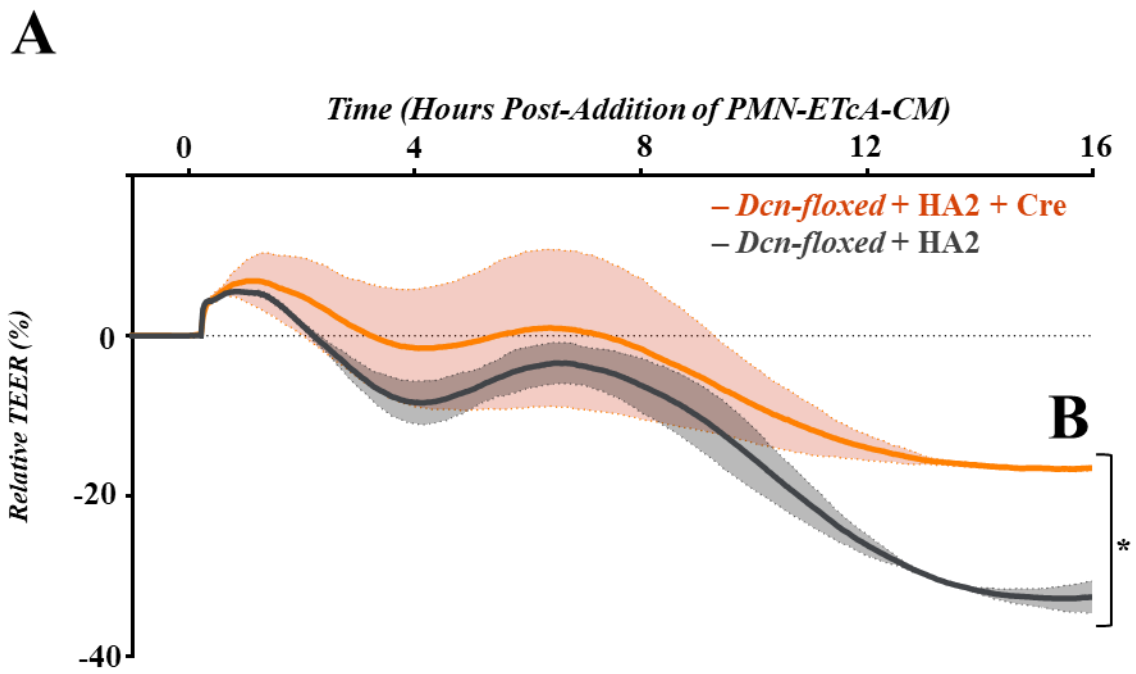

Figure 2.16. Loss of Decorin Expression Partially Rescues BBB Dysfunction.

A. Mouse BBB-ECs isolated from *Dcn-floxed* mice were seeded at confluence into 8W10E+ arrays coated with collagen type IV. Following maturation, monolayers were incubated with TAT-HA2 in serum-free media alone (*grey*) or additionally with TAT-Cre (*orange*) to ablate decorin gene expression. Following a media change and overnight recovery, monolayers were incubated with PMN-ETcA-CM and data was continuously collected at 4 kHz. Tracings were normalized to the zero-time point to determine the relative change in TEER (n = 2 wells each). Error bars represent the standard deviation. **B.** The peak change in TEER at 16 hours was significantly different between the two groups (*$p < 0.05$, unpaired Student's *t*-Test).

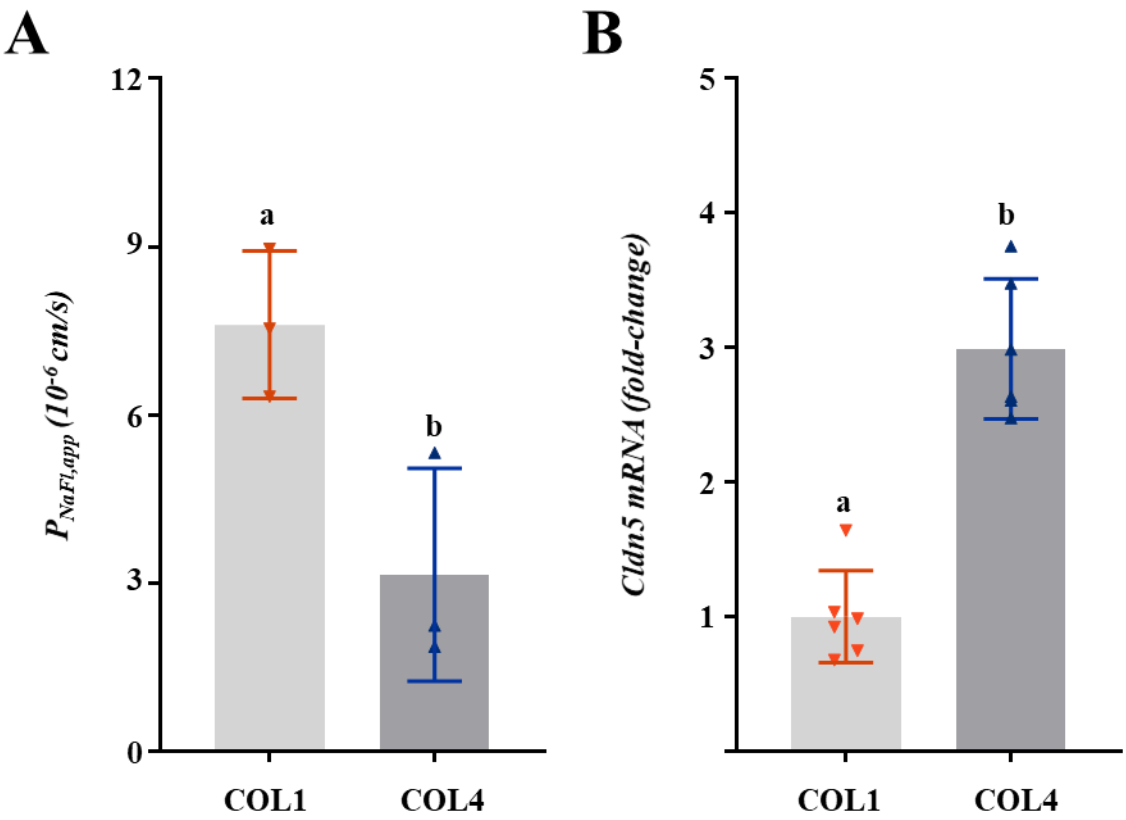

Figure 2.17. Influence of Collagen Type on Permeability & *Cldn5* Expression.

A. Mouse BBB-ECs were seeded at confluence into transwell inserts coated with collagen type I (COL1 – *orange*) or collagen type IV (COL4 – *blue*). Following maturation, the apparent permeability coefficient (P_{app}) for the small solute tracer sodium fluorescein (NaFluor) was used to assess barrier permeability for each collagen (n = 3 inserts each). Error bars represent the standard deviation of the mean. Groups marked with different letters are statistically different from each other ($p < 0.05$, Student's *t*-test). **B.** Mouse BBB-ECs were seeded at confluence into wells coated with collagen type I (COL1 – *orange*) or collagen type IV (COL4 – *blue*). Following maturation, cells were lysed and assessed for expression of *Cldn5* or *Actb* as a reference gene. Technical duplicates were performed for each collagen (n = 3 wells each), and then $2^{-\Delta\Delta Cq}$ values were calculated with the COL1 group arbitrarily set as the control group. Error bars represent the standard deviation of the mean. Groups marked with different letters are statistically different from each other ($p < 0.05$, Student's *t*-test).

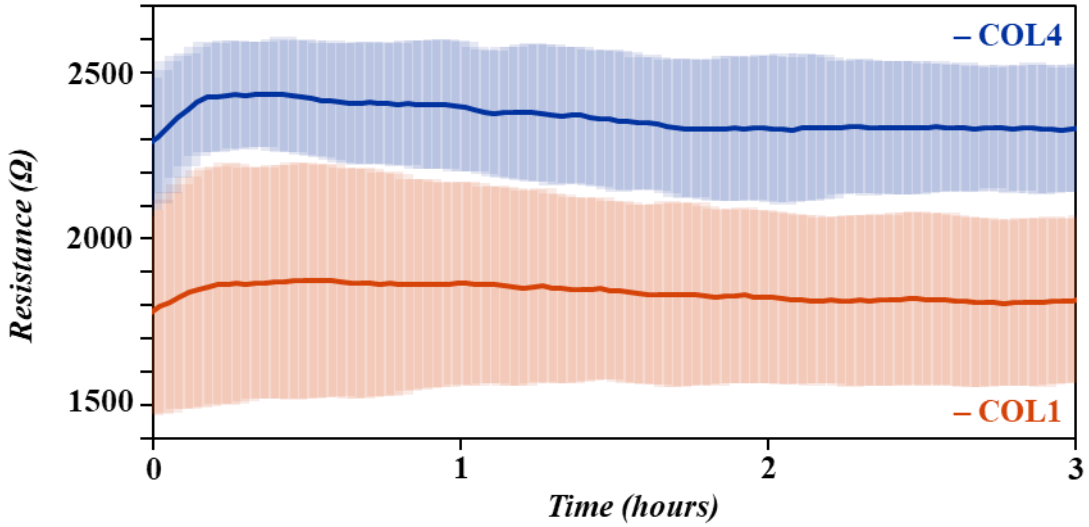

Figure 2.18. Influence of Collagen Type on TEER.

Mouse BBB-ECs were seeded at confluence into 8W10E+ arrays coated with collagen type IV (COL4 – *blue*) or collagen type I (COL1 – *orange*). Following maturation, data was continuously collected over a range of frequencies (62.5 Hz to 64 kHz) for three hours following an initial period of stabilization in the incubator (*not shown*). For this figure, the mean resistance value (**Ω**) and standard deviations for each collagen type (n = 3 wells each) collected at 4 kHz are plotted as a function of time.

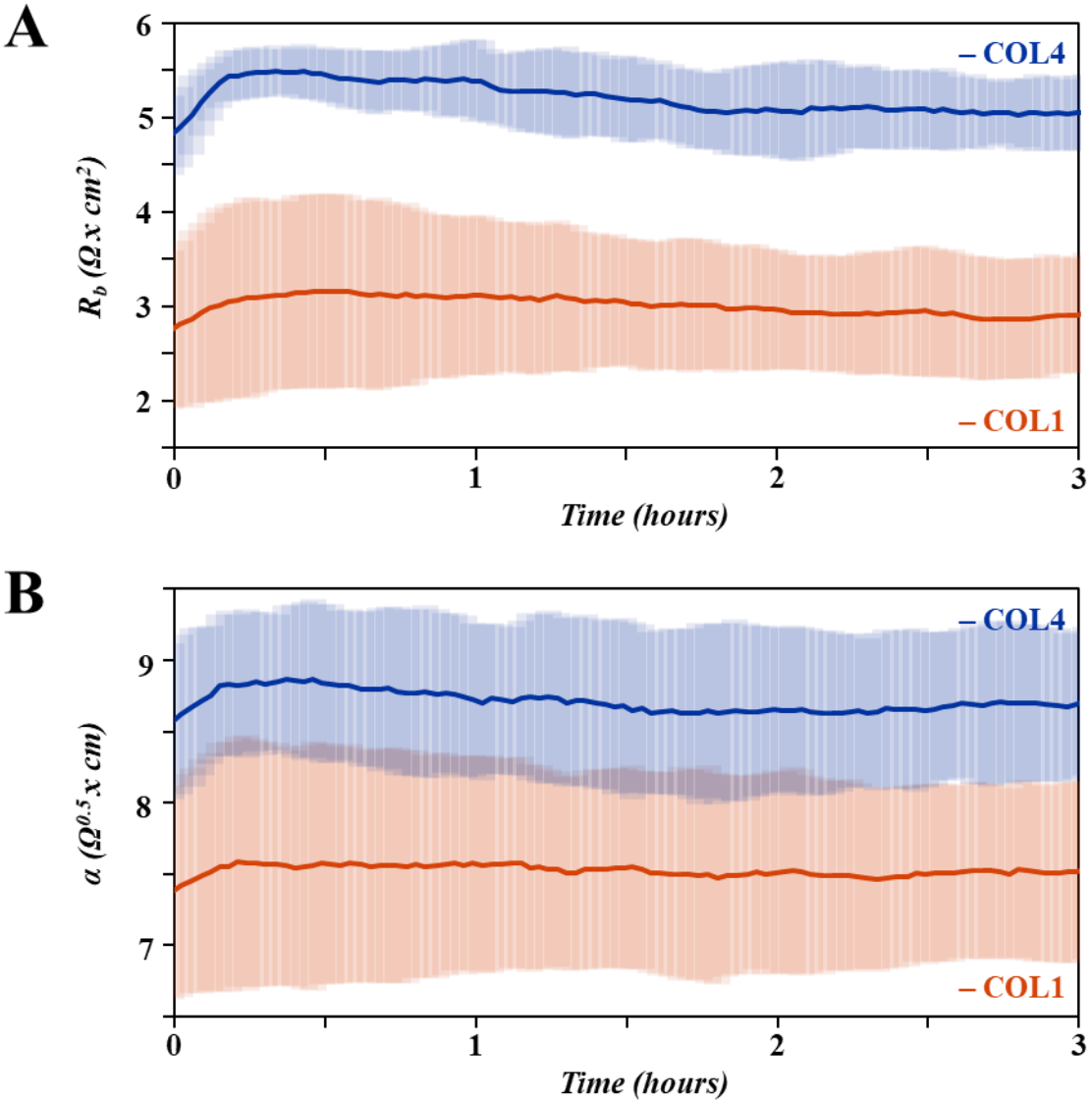

Figure 2.19. Influence of Collagen Type on R_b & α.

A. The mean **R_b** value (**Ω x cm^2**) and standard deviations for each collagen type (COL4 – *blue*, COL1 – *orange*) for the data presented in **Figure 2.7**. **B.** The mean **α** value (**$\Omega^{0.5}$ x cm**) and standard deviations for each collagen type (COL4 – *blue*, COL1 – *orange*) for the data presented in **Figure 2.7**.

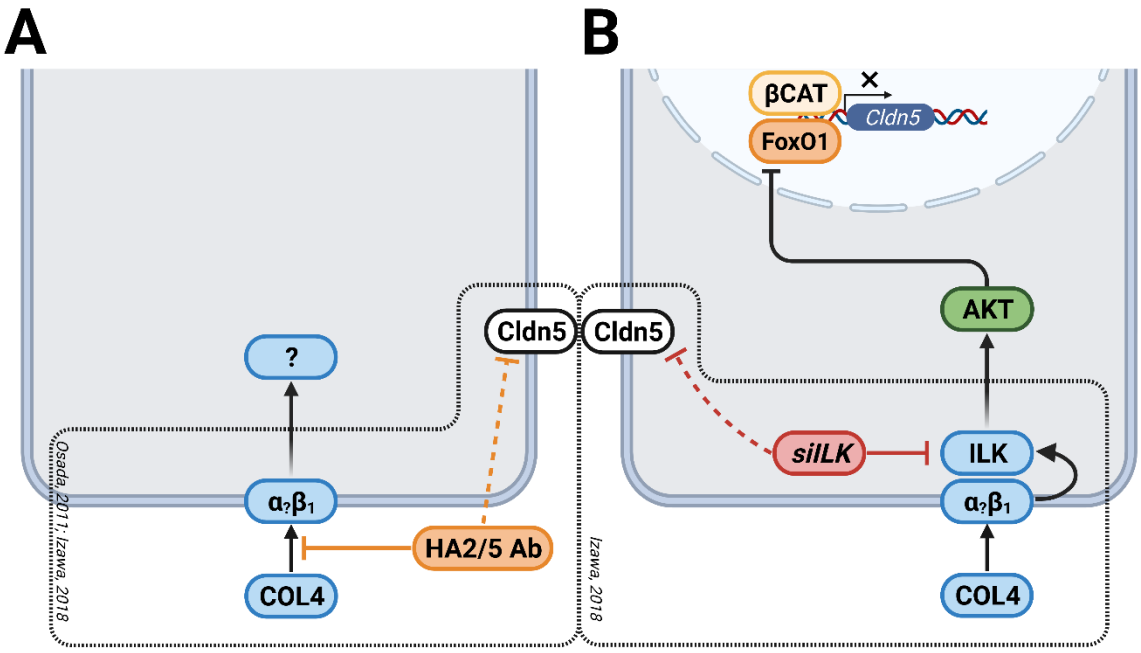

Figure 2.20. Known Collagen Type IV-involved Pathways in Endothelial Cells.

A. Antibody (Ab)-mediated blockade of collagen type IV (COL4)-β_1 integrin interactions (*orange – solid line*) suppresses claudin-5 (CLDN5) expression (*orange – dotted line*) through undetermined intermediaries.[190,191] $\alpha_?\beta_1$: Unknown α isoform. **B.** Silencing of integrin-linked kinase (ILK; *red – solid line*), a putative pseudo-kinase kinase that interacts with the cytoplasmic tail of β1, suppresses claudin-5 expression (*red – dotted line*) through undetermined intermediaries.[191] As the kinase Akt is a known downstream target of ILK, it is possible that loss of ILK lowers Akt activity, in turn impairing its ability to phosphorylate the transcription factor forkhead box protein O1 (FoxO1 - *orange*) so as to prevent formation of a transcriptional repressor complex with beta-catenin (βCAT - *yellow*) at the *Cldn5* promotor. siILK: siRNA-mediated silencing of *ILK*. Created with BioRender.com.

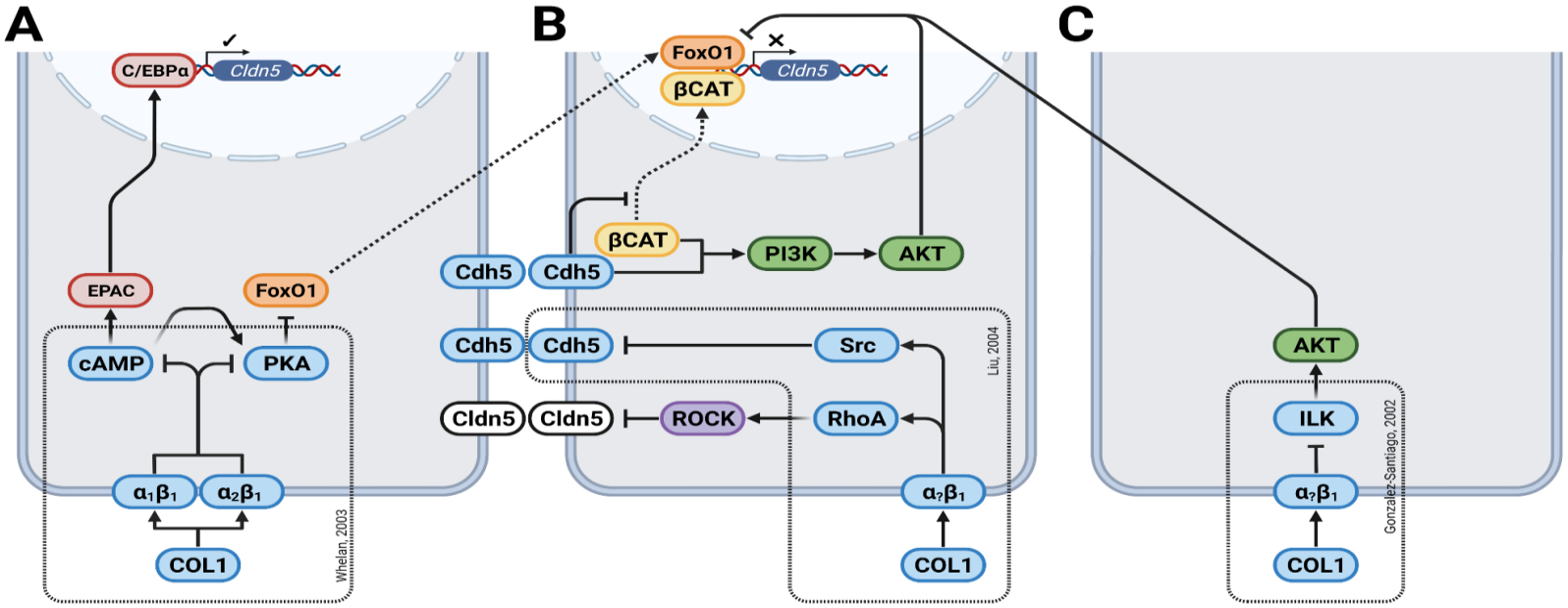

Figure 2.21. Known Collagen Type I-involved Pathways in Endothelial Cells.

A. Collagen type I (COL1) lowers cyclic AMP (cAMP) levels and protein kinase A (PKA) activity in an $\alpha_1\beta_1$- and $\alpha_2\beta_1$-dependent manner.[230] As cAMP and PKA are positively associated barrier function and claudin-5 (CLDN5) expression,[231] COL1 may impair a cAMP-exchange protein directly activated by cAMP (EPAC)-CCAAT/enhancer-binding protein-α (C/EBPα) axis (*red*).[232] Alternatively, COL1 may impair the ability of PKA to phosphorylate FoxO1 (*orange*).[233] **B.** COL1 elevates the activities of the small GTPase Ras homologue family member A (RhoA) and the kinase Src in a β_1-dependent manner.[234] Inhibition of either protein rescued the destabilization of vascular endothelial-cadherin (CDH5).[234] As CLDN5 is known to be phosphorylated by Rho-associated kinase (ROCK), a known downstream target of RhoA,[58] COL1 may directly signal for the removal of CLDN5 from tight junctions. Alternatively, destabilization of CDH5 liberates beta-catenin (βCAT – *yellow*) from the cell-cell contacts, in turn impairing a phosphoinositide 3-kinase (PI3K)-Akt signaling pathway (*green*) that phosphorylates FoxO1 (*orange*). $\alpha_?\beta_1$: Unknown α isoform. **C.** COL1 impairs ILK in a β_1-dependent manner.[236] As the kinase Akt is a known downstream target of ILK, it is possible that loss of ILK lowers Akt activity, impairing its ability to phosphorylate FoxO1 (*orange*). $\alpha_?\beta_1$: Unknown α isoform. Created with BioRender.com.

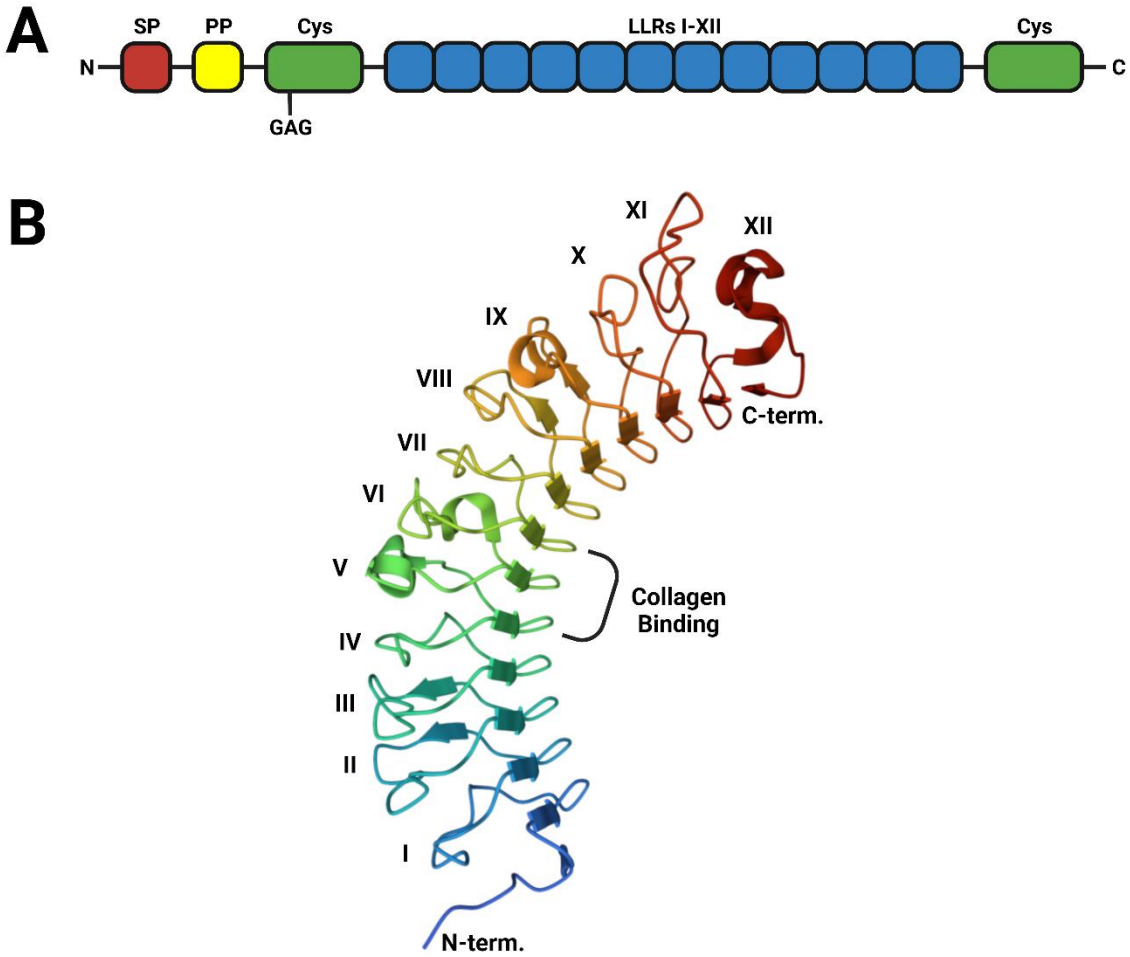

Figure 2.22. Structural Features of Decorin.

A. Domain structure of the protein core. N: N-terminus. SP: signal peptide. PP: Propeptide. GAG: Point of GAG chain attachment (Ser34). Cys: Cysteine-rich region. LRR: Leucine-rich repeat. C: C-terminus. **B.** Solved crystal structure for the protein core of bovine tissue-derived decorin (PDB: 1XCD). Each LRR is denoted by Roman numerals (I-XII). The crystal structure was visualized using MolStar (M*) viewer[279] and colored by sequence. Note: The first 21 residues of the mature protein, within which resides the DEASGIG motif for GAGylation, are not shown due to conformational disorder. Created with BioRender.com.

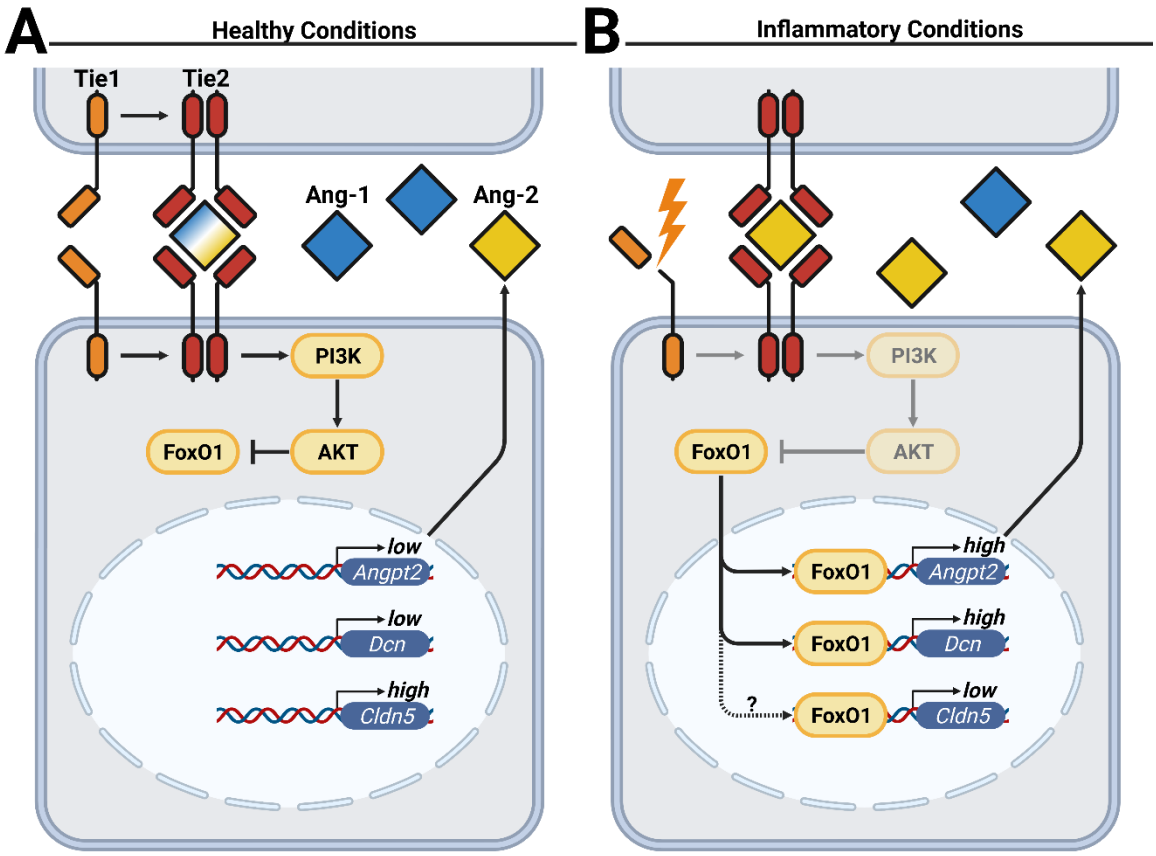

Figure 2.23. Angiopoietin-Tie Signaling in Health & Disease.

A. Under healthy conditions, Ang-1 (*blue*) is the primary Ang member and binds to Tie2 receptors (*red*) enriched at cell-cell contacts which, in turn, suppresses FoxO1 transcriptional activity in a PI3K-AKT-dependent manner (*yellow*). Consequently, claudin-5 gene expression is high, while decorin and Ang-2 expression are low. For poorly understood reasons, basal Ang-2 (*gold*) expression also promotes Tie2 signaling provided that the orphan receptor Tie1 is present (*orange*). **B.** Under inflammatory conditions, Ang-2 predominates and the ectodomain of Tie1 is cleaved. These changes shift Ang-2 to an antagonist of Tie2 signaling. This permits the nuclear accumulation of FoxO1 which, in turn, suppresses claudin-5 gene expression and promotes decorin and Ang-2 gene expression of decorin. Consequently, a positive feedback between FoxO1 and Ang-2 is formed. Note: Not illustrated is the fact that under inflammatory conditions, Tie2 can be sequestered away from the cell-cell contacts, further impairing signaling. Created with BioRender.com.

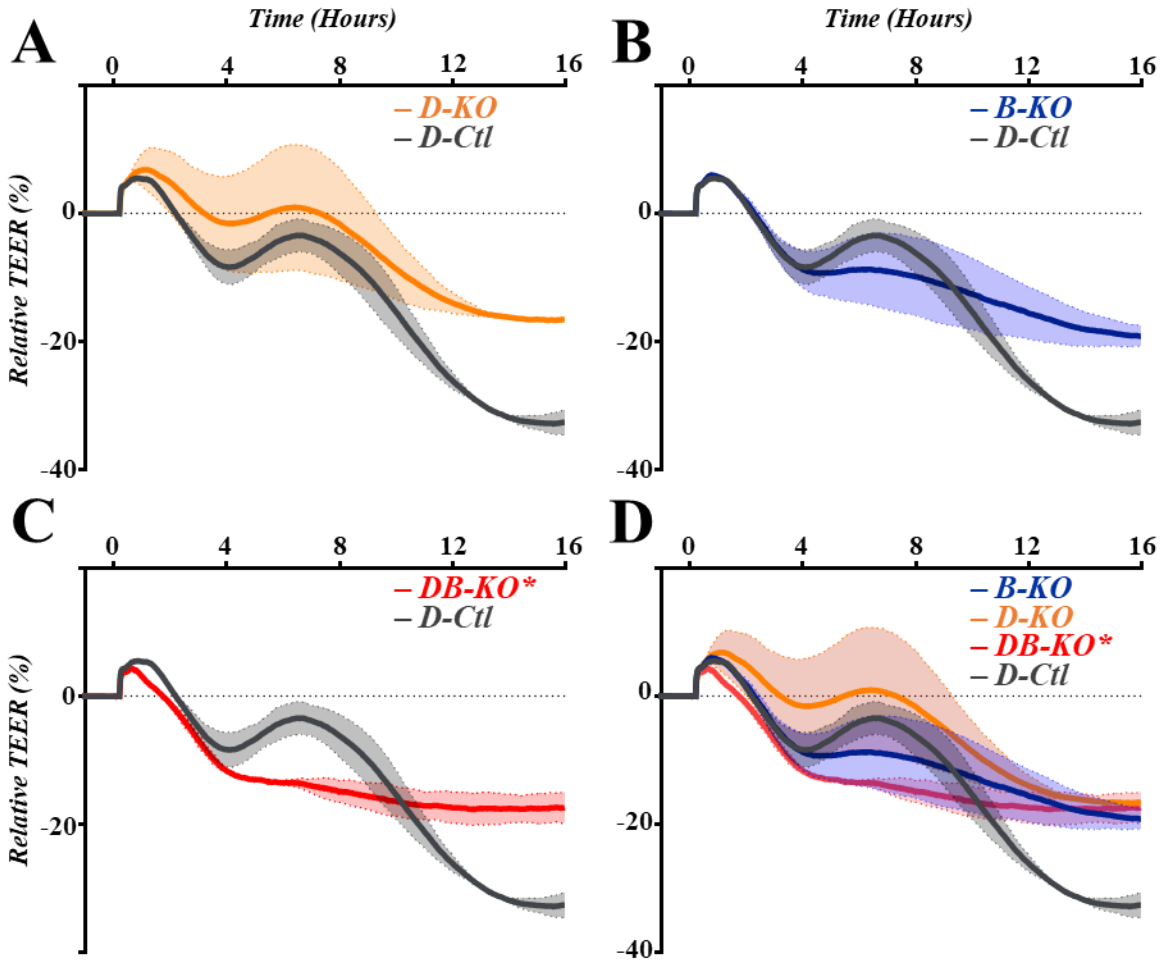

Figure 2.24. Loss of SLRP Expression Partially Rescues Barrier Dysfunction.

A-D. Mouse BBB-ECs isolated from *Dcn*$^{fl/fl}$ mice (*orange*), *Bgn*$^{fl/fl}$ mice (*blue*), or *Dcn*$^{fl/wt}$ x *Bgn*$^{fl/fl}$ mice (*red*) were seeded at confluence into 8W10E+ arrays coated with collagen type IV. Following maturation, monolayers were incubated with TAT-HA2 and TAT-Cre in serum-free media to ablate gene expression. To serve as a "wild-type" control, some wells containing *Dcn*$^{fl/fl}$ BBB-ECs were incubated with TAT-HA2 alone in serum-free media (*grey*). Following a media change and overnight recovery, monolayers were incubated with PMN-ETcA-CM and data was continuously collected at 4 kHz. Tracings were normalized to the zero-time point to determine the relative change in TEER (n = 2 wells each). Error bars represent the standard deviation. **Note:** The data presented for decorin-knockout is the same as that shown in Figure 2.17. Additionally, at the time of this experiment, a complete *Dcn*$^{fl/fl}$ *x Bgn*$^{fl/fl}$ genotype had not been achieved, so *Dcn*$^{fl/wt}$ *x Bgn*$^{fl/fl}$ mice were used.

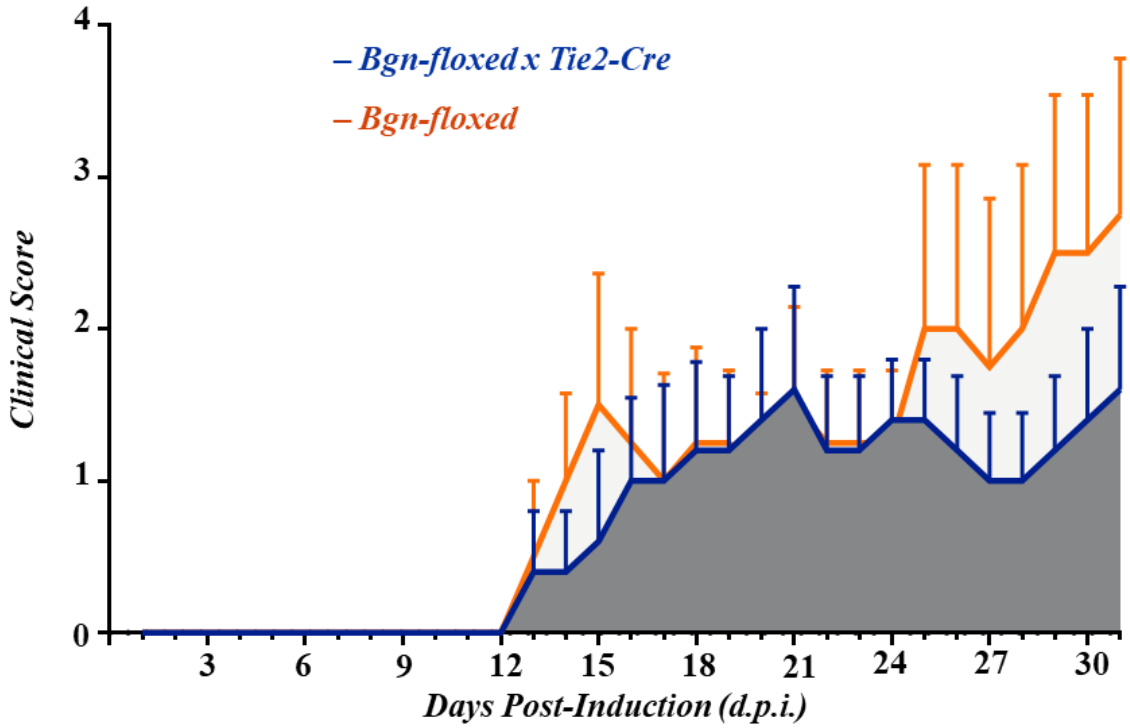

Figure 2.25. No rescue in EAE with *Bgn-floxed x Tie2-Cre* Mice Post-Tamoxifen.

In a pilot study with *Bgn*-floxed *x Tie2-Cre* mice (*blue*; n = 5) and their *Cre*-negative littermates (*orange*; n = 4), animals were injected *i.p.* with tamoxifen (50 mg/kg) every 12 hours for five consecutive days, then allowed to recover for 14 days. Subsequently, active EAE was induced and clinical scoring was performed daily. Error bars represent the standard error of the mean. **Note:** One *Cre*-negative animal reached a severity of disease requiring humane euthanasia on 25 *d.p.i.* Per standard scoring procedure, a clinical score of 5 was logged for the animal through the end of the experiment.

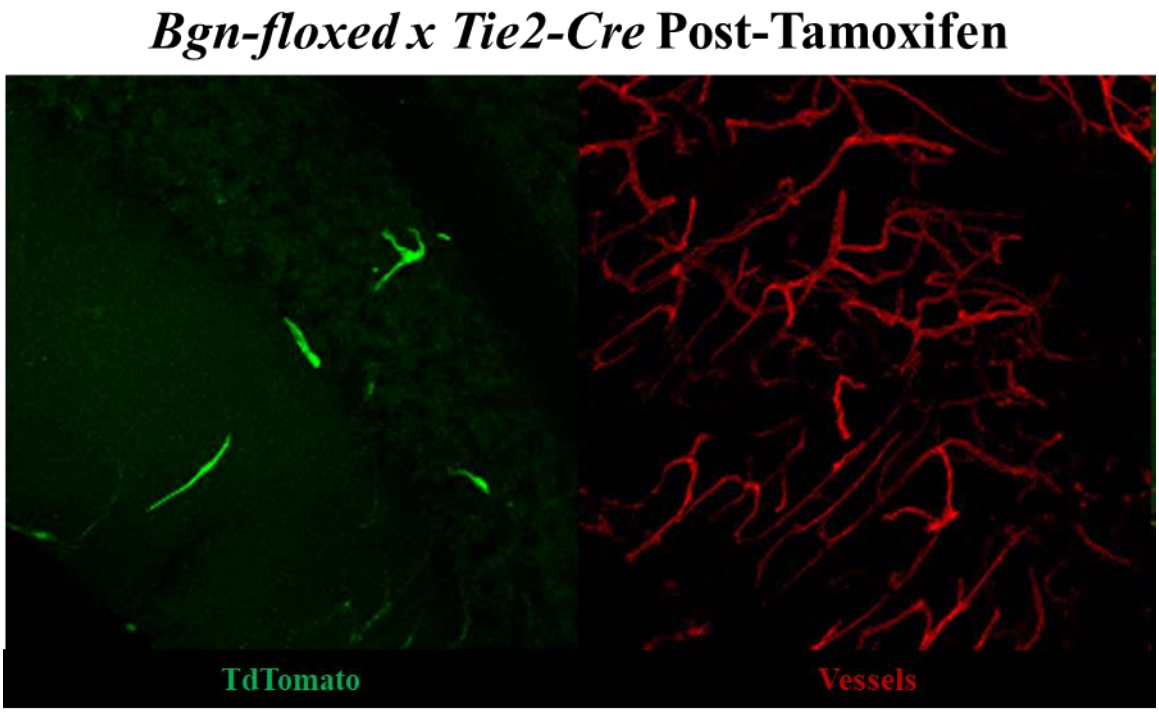

Figure 2.26. ***Ai14 x Tie2-Cre*** **Mice Exhibit Poor Recombination** ***in vivo*****.**

An *Ai14 x Tie2-Cre* mouse was injected *i.p.* with tamoxifen (50 mg/kg) every 12 hours for five consecutive days, then allowed to recover for 14 days. Subsequently, the animal was anesthetized and injected *t.c.* with TL-DyLight 649 to label the endothelium (*red*). The animal was then flushed, decapitated, and its brain processed for confocal microscopy to assess TdTomato (*green*) expression as a marker of recombination. A representative micrograph is shown.

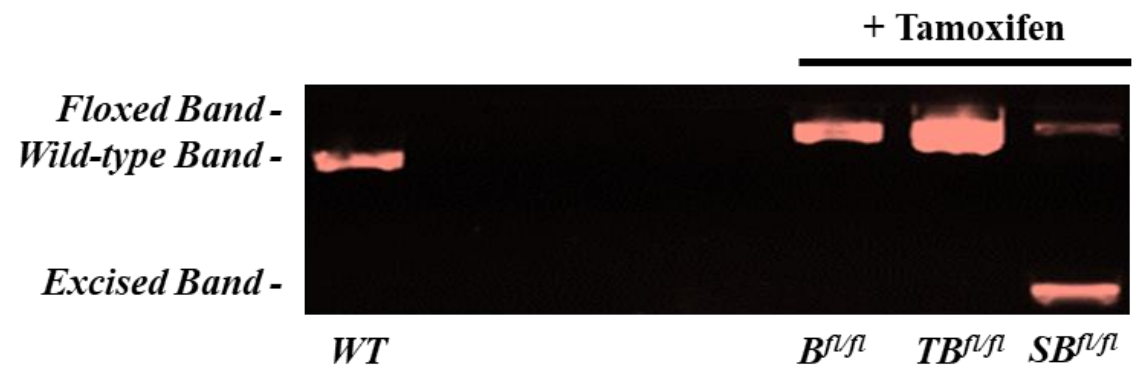

Figure 2.27. *Slco1c1-Cre* Efficiently Recombines *in vivo*.

Bgn-floxed mice (***B*$^{fl/fl}$**), *Bgn*-floxed *x Tie2-Cre* mice (***TB*$^{fl/fl}$**), or *Bgn*-floxed *x Slco1c1-Cre* mice (***SB*$^{fl/fl}$**) were injected *i.p.* with tamoxifen (50 mg/kg) every 12 hours for five consecutive days, then allowed to recover for 14 days. Microvessel-enriched pellets were isolated from these three lines, then lysed for genomic DNA analysis. As an additional control, wild-type (***WT***) animals were included. **Note:** Lanes represent the isolated microvessels of a single animal.

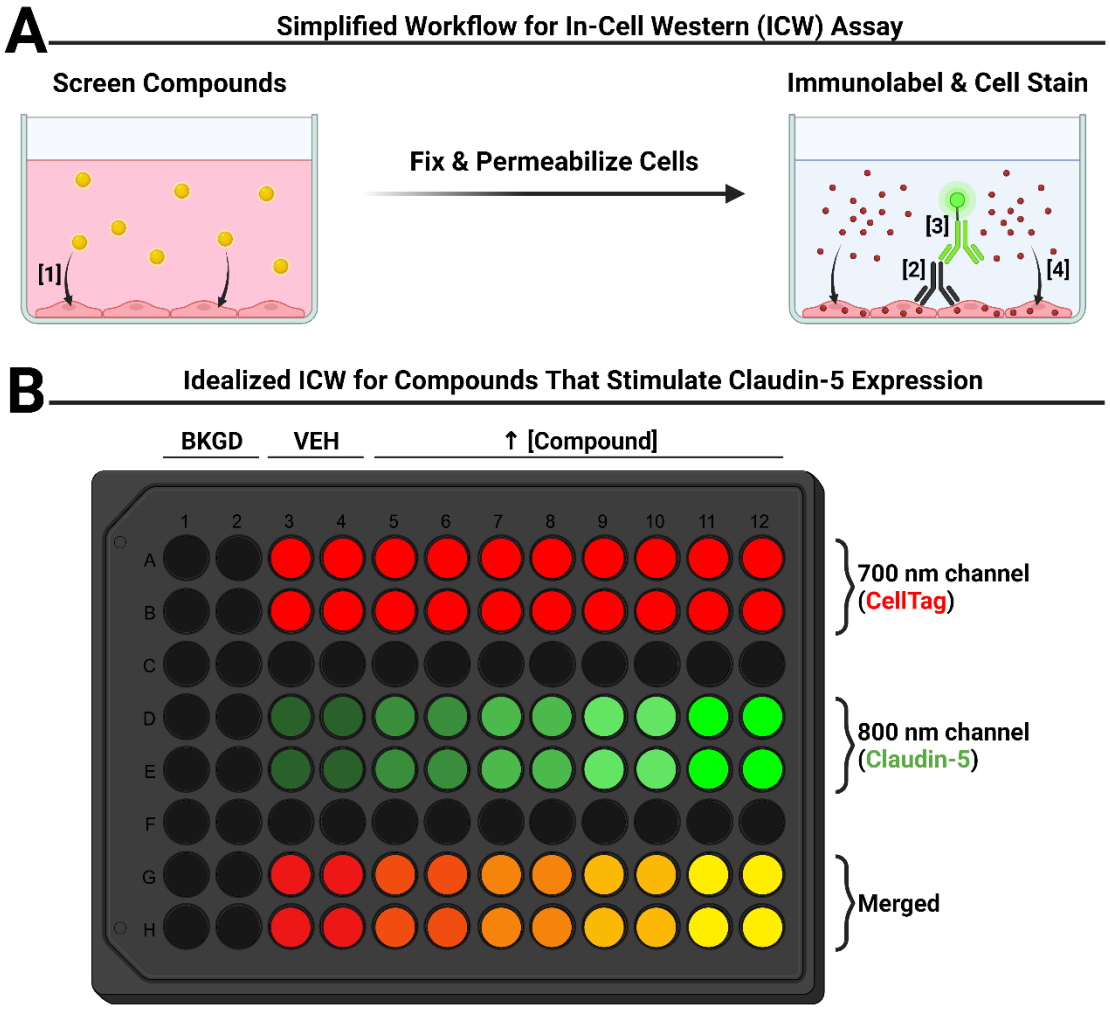

Figure 2.28. Principle of In-Cell Western Assay.

A. BBB-EC monolayers are cultured in a 96-well plate to a partially mature state, then screened with compounds predicted to promote claudin-5 expression **[1]**. Following fixation and permeabilization, monolayers are first labeled with a primary antibody against claudin-5 **[2]**, then a secondary antibody conjugated with IRDye® 800CW **[3]**. To normalize cell count between wells, CellTag 700™ is used **[4]**. **B**. When visualized using a near-infrared (NIR) imaging system, compounds that promote claudin-5 expression can be identified by increased signal in the 800 channel (*middle*) relative to the signal in the 700 channel (*top*) compared to wells administered vehicle controls (VEH). For background correction, a subset of wells are incubated only with the secondary antibody (BKGD). Created with BioRender.com.

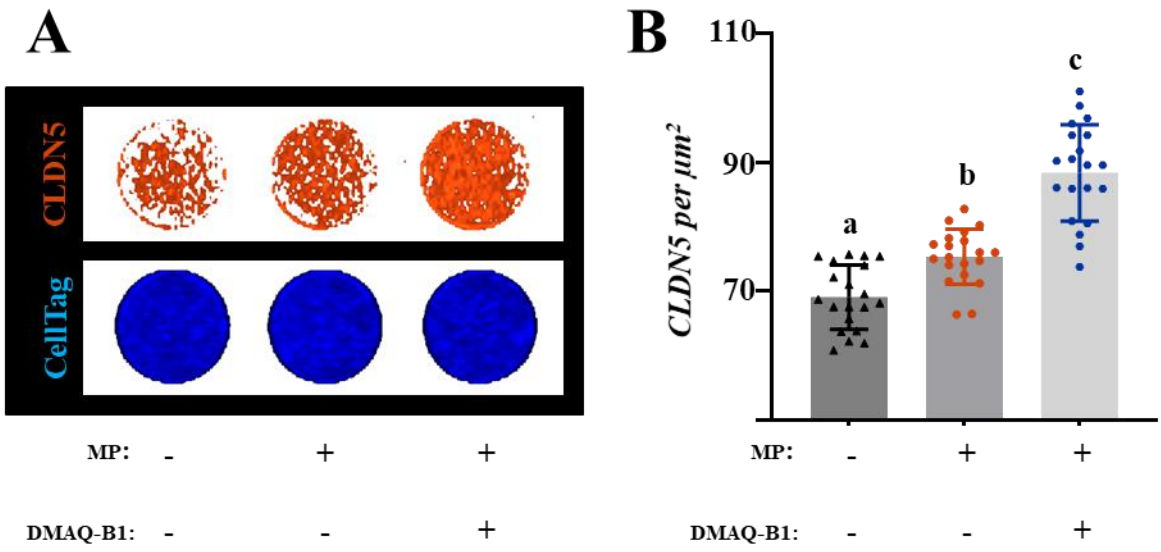

Figure 2.29. In-cell Western Assay for Screening pro-Claudin-5 Compounds.

A. Mouse BBB-ECs were seeded at confluence into a 96-well plate coated with collagen type IV. Monolayers were allowed to partially mature (3 days), then were administered methylprednisolone (MP; 10 µg/mL) with or without demethylasterriquinone B1 (DMAQ-B1; 5 mM), or neither. Six hours later, cells were fixed and analyzed via in-cell western (ICW) assay for claudin-5 (*orange*). For normalization, monolayers were counterstained with CellTag 700 (*blue*). **B.** Normalized and corrected mean claudin-5 signal value per μm^2 for each group (n = 20 wells each). Error bars represent the standard deviation of the mean. Groups marked with different letters are statistically different from each other ($p < 0.05$, one-way ANOVA with post-hoc Tukey's).

REFERENCES

1. Popescu BFG, Lucchinetti CF. Pathology of demyelinating diseases. *Annual Review of Pathology: Mechanisms of Disease*; 7. Epub ahead of print 2012. DOI: 10.1146/annurev-pathol-011811-132443.

2. Höftberger R, Lassmann H. Inflammatory demyelinating diseases of the central nervous system. 2018. Epub ahead of print 2018. DOI: 10.1016/B978-0-12-802395-2.00019-5.

3. Kim HJ, Paul F, Lana-Peixoto MA, et al. MRI characteristics of neuromyelitis optica spectrum disorder: An international update. *Neurology* 2015; 84: 1165–1173.

4. Filippi M, Rocca MA. Acute Disseminated Encephalomyelitis. In: *White Matter Diseases*. Cham: Springer International Publishing, 2020. Epub ahead of print 2020. DOI: 10.1007/978-3-030-38621-4_5.

5. Tenembaum SN. Treatment of multiple sclerosis and neuromyelitis optica in children and adolescents. *Clin Neurol Neurosurg*; 115. Epub ahead of print 2013. DOI: 10.1016/j.clineuro.2013.09.016.

6. Brenton JN, Banwell BL. Therapeutic Approach to the Management of Pediatric Demyelinating Disease: Multiple Sclerosis and Acute Disseminated Encephalomyelitis. *Neurotherapeutics*; 13. Epub ahead of print 2016. DOI: 10.1007/s13311-015-0396-0.

7. Spencer JI, Bell JS, DeLuca GC. Vascular pathology in multiple sclerosis: Reframing pathogenesis around the blood-brain barrier. *Journal of Neurology, Neurosurgery and Psychiatry* 2018; 89: 42–52.

8. Lassmann H. Pathogenic mechanisms associated with different clinical courses of multiple sclerosis. *Frontiers in Immunology*; 10. Epub ahead of print 2019. DOI: 10.3389/fimmu.2018.03116.

9. Alvarez JI, Saint-Laurent O, Godschalk A, et al. Focal disturbances in the blood-brain barrier are associated with formation of neuroinflammatory lesions. *Neurobiol Dis* 2015; 74: 14–24.

10. Petersen MA, Ryu JK, Akassoglou K. Fibrinogen in neurological diseases: Mechanisms, imaging and therapeutics. *Nature Reviews Neuroscience* 2018; 19: 283–301.

11. Hemmer B, Kerschensteiner M, Korn T. Role of the innate and adaptive immune responses in the course of multiple sclerosis. *The Lancet Neurology*; 14. Epub ahead of print 2015. DOI: 10.1016/S1474-4422(14)70305-9.

12. Loma I, Heyman R. Multiple Sclerosis: Pathogenesis and Treatment. *Curr Neuropharmacol* 2011; 9: 409–416.

13. Inojosa H, Proschmann U, Akgün K, et al. A focus on secondary progressive multiple sclerosis (SPMS): challenges in diagnosis and definition. *Journal of Neurology*. Epub ahead of print 2019. DOI: 10.1007/s00415-019-09489-5.

14. Miller DH, Leary SM. Primary-progressive multiple sclerosis. *Lancet Neurology* 2007; 6: 903–912.

15. Hu W, Lucchinetti CF. The pathological spectrum of CNS inflammatory demyelinating diseases. *Seminars in Immunopathology* 2009; 31: 439–453.

16. Rahmlow MR, Kantarci O. Fulminant Demyelinating Diseases. *The Neurohospitalist* 2013; 3: 81–91.

17. Jarius S, Wildemann B. The history of neuromyelitis optica. *Journal of Neuroinflammation*; 10. Epub ahead of print 2013. DOI: 10.1186/1742-2094-10-8.

18. Wingerchuk DM, Hogancamp WF, O'Brien PC, et al. The clinical course of neuromyelitis optica (Devic's syndrome). *Neurology*; 53. Epub ahead of print 1 September 1999. DOI: 10.1212/WNL.53.5.1107.

19. Wingerchuk DM, Banwell B, Bennett JL, et al. International consensus diagnostic criteria for neuromyelitis optica spectrum disorders. *Neurology*; 85. Epub ahead of print 14 July 2015. DOI: 10.1212/WNL.0000000000001729.

20. Winkler A, Wrzos C, Haberl M, et al. Blood-brain barrier resealing in neuromyelitis optica occurs independently of astrocyte regeneration. *J Clin Invest*; 131. Epub ahead of print 1 March 2021. DOI: 10.1172/JCI141694.

21. Lucchinetti CF, Guo Y, Popescu BFG, et al. The pathology of an autoimmune astrocytopathy: Lessons learned from neuromyelitis optica. In: *Brain Pathology*. NIH Public Access, pp. 83–97.

22. Khalilidehkordi E, Clarke L, Arnett S, et al. Relapse Patterns in NMOSD: Evidence for Earlier Occurrence of Optic Neuritis and Possible Seasonal Variation. *Front Neurol*; 11. Epub ahead of print 2020. DOI: 10.3389/fneur.2020.00537.

23. Tenembaum SN. Acute disseminated encephalomyelitis. 2013. Epub ahead of print 2013. DOI: 10.1016/B978-0-444-52910-7.00048-9.

24. Iadecola C. The Neurovascular Unit Coming of Age: A Journey through Neurovascular Coupling in Health and Disease. *Neuron*; 96. Epub ahead of print 2017. DOI: 10.1016/j.neuron.2017.07.030.

25. Stackhouse TL, Mishra A. Neurovascular Coupling in Development and Disease: Focus on Astrocytes. *Frontiers in Cell and Developmental Biology*; 9. Epub ahead of print 2021. DOI: 10.3389/fcell.2021.702832.

26. Zlokovic B V. The Blood-Brain Barrier in Health and Chronic Neurodegenerative Disorders. *Neuron* 2008; 57: 178–201.

27. Daneman R, Prat A. The Blood–Brain Barrier. *Cold Spring Harb Perspect Biol* 2015; 7: a020412.

28. Dias MC, Mapunda JA, Vladymyrov M, et al. Structure and junctional complexes of endothelial, epithelial and glial brain barriers. *International Journal of Molecular Sciences*; 20. Epub ahead of print 1 November 2019. DOI: 10.3390/ijms20215372.

29. Profaci CP, Munji RN, Pulido RS, et al. The blood–brain barrier in health and disease: Important unanswered questions. *Journal of Experimental Medicine*; 217. Epub ahead of print 6 April 2020. DOI: 10.1084/jem.20190062.

30. Bauer HC, Krizbai IA, Bauer H, et al. 'You shall not pass'-tight junctions of the blood brain barrier. *Frontiers in Neuroscience* 2014; 8: 392.

31. Higashi T, Miller AL. Tricellular junctions: How to build junctions at the TRICkiest points of epithelial cells. *Molecular Biology of the Cell* 2017; 28: 2023–2034.

32. Günzel D, Yu ASL. Claudins and the modulation of tight junction permeability. *Physiol Rev* 2013; 93: 525–569.

33. Luissint AC, Federici C, Guillonneau F, et al. Guanine nucleotide-binding protein Gαi2: A new partner of claudin-5 that regulates tight junction integrity in human brain endothelial cells. *J Cereb Blood Flow Metab*; 32. Epub ahead of print 2012. DOI: 10.1038/jcbfm.2011.202.

34. Beard RS, Hoettels BA, Meegan JE, et al. AKT2 maintains brain endothelial claudin-5 expression and selective activation of IR/AKT2/FOXO1-signaling reverses barrier dysfunction. *J Cereb Blood Flow Metab* 2020; 40: 374–391.

35. Nitta T, Hata M, Gotoh S, et al. Size-selective loosening of the blood-brain barrier in claudin-5–deficient mice. *J Cell Biol* 2003; 161: 653–660.

36. Greene C, Kealy J, Humphries MM, et al. Dose-dependent expression of claudin-5 is a modifying factor in schizophrenia. *Mol Psychiatry*. Epub ahead of print 10 October 2017. DOI: 10.1038/mp.2017.156.

37. Cleynen I, Engchuan W, Hestand MS, et al. Genetic contributors to risk of schizophrenia in the presence of a 22q11.2 deletion. *Mol Psychiatry*. Epub ahead of print 2020. DOI: 10.1038/s41380-020-0654-3.

38. Greene C, Hanley N, Campbell M. Claudin-5: Gatekeeper of neurological function. *Fluids and Barriers of the CNS* 2019; 16: 1–15.

39. Berndt P, Winkler L, Cording J, et al. Tight junction proteins at the blood–brain barrier: far more than claudin-5. *Cell Mol Life Sci* 2019; 76: 1987–2002.

40. Uchida Y, Sumiya T, Tachikawa M, et al. Involvement of Claudin-11 in Disruption of Blood-Brain, -Spinal Cord, and -Arachnoid Barriers in Multiple Sclerosis. *Mol Neurobiol* 2019; 56: 2039–2056.

41. Ohtsuki S, Yamaguchi H, Katsukura Y, et al. mRNA expression levels of tight junction protein genes in mouse brain capillary endothelial cells highly purified by magnetic cell sorting. *J Neurochem* 2008; 104: 147–154.

42. Kratzer I, Vasiljevic A, Rey C, et al. Complexity and developmental changes in the expression pattern of claudins at the blood-CSF barrier. *Histochem Cell Biol* 2012; 138: 861–879.

43. Hashimoto Y, Zhou W, Hamauchi K, et al. Engineered membrane protein antigens successfully induce antibodies against extracellular regions of claudin-5. *Sci Rep*; 8. Epub ahead of print 2018. DOI: 10.1038/s41598-018-26560-9.

44. Wolburg H, Wolburg-Buchholz K, Kraus J, et al. Localization of claudin-3 in tight junctions of the blood-brain barrier is selectively lost during experimental autoimmune encephalomyelitis and human glioblastoma multiforme. *Acta Neuropathol* 2003; 105: 586–592.

45. Pfeiffer F, Schäfer J, Lyck R, et al. Claudin-1 induced sealing of blood-brain barrier tight junctions ameliorates chronic experimental autoimmune encephalomyelitis. *Acta Neuropathol* 2011; 122: 601–614.

46. Sladojevic N, Stamatovic SM, Johnson AM, et al. Claudin-1-dependent destabilization of the blood–brain barrier in chronic stroke. *J Neurosci* 2019; 39: 743–757.

47. Castro Dias M, Coisne C, Lazarevic I, et al. Claudin-3-deficient C57BL/6J mice display intact brain barriers. *Sci Rep*; 9. Epub ahead of print 1 December 2019. DOI: 10.1038/s41598-018-36731-3.

48. M CD, C C, P B, et al. Claudin-12 is not required for blood-brain barrier tight junction function. *Fluids Barriers CNS*; 16. Epub ahead of print 2019. DOI: 10.1186/S12987-019-0150-9.

49. Raleigh DR, Marchiando AM, Zhang Y, et al. Tight junction-associated MARVEL proteins marvelD3, tricellulin, and occludin have distinct but overlapping functions. *Mol Biol Cell* 2010; 21: 1200–1213.

50. Mariano C, Palmela I, Pereira P, et al. Tricellulin expression in brain endothelial and neural cells. *Cell Tissue Res* 2013; 351: 397–407.

51. Sánchez-Pulido L, Martín-Belmonte F, Valencia A, et al. MARVEL: A conserved domain involved in membrane apposition events. *Trends in Biochemical Sciences* 2002; 27: 599–601.

52. Buschmann MM, Shen L, Rajapakse H, et al. Occludin OCEL-domain interactions are required for maintenance and regulation of the tight junction barrier to macromolecular flux. *Mol Biol Cell*; 24. Epub ahead of print 2013. DOI: 10.1091/mbc.E12-09-0688.

53. Van Itallie CM, Anderson JM. Phosphorylation of tight junction transmembrane proteins: Many sites, much to do. *Tissue Barriers*; 6. Epub ahead of print 2018. DOI: 10.1080/21688370.2017.1382671.

54. Haorah J, Heilman D, Knipe B, et al. Ethanol-induced activation of myosin light chain kinase leads to dysfunction of tight junctions and blood-brain barrier compromise. *Alcohol Clin Exp Res*; 29. Epub ahead of print 2005. DOI: 10.1097/01.ALC.0000166944.79914.0A.

55. Haorah J, Knipe B, Gorantla S, et al. Alcohol-induced blood-brain barrier dysfunction is mediated via inositol 1,4,5-triphosphate receptor (IP3R)-gated intracellular calcium release. *J Neurochem*; 100. Epub ahead of print 2007. DOI: 10.1111/j.1471-4159.2006.04245.x.

56. Haorah J, Ramirez SH, Schall K, et al. Oxidative stress activates protein tyrosine kinase and matrix metalloproteinases leading to blood-brain barrier dysfunction. *J Neurochem*; 101. Epub ahead of print 2007. DOI: 10.1111/j.1471-4159.2006.04393.x.

57. Persidsky Y, Heilman D, Haorah J, et al. Rho-mediated regulation of tight junctions during monocyte migration across the blood-brain barrier in HIV-1 encephalitis (HIVE). *Blood*; 107. Epub ahead of print 2006. DOI: 10.1182/blood-2005-11-4721.

58. Yamamoto M, Ramirez SH, Sato S, et al. Phosphorylation of claudin-5 and occludin by Rho kinase in brain endothelial cells. *Am J Pathol*; 172. Epub ahead of print 2008. DOI: 10.2353/ajpath.2008.070076.

59. Murakami T, Felinski EA, Antonetti DA. Occludin phosphorylation and ubiquitination regulate tight junction trafficking and vascular endothelial growth factor-induced permeability. *J Biol Chem*; 284. Epub ahead of print 2009. DOI: 10.1074/jbc.M109.016766.

60. Riazuddin S, Ahmed ZM, Fanning AS, et al. Tricellulin is a tight-junction protein necessary for hearing. *Am J Hum Genet* 2006; 79: 1040–1051.

61. Steed E, Rodrigues NTL, Balda MS, et al. Identification of MarvelD3 as a tight junction-associated transmembrane protein of the occludin family. *BMC Cell Biol*; 10. Epub ahead of print 22 December 2009. DOI: 10.1186/1471-2121-10-95.

62. Blasig IE, Bellmann C, Cording J, et al. Occludin protein family: Oxidative stress and reducing conditions. *Antioxidants and Redox Signaling*; 15. Epub ahead of print 2011. DOI: 10.1089/ars.2010.3542.

63. Iwamoto N, Higashi T, Furuse M. Localization of angulin-1/LSR and tricellulin at tricellular contacts of brain and retinal endothelial cells in vivo. *Cell Struct Funct* 2013; 39: 1–8.

64. Sohet F, Lin C, Munji RN, et al. LSR/angulin-1 is a tricellular tight junction protein involved in blood-brain barrier formation. *J Cell Biol* 2015; 208: 703–711.

65. Dias MC, Quesada AO, Soldati S, et al. Brain endothelial tricellular junctions as novel sites for T cell diapedesis across the blood-brain barrier. *J Cell Sci*; 134. Epub ahead of print 2021. DOI: 10.1242/jcs.253880.

66. Saito AC, Higashi T, Fukazawa Y, et al. Occludin and tricellulin facilitate formation of anastomosing tight-junction strand network to improve barrier function. *Mol Biol Cell*; 32. Epub ahead of print 2021. DOI: 10.1091/mbc.E20-07-0464.

67. Ikenouchi J, Sasaki H, Tsukita S, et al. Loss of occludin affects tricellular localization of tricellulin. *Mol Biol Cell* 2008; 19: 4687–4693.

68. Kitajiri SI, Katsuno T, Sasaki H, et al. Deafness in occludin-deficient mice with dislocation of tricellulin and progressive apoptosis of the hair cells. *Biol Open* 2014; 3: 759–766.

69. Kamitani T, Sakaguchi H, Tamura A, et al. Deletion of Tricellulin Causes Progressive Hearing Loss Associated with Degeneration of Cochlear Hair Cells. *Sci Rep*; 5. Epub ahead of print 2015. DOI: 10.1038/srep18402.

70. Higashi T, Katsuno T, Kitajiri SI, et al. Deficiency of angulin-2/ILDR1, a tricellular tight junction-associated membrane protein, causes deafness with cochlear hair cell degeneration in mice. *PLoS One*; 10. Epub ahead of print 2015. DOI: 10.1371/journal.pone.0120674.

71. Hempstock W, Sugioka S, Ishizuka N, et al. Angulin-2/ILDR1, a tricellular tight junction protein, does not affect water transport in the mouse large intestine. *Sci Rep*; 10. Epub ahead of print 2020. DOI: 10.1038/s41598-020-67319-5.

72. Liberati A, Altman DG, Tetzlaff J, et al. The PRISMA Statement for Reporting Systematic Reviews and Meta-Analyses of Studies That Evaluate Health Care Interventions: Explanation and Elaboration. *PLoS Med* 2009; 6: e1000100.

73. Reijerkerk A, Alejandro Lopez-Ramirez M, van het Hof B, et al. MicroRNAs regulate human brain endothelial cell-barrier function in inflammation: Implications for multiple sclerosis. *J Neurosci* 2013; 33: 6857–6863.

74. Lengfeld JE, Lutz SE, Smith JR, et al. Endothelial Wnt/β-catenin signaling reduces immune cell infiltration in multiple sclerosis. *Proc Natl Acad Sci U S A* 2017; 114: E1168–E1177.

75. Opsahl ML, Kennedy PGE. Investigating the presence of human herpesvirus 7 and 8 in multiple sclerosis and normal control brain tissue. *J Neurol Sci* 2006; 240: 37–44.

76. Lopez-Ramirez MA, Wu D, Pryce G, et al. MicroRNA-155 negatively affects blood-brain barrier function during neuroinflammation. *FASEB J* 2014; 28: 2551–2565.

77. Podjaski C, Alvarez JI, Bourbonniere L, et al. Netrin 1 regulates blood-brain barrier function and neuroinflammation. *Brain* 2015; 138: 1598–1612.

78. Van Der Valk P, De Groot CJA. Staging of multiple sclerosis (MS) lesions: Pathology of the time frame of MS. *Neuropathology and Applied Neurobiology* 2000; 26: 2–10.

79. Kuhlmann T, Ludwin S, Prat A, et al. An updated histological classification system for multiple sclerosis lesions. *Acta Neuropathol* 2017; 133: 13–24.

80. Klaver R, De Vries HE, Schenk GJ, et al. Grey matter damage in multiple sclerosis A pathology perspective. In: *Prion*. Taylor & Francis, pp. 66–75.

81. van der Valk P, Amor S. Preactive lesions in multiple sclerosis. *Curr Opin Neurol* 2009; 22: 1.

82. van Horssen J, Singh S, van der Pol S, et al. Clusters of activated microglia in normal-appearing white matter show signs of innate immune activation. *J Neuroinflammation* 2012; 9: 602.

83. Plumb J, McQuaid S, Mirakhur M, et al. Abnormal endothelial tight junctions in active lesions and normal-appearing white matter in multiple sclerosis. *Brain Pathol* 2002; 12: 154–169.

84. Frischer JM, Weigand SD, Guo Y, et al. Clinical and pathological insights into the dynamic nature of the white matter multiple sclerosis plaque. *Ann Neurol* 2015; 78: 710–721.

85. Wosik K, Cayrol R, Dodelet-Devillers A, et al. Angiotensin II controls occludin function and is required for blood-brain barrier maintenance: Relevance to multiple sclerosis. *J Neurosci* 2007; 27: 9032–9042.

86. Van Horssen J, Brink BP, De Vries HE, et al. The blood-brain barrier in cortical multiple sclerosis lesions. *J Neuropathol Exp Neurol* 2007; 66: 321–328.

87. Cunnea P, McMahon J, O'Connell E, et al. Gene expression analysis of the microvascular compartment in multiple sclerosis using laser microdissected blood vessels. *Acta Neuropathol* 2010; 119: 601–615.

88. Lassmann H. Cortical lesions in multiple sclerosis: Inflammation versus neurodegeneration. *Brain*; 135. Epub ahead of print 2012. DOI: 10.1093/brain/aws260.

89. Gh Popescu BF, Lucchinetti CF. Meningeal and cortical grey matter pathology in multiple sclerosis. *BMC Neurology*; 12. Epub ahead of print 2012. DOI: 10.1186/1471-2377-12-11.

90. Musolino PL, Gong Y, Snyder JMT, et al. Brain endothelial dysfunction in cerebral adrenoleukodystrophy. *Brain* 2015; 138: 3206–3220.

91. Weksler BB, Subileau EA, Perrière N, et al. Blood-brain barrier-specific properties of a human adult brain endothelial cell line. *FASEB J* 2005; 19: 1872–1874.

92. Sano Y, Shimizu F, Abe M, et al. Establishment of a new conditionally immortalized human brain microvascular endothelial cell line retaining an in vivo blood-brain barrier function. *J Cell Physiol* 2010; 225: 519–528.

93. Sano Y, Kashiwamura Y, Abe M, et al. Stable human brain microvascular endothelial cell line retaining its barrier-specific nature independent of the passage number. *Clin Exp Neuroimmunol* 2013; 4: 92–103.

94. Maeda T, Sano Y, Abe M, et al. Establishment and characterization of spinal cord microvascular endothelial cell lines. *Clin Exp Neuroimmunol* 2013; 4: 326–338.

95. Shimizu F, Sano Y, Takahashi T, et al. Sera from neuromyelitis optica patients disrupt the blood-brain barrier. *J Neurol Neurosurg Psychiatry* 2012; 83: 288–297.

96. Tasaki A, Shimizu F, Sano Y, et al. Autocrine MMP-2/9 secretion increases the BBB permeability in neuromyelitis optica. *J Neurol Neurosurg Psychiatry* 2014; 85: 419–430.

97. Shimizu F, Tasaki A, Sano Y, et al. Sera from remitting and secondary progressive multiple sclerosis patients disrupt the blood-brain barrier. *PLoS One*; 9. Epub ahead of print 31 March 2014. DOI: 10.1371/journal.pone.0092872.

98. Sheikh MH, Henson SM, Loiola RA, et al. Immuno-metabolic impact of the multiple sclerosis patients' sera on endothelial cells of the blood-brain barrier. *J Neuroinflammation*; 17. Epub ahead of print 9 May 2020. DOI: 10.1186/s12974-020-01810-8.

99. Willis M, Cohen J. Fingolimod Therapy for Multiple Sclerosis. *Semin Neurol*; 33. Epub ahead of print 25 May 2013. DOI: 10.1055/s-0033-1343794.

100. Nishihara H, Shimizu F, Sano Y, et al. Fingolimod prevents blood-brain barrier disruption induced by the sera from patients with multiple sclerosis. *PLoS One*; 10. Epub ahead of print 16 March 2015. DOI: 10.1371/journal.pone.0121488.

101. Takahashi S, Maeda T, Sano Y, et al. Active form of vitamin D directly protects the blood-brain barrier in multiple sclerosis. *Clin Exp Neuroimmunol* 2017; 8: 244–254.

102. Mestas J, Hughes CCW. Of Mice and Not Men: Differences between Mouse and Human Immunology. *J Immunol*; 172. Epub ahead of print 2004. DOI: 10.4049/jimmunol.172.5.2731.

103. Misu T, Höftberger R, Fujihara K, et al. Presence of six different lesion types suggests diverse mechanisms of tissue injury in neuromyelitis optica. *Acta Neuropathol*; 125. Epub ahead of print 2013. DOI: 10.1007/s00401-013-1116-7.

104. Takai Y, Misu T, Suzuki H, et al. Staging of astrocytopathy and complement activation in neuromyelitis optica spectrum disorders. *Brain*. Epub ahead of print 12 March 2021. DOI: 10.1093/brain/awab102.

105. Takeshita Y, Obermeier B, Cotleur AC, et al. Effects of neuromyelitis optica - IgG at the blood - Brain barrier in vitro. *Neurol Neuroimmunol NeuroInflammation*; 4. Epub ahead of print 2017. DOI: 10.1212/NXI.0000000000000311.

106. Shimizu F, Schaller KL, Owens GP, et al. Glucose-regulated protein 78 autoantibody associates with blood-brain barrier disruption in neuromyelitis optica. *Sci Transl Med*; 9. Epub ahead of print 5 July 2017. DOI: 10.1126/scitranslmed.aai9111.

107. Miller SD, Karpus WJ, Davidson TS. Experimental autoimmune encephalomyelitis in the mouse. *Current Protocols in Immunology* 2010; CHAPTER: Unit.

108. Robinson AP, Harp CT, Noronha A, et al. The experimental autoimmune encephalomyelitis (EAE) model of MS. utility for understanding disease pathophysiology and treatment. In: *Handbook of Clinical Neurology*. Elsevier B.V., pp. 173–189.

109. Paul D, Ge S, Lemire Y, et al. Cell-selective knockout and 3D confocal image analysis reveals separate roles for astrocyte-and endothelial-derived CCL2 in neuroinflammation. *J Neuroinflammation*; 11. Epub ahead of print 21 January 2014. DOI: 10.1186/1742-2094-11-10.

110. Paul D, Cowan AE, Ge S, et al. Novel 3D analysis of Claudin-5 reveals significant endothelial heterogeneity among CNS microvessels. *Microvasc Res* 2013; 86: 1–10.

111. Paul D, Baena V, Ge S, et al. Appearance of claudin-5+ leukocytes in the central nervous system during neuroinflammation: A novel role for endothelial-derived extracellular vesicles. *J Neuroinflammation*; 13. Epub ahead of print 16 November 2016. DOI: 10.1186/s12974-016-0755-8.

112. Argaw AT, Gurfein BT, Zhang Y, et al. VEGF-mediated disruption of endothelial CLN-5 promotes blood-brain barrier breakdown. *Proc Natl Acad Sci U S A* 2009; 106: 1977–82.

113. Errede M, Girolamo F, Ferrara G, et al. Blood-brain barrier alterations in the cerebral cortex in experimental autoimmune encephalomyelitis. *J Neuropathol Exp Neurol* 2012; 71: 840–854.

114. Welser J V., Halder SK, Kant R, et al. Endothelial α6β4 integrin protects during experimental autoimmune encephalomyelitis-induced neuroinflammation by maintaining vascular integrity and tight junction protein expression. *J Neuroinflammation*; 14. Epub ahead of print 9 November 2017. DOI: 10.1186/s12974-017-0987-2.

115. Niu X, Sang H, Wang J. Naringenin attenuates experimental autoimmune encephalomyelitis by protecting the intact of blood-brain barrier and controlling inflammatory cell migration. *J Nutr Biochem*; 89. Epub ahead of print 1 March 2021. DOI: 10.1016/j.jnutbio.2020.108560.

116. Li B, Cui W, Liu J, et al. Sulforaphane ameliorates the development of experimental autoimmune encephalomyelitis by antagonizing oxidative stress and Th17-related inflammation in mice. *Exp Neurol* 2013; 250: 239–249.

117. Wang C, Wang C, Dong H, et al. Immune-related GTPase Irgm1 exacerbates experimental auto-immune encephalomyelitis by promoting the disruption of blood-brain barrier and blood-cerebrospinal fluid barrier. *Mol Immunol* 2013; 53: 43–51.

118. Bittner S, Ruck T, Schuhmann MK, et al. Endothelial TWIK-related potassium channel-1 (TREK1) regulates immune-cell trafficking into the CNS. *Nat Med* 2013; 19: 1161–1165.

119. Zhang L, Lu X, Gong L, et al. Tetramethylpyrazine Protects Blood-Spinal Cord Barrier Integrity by Modulating Microglia Polarization Through Activation of STAT3/SOCS3 and Inhibition of NF-κB Signaling Pathways in Experimental Autoimmune Encephalomyelitis Mice. *Cell Mol Neurobiol*. Epub ahead of print 2020. DOI: 10.1007/s10571-020-00878-3.

120. Bénardais K, Pul R, Singh V, et al. Effects of fumaric acid esters on blood-brain barrier tight junction proteins. *Neurosci Lett* 2013; 555: 165–170.

121. Eilam R, Segal M, Malach R, et al. Astrocyte disruption of neurovascular communication is linked to cortical damage in an animal model of multiple sclerosis. *Glia* 2018; 66: 1098–1117.

122. Chapouly C, Argaw AT, Horng S, et al. Astrocytic TYMP and VEGFA drive blood-brain barrier opening in inflammatory central nervous system lesions. *Brain* 2015; 138: 1548–1567.

123. Becker KA, Halmer R, Davies L, et al. Blockade of experimental multiple sclerosis by inhibition of the acid sphingomyelinase/ceramide system. *NeuroSignals* 2018; 25: 88–97.

124. Mora P, Hollier PL, Guimbal S, et al. Blood-brain barrier genetic disruption leads to protective barrier formation at the Glia Limitans. *PLoS Biol*; 18. Epub ahead of print 30 November 2020. DOI: 10.1371/journal.pbio.3000946.

125. Alt C, Duvefelt K, Franzén B, et al. Gene and protein expression profiling of the microvascular compartment in experimental autoimmune encephalomyelitis in C57BI/6 and SJL mice. *Brain Pathol* 2005; 15: 1–16.

126. Ferrara G, Errede M, Girolamo F, et al. NG2, a common denominator for neuroinflammation, blood–brain barrier alteration, and oligodendrocyte precursor response in EAE, plays a role in dendritic cell activation. *Acta Neuropathol* 2016; 132: 23–42.

127. Girolamo F, Errede M, Longo G, et al. Defining the role of NG2-expressing cells in experimental models of multiple sclerosis. A biofunctional analysis of the neurovascular unit in wild type and NG2 null mice. *PLoS One*; 14. Epub ahead of print 1 March 2019. DOI: 10.1371/journal.pone.0213508.

128. Argaw AT, Asp L, Zhang J, et al. Astrocyte-derived VEGF-A drives blood-brain barrier disruption in CNS inflammatory disease. *J Clin Invest* 2012; 122: 2454–2468.

129. Gopal S, Mikulskis A, Gold R, et al. Evidence of activation of the Nrf2 pathway in multiple sclerosis patients treated with delayed-release dimethyl fumarate in the Phase 3 DEFINE and CONFIRM studies. *Mult Scler* 2017; 23: 1875–1883.

130. Hou Y, Heon Ryu C, Jun JA, et al. Interferon β-secreting mesenchymal stem cells combined with minocycline attenuate experimental autoimmune encephalomyelitis. *J Neuroimmunol* 2014; 274: 20–27.

131. Bell C, Anderson J, Ganguly T, et al. Development of Glatopa® (Glatiramer Acetate): The First FDA-Approved Generic Disease-Modifying Therapy for Relapsing Forms of Multiple Sclerosis. *Journal of Pharmacy Practice* 2018; 31: 481–488.

132. Göbel K, Pankratz S, Schneider-Hohendorf T, et al. Blockade of the kinin receptor B1 protects from autoimmune CNS disease by reducing leukocyte trafficking. *J Autoimmun* 2011; 36: 106–114.

133. Wouters E, de Wit NM, Vanmol J, et al. Liver X Receptor Alpha Is Important in Maintaining Blood-Brain Barrier Function. *Front Immunol* 2019; 10: 1811.

134. Ni C, Wang C, Zhang J, et al. Interferon-γ safeguards blood-brain barrier during experimental autoimmune encephalomyelitis. *Am J Pathol* 2014; 184: 3308–3320.

135. Ouyang S, Hsuchou H, Kastin AJ, et al. Leukocyte infiltration into spinal cord of EAE mice is attenuated by removal of endothelial leptin signaling. *Brain Behav Immun* 2014; 40: 61–73.

136. Brambilla R, Morton PD, Ashbaugh JJ, et al. Astrocytes play a key role in EAE pathophysiology by orchestrating in the CNS the inflammatory response of resident and peripheral immune cells and by suppressing remyelination. *Glia* 2014; 62: 452–467.

137. Lutz SE, Smith JR, Kim DH, et al. Caveolin1 Is Required for Th1 Cell Infiltration, but Not Tight Junction Remodeling, at the Blood-Brain Barrier in Autoimmune Neuroinflammation. *Cell Rep* 2017; 21: 2104–2117.

138. Merrill JE. In vitro and in vivo pharmacological models to assess demyelination and remyelination. *Neuropsychopharmacology* 2009; 34: 55–73.

139. Adzemovic MZ, Öckinger J, Zeitelhofer M, et al. Expression of Ccl11 associates with immune response modulation and protection against neuroinflammation in rats. *PLoS One*; 7. Epub ahead of print 2012. DOI: 10.1371/journal.pone.0039794.

140. Morgan L, Shah B, Rivers LE, et al. Inflammation and dephosphorylation of the tight junction protein occludin in an experimental model of multiple sclerosis. *Neuroscience* 2007; 147: 664–673.

141. Ninkovic M, Stevanovic I, Stojanovic I, et al. The Use of Agmatine Provides the New Insight in an Experimental Model of Multiple Sclerosis. *Neurochem Res* 2015; 40: 1719–1727.

142. Halder SK, Kant R, Milner R. Hypoxic pre-conditioning suppresses experimental autoimmune encephalomyelitis by modifying multiple properties of blood vessels. *Acta Neuropathol Commun* 2018; 6: 86.

143. Halder SK, Milner R. Chronic mild hypoxia accelerates recovery from preexisting EAE by enhancing vascular integrity and apoptosis of infiltrated monocytes. *Proc Natl Acad Sci U S A* 2020; 117: 11126–11135.

144. Lanz T V., Becker S, Osswald M, et al. Protein kinase Cβ as a therapeutic target stabilizing blood-brain barrier disruption in experimental autoimmune encephalomyelitis. *Proc Natl Acad Sci U S A* 2013; 110: 14735–14740.

145. Huang J, Han S, Sun Q, et al. Kv1.3 channel blocker (ImKTx88) maintains blood-brain barrier in experimental autoimmune encephalomyelitis. *Cell Biosci*; 7. Epub ahead of print 7 June 2017. DOI: 10.1186/s13578-017-0158-2.

146. Shou J, Peng J, Zhao Z, et al. CCL26 and CCR3 are associated with the acute inflammatory response in the CNS in experimental autoimmune encephalomyelitis. *J Neuroimmunol*; 333. Epub ahead of print 15 August 2019. DOI: 10.1016/j.jneuroim.2019.576967.

147. Yang X, Yan J, Feng J. Treatment with tanshinone IIA suppresses disruption of the blood-brain barrier and reduces expression of adhesion molecules and chemokines in experimental autoimmune encephalomyelitis. *Eur J Pharmacol* 2016; 771: 18–28.

148. Grygorowicz T, Dąbrowska-Bouta B, Strużyńska L. Administration of an antagonist of P2X7 receptor to EAE rats prevents a decrease of expression of claudin-5 in cerebral capillaries. *Purinergic Signal* 2018; 14: 385–393.

149. Viñuela-Berni V, Gómez-González B, Quintanar-Stephano A. Blockade of Arginine Vasopressin receptors prevents blood-brain barrier breakdown in Experimental Autoimmune Encephalomyelitis. *Sci Rep*; 10. Epub ahead of print 1 December 2020. DOI: 10.1038/s41598-019-57134-y.

150. Schrempf W, Ziemssen T. Glatiramer acetate: Mechanisms of action in multiple sclerosis. *Autoimmunity Reviews*; 6. Epub ahead of print 2007. DOI: 10.1016/j.autrev.2007.02.003.

151. Salvador E, Shityakov S, Förster C. Glucocorticoids and endothelial cell barrier function. *Cell and Tissue Research*; 355. Epub ahead of print 2014. DOI: 10.1007/s00441-013-1762-z.

152. Prager B, Spampinato SF, Ransohoff RM. Sphingosine 1-phosphate signaling at the blood-brain barrier. *Trends in Molecular Medicine*; 21. Epub ahead of print 2015. DOI: 10.1016/j.molmed.2015.03.006.

153. Kraus J, Oschmann P. The impact of interferon-β treatment on the blood-brain barrier. *Drug Discovery Today*; 11. Epub ahead of print 2006. DOI: 10.1016/j.drudis.2006.06.008.

154. Duan T, Verkman AS. Experimental animal models of aquaporin-4-IgG-seropositive neuromyelitis optica spectrum disorders: progress and shortcomings. *Brain Pathology* 2020; 30: 13–25.

155. Oleszak EL, Chang JR, Friedman H, et al. Theiler's Virus Infection: A Model for Multiple Sclerosis. *Clinical Microbiology Reviews* 2004; 17: 174–207.

156. Kang SS, McGavern DB. Microbial induction of vascular pathology in the CNS. *Journal of Neuroimmune Pharmacology* 2010; 5: 370–386.

157. L. H, Pirko I, J. A. Experimental Model Systems to Define Mechanisms of Immune-Mediated Blood Brain Barrier Disruption in Acute Disseminated Encephalomyelitis (ADEM) and Acute Hemorrhagic Leukoencephalitis (AHLE). In: *Pathogenesis of Encephalitis*. InTech. Epub ahead of print 9 December 2011. DOI: 10.5772/27069.

158. Johnson AJ, Mendez-Fernandez Y, Moyer AM, et al. Antigen-Specific CD8 + T Cells Mediate a Peptide-Induced Fatal Syndrome . *J Immunol* 2005; 174: 6854–6862.

159. Suidan GL, Mcdole JR, Chen Y, et al. Induction of blood brain barrier tight junction protein alterations by CD8 T cells. *PLoS One*; 3. Epub ahead of print 22 August 2008. DOI: 10.1371/journal.pone.0003037.

160. Johnson HL, Jin F, Pirko I, et al. Theiler's murine encephalomyelitis virus as an experimental model system to study the mechanism of blood-brain barrier disruption. *Journal of NeuroVirology* 2014; 20: 107–112.

161. Johnson HL, Chen Y, Jin F, et al. CD8 T Cell-Initiated Blood–Brain Barrier Disruption Is Independent of Neutrophil Support. *J Immunol* 2012; 189: 1937–1945.

162. Willenbring RC, Jin F, Hinton DJ, et al. Modulatory effects of perforin gene dosage on pathogen-associated blood-brain barrier (BBB) disruption. *J Neuroinflammation*; 13. Epub ahead of print 31 August 2016. DOI: 10.1186/s12974-016-0673-9.

163. Suidan GL, Dickerson JW, Chen Y, et al. CD8 T Cell-Initiated Vascular Endothelial Growth Factor Expression Promotes Central Nervous System Vascular Permeability under Neuroinflammatory Conditions. *J Immunol* 2010; 184: 1031–1040.

164. Johnson HL, Willenbring RC, Jin F, et al. Perforin competent CD8 T cells are sufficient to cause immune-mediated blood-brain barrier disruption. *PLoS One*; 9. Epub ahead of print 22 October 2014. DOI: 10.1371/journal.pone.0111401.

165. Eisele P, Alonso A, Griebe M, et al. Investigation of cerebral microbleeds in multiple sclerosis as a potential marker of blood-brain barrier dysfunction. *Mult Scler Relat Disord*; 7. Epub ahead of print 2016. DOI: 10.1016/j.msard.2016.03.010.

166. Nishigori R, Warabi Y, Isozaki E. Intracranial hemorrhagic lesions in neurosarcoidosis: The difference from neuromyelitis optica spectrum disorders. *Clin Exp Neuroimmunol*; 9. Epub ahead of print March 2018. DOI: 10.1111/cen3.12439.

167. Gross CC, Meyer C, Bhatia U, et al. CD8+ T cell-mediated endotheliopathy is a targetable mechanism of neuro-inflammation in Susac syndrome. *Nat Commun*; 10. Epub ahead of print 18 December 2019. DOI: 10.1038/s41467-019-13593-5.

168. Kipp M, Clarner T, Dang J, et al. The cuprizone animal model: New insights into an old story. *Acta Neuropathologica* 2009; 118: 723–736.

169. Praet J, Guglielmetti C, Berneman Z, et al. Cellular and molecular neuropathology of the cuprizone mouse model: Clinical relevance for multiple sclerosis. *Neuroscience and Biobehavioral Reviews* 2014; 47: 485–505.

170. Bakker DA, Ludwin SK. Blood-brain barrier permeability during Cuprizone-induced demyelination. Implications for the pathogenesis of immune-mediated demyelinating diseases. *J Neurol Sci* 1987; 78: 125–137.

171. McMahon EJ, Suzuki K, Matsushima GK. Peripheral macrophage recruitment in cuprizone-induced CNS demyelination despite an intact blood-brain barrier. *J Neuroimmunol* 2002; 130: 32–45.

172. Berghoff SA, Düking T, Spieth L, et al. Blood-brain barrier hyperpermeability precedes demyelination in the cuprizone model. *Acta Neuropathol Commun* 2017; 5: 94.

173. Berghoff SA, Gerndt N, Winchenbach J, et al. Dietary cholesterol promotes repair of demyelinated lesions in the adult brain. *Nat Commun*; 8. Epub ahead of print 24 January 2017. DOI: 10.1038/ncomms14241.

174. Shelestak J, Singhal N, Frankle L, et al. Increased blood-brain barrier hyperpermeability coincides with mast cell activation early under cuprizone administration. *PLoS One*; 15. Epub ahead of print 1 June 2020. DOI: 10.1371/journal.pone.0234001.

175. Ramirez SH, Fan S, Dykstra H, et al. Inhibition of Glycogen Synthase Kinase 3β Promotes Tight Junction Stability in Brain Endothelial Cells by Half-Life Extension of Occludin and Claudin-5. *PLoS One*; 8. Epub ahead of print 13 February 2013. DOI: 10.1371/journal.pone.0055972.

176. Francisco DMF, Marchetti L, Rodríguez-Lorenzo S, et al. Advancing brain barriers RNA sequencing: Guidelines from experimental design to publication. *Fluids and Barriers of the CNS* 2020; 17: 51.

177. Brown LS, Foster CG, Courtney JM, et al. Pericytes and neurovascular function in the healthy and diseased brain. *Frontiers in Cellular Neuroscience*; 13. Epub ahead of print 2019. DOI: 10.3389/fncel.2019.00282.

178. Daneman R. The blood-brain barrier in health and disease. *Ann Neurol* 2012; 72: 648–672.

179. Nishihara H, Engelhardt B. Brain Barriers and Multiple Sclerosis: Novel Treatment Approaches from a Brain Barriers Perspective. *Handb Exp Pharmacol*. Epub ahead of print 26 November 2020. DOI: 10.1007/164_2020_407.

180. Yamazaki Y, Kanekiyo T. Blood-Brain Barrier Dysfunction and the Pathogenesis of Alzheimer's Disease. *Int J Mol Sci*; 18. Epub ahead of print 13 September 2017. DOI: 10.3390/ijms18091965.

181. Yamazaki Y, Shinohara M, Shinohara M, et al. Selective loss of cortical endothelial tight junction proteins during Alzheimer's disease progression. *Brain*; 142. Epub ahead of print 2019. DOI: 10.1093/brain/awz011.

182. Abdullahi W, Tripathi D, Ronaldson PT. Blood-brain barrier dysfunction in ischemic stroke: targeting tight junctions and transporters for vascular protection. *Am J Physiol Physiol* 2018; 315: C343–C356.

183. Price L, Wilson C, Grant G. *Blood–Brain Barrier Pathophysiology following Traumatic Brain Injury*. 2016.

184. Bodnar CN, Watson JB, Higgins EK, et al. Inflammatory Regulation of CNS Barriers After Traumatic Brain Injury: A Tale Directed by Interleukin-1. *Front Immunol*; 12. Epub ahead of print 21 May 2021. DOI: 10.3389/fimmu.2021.688254.

185. Greene C, Hanley N, Campbell M. Blood-brain barrier associated tight junction disruption is a hallmark feature of major psychiatric disorders. *Transl Psychiatry*; 10. Epub ahead of print 2020. DOI: 10.1038/s41398-020-01054-3.

186. Thomsen MS, Routhe LJ, Moos T. The vascular basement membrane in the healthy and pathological brain. *J Cereb Blood Flow Metab*; 37. Epub ahead of print 28 October 2017. DOI: 10.1177/0271678X17722436.

187. Baeten KM, Akassoglou K. Extracellular matrix and matrix receptors in blood-brain barrier formation and stroke. *Dev Neurobiol*; 71. Epub ahead of print November 2011. DOI: 10.1002/dneu.20954.

188. Reed MJ, Damodarasamy M, Banks WA. The extracellular matrix of the blood–brain barrier: structural and functional roles in health, aging, and Alzheimer's disease. *Tissue Barriers*; 7. Epub ahead of print 2 October 2019. DOI: 10.1080/21688370.2019.1651157.

189. Xu L, Nirwane A, Yao Y. Basement membrane and blood–brain barrier. *Stroke Vasc Neurol*; 4. Epub ahead of print June 2019. DOI: 10.1136/svn-2018-000198.

190. Osada T, Gu Y-H, Kanazawa M, et al. Interendothelial Claudin-5 Expression Depends on Cerebral Endothelial Cell–Matrix Adhesion by β_1 -Integrins. *J Cereb Blood Flow Metab*; 31. Epub ahead of print 20 October 2011. DOI: 10.1038/jcbfm.2011.99.

191. Izawa Y, Gu Y-H, Osada T, et al. β1-integrin–matrix interactions modulate cerebral microvessel endothelial cell tight junction expression and permeability. *J Cereb Blood Flow Metab*; 38. Epub ahead of print 8 April 2018. DOI: 10.1177/0271678X17722108.

192. Van Horssen J, Dijkstra CD, De Vries HE. The extracellular matrix in multiple sclerosis pathology. *Journal of Neurochemistry*; 103. Epub ahead of print 2007. DOI: 10.1111/j.1471-4159.2007.04897.x.

193. Mohan H, Krumbholz M, Sharma R, et al. Extracellular matrix in multiple sclerosis lesions: Fibrillar collagens, biglycan and decorin are upregulated and associated with infiltrating immune cells. *Brain Pathol*; 20. Epub ahead of print 2010. DOI: 10.1111/j.1750-3639.2010.00399.x.

194. Munji RN, Soung AL, Weiner GA, et al. Profiling the mouse brain endothelial transcriptome in health and disease models reveals a core blood–brain barrier dysfunction module. *Nat Neurosci*; 22. Epub ahead of print 2019. DOI: 10.1038/s41593-019-0497-x.

195. Tagami M, Yamagata K, Fujino H, et al. Morphological differentiation of endothelial cells co-cultured with astrocytes on type-I or type-IV collagen. *Cell Tissue Res* 1992; 268: 225–232.

196. Tilling T, Korte D, Hoheisel D, et al. Basement membrane proteins influence brain capillary endothelial barrier function in vitro. *J Neurochem*; 71. Epub ahead of print 1998. DOI: 10.1046/j.1471-4159.1998.71031151.x.

197. Zhang Y, Chen K, Sloan SA, et al. An RNA-sequencing transcriptome and splicing database of glia, neurons, and vascular cells of the cerebral cortex. *J Neurosci* 2014; 34: 11929–47.

198. Zhang Y, Sloan SA, Clarke LE, et al. Purification and Characterization of Progenitor and Mature Human Astrocytes Reveals Transcriptional and Functional Differences with Mouse. *Neuron*; 89. Epub ahead of print 6 January 2016. DOI: 10.1016/j.neuron.2015.11.013.

199. Sabbagh MF, Heng JS, Luo C, et al. Transcriptional and epigenomic landscapes of CNS and non-CNS vascular endothelial cells. *Elife*; 7. Epub ahead of print 6 September 2018. DOI: 10.7554/eLife.36187.

200. Vanlandewijck M, He L, Mäe MA, et al. A molecular atlas of cell types and zonation in the brain vasculature. *Nature* 2018; 554: 475–480.

201. Robertson RT, Levine ST, Haynes SM, et al. Use of labeled tomato lectin for imaging vasculature structures. *Histochem Cell Biol*; 143. Epub ahead of print 2015. DOI: 10.1007/s00418-014-1301-3.

202. Watson PMD, Paterson JC, Thom G, et al. Modelling the endothelial blood-CNS barriers: A method for the production of robust in vitro models of the rat blood-brain barrier and blood-spinal cord barrier. *BMC Neurosci*; 14. Epub ahead of print 2013. DOI: 10.1186/1471-2202-14-59.

203. Wadia JS, Stan R V., Dowdy SF. Transducible TAT-HA fusogenic peptide enhances escape of TAT-fusion proteins after lipid raft macropinocytosis. *Nat Med*; 10. Epub ahead of print 2004. DOI: 10.1038/nm996.

204. Szulcek R, Bogaard HJ, van Nieuw Amerongen GP. Electric Cell-substrate Impedance Sensing for the Quantification of Endothelial Proliferation, Barrier Function, and Motility. *J Vis Exp*. Epub ahead of print 28 March 2014. DOI: 10.3791/51300.

205. Chen H, Kovar J, Sissons S, et al. A cell-based immunocytochemical assay for monitoring kinase signaling pathways and drug efficacy. *Anal Biochem*; 338. Epub ahead of print 2005. DOI: 10.1016/j.ab.2004.11.015.

206. Boveia V, Schutz-Geschwender A. Quantitative analysis of signal transduction with in-cell western immunofluorescence assays. In: *Methods in Molecular Biology*. 2015. Epub ahead of print 2015. DOI: 10.1007/978-1-4939-2718-0_13.

207. Göbel K, Ruck T, Meuth SG. Cytokine signaling in multiple sclerosis: Lost in translation. *Multiple Sclerosis Journal*; 24. Epub ahead of print 2018. DOI: 10.1177/1352458518763094.

208. Karpus WJ. Cytokines and Chemokines in the Pathogenesis of Experimental Autoimmune Encephalomyelitis. *J Immunol*; 204. Epub ahead of print 2020. DOI: 10.4049/jimmunol.1900914.

209. Borjini N, Fernández M, Giardino L, et al. Cytokine and chemokine alterations in tissue, CSF, and plasma in early presymptomatic phase of experimental allergic encephalomyelitis (EAE), in a rat model of multiple sclerosis. *J Neuroinflammation*; 13. Epub ahead of print 2016. DOI: 10.1186/s12974-016-0757-6.

210. Palle P, Monaghan KL, Milne SM, et al. Cytokine Signaling in Multiple Sclerosis and Its Therapeutic Applications. *Med Sci*; 5. Epub ahead of print 2017. DOI: 10.3390/medsci5040023.

211. Yang JF, Tao HQ, Liu YM, et al. Characterization of the interaction between astrocytes and encephalitogenic lymphocytes during the development of experimental autoimmune encephalitomyelitis (EAE) in mice. *Clin Exp Immunol*; 170. Epub ahead of print 2012. DOI: 10.1111/j.1365-2249.2012.04661.x.

212. Xie L, Yang SH. Interaction of astrocytes and T cells in physiological and pathological conditions. *Brain Research*; 1623. Epub ahead of print 2015. DOI: 10.1016/j.brainres.2015.03.026.

213. Pierson ER, Wagner CA, Goverman JM. The contribution of neutrophils to CNS autoimmunity. *Clin Immunol*; 189. Epub ahead of print 2018. DOI: 10.1016/j.clim.2016.06.017.

214. Woodberry T, Bouffler SE, Wilson AS, et al. The emerging role of neutrophil granulocytes in multiple sclerosis. *Journal of Clinical Medicine*; 7. Epub ahead of print 2018. DOI: 10.3390/jcm7120511.

215. Savettieri G, Di Liegro I, Catania C, et al. Neurons and ECM regulate occludin localization in brain endothelial cells. *Neuroreport*; 11. Epub ahead of print 2000. DOI: 10.1097/00001756-200004070-00035.

216. Leclech C, Natale CF, Barakat AI. The basement membrane as a structured surface – role in vascular health and disease. *Journal of Cell Science*; 133. Epub ahead of print 2021. DOI: 10.1242/jcs.239889.

217. Yuan SY, Rigor RR. *Regulation of Endothelial Barrier Function*. Morgan & Claypool Life Sciences, http://www.ncbi.nlm.nih.gov/pubmed/21634066 (2010, accessed 22 March 2018).

218. Pulous FE, Petrich BG. Integrin-dependent regulation of the endothelial barrier. *Tissue Barriers*; 7. Epub ahead of print 2019. DOI: 10.1080/21688370.2019.1685844.

219. Heino J. The collagen receptor integrins have distinct ligand recognition and signaling functions. *Matrix Biol*; 19. Epub ahead of print August 2000. DOI: 10.1016/S0945-053X(00)00076-7.

220. Silva R, D'Amico G, Hodivala-Dilke KM, et al. Integrins: The keys to unlocking angiogenesis. *Arteriosclerosis, Thrombosis, and Vascular Biology*; 28. Epub ahead of print 2008. DOI: 10.1161/ATVBAHA.108.172015.

221. Wickström SA, Lange A, Montanez E, et al. The ILK/PINCH/parvin complex: The kinase is dead, long live the pseudokinase! *EMBO Journal*; 29. Epub ahead of print 2010. DOI: 10.1038/emboj.2009.376.

222. Qin J, Wu C. ILK: a pseudokinase in the center stage of cell-matrix adhesion and signaling. *Current Opinion in Cell Biology*; 24. Epub ahead of print 2012. DOI: 10.1016/j.ceb.2012.06.003.

223. Friedrich EB, Liu E, Sinha S, et al. Integrin-Linked Kinase Regulates Endothelial Cell Survival and Vascular Development. *Mol Cell Biol*; 24. Epub ahead of print 2004. DOI: 10.1128/mcb.24.18.8134-8144.2004.

224. Park H, Yamamoto H, Mohn L, et al. Integrin-linked kinase controls retinal angiogenesis and is linked to Wnt signaling and exudative vitreoretinopathy. *Nat Commun*; 10. Epub ahead of print 2019. DOI: 10.1038/s41467-019-13220-3.

225. Jang AS, Concel VJ, Bein K, et al. Endothelial dysfunction and Claudin 5 regulation during acrolein-induced lung injury. *Am J Respir Cell Mol Biol*; 44. Epub ahead of print 2011. DOI: 10.1165/rcmb.2009-0391OC.

226. Beard RS, Haines RJ, Wu KY, et al. Non-muscle Mlck is required for ß-catenin- and FoxO1-dependent downregulation of Cldn5 in IL-1ß-mediated barrier dysfunction in brain endothelial cells. *J Cell Sci*; 127. Epub ahead of print 2014. DOI: 10.1242/jcs.144550.

227. Yau CYF, Wheeler JJ, Sutton KL, et al. Inhibition of Integrin-Linked Kinase by a Selective Small Molecule Inhibitor, QLT0254, Inhibits the PI3K/PKB/mTOR, Stat3, and FKHR Pathways and Tumor Growth, and Enhances Gemcitabine-Induced Apoptosis in Human Orthotopic Primary Pancreatic Cancer Xenografts. *Cancer Res*; 65. Epub ahead of print 2005. DOI: 10.1158/0008-5472.can-04-2940.

228. Vaynberg J, Fukuda K, Lu F, et al. Non-catalytic signaling by pseudokinase ILK for regulating cell adhesion. *Nat Commun*; 9. Epub ahead of print 2018. DOI: 10.1038/s41467-018-06906-7.

229. Proia P, Schiera G, Salemi G, et al. Neuronal and BBB damage induced by sera from patients with secondary progressive multiple sclerosis. *Int J Mol Med* 2009; 24: 743–747.

230. Whelan MC, Senger DR. Collagen I Initiates Endothelial Cell Morphogenesis by Inducing Actin Polymerization through Suppression of Cyclic AMP and Protein Kinase A. *J Biol Chem*; 278. Epub ahead of print January 2003. DOI: 10.1074/jbc.M207554200.

231. Ishizaki T, Chiba H, Kojima T, et al. Cyclic AMP induces phosphorylation of claudin-5 immunoprecipitates and expression of claudin-5 gene in blood–brain-barrier endothelial cells via protein kinase A-dependent and -independent pathways. *Exp Cell Res*; 290. Epub ahead of print November 2003. DOI: 10.1016/S0014-4827(03)00354-9.

232. Kakogiannos N, Ferrari L, Giampietro C, et al. JAM-A acts via C/EBP-α to promote claudin-5 expression and enhance endothelial barrier function. *Circ Res*. Epub ahead of print 2020. DOI: 10.1161/CIRCRESAHA.120.316742.

233. Lee JW, Chen H, Pullikotil P, et al. Protein kinase A-α directly phosphorylates FoxO1 in vascular endothelial cells to regulate expression of vascular cellular adhesion molecule-1 mRNA. *J Biol Chem*; 286. Epub ahead of print 2011. DOI: 10.1074/jbc.M110.180661.

234. Liu Y, Senger DR. Matrix-specific activation of Src and Rho initiates capillary morphogenesis of endothelial cells. *FASEB J*; 18. Epub ahead of print March 2004. DOI: 10.1096/fj.03-0948com.

235. Giannotta M, Trani M, Dejana E. VE-cadherin and endothelial adherens junctions: Active guardians of vascular integrity. *Developmental Cell*; 26. Epub ahead of print 2013. DOI: 10.1016/j.devcel.2013.08.020.

236. González-Santiago L, López-Ongil S, Rodríguez-Puyol M, et al. Decreased nitric oxide synthesis in human endothelial cells cultured on type I collagen. *Circ Res*; 90. Epub ahead of print 2002. DOI: 10.1161/01.RES.0000012445.68979.9D.

237. Fukuda K, Gupta S, Chen K, et al. The Pseudoactive Site of ILK Is Essential for Its Binding to α-Parvin and Localization to Focal Adhesions. *Mol Cell*; 36. Epub ahead of print 2009. DOI: 10.1016/j.molcel.2009.11.028.

238. Fukuda K, Knight JDR, Piszczek G, et al. Biochemical, proteomic, structural, and thermodynamic characterizations of integrin-linked kinase (ILK): Cross-validation of the pseudokinase. *J Biol Chem*; 286. Epub ahead of print 2011. DOI: 10.1074/jbc.M111.240093.

239. Neill T, Schaefer L, Iozzo R V. Decorin: A guardian from the matrix. *American Journal of Pathology*; 181. Epub ahead of print 2012. DOI: 10.1016/j.ajpath.2012.04.029.

240. Chen S, Birk DE. Focus on Molecules: Decorin. *Experimental Eye Research*; 92. Epub ahead of print 2011. DOI: 10.1016/j.exer.2010.05.008.

241. Rühland C, Schönherr E, Robenek H, et al. The glycosaminoglycan chain of decorin plays an important role in collagen fibril formation at the early stages of fibrillogenesis. *FEBS J*; 274. Epub ahead of print 2007. DOI: 10.1111/j.1742-4658.2007.05951.x.

242. Esmaeili M, Berry M, Logan A, et al. Decorin treatment of spinal cord injury. *Neural Regen Res*; 9. Epub ahead of print 2014. DOI: 10.4103/1673-5374.141797.

243. Neill T, Schaefer L, Iozzo R V. Oncosuppressive functions of decorin. *Molecular and Cellular Oncology*; 2. Epub ahead of print 2015. DOI: 10.4161/23723556.2014.975645.

244. Gubbiotti MA, Vallet SD, Ricard-Blum S, et al. Decorin interacting network: A comprehensive analysis of decorin-binding partners and their versatile functions. *Matrix Biology*; 55. Epub ahead of print 2016. DOI: 10.1016/j.matbio.2016.09.009.

245. Neill T, Buraschi S, Kapoor A, et al. Proteoglycan-driven Autophagy: A Nutrient-independent Mechanism to Control Intracellular Catabolism. *Journal of Histochemistry and Cytochemistry*; 68. Epub ahead of print 2020. DOI: 10.1369/0022155420937370.

246. Fiedler LR, Schönherr E, Waddington R, et al. Decorin regulates endothelial cell motility on collagen I through activation of insulin-like growth factor I receptor and modulation of α2β1 integrin activity. *J Biol Chem*; 283. Epub ahead of print 2008. DOI: 10.1074/jbc.M710025200.

247. Zhang Y, Yang X. The Roles of TGF-β Signaling in Cerebrovascular Diseases. *Frontiers in Cell and Developmental Biology*; 8. Epub ahead of print 2020. DOI: 10.3389/fcell.2020.567682.

248. Fresegna D, Bullitta S, Musella A, et al. Re-Examining the Role of TNF in MS Pathogenesis and Therapy. *Cells*; 9. Epub ahead of print 2020. DOI: 10.3390/cells9102290.

249. Girolamo F, Coppola C, Ribatti D, et al. Angiogenesis in multiple sclerosis and experimental autoimmune encephalomyelitis. *Acta Neuropathologica Communications*; 2. Epub ahead of print 2014. DOI: 10.1186/s40478-014-0084-z.

250. Derada Troletti C, Fontijn RD, Gowing E, et al. Inflammation-induced endothelial to mesenchymal transition promotes brain endothelial cell dysfunction and occurs during multiple sclerosis pathophysiology. *Cell Death Dis*; 10. Epub ahead of print 1 February 2019. DOI: 10.1038/s41419-018-1294-2.

251. Aslam M, Ahmad N, Srivastava R, et al. TNF-alpha induced NFκB signaling and p65 (RelA) overexpression repress Cldn5 promoter in mouse brain endothelial cells. *Cytokine*; 57. Epub ahead of print 2012. DOI: 10.1016/j.cyto.2011.10.016.

252. Daly C, Wong V, Burova E, et al. Angiopoietin-1 modulates endothelial cell function and gene expression via the transcription factor FKHR (FOXO1). *Genes Dev*; 18. Epub ahead of print 2004. DOI: 10.1101/gad.1189704.

253. Daly C, Pasnikowski E, Burova E, et al. Angiopoietin-2 functions as an autocrine protective factor in stressed endothelial cells. *Proc Natl Acad Sci U S A*; 103. Epub ahead of print 2006. DOI: 10.1073/pnas.0607538103.

254. Sweeney MD, Ayyadurai S, Zlokovic B V. Pericytes of the neurovascular unit: key functions and signaling pathways. *Nat Neurosci* 2016; 19: 771–783.

255. Liebner S, Dijkhuizen RM, Reiss Y, et al. Functional morphology of the blood–brain barrier in health and disease. *Acta Neuropathologica*; 135. Epub ahead of print 2018. DOI: 10.1007/s00401-018-1815-1.

256. Kim M, Allen B, Korhonen EA, et al. Opposing actions of angiopoietin-2 on Tie2 signaling and FOXO1 activation. *J Clin Invest*; 126. Epub ahead of print 2016. DOI: 10.1172/JCI84871.

257. Si Y, Huang J, Li X, et al. AKT/FOXO1 axis links cross-talking of endothelial cell and pericyte in TIE2-mutated venous malformations. *Cell Commun Signal*; 18. Epub ahead of print 2020. DOI: 10.1186/s12964-020-00606-w.

258. Mueller SB, Kontos CD. Tie1: An orphan receptor provides context for angiopoietin-2/Tie2 signaling. *Journal of Clinical Investigation*; 126. Epub ahead of print 2016. DOI: 10.1172/JCI89963.

259. Maisonpierre PC, Suri C, Jones PF, et al. Angiopoietin-2, a natural antagonist for Tie2 that disrupts in vivo angiogenesis. *Science (80-)*; 277. Epub ahead of print 1997. DOI: 10.1126/science.277.5322.55.

260. Gurnik S, Devraj K, Macas J, et al. Angiopoietin-2-induced blood–brain barrier compromise and increased stroke size are rescued by VE-PTP-dependent restoration of Tie2 signaling. *Acta Neuropathol*; 131. Epub ahead of print 2016. DOI: 10.1007/s00401-016-1551-3.

261. Li Z, Korhonen EA, Merlini A, et al. Angiopoietin-2 blockade ameliorates autoimmune neuroinflammation by inhibiting leukocyte recruitment into the CNS. *J Clin Invest*; 130. Epub ahead of print 2020. DOI: 10.1172/JCI130308.

262. Blecharz KG, Frey D, Schenkel T, et al. Autocrine release of angiopoietin-2 mediates cerebrovascular disintegration in Moyamoya disease. *J Cereb Blood Flow Metab*; 37. Epub ahead of print 2017. DOI: 10.1177/0271678X16658301.

263. Robinson KA, Sun M, Barnum CE, et al. Decorin and biglycan are necessary for maintaining collagen fibril structure, fiber realignment, and mechanical properties of mature tendons. *Matrix Biol*; 64. Epub ahead of print 2017. DOI: 10.1016/j.matbio.2017.08.004.

264. McBride OW, Fisher LW, Young MF. Localization of PGI (biglycan, BGN) and PGII (decorin, DCN, PG-40) genes on human chromosomes Xq13-qter and 12q, respectively. *Genomics*; 6. Epub ahead of print 1990. DOI: 10.1016/0888-7543(90)90560-H.

265. Ridder DA, Lang M-F, Salinin S, et al. TAK1 in brain endothelial cells mediates fever and lethargy. *J Exp Med* 2011; 208: 2615–2623.

266. Felinski EA, Cox AE, Phillips BE, et al. Glucocorticoids induce transactivation of tight junction genes occludin and claudin-5 in retinal endothelial cells via a novel cis-element. *Exp Eye Res*; 86. Epub ahead of print 2008. DOI: 10.1016/j.exer.2008.01.002.

267. Keil JM, Liu X, Antonetti DA. Glucocorticoid induction of occludin expression and endothelial barrier requires transcription factor p54 NONO. *Investig Ophthalmol Vis Sci*; 54. Epub ahead of print 2013. DOI: 10.1167/iovs.13-11980.

268. Förster C, Silwedel C, Golenhofen N, et al. Occludin as direct target for glucocorticoid-induced improvement of blood-brain barrier properties in a murine in vitro system. *J Physiol* 2005; 565: 475–486.

269. Burek M, Förster CY. Cloning and characterization of the murine claudin-5 promoter. *Mol Cell Endocrinol*; 298. Epub ahead of print January 2009. DOI: 10.1016/j.mce.2008.09.041.

270. Na W, Shin JY, Lee JY, et al. Dexamethasone suppresses JMJD3 gene activation via a putative negative glucocorticoid response element and maintains integrity of tight junctions in brain microvascular endothelial cells. *J Cereb Blood Flow Metab*; 37. Epub ahead of print 2017. DOI: 10.1177/0271678X17701156.

271. Winkelmann A, Loebermann M, Reisinger EC, et al. Disease-modifying therapies and infectious risks in multiple sclerosis. *Nature Reviews Neurology*; 12. Epub ahead of print 2016. DOI: 10.1038/nrneurol.2016.21.

272. Coutinho AE, Chapman KE. The anti-inflammatory and immunosuppressive effects of glucocorticoids, recent developments and mechanistic insights. *Molecular and Cellular Endocrinology*; 335. Epub ahead of print 2011. DOI: 10.1016/j.mce.2010.04.005.

273. Zhao Z, Ma CL, Gu ZC, et al. Incidence and Risk of Infection Associated With Fingolimod in Patients With Multiple Sclerosis: A Systematic Review and Meta-Analysis of 8,448 Patients From 12 Randomized Controlled Trials. *Frontiers in Immunology*; 12. Epub ahead of print 2021. DOI: 10.3389/fimmu.2021.611711.

274. Vargas W s., Perumal J s. Fingolimod and cardiac risk: Latest findings and clinical implications. *Ther Adv Drug Saf*; 4. Epub ahead of print 2013. DOI: 10.1177/2042098613481023.

275. Qureshi SA, Ding V, Li Z, et al. Activation of insulin signal transduction pathway and anti-diabetic activity of small molecule insulin receptor activators. *J Biol Chem*; 275. Epub ahead of print 2000. DOI: 10.1074/jbc.M006287200.

276. Liu K, Xu L, Szalkowski D, et al. Discovery of a potent, highly selective, and orally efficacious small-molecule activator of the insulin receptor. *J Med Chem*; 43. Epub ahead of print 2000. DOI: 10.1021/jm000285q.

277. Bolton JL, Dunlap T. Formation and biological targets of quinones: Cytotoxic versus cytoprotective effects. *Chemical Research in Toxicology*; 30. Epub ahead of print 2017. DOI: 10.1021/acs.chemrestox.6b00256.

278. Robilliard LD, Kho DT, Johnson RH, et al. The importance of multifrequency impedance sensing of endothelial barrier formation using ECIS technology for the generation of a strong and durable paracellular barrier. *Biosensors*; 8. Epub ahead of print 2018. DOI: 10.3390/bios8030064.

279. Sehnal D, Bittrich S, Deshpande M, et al. Mol∗Viewer: Modern web app for 3D visualization and analysis of large biomolecular structures. *Nucleic Acids Res*; 49. Epub ahead of print 2021. DOI: 10.1093/nar/gkab314.

280. Mandel I, Paperna T, Glass-Marmor L, et al. Tight junction proteins expression and modulation in immune cells and multiple sclerosis. *J Cell Mol Med* 2012; 16: 765–775.

281. Hassanzadeh G, Hosseini Quchani S, Sahraian MA, et al. Leukocyte Gene Expression and Plasma Concentration in Multiple Sclerosis: Alteration of Transforming Growth Factor-βs, Claudin-11, and Matrix Metalloproteinase-2. *Cell Mol Neurobiol* 2016; 36: 865–872.

282. Annunziata P, Cioni C, Masi G, et al. Fingolimod reduces circulating tight-junction protein levels and in vitro peripheral blood mononuclear cells migration in multiple sclerosis patients. *Sci Rep*; 8. Epub ahead of print 1 December 2018. DOI: 10.1038/s41598-018-33672-9.

283. Camara-Lemarroy CR, Silva C, Greenfield J, et al. Biomarkers of intestinal barrier function in multiple sclerosis are associated with disease activity. *Mult Scler J*. Epub ahead of print 2019. DOI: 10.1177/1352458519863133.

284. Masaki K, Suzuki SO, Matsushita T, et al. Extensive loss of connexins in Baló's disease: Evidence for an auto-antibody-independent astrocytopathy via impaired astrocyte-oligodendrocyte/ myelin interaction. *Acta Neuropathol* 2012; 123: 887–900.

285. Kooij G, Kopplin K, Blasig R, et al. Disturbed function of the blood-cerebrospinal fluid barrier aggravates neuro-inflammation. *Acta Neuropathol* 2014; 128: 267–277.

286. Cui C, Tan S, Tao L, et al. Intestinal Barrier Breakdown and Mucosal Microbiota Disturbance in Neuromyelitis Optical Spectrum Disorders. *Front Immunol*; 11. Epub ahead of print 2 September 2020. DOI: 10.3389/fimmu.2020.02101.

287. Minagar A, Ostanin D, Long AC, et al. Serum from patients with multiple sclerosis downregulates occludin and VE-cadherin expression in cultured endothelial cells. *Mult Scler* 2003; 9: 235–238.

288. Blecharz KG, Haghikia A, Stasiolek M, et al. Glucocorticoid effects on endothelial barrier function in the murine brain endothelial cell line cEND incubated with sera from patients with multiple sclerosis. *Mult Scler* 2010; 16: 293–302.

289. Cobo-Calvo A, Ruiz A, Richard C, et al. Purified IgG from aquaporin-4 neuromyelitis optica spectrum disorder patients alters blood-brain barrier permeability. *PLoS One*; 15. Epub ahead of print 1 September 2020. DOI: 10.1371/journal.pone.0238301.

290. Wang XS, Fang HL, Chen Y, et al. Idazoxan reduces blood-brain barrier damage during experimental autoimmune encephalomyelitis in mouse. *Eur J Pharmacol* 2014; 736: 70–76.

291. Wang D, Li SP, Fu JS, et al. Resveratrol defends blood-brain barrier integrity in experimental autoimmune encephalomyelitis mice. *J Neurophysiol* 2016; 116: 2173–2179.

292. Choi JH, Lee MJ, Jang M, et al. An oriental medicine, hyungbangpaedok-san attenuates motor paralysis in an experimental model of multiple sclerosis by regulating the T cell response. *PLoS One*; 10. Epub ahead of print 7 October 2015. DOI: 10.1371/journal.pone.0138592.

293. Liu Y, Ma Y, Du B, et al. Mesenchymal Stem Cells Attenuated Blood-Brain Barrier Disruption via Downregulation of Aquaporin-4 Expression in EAE Mice. *Mol Neurobiol* 2020; 57: 3891–3901.

294. Horng S, Therattil A, Moyon S, et al. Astrocytic tight junctions control inflammatory CNS lesion pathogenesis. *J Clin Invest* 2017; 127: 3136–3151.

295. Kebir H, Kreymborg K, Ifergan I, et al. Human TH17 lymphocytes promote blood-brain barrier disruption and central nervous system inflammation. *Nat Med* 2007; 13: 1173–1175.

296. Souza PS, Gonçalves ED, Pedroso GS, et al. Physical Exercise Attenuates Experimental Autoimmune Encephalomyelitis by Inhibiting Peripheral Immune Response and Blood-Brain Barrier Disruption. *Mol Neurobiol* 2017; 54: 4723–4737.

297. Kim HN, Kim YR, Ahn SM, et al. Protease activated receptor-1 antagonist ameliorates the clinical symptoms of experimental autoimmune encephalomyelitis via inhibiting breakdown of blood-brain barrier. *J Neurochem* 2015; 135: 577–588.

298. Shrestha B, Paul D, Pachter JS. Alterations in tight junction protein and igg permeability accompany leukocyte extravasation across the choroid plexus during neuroinflammation. *J Neuropathol Exp Neurol* 2014; 73: 1047–1061.

299. Giacoppo S, Galuppo M, Iori R, et al. The protective effects of bioactive (RS)-glucoraphanin on the permeability of the mice blood-brain barrier following experimental autoimmune encephalomyelitis. *Eur Rev Med Pharmacol Sci* 2014; 18: 194–204.

300. Zheng M, Wei J, Tang Y, et al. ApoE-Deficient Promotes Blood–Brain Barrier Disruption in Experimental Autoimmune Encephalomyelitis via Alteration of MMP-9. *J Mol Neurosci* 2014; 54: 282–290.

301. Becanovic K, Jagodic M, Sheng JR, et al. Advanced Intercross Line Mapping of Eae5 Reveals Ncf-1 and CLDN4 as Candidate Genes for Experimental Autoimmune Encephalomyelitis . *J Immunol* 2006; 176: 6055–6064.

302. Fairless R, Williams SK, Hoffmann DB, et al. Preclinical retinal neurodegeneration in a model of multiple sclerosis. *J Neurosci* 2012; 32: 5585–5597.

303. Stevens DB, Chen K, Seitz RS, et al. Oligodendrocyte-specific protein peptides induce experimental autoimmune encephalomyelitis in SJL/J mice. *J Immunol* 1999; 162: 7501–7509.

304. Wolburg H, Wolburg-Buchholz K, Liebner S, et al. Claudin-1, claudin-2 and claudin-11 are present in tight junctions of choroid plexus epithelium of the mouse. *Neurosci Lett* 2001; 307: 77–80.

305. Huang XN, Wang WZ, Fu J, et al. The Relationship Between Aquaporin-4 Expression and Blood-Brain and Spinal Cord Barrier Permeability Following Experimental Autoimmune Encephalomyelitis in the Rat. *Anat Rec* 2011; 294: 46–54.

306. Huang XN, Fu J, Wang WZ. The effects of fasudil on the permeability of the rat blood-brain barrier and blood-spinal cord barrier following experimental autoimmune encephalomyelitis. *J Neuroimmunol* 2011; 239: 61–67.

APPENDIX A

Recent Transcriptional Studies Involving Claudin or TAMPs in Brain Microvessels.

Table A.1. Summary of Recent Transcriptional Studies Involving Claudin or TAMP Expression in Brain MVs.

Gene	Human (LCM)[39] Exp. (% Overall)	Mouse (LCM)[39] Exp. (% Overall)	Mouse (Dex-40 µm)[39] Exp. (% Overall)	Mouse (MACS)[41] Exp. (% Overall)	Rat (Dex-40 µm)[42] Exp. (% Overall)
Claudin-1	✓ 2.3%	✓ 2.3%	✓ 3.0%	✓ < 0.1%	✓ 0.5%
Claudin-2	✓ < 0.1%	✓ < 0.1%	✓ 1.4%	✓ < 0.1%	✓ < 0.1%
Claudin-3	✓ 0.5%	✓ 0.2%	✓ 0.1%	✓ 0.2%	✓ 0.2%
Claudin-4	✓ 0.3%	✓ 0.2%	✓ 0.4%	✗	✓ < 0.1%
Claudin-5	✓ 15.8%	✓ 37.1%	✓ 83.9%	✓ 91.6%	✓ 90.7%
Claudin-6	✓ 0.6%	✓ < 0.1%	✓ < 0.1%	✗	✓ 0.2%
Claudin-7	✗	✗	✗	✗	
Claudin-8	✗	✗	✓ < 0.1%	✓ 0.2%	
Claudin-9	✓ 1.0%	✓ 0.2%	✓ < 0.1%	✓ < 0.1%	✓ 1.2%
Claudin-10	✗	✗	✗	✓ 1.5%	✓ 0.4%
Claudin-11	✓ 12.5%	✓ 29.2%	✓ 0.3%	✓ < 0.1%	✓ 0.9%
Claudin-12	✓ 8.8%	✓ 8.3%	✓ 1.1%	✓ 0.1%	✓ 0.8%
[a]***Claudin-13***	*No Orthologue*	✗	✓ < 0.1%	✗	
Claudin-14	✗	✓ 0.9%	✓ < 0.1%	✗	
Claudin-15	✓ 0.5%	✓ < 0.1%	✓ < 0.1%	✓ 0.1%	
Claudin-16	✗	✗	✗	✗	✓ 0.9%

Note: Genes detected by qPCR-based assays are demarked by a check mark (✓) and those not detected by a cross mark (✗). Genes not tested are demarked by two dashes (--). For relative expression, the mRNA amounts for all transcripts was summed, then the percentage for each gene calculated.

[a]Mouse claudin-13 has no known human orthologue. Although there is a claudin-13-like gene in rats, no evidence exists that it is expressed.

LCM: Laser-capture microdissection. **Dex-40 µm:** Dextran-based sedimentation followed by the usage of a 40 µm filter. **MACS:** Magnetic-activated cell sorting.

Gene	Human (LCM)[39] Exp. (% Overall)	Mouse (LCM)[39] Exp. (% Overall)	Mouse (Dex-40 µm)[39] Exp. (% Overall)	Mouse (MACS)[41] Exp. (% Overall)	Rat (Dex-40 µm)[42] Exp. (% Overall)
Claudin-17	✓ 0.5%	✓ 0.4%	✓ 0.1%	✓ 0.3%	--
Claudin-18	✗	✗	✗	✗	--
Claudin-19	✗	✗	✗	✓ 0.5%	✓ < 0.1%
Claudin-20	✓ 0.3%	✓ 4.3%	✗	✓ 0.2%	--
[b]***Claudin-21***	*No Orthologue*	*No Orthologue*	*No Orthologue*	*No Orthologue*	*No Orthologue*
[b]***Claudin-22***	✓ 0.3%	✓ 0.6%	✓ < 0.1%	✓ 1.8%	✓ 0.5%
Claudin-23	✓ 0.1%	✗	✓ < 0.1%	✓ 0.5%	--
[b]***Claudin-24***	✗	✓ 0.9%	✓ 0.6%	--	--
[c]***Claudin-25***	✗	✗	✗	--	--
[d]***Claudin-26***	✗	✓ 0.8%	✗	--	--
[d]***Claudin-27***	✓ 6.0%	✗	✗	--	--
[c]***Cldnd1***	✓ 49.0%	✓ 8.8%	✓ 3.6%	--	--
Occludin	✓ 1.3%	✓ 5.5%	✓ 4.7%	✓ 2.7%	✓ 3.6%
MarvelD2	✓ 0.2%	✓ 0.2%	✓ 0.3%	--	--
MarvelD3	--	--	--	--	--

Note: Genes detected by qPCR-based assays are demarked by a check mark (✓) and those not detected by a cross mark (✗). Genes not tested are demarked by two dashes (--). For relative expression, the mRNA amounts for all transcripts was summed, then the percentage for each gene calculated.

[b]Claudins 22 and 24 are paralogues. Previously, they were designated singularly as claudin-21. There are no genes currently designated claudin-21 in humans or rodents. [c]Claudin domain-containing protein 1 was previously designated claudin-25, and a separate gene is now designated as claudin-25 in humans and rodents. [4]Claudins 26 and 27 are putative members of the claudin family, but more recent phylogenetic analysis suggests they may actually belong to the voltage-dependent calcium channel gamma subunit (CACNG) family.

LCM: Laser-capture microdissection. **Dex-40 µm:** Dextran-based sedimentation followed by the usage of a 40 µm filter. **MACS:** Magnetic-activated cell sorting.

APPENDIX B

Search Strategies Used to Identify Relevant Studies

Table B.0. Search Strategy Parameters.

Search #	Member	Gene ID	Search	Results	Notes
#0	***Gene***	Human Mouse Rat	TS=("keyword") Databases=WOS, BIOSIS, KJD, MEDLINE, RSCI, SCIELO Timespan=All years Search language=Auto	--	TS refers to a topic search which includes the title, abstract, author-submitted keywords, and Keywords Plus® (based on the titles of the references of the article - specific to Clarivate Analytics). All searches used the same search settings for databases, timespan, and language.

Table B.1. Search Strategy for the [CLAUDIN] data set.

Search #	Member	Gene ID	Search	Results	Notes
#1	***Cldn1***	9076 12737 65129	TS=("claudin-1" OR "cldn1" OR "cldn-1" OR "cld1" OR "cld-1" OR "cln1" OR "cln-1")	**5,163**	--
#2	***Cldn2***	9075 12738 300920	TS=("claudin-2" OR "cldn2" OR "cldn-2" OR "cld2" OR "cld-2" OR "cln2" OR "cln-2")	**3,096**	--
#3	***Cldn3***	1365 12739 65130	TS=("claudin-3" OR "cldn3" OR "cldn-3" OR "cld3" OR "cld-3" OR "cln3" OR "cln-3")	**3,209**	--
#4	***Cldn4***	1364 12740 304407	TS=("claudin-4" OR "cldn4" OR "cldn-4" OR "cld4" OR "cld-4" OR "cln4" OR "cln-4")	**2,439**	--
#5	***Cldn5***	7122 12741 65131	TS=("claudin-5" OR "cldn5" OR "cldn-5" OR "cld5" OR "cld-5" OR "cln5" OR "cln-5")	**2,926**	--
#6	***Cldn6***	9074 54419 287098	TS=("claudin-6" OR "cldn6" OR "cldn-6" OR "cld6" OR "cld-6" OR "cln6" OR "cln-6")	**603**	--
#7	***Cldn7***	1366 53624 65132	TS=("claudin-7" OR "cldn7" OR "cldn-7" OR "cld7" OR "cld-7" OR "cln7" OR "cln-7")	**1,092**	--
#8	***Cldn8***	9073 54420 304124	TS=("claudin-8" OR "cldn8" OR "cldn-8" OR "cld8" OR "cld-8" OR "cln8" OR "cln-8")	**547**	--
#9	***Cldn9***	9080 56863 287099	TS=("claudin-9" OR "cldn9" OR "cldn-9" OR "cld9" OR "cld-9" OR "cln9" OR "cln-9")	**124**	--
#10	***Cldn10***	9071 58187 290485	TS=("claudin-10*" OR "cldn10*" OR "cldn-10*" OR "cld10*" OR "cld-10*" OR "cln10*" OR "cln-10*")	**364**	Two isoforms of claudin-10 (10a and 10b).

Search #	Member	Gene ID	Search	Results	Notes
#11	***Cldn11***	5010 18417 84588	TS=("claudin-11" OR "cldn11" OR "cldn-11" OR "cld11" OR "cld-11" OR "cln11" OR "cln-11" OR "oligodendrocyte-specific protein" OR "OSP" OR "oligodendrocyte transmembrane protein" OR "OTP")	**4,735**	Claudin-11 has historically been referred to as OSP (oligodendrocyte-specific protein).
#12	***Cldn12***	9069 64945 500000	TS=("claudin-12" OR "cldn12" OR "cldn-12" OR "cld12" OR "cld-12" OR "cln12" OR "cln-12")	**225**	--
#13	***Cldn13***	-- 57255 --	TS=("claudin-13" OR "cldn13" OR "cldn-13" OR "cld13" OR "cld-13" OR "cln13" OR "cln-13")	**36**	Claudin-13 is expressed in mice, but not humans or rats.
#14	***Cldn14***	23562 56173 304073	TS=("claudin-14" OR "cldn14" OR "cldn-14" OR "cld14" OR "cld-14" OR "cln14" OR "cln-14")	**228**	--
#15	***Cldn15***	24146 60363 304388	TS=("claudin-15" OR "cldn15" OR "cldn-15" OR "cld15" OR "cld-15" OR "cln15" OR "cln-15")	**207**	--
#16	***Cldn16***	10686 114141 155268	TS=("claudin-16" OR "cldn16" OR "cldn-16" OR "cld16" OR "cld-16" OR "cln16" OR "cln-16")	**335**	--
#17	***Cldn17***	26285 239931 304125	TS=("claudin-17" OR "cldn17" OR "cldn-17" OR "cld17" OR "cld-17" OR "cln17" OR "cln-17")	**39**	--
#17	***Cldn17***	26285 239931 304125	TS=("claudin-17" OR "cldn17" OR "cldn-17" OR "cld17" OR "cld-17" OR "cln17" OR "cln-17")	**39**	--
#18	***Cldn18***	51208 56492 315953	TS=("claudin-18" OR "cldn18" OR "cldn-18" OR "cld18" OR "cld-18" OR "cln18" OR "cln-18")	**382**	--
#19	***Cldn19***	149461 242653 298487	TS=("claudin-19" OR "cldn19" OR "cldn-19" OR "cld19" OR "cld-19" OR "cln19" OR "cln-19")	**206**	--

Search #	Member	Gene ID	Search	Results	Notes
#20	***Cldn20***	49861 621628 680178	TS=("claudin-20" OR "cldn20" OR "cldn-20" OR "cld20" OR "cld-20" OR "cln20" OR "cln-20")	**20**	--
#21	***Cldn21***	-- -- --	TS=("claudin-21" OR "cldn21" OR "cldn-21" OR "cld21" OR "cld-21" OR "cln21" OR "cln-21")	**12**	No gene is currently designated Claudin-21 in humans or rodents.
#22	***Cldn22***	53842 75677 306454	TS=("claudin-22" OR "cldn22" OR "cldn-22" OR "cld22" OR "cld-22" OR "cln22" OR "cln-22")	**14**	--
#23	***Cldn23***	137075 71908 290789	TS=("claudin-23" OR "cldn23" OR "cldn-23" OR "cld23" OR "cld-23" OR "cln23" OR "cln-23")	**72**	--
#24	***Cldn24***	100132463 100039801 502083	TS=("claudin-24" OR "cldn24" OR "cldn-24" OR "cld24" OR "cld-24" OR "cln24" OR "cln-24")	**9**	--
#25	***Cldn25***	644672 100042785 100360390	TS=("claudin-25" OR "cldn25" OR "cldn-25" OR "cld25" OR "cld-25" OR "cln25" OR "cln-25")	**20**	The current gene designated claudin-25 is different than the gene originally named claudin-25 (see: Cldnd1).
#26	***Cldn26***	283953 74720 501675	TS=("claudin-26" OR "cldn26" OR "cldn-26" OR "cld26" OR "cld-26" OR "cln26" OR "cln-26" OR "transmembrane protein 114" OR "tmem114")	**21**	The gene name for claudin-26 is transmembrane protein 114.
#27	***Cldn27***	283999 546519 688285	TS=("claudin-27" OR "cldn27" OR "cldn-27" OR "cld27" OR "cld-27" OR "cln27" OR "cln-27" OR "transmembrane protein 235" OR "tmem235")	**10**	The gene name for claudin-27 is transmembrane protein 235.
#28	***Cldnd1***	56650 224250 288182	TS=("claudin domain-containing protein 1" OR "claudin domain-containing 1" OR "cldnd1")	**21**	Cldnd1 was formerly called claudin-25, with a separate gene now designated claudin-25.
#29	**--**	--	**#1 OR #2 OR #3 OR #4 OR #5 OR #6 OR #7 OR #8 OR #9 OR #10 OR #11 OR #12 OR #13 OR #14 OR #15 OR #16 OR #17 OR #18 OR #19 OR #20 OR #21 OR #22 OR #23 OR #24 OR #25 OR #26 OR #27 OR #28**	**19,451**	This represents the **[CLAUDIN]** data set.

Table B.2. Search Strategy for the [TAMP] data set.

Search #	Member	Gene ID	Search	Results	Notes
#1	*Ocln*	100506658 18260 83497	TS=("occludin" OR "ocln")	**9,027**	MarvelD1 is a different gene than occludin.
#2	*MarvelD2*	153562 218518 365657	TS=("tricellulin" OR "tric" OR "marvel domain-containing protein 2" OR "marvel domain-containing 2" OR "marveld2")	**1,407**	The gene name for tricellulin is MarvelD2.
#3	*MarvelD3*	91862 73608 498950	TS=("marvel domain-containing protein 3" OR "marvel domain-containing 3" OR "marveld3")	**40**	--
#4	--	--	**#1 OR #2 OR #3**	**10,263**	This represents the **[TAMP]** data set.

Table B.3. Search Strategy for the [ANGULIN] data set.

Search #	Member	Gene ID	Search	Results	Notes
#1	*Lsr*	51599 54135 64355	TS=("angulin-1" OR "Lipolysis Stimulated Lipoprotein Receptor" OR "lsr" OR "Immunoglobulin-Like Domain Containing Receptor 3" OR "ildr3")	**2,797**	--
#2	*Ildr1*	286676 106347 303914	TS=("Immunoglobulin Like Domain Containing Receptor 1" OR "ILDR1" OR "angulin-2")	**57**	--
#3	*Ildr2*	387597 100039795 685277	TS=("Immunoglobulin Like Domain Containing Receptor 2" OR "ILDR2" OR "angulin-3")	**32**	--
#4	--	--	**#1 OR #2 OR #3**	**2,853**	This represents the **[ANGULIN]** data set.

Table B.4. Search Strategy for the [TJ] data set.

Search #	Search	Results	Notes
#1	TS=("tight junction*")	**30,418**	Wildcard approach. This represents the **[TJ]** data set.

Table B.5. Search Strategy for the [UNIFIED] data set.

Search #	Search	Results	Notes
#1	**[CLAUDIN]**	**19,451**	Claudin family data set.
#2	**[TAMP]**	**10,263**	TAMP family data set.
#3	**[ANGULIN]**	**2,853**	Angulin family data set.
#4	**[TJ]**	**30,418**	Generic tight junction data set.
#5	**#1 OR #2 OR #3 OR #4**	**48,715**	This represents the **[UNIFIED]** data set.

Table B.6. Search Strategy for the [MS] data set.

Search #	Search	Results	Notes
#1	TS=("multiple sclerosis")	**157,585**	--
#2	TS=("relapse-remitting MS" OR "RR-MS" OR "RRMS" OR "relapse-remit*")	**6,162**	Most common of the main clinical forms.
#3	TS=("secondary-progressive MS" OR "SP-MS" OR "SPMS" OR "secondary-progress*")	**5,833**	Second-most common of the main clinical forms.
#4	TS=("primary-progressive MS" OR "PP-MS" OR "PPMS" OR "primary-progress*")	**6,979**	Second-least common of the main clinical forms.
#5	TS=("progressive-relapsing MS" OR "PR-MS" OR "PRMS" OR "progressive-relaps*")	**846**	Least common of the main clinical forms.
#6	TS=("acute multiple sclerosis" OR "acute MS" OR "Marburg's disease" OR "Marbug disease" OR "Marburg's type" OR "Marburg type" OR "Marburg's variant" OR "Marburg variant")	**523**	Atypical variant.
#7	TS=("concentric sclerosis" OR "Balo's disease" OR "Balo disease" OR "Balo's type" OR "Balo type" OR "Balo's variant" OR "Balo variant")	**346**	Atypical variant.
#8	TS=("Tumefactive multiple sclerosis" OR "Tumefactive MS")	**179**	Atypical variant.
#9	**#1 OR #2 OR #3 OR #4 OR #5 OR #6 OR #7 OR #8**	**165,410**	This represents the **[MS]** data set.

Table B.7. Search Strategy for the [NMOSD] data set.

Search #	Search	Results	Notes
#1	TS=("neuromyelitis" OR "neuromyelitis optica" OR "NMO" OR "neuromyelitis" OR "neuromyelitis optica spectrum" OR "neuromyelitis optica spectrum disorder*" OR "NMOSD" OR "Devic's disease" OR "Devic disease")	**20,611**	This represents the **[NMOSD]** data set.

Table B.8. Search Strategy for the [ADEM] data set.

Search #	Search	Results	Notes
#1	TS=("acute disseminated" OR "acute disseminated encephalomyelitis" OR "disseminated encephalomyelitis" OR "ADEM")	**5,380**	Common form.
#2	TS=("acute hemorrhagic" OR "acute hemorrhagic leukoencephalitis" OR "hemorrhagic leukoencephalitis" OR "AHLE" OR "acute hemorrhagic encephalomyelitis" OR "hemorrhagic encephalomyelitis" OR "AHEM" OR "Hurst's disease" OR "Hurst disease" OR "Weston-Hurst syndrome")	**3,572**	Rare variant of ADEM.
#3	**#1 OR #2**	**8,836**	This represents the **[ADEM]** data set.

Table B.9. Search Strategy for the [EAE] data set.

Search #	Search	Results	Notes
#1	TS=("experimental autoimmune encephalomyelitis" OR "experimental autoimmune" OR "autoimmune encephalomyelitis" OR "EAE" OR "experimental allergic encephalomyelitis" OR "experimental allergic" OR "allergic encephalomyelitis")	**44,305**	This represents the **[EAE]** data set.

Table B.10. Search Strategy for the [E-NMOSD] data set.

Search #	Search	Results	Notes
#1	TS=("experimental neuromyelitis" OR "experimental NMO*" OR "model of neuromyelitis" OR "model of NMO*" OR "neuromyelitis optica model" OR "neuromyelitis optica rodent model*" OR "neuromyelitis optica mouse model*" OR "neuromyelitis optica rat model*" OR "NMO rodent model*" OR "NMO mouse model*" OR "NMO rat model*" OR "neuromyelitis optica spectrum disorder model*" OR "neuromyelitis optica spectrum disorder rodent model*" OR "neuromyelitis optica spectrum disorder mouse model*" OR "neuromyelitis optica spectrum disorder rat model*" OR "NMOSD rodent model*" OR "NMOSD mouse model*" OR "NMOSD rat model*" OR "neuromyelitis optica IgG" OR "NMO-IgG" OR "neuromyelitis optica spectrum disorder IgG" OR "NMOSD-IgG" OR "neuromyelitis optica recombinant antibod*" OR "neuromyelitis optica rAb*" OR "neuromyelitis optica antibod*" OR "neuromyelitis optica Ab*" OR "NMO recombinant antibod*" OR "NMO rAb*" OR "NMO antibod*" OR "NMO Ab*" OR "neuromyelitis optica spectrum disorder recombinant antibod*" OR "neuromyelitis optica spectrum disorder rAb*" OR "neuromyelitis optica spectrum disorder antibod*" OR "neuromyelitis optica spectrum disorder Ab*" OR "NMOSD recombinant antibod*" OR "NMOSD rAb*" OR "NMOSD antibod*" OR "NMOSD Ab*" OR "Aquaporin-4-IgG" OR "AQP4-IgG" OR "aquaporin-4 recombinant antibod*" OR "aquaporin-4 rAb*" OR "aquaporin-4 antibod*" OR "aquaporin-4 Ab*" OR "AQP4 recombinant antibod*" OR "AQP4 rAb*" OR "AQP4 antibod*" OR "AQP4 Ab*")	**2,997**	There is no set disease model name. Therefore, as many phrases involving key words in different orders were queried. This represents the **[E-NMOSD]** data set.

Table B.11. Search Strategy for the [TMEV] data set.

Search #	Search	Results	Notes
#1	TS=("Theiler's murine encephalomyelitis virus" OR "TMEV" OR "Theiler's murine encephalomyelitis" OR "Theiler's murine" OR "Theiler's encephalomyelitis virus" OR "Theiler's encephalomyelitis" OR "Theiler's virus" OR "murine encephalomyelitis virus" OR "encephalomyelitis virus")	**4,831**	Classic TMEV model
#2	TS=("peptide-induced fatal syndrome" OR "PIFS" OR "peptide-induced fatal")	**536**	Fulminant TMEV model
#3	**#1 OR #2**	**5,360**	This represents the **[TMEV]** data set.

Table B.12. Search Strategy for the [CUP] data set.

Search #	Search	Results	Notes
#1	TS=("cuprizone" OR "oxalic acid bis(cyclohexylidene hydrazide)" OR "N,N-Oxalylbis(cyclohexanone hydrazone)" OR "biscyclohexanone oxaldihydrazone" OR "biscyclohexanoneoxalyhydrazone")	**1,588**	Cuprizone model. This represents the [CUP] data set.

Table B.13. Search Strategy for the [DISEASE] data set.

Search #	Search	Results	Notes
#1	**[MS]**	**165,410**	MS data set.
#2	**[NMOSD]**	**10,611**	NMOSD data set.
#3	**[ADEM]**	**8,836**	ADEM data set.
#4	**[EAE]**	**44,305**	EAE data set.
#	**[E-NMOSD]**	**2,997**	E-NMOSD data set.
#6	**[TMEV]**	**5,360**	TMEV data set.
#7	**[CUP]**	**1,588**	Cuprizone data set.
#8	**#1 OR #2 OR #3 OR #4 OR #5 OR #6 OR #7**	**205,981**	This represents the **[DISEASE]** data set.

Table B.14. Search Strategy for the [OVERLAP] data set.

Search #	Search	Results	Notes
#1	**[UNIFIED]**	**48,715**	Tight junction data set (all families and generic tight junction).
#2	**[DISEASE]**	**205,981**	Disease model set (all diseases and models).
#3	**#1 AND #2**	**657**	This represents the overlap between the **[DISEASE]** and **[UNIFIED]** data sets.

APPENDIX C

Summary Tables for Studies with CNS-IDDs.

Table C.1. CNS-EC-specific Alterations in MS.

Study	Patients (n)[@]	Origin	Matter	Stage/Type[†]	Histology[†]	Tight Junction Protein Alterations[#]	Methods
Van Horssen et al.[82,a]	• ***PP*** *(2)** • ***SP*** *(2)** • ***ND*** *(1)**	Brain	White	Pre-Active	• Activated microglial clusters • No astrogliosis • No fibrinogen deposition	No apparent alteration of **CLDN5** reactivity detected in pre-lesional vessels near HLA-DR+ microglial clusters.	IHC-IF
Alvarez et al.[9]	• ***SP*** *(6)* • ***RR*** *(4)*	Brain	White	Pre-Active	•Activated microglia/macrophages • Astrogliosis • Fibrinogen & ApoBs deposition • CD3+ infiltrates	Disruption & loss of **CLDN5** & **OCLN** reactivity in pre-lesional vessels vs. NAWM. Also, ↓ **CLDN5** & ↓ **OCLN** pixel intensity.	IHC-IF
Plumb et al.[83,b,c]	• ***SP*** *(10)* • ***Acute*** *(2)* • ***OND*** *(5)* • ***CD*** *(2)*	Brain	White	Pre-Active	• Activated microglia/macrophages • CD45+ infiltrates	↑ Proportion of abnormal tight junctions for pre-lesional vessels in HLA-DR+ NAWM vs. HLA-DR- NAWM based on altered **OCLN** & ZO-1 reactivity.	IHC-IF
				Active	• Demyelination • Activated microglia/macrophages • Fibrinogen deposition • CD45+ infiltrates	Disruption & loss of **OCLN** reactivity in lesional vessels near HLA-DR+ macrophages, CD45+ infiltrates, or fibrinogen deposition. ↑ Proportion of abnormal tight junctions in lesional vessels vs. ONDs or CDs based on altered **OCLN** & ZO-1 reactivity.	IHC-IF
Wosik et al.[85,d]	• ***ND*** *(6)*	Brain	White	Active	• Demyelination • Cellular Infiltration (H&E)	↓ **OCLN** intensity & strand thickness at tight junctions in lesional vessels vs. NAWM.	IHC-IF

Note: [@]When studies specified the patients involved in tight junction protein analyses, only those patients are listed and are marked by an asterisk (*). [†]Where available, lesion staging and histology are included. [#]Unless otherwise noted, comparisons are between patients and control donors. Increases are marked by an upwards arrow (↑), decreases by a downwards arrow (↓), and no change by a left-right arrow (↔).

[a]Comparisons with HLA-DR$^-$ NAWM or control donors were not performed. [b]Quantification used a combination of occludin- and ZO-1-labeling. [c]Micrographs of occludin from HLA-DR$^+$ NAWM or control donors were not provided. [d]Micrographs were not provided.

PP: Primary-Progressive MS. SP: Secondary-Progressive MS. ND: Clinical form not determined or not provided. RR: Relapse-remitting MS. Acute: Acute MS (Marburg's disease). OND: Other neurological disease. CD: Control Donor. NP: Not provided. ApoB: Apolipoprotein B. CD3: Cluster of differentiation 3. CD45: Cluster of differentiation 45. HLA-DR: Human leukocyte antigen DR isotype. NAWM: Normal-appearing white matter. CLDN5: claudin-5. OCLN: occludin. IHC-IF: Immunofluorescent-based immunohistochemistry.

Study	Patients (n)[@]	Origin	Matter	Stage/Type[†]	Histology[†]	Tight Junction Protein Alterations[#]	Methods
Cunnea et al.[87,e]	• ***PP*** *(3)** • ***SP*** *(4)**	Brain MVs	White	Chronic Active	• Demyelination • Sparse ORO+ cell presence • HLA-DR+ presence at edge	↑ ***Ocln*** mRNA in brain MVs isolated from patients vs. NAWM using MA, but ↓ ***Ocln*** mRNA in BMVs isolated from patients vs. NAWM using qPCR.	MA, qPCR
				Inactive	• Demyelination • No ORO+ cell presence	↓ ***Ocln*** mRNA in BMVs isolated from patients vs. NAWM.	qPCR
Van Horssen et al.[86,f]	• ***ND*** *(2)* • ***RR*** *(1)* • ***PP*** *(2)* • ***SP*** *(14)* • ***Prog*** *(2*	Brain	White	Inactive	• Demyelination • Sparse HLA-DR+ cell presence	Sporadic loss of **CLDN5+** in lesional vessels.	IHC-IE
			Grey	Pure Grey	• Demyelination • No astrogliosis • No fibrinogen or IgG deposition	No apparent loss of **CLDN5** reactivity detected in lesional vessels vs. adjacent NAGM.	IHC-IE
Musolino et al.[90]	• ***RR*** *(6)* • ***CD*** *(11)*	Brain	White	*NP*	• Demyelination	Disruption & loss of **CLDN5** reactivity in lesional vessels.	IHC-IF
Uchida et al.[40,g]	• ***ND*** *(2)* • ***CD*** *(3)*	Brain & Spine	*NP*	*NP*	• *NP*	Disruption & loss of **CLDN11** reactivity in patient brain & spine vessels. Also, ↓ **CLDN11** per GLUT1 intensity for brain & spine.	IHC-IF

Note: [@]When studies specified the patients involved in tight junction protein analyses, only those patients are listed and are marked by an asterisk (*****). [†]Where available, lesion staging and histology are included. [#]Unless otherwise noted, comparisons are between patients and control donors. Increases are marked by an upwards arrow (↑), decreases by a downwards arrow (↓), and no change by a left-right arrow (↔).

[e]Statistics were not enumerated for the qPCR data. [f]Micrographs of control donors were not provided. [f]Tissues were analyzed without distinction between matter type or lesion status.

PP: Primary-Progressive MS. SP: Secondary-Progressive MS. ND: Clinical form not determined or not provided. RR: Relapse-remitting MS. Prog: Progressive MS. CD: Control Donor. NP: Not provided. MV: Microvessel. ORO: Oil Red O stain. HLA-DR: Human leukocyte antigen DR isotype. IgG: Immunoglobulin G. NAWM: Normal-appearing white matter. NAGM: Normal-appearing grey matter. CLDN5: claudin-5. OCLN: occludin. CLDN11: claudin-11. GLUT1: Glucose transporter 1. MA: Microarray. qPCR: Quantitative Polymerase Chain Reaction. IHC-IE: Immunoenzyme-based immunohistochemistry. IHC-IF: Immunofluorescent-based immunohistochemistry.

Table C.2. Non-CNS-EC-specific Alterations in MS.

Study	Patients (n)[@]	Origin	Intervention(s)	Tight Junction Protein Alterations[#]	Methods
Mandel et al.[280,a]	• ***RR-R*** *(51)* • ***RR-S*** *(53)* • ***CD*** *(40)*	• Peripheral Blood Leukocytes	--	↑ ***Cldn5*** mRNA in PBLs isolated from RR-R patients vs. RR-S patients or control donors.	qPCR
				↑ Total **CLDN1** & ↑ total **CLDN5** protein in PBLs isolated from RR-R patients vs. RR-S patients or control donors.	WB
			• Glucocorticoids for 7 days	↓ ***Cldn5*** mRNA in PBLs isolated from RR-R patients after treatment vs. before.	qPCR
				↓ Total **CLDN5** protein in PBLs isolated from RR-R patients after treatment vs. before.	WB
			• Interferon-β for 3-6 months	↔ ***Cldn5*** mRNA in PBLs isolated from RR-S patients after treatment vs. before.	qPCR
Hassanzadeh et al.[281]	• ***RR-S*** *(13)* • ***CD*** *(15)*	• Peripheral Blood Leukocytes	--	↑ ***Cldn11*** mRNA in PBLs.	qPCR
		• Plasma	--	↔ **CLDN11** protein concentration.	ELISA
Annunziata et al.[282]	• ***RR*** *(20)* • ***CD*** *(20)*	• Serum	• FTY720 for 12 months	↑ **CLDN5** & ↑ **OCLN** protein concentration at 0, 6, and 12 months of treatment vs. control donor serum.	ELISA
				↑ **CLDN5** & ↑ **OCLN** protein concentration in RR serum at 6 & 12 months of treatment vs. 0 months.	
Camara-Lemarroy et al.[283]	• ***RR*** *(29)** • ***Gad+*** (15) • ***Gad-*** (14) • ***CD*** (17)	• Plasma	--	↑ **OCLN** protein concentration.	ELISA
				↑ **OCLN** protein concentration in RR-Gad+ plasma vs. RR-Gad- plasma.	

Note: [@]When studies specified the patients involved in tight junction protein analyses, only those patients are listed and are marked by an asterisk (*****). [#]Unless otherwise noted, comparisons are between patients and control donors. Increases are marked by an upwards arrow (↑), decreases by a downwards arrow (↓), and no change by a left-right arrow (↔).

[a]Patients who positively responded to IFN-β treatment had lower initial claudin-5 mRNA levels than those who poorly responded to IFN-β treatment.

RR-R: Relapsing-remitting MS during relapse. RR-S: Relapse-remitting MS during remission (stable). CD: Control donor. Gad+/Gad-: Presence/absence of gadolinium-enhancing lesion at time of blood draw. CLDN5: Claudin-5. PBLs: Peripheral blood leukocytes. CLDN1: Caudin-1. CLDN11: Claudin-11. OCLN: Occludin. qPCR: Quantitative polymerase chain reaction. WB: Western blotting. ELISA: Enzyme-linked immunosorbent assay.

Study	Patients (n)[@]	Origin	Intervention(s)	Tight Junction Protein Alterations[#]	Methods
Masaki et al.[284,b]	• ***CS*** (4)	• Brain Myelin	--	Disruption & loss of **CLDN11** reactivity in demyelinated rings vs. adjacent myelinated rings.	IHC-IE
Kooij et al.[285,c]	• ***PP*** *(3)* • ***SP*** *(10)* • ***CD*** *(13)*	• Choroid Plexus	--	Disruption & loss of **CLDN3** reactivity in tissue sections.	IHC-IF
				↓ ***Cldn3*** mRNA & ↓ total **CLDN3** protein in homogenate.	qPCR, WB
				↔ ***Cldn1*** & ↔ ***Cldn5*** mRNA in homogenate.	qPCR
Mora et al.[124]	• ***ND*** *(NP)*	• Cortical Astrocytes	--	**CLDN4** reactivity detected at the glial limitans of astrocytes within active cortical lesions.	IHC-IF

Note: [@]When studies specified the patients involved in tight junction protein analyses, only those patients are listed and are marked by an asterisk (*). [#]Unless otherwise noted, comparisons are between patients and control donors. Increases are marked by an upwards arrow (↑), decreases by a downwards arrow (↓), and no change by a left-right arrow (↔).

[b]Claudin-11 is expressed by oligodendrocytes, hence its usage here as a myelin marker. [c]Clinical form-specific analysis was not performed.

CS: Concentric sclerosis (Balo's disease). PP: Primary-Progressive MS. SP: Secondary-Progressive MS. CD: Control donor. ND: Clinical form not determined or not provided. NP: Information not provided. CLDN11: Claudin-11. CLDN3: Claudin-3. CLDN1: Caudin-1. CLDN5: Caudin-5. CLDN4: Caudin-4. IHC-IE: Immunoenzyme-based immunohistochemistry. IHC-IF: Immunofluorescent-based immunohistochemistry. qPCR: Quantitative polymerase chain reaction. WB: Western blotting.

Table C.3. CNS-EC-specific Alterations in NMOSD.

Study	Patients (n)[@]	Origin	Staging[†]	Histology[†]	Tight Junction Protein Alterations[#]	Methods
Winkler et al.[20,a,b,c]	• ***NMOSD*** *(4)** • ***CD*** *(5)*	• Brain & Spine	Early[‡]	• Completed astrocyte loss • Demyelination • Activated macrophages/microglia • Inflammatory infiltrates • No fibrinogen deposition	No apparent alteration of **CLDN5** reactivity in lesional vessels. Also, ↔ proportion of **CLDN5+** lesional or perilesional vessels vs. control donors.	IHC-IF
	• ***NMOSD*** *(1)** • ***CD*** *(3)*	• Spine	Sub-Acute[‡]	• Partial astrocyte repopulation • Demyelination • Activated macrophages/microglia • No inflammatory infiltrates • Focal fibrinogen deposition	No apparent alteration of **CLDN3** & **OCLN** reactivity in lesional vessels vs. control donors.	IHC-IF

Note: [@]When studies specified the patients involved in tight junction protein analyses, only those patients are listed and are marked by an asterisk (*). [†]Where available, lesion staging and histology are included. Original author-reported staging marked by a double dagger (‡). [#] Increases are marked by an upwards arrow (↑), decreases by a downwards arrow (↓), and no change by a left-right arrow (↔).

[a]Patients autopsied after 2005 were seropositive for AQP4. Although the serostatus for patients autopsied prior to 2005 was not available, the patients all fulfilled at least two of the core NMOSD characteristics [b]Micrographs of claudin-5 from control donors were not provided. [c]The originals authors suggest that the fibrinogen in the sub-acute lesion may be old and not yet cleared, rather than freshly deposited.

CD: Control Donor. CLDN5: Claudin-5. CLDN3: Claudin-3. OCLN: Occludin. IHC-IF: Immunofluorescent-based immunohistochemistry.

Table C.4. Non-CNS-EC-specific Alterations in NMOSD.

Study	Patients (n)	Origin	Intervention(s)	Tight Junction Protein Alterations[#]	Methods
Cui et al.[286,a]	• ***NMOSD*** *(6)* • ***CD*** *(5)*	• Sigmoid colon	--	Disruption & loss of **CLDN1** & **OCLN** reactivity in the colonic mucosa. Additionally, ↓ **CLDN1** & ↓ **OCLN** average optical density.	IHC-IF

Note: [#]Increases are demarked by an upwards arrow (↑), decreases by a downwards arrow (↓), and no change by a left-right arrow (↔).

[a]All patients were AQP4-seropositive.

CD: Control donor. CLDN1: Claudin-1. OCLN: Occludin. IHC-IF: Immunofluorescent-based immunohistochemistry.

APPENDIX D

Summary Tables for Studies with Cell Culture Models of CNS-IDDs.

Table D.1. MS Sera/IgG-induced Alterations in Human CNS-EC Culture Models.

Study	Patients (n)	Cell Line	Sample	Intervention(s)	Barrier Alterations	Tight Junction Protein Alterations[#]	Methods
Shimizu et al.[95,a,b]	• ***ND-Acute*** (7)	TY08	Serum	--	↔ TEER with patient serum vs. FBS.	↔ Total **CLDN5** & ↔ total **OCLN** protein for patient serum vs. FBS.	WB
Tasaki et al.[96,a,b]	• ***ND-Acute*** (10)	TY08	Serum	--	↔ TEER with patient serum vs. FBS.	↔ Total **CLDN5** protein for patient serum vs. FBS.	WB
				• MMP inhibition (GM6001)	↔ TEER or perm. to NaFl for patient serum with GM6001 vs. without.	↔ Total **CLDN5** protein for patient serum with GM6001 vs. without.	WB
Shimizu et al.[97,b]	• ***RR-R*** (6) • ***RR-S*** (9) • ***SP*** (8)	TY09	Serum	--	↓ TEER for SP or RR-R sera vs. FBS. ↔ TEER for RR-S sera vs FBS.	↓ Total **CLDN5** protein for RR-R or SP sera vs. FBS, but ↔ total **CLDN5** protein for RR-S sera vs. FBS. ↓ Total **OCLN** protein for SP sera vs. FBS, but ↔ total **OCLN** protein for either RR sera vs. FBS.	WB
				• Neutralizing Abs (TNF-α, IFN-γ, IL17, VEGF) • MMP inhibition (GM6001)	↑ TEER for RR-R sera with VEGF Ab or GM6001 vs. without.	↑ Total **CLDN5** for RR-R sera with VEGF Ab or GM6001 vs. without, but ↔ total **CLDN5** protein for RR-R sera with other Abs vs. without. ↔ Total **OCLN** protein for RR-R sera with Abs or inhibitor vs. without. ↔ Total **CLDN5** & ↔ total **OCLN** protein for SP sera with Abs or inhibitor vs. without.	WB
			IgG	--	↓ TEER for SP IgG vs. FBS IgG. ↔ TEER for either RR IgG vs. FBS IgG.	↓ Total **CLDN5** protein for SP IgG vs. FBS IgG, but ↔ total **CLDN5** protein for either RR patient IgG vs. FBS IgG. ↔ Total **OCLN** protein for any patient IgG type vs. FBS IgG	WB

Note: [#]Increases are marked by an upwards arrow (↑), decreases by a downwards arrow (↓), and no change by a left-right arrow (↔).

[a]These patients fulfilled the 2010 revised McDonald diagnostic criteria. As the authors contrast patients during "acute phase" with those during "stable disease", "acute phase" suggests following an episode of neurologic symptoms. [b]Although control donor sera and IgG were used, only comparisons against FBS or FBS-derived IgG were performed.

ND-Acute: Clinical form not determined or not provided during the acute phase of disease. RR-R: Relapsing-Remitting MS during relapse. RR-S: Relapse-Remitting MS in remission (stable). SP: Secondary-Progressive MS. IgG: Immunoglobulin G. TY08: Human brain endothelial cells (BECs) that express a temperature-sensitive SV40-T antigen variant. TY09/TY10: TY08-derived cells that additionally express human telomerase reverse transcriptase (hTERT). Ab: Antibody. TNF-α: Tumor Necrosis Factor alpha. IFN-γ: Interferon gamma. IL17: Interleukin 17. VEGF: Vascular endothelial growth factor. MMP: Matrix metalloproteinase. TEER: Transendothelial electrical resistance. NaFl: Sodium fluorescein. CLDN5: Claudin-5. OCLN: Occludin. FBS: Fetal bovine serum. WB: Western blotting.

Study	Patients (n)	Cell Line	Sample	Intervention(s)	Barrier Alterations	Tight Junction Protein Alterations[#]	Methods
Takahashi et al.[101]	• ***RR-R*** (3) • ***RR-S*** (3) • ***SP*** (3)	TY10	Serum	• VDR Agonism ($Vitamin\ D_3$)	--	↑ Total **CLDN5** protein for RR-R sera with pre-treatment vs. without, but ↔ total **CLDN5** protein for RR-S or SP sera under same conditions.	WB
Nishihara et al.[100,c,d]	• ***RR-R*** (3) • ***RR-S*** (3) • ***SP*** (3)	TY*	Serum	• S1PR inhibition (FTY720P)	↑ TEER for all patient serum types with FTY720P vs. without.	↑ Total **CLDN5** & ↔ total **OCLN** protein for all patient serum types with pre-treatment vs. without.	WB
						↑ ***Cldn5*** mRNA for MS sera with pre-treatment vs. without.	qPCR
Sheikh et al.[98,e]	• ***RR*** (12-24) • ***CD*** (12-24)	hCMEC/D3	Serum	--	↓ TEER & ↓ perm. to 70 kDa FITC-Dextran for RR sera vs. CD sera.	↓ Mean intensity fluorescence of **OCLN** for RR sera vs. CD sera.	FC

Note: [#]Increases are marked by an upwards arrow (↑), decreases by a downwards arrow (↓), and no change by a left-right arrow (↔).

[c]The exact TY cell line was not defined. [d]Patients were grouped into a single disease category for the qPCR data. [e]Serum samples were pooled and the exact number of patients was not enumerated.

RR-R: Relapsing-Remitting MS during relapse. RR-S: Relapse-Remitting MS in remission (stable). SP: Secondary-Progressive MS. CD: Control Donor. TY08: Human brain endothelial cells (BECs) that express a temperature-sensitive SV40-T antigen variant. TY09/TY10: TY08-derived cells that additionally express human telomerase reverse transcriptase (hTERT). hCMEC/D3: Human BECs that express SV40-T antigen and hTERT. S1PR: Sphingosine 1 phosphate receptor. TEER: Transendothelial electrical resistance. FITC: Fluorescein isothiocyanate. CLDN5: Claudin-5. OCLN: Occludin. WB: Western blotting. qPCR: Quantitative polymerase chain reaction. FC: Flow cytometry.

Table D.2. MS Sera/IgG-induced Alterations in Non-human or Non-CNS EC Culture Models.

Study	Patients (n)[@]	Sample	Cell line	Intervention	Barrier Alterations	Tight Junction Protein Alterations[#]	Methods
Minagar et al.[287,a]	• ***ND-R*** (*6*)* • ***CD*** (6)	Serum	SVEC4-10	--	--	↓ Total **OCLN** protein for ND-R sera vs. CD sera.	WB
Proia et al.[229,b]	• ***SP*** (*NP*) • ***CD*** (15)	Serum	RBE4	--	↓ TEER for SP sera vs. CD sera.	Loss of **OCLN** reactivity & ↓ total **OCLN** protein for SP sera vs. CD sera.	IHC-IF, WB
Blecharz et al.[288]	• ***RR-R*** (*NP*) • ***RR-S*** (*NP*) • ***CD*** (3)	Serum	cEND	--	↓ TEER for both patient serum types vs. CD sera.	↓ Total **CLDN5** & ↓ total **OCLN** protein for both patient sera vs. CD sera.	WB
						↓ ***Cldn5*** & ↓ ***Ocln*** mRNA for RR-R sera vs. CD sera.	qPCR
						↓ ***Cldn5*** mRNA & ↔ ***Ocln*** mRNA for RR-S sera vs. CD sera.	
				• Dex	↑ TEER for RR-S sera with Dex vs. without. ↔ TEER for RR-R sera with Dex vs. without.	↑ Total **CLDN5** & ↑ total **OCLN** protein for RR-S sera with Dex vs. without.	WB
						↑ Total **CLDN5** protein & ↓ total **OCLN** protein for RR-R sera with Dex vs. without.	
						↑ ***Cldn5*** & ***Ocln*** mRNA for RR-S sera with Dex vs. without.	qPCR
						↑ ***Cldn5*** mRNA & ↔ ***Ocln*** mRNA for RR-R sera with Dex vs. without.	

Note: [@]When studies specified the patients involved in tight junction protein analyses, only those patients are listed and are marked by an asterisk (*****). [#]Increases are demarked by an upwards arrow (↑), decreases – by a downwards arrow (↓), and no change – by a left-right arrow (↔).

[a]These patients met the 2001 McDonald diagnostic criteria. Additionally, patients in remission were recruited for the study, but their data was not shown. [b]A tri-culture model with rat astrocytes and rat neurons was used. [a]All patients were AQP4-seropositive.

ND-R: Clinical form not determined or provided during relapse. CD: Control donor. SP: Secondary-Progressive MS. NP: Information not provided. RR-R: Relapsing-Remitting MS during relapse. RR-S: Relapse-Remitting MS in remission (stable). SVEC4-10: Mouse lymphatic endothelial cell line transformed by simian virus 40. RBE4: Rat brain endothelial cell (BEC) line that expresses the adenovirus E1A gene. cEND: Mouse BEC line that expresses the murine polyoma middle T oncogene. Dex: Dexamethasone. TEER: Transendothelial electrical resistance. OCLN: Occludin. CLDN5: Claudin-5. WB: Western blotting. IHC-IF: Immunofluorescent-based immunohistochemistry. qPCR: quantitative polymerase chain reaction.

Table D.3. NMOSD Sera/IgG-induced Alterations in Human CNS-EC Culture Models.

Study	Cell Line	Sample	Patient (n)	Intervention(s)	Barrier Alterations	Tight Junction Protein Alterations[#]	Methods
Shimizu et al.[95,a,b]	TY08	Serum	• ***NMO-A*** (14)	--	↓ TEER with patient serum vs. FBS.	↓ Total **CLDN5** protein for patient serum vs. FBS, but ↔ total **OCLN** protein for patient serum vs. FBS.	WB
			• ***NMO-A*** (2)	• Plasma exchange	↑ TEER with patient serum after TPE vs. before TPE.	↑ Total **CLDN5** protein for patient serum after PE vs. before PE.	WB
			• ***NMO-A*** (8) **(+) α-BEC Abs** (5) **(-) α-BEC Abs** (3)	• Neutralizing Abs (TNF-α, IFN-γ, IL6, IL17, VEGF, TGFβ)	↑ TEER for patient serum containing α-BEC Abs with VEGF Ab vs. without. ↔ TEER for patient serum containing α-BEC Abs with IL17 Ab vs. without.	↑ ***Cldn5*** mRNA for patient serum containing α-BEC Abs with VEGF Ab vs. without, but no alteration with other Abs vs. without, regardless of α-BEC status. ↑ ***Ocln*** mRNA for patient serum, regardless of α-BEC status, with IL17 Ab vs. without, but no alteration with other Abs vs. without, regardless of α-BEC status.	qPCR
						↑ Total **CLDN5** & ↔ total **OCLN** protein for patient serum containing α-BEC Abs with VEGF Ab vs. without. ↔ Total **CLDN5** & ↔ total **OCLN** protein for patient serum containing α-BEC Abs with IL17 Ab vs. without.	WB
			• ***NMO-A*** (2)	• Ab depletion (Incubation with ACs for 30 or 150 min)	↑ TEER for patient serum following 30 or 150 minutes of depletion vs. none.	↑ Total **CLDN5** protein for patient serum following 30 or 150 minutes of depletion vs. none.	WB

Note: [#]Increases are marked by an upwards arrow (↑), decreases by a downwards arrow (↓), and no change by a left-right arrow (↔).

[a]As the authors contrast patients during "acute phase" with those during "stable disease", "acute phase" suggests following an episode of neurologic symptoms. [b]Although control donor sera and IgG were used, only comparisons against FBS or FBS-derived IgG were performed.

TY08: Human brain endothelial cells (BECs) that express a temperature-sensitive SV40-T antigen variant. NMO-A: NMO during the acute phase of disease. Ab: Antibody. TPE: Therapeutic plasma exchange. TNF-α: Tumor Necrosis Factor alpha. IFN-γ: Interferon gamma. IL6: Interleukin 6. IL17: Interleukin 17. VEGF: Vascular endothelial growth factor. TGFβ: Transforming growth factor beta. AC: Astrocyte. TEER: Transendothelial electrical resistance. FBS: Fetal bovine serum. CLDN5: Claudin-5. OCLN: Occludin. WB: Western blotting. qPCR: Quantitative polymerase chain reaction.

Study	Cell Line	Sample	Patient (n)	Intervention(s)	Barrier Alterations	Tight Junction Protein Alterations[#]	Methods
Tasaki et al.[96,a,b,c,d]	TY08	Serum	• ***NMOSD-A*** (10) • ***NMO*** (7) • ***LETM*** (3)	--	↓ TEER and ↑ perm. to NaF with patient serum vs. FBS.	↓ Total **CLDN5** protein for patient serum vs. FBS, but ↔ total **CLDN5** protein for NMO serum vs. LETM.	WB
				• MMP inhibition (GM6001 or inhibitors specific to MMPs 2 or -9)	↑ TEER & ↓ perm. to NaF for patient serum with GM6001 vs. without. ↑ TEER for patient serum with MMP-2 or MMP-9 inhibitors vs. without.	↑ Total **CLDN5** protein for patient serum with any of the inhibitors vs. without.	WB
			• ***NMOSD-S*** (4) • ***NMO*** (2) • ***LETM*** (2)	--	--	↔ Total **CLDN5** protein for patient serum vs. FBS.	WB
		IgG	• ***NMOSD-A*** (5) • ***NMO*** (4) • ***LETM*** (1)	--	↔ TEER and ↔ perm. to NaF with patient IgG vs. FBS IgG.	↔ Total **CLDN5** protein for patient IgG vs. FBS IgG.	WB
Takeshita et al.[105]	TY08	IgG	• ***NMO*** (50 pooled) • ***CD*** (*NP* pooled)	• AQP4 Expression (Co-culture with AQP4+ or AQP4- ACs)	↑ Perm. to 10 kDa FITC-Dextran with AQP4+ ACs & patient IgG vs. AQP4+ & CD IgG or AQP4- ACs & patient IgG.	Disruption & loss of **CLDN5** reactivity with AQP4+ ACs & patient IgG vs. AQP4+ ACs & CD IgG or AQP4- ACs & patient IgG. Also, ↓ **CLDN5+** area fraction vs. both conditions.	IHC-IF
Shimizu et al.[106,e]	TY08	IgG	• ***NMO*** (50 pooled) • ***CD*** (*NP* pooled)	--	--	Disruption & loss of **CLDN5** reactivity with patient IgG vs. CD IgG. Also, ↓ **CLDN5+** area fraction.	IHC-IF
		rAb	• ***NMO*** (7) • ***ICD*** (2)	--	↑ Perm. to 10 kDa Dextran with patient rAb vs. ICD rAb.	Disruption & loss of **CLDN5** reactivity with patient rAb vs. ICD rAb. Also, ↓ **CLDN5+** area fraction.	IHC-IF

Note: [#]Increases are marked by an upwards arrow (↑), decreases by a downwards arrow (↓), and no change by a left-right arrow (↔).

[a]As the authors contrast patients during "acute phase" with those during "stable disease", "acute phase" suggests following an episode of neurologic symptoms. [b]Although control donor sera and IgG were used, only comparisons against FBS or FBS-derived IgG were performed. [c]The patients who donated stable disease serum also donated acute phase serum. [d]The names of the MMP2 and MMP9 inhibitors were not defined. [e]The patient-derived recombinant antibody recognizes glucose-regulated protein 78 (GRP78).

TY08: Human brain endothelial cells (BECs) that express a temperature-sensitive SV40-T antigen variant. IgG: Immunoglobulin G. rAb: Recombinant antibody. NMOSD-A: NMOSD during the acute phase of disease. NMOSD-S: NMOSD in remission (stable). LETM: Longitudinal extensive transverse myelitis. CD: Control Donor. ICD: Inflammatory control. MMP: Matrix metalloproteinase. AQP4: Aquaporin 4. AC: Astrocyte. TEER: Transendothelial electrical resistance. FBS: Fetal bovine serum. NaF: Sodium fluorescein. FITC: Fluorescein isothiocyanate. kDa: Kilodalton. CLDN5: Claudin-5. OCLN: Occludin. WB: Western blotting. qPCR: Quantitative polymerase chain reaction. IHC-IF: Immunofluorescent-based immunohistochemistry.

Table D.4. NMOSD Sera/IgG-induced Alterations in Non-human or Non-CNS EC Culture Models.

Study	Patients (n)	Sample	Cell	Intervention	Barrier Alterations	Tight Junction Protein Alterations[#]	Methods
Cobo-Calvo et al.[289,a]	• ***NMOSD-R*** (6) • ***CD*** (4)	IgG	Rat BMVs	--	--	↓ Total **CLDN5** & ↔ total **OCLN** protein for patient IgG vs. CD IgG.	WB
			Rat BECs	--	↑ Perm. to sucrose for patient IgG vs. CD IgG.	↓ Total **CLDN5** & ↔ total **OCLN** protein for patient IgG vs. CD IgG.	WB

Note: [@]When studies specified the patients involved in tight junction protein analyses, only those patients are listed and are marked by an asterisks (*****). [#]Increases are demarked by an upwards arrow (↑), decreases – by a downwards arrow (↓), and no change – by a left-right arrow (↔).

[a]All patients were AQP4-seropositive.

NMOSD-R: NMOSD during relapse. CD: Control donor. IgG: Immunoglobulin G. BMV: Brain microvessel. Perm: Permeability. CLDN5: Claudin-5. OCLN: Occludin. WB: Western blotting.

APPENDIX E

Summary Tables for Studies with EAE-based Animal Models of CNS-IDDs.

Table E.1. CNS-EC-specific Alterations in MOG_{35-55}-induced EAE Models (Base Disease).

Pre-onset to Early

Study	Strain	Origin	Stage & Severity†	Tight Junction Protein Alterations#	Methods
Paul et al.[110,a]	**C57BL/6 Mice**	• Spine (*Thoraco-lumbar*)	Pre-onset: No CS (6 *dpi*‡)	No apparent alteration of **CLDN5** reactivity in venules or capillaries with focal IgG deposition in diseased animals.	IHC-IF
Paul et al.[109,b]	**C57BL/6 Mice**	• Spine (*Thoraco-lumbar*)	Pre-onset: No CS (9 *dpi*‡)	Disruption & loss of **CLDN5** reactivity in the venules of diseased animals.	IHC-IF
Paul et al.[111,a]	**C57BL/6 Mice**	• Spine (*Thoraco-Lumbar*)	Pre-onset: No CS (9 *dpi*‡)	Disruption & loss of **CLDN5** reactivity in venules of diseased animals.	IHC-IF
Beard et al.[34]	**C57BL/6 Mice**	• Brain MVs	Pre-onset: No CS (8 *dpi*‡)	Disruption & loss of **CLDN5** reactivity in isolated brain MVs. Additionally, ↓ **CLDN5** density at tight junctions.	IHC-IF
				↓ Total **CLDN5** protein in isolated brain MVs.	WB
Argaw et al.[112]	**C57BL/6 Mice**	• Spine (*Lumbar*)	Onset: T-L	Disruption & loss of **CLDN5** in vessels with fibrinogen deposition.	IHC-IF
			Early: HL-W/-PL	Disruption & loss of **CLDN5** or **OCLN** reactivity in vessels with fibrinogen or albumin deposition, or with strong VEGFA reactivity.	IHC-IF

Note: †Where possible, the disease stage & clinical scores are provided. Otherwise, original author-reported staging marked by a double dagger (‡), with estimated staging marked by a tilde (~). #Unless otherwise noted, comparisons are with respect to a healthy control animal. Increases are marked by an upwards arrow (↑), decreases by a downwards arrow (↓), and no change by a left-right arrow (↔).

[a]Comparisons with naïve animals were not performed. [b]Although naïve wild-type animals were included, no comparisons for claudin-5 density were performed.

MV: Microvessel. dpi: Days post-induction. CS: Clinical score. T-L: Tail limpness. HL-W: Hind limb weakness. HL-PL: Hind limb paralysis. CLDN5: Claudin-5. OCLN: Occludin. VEGFA: Vascular endothelial growth factor A. IHC-IF: Immunofluorescent-based immunohistochemistry. WB: Western blotting.

Onset to Early

Study	Strain	Origin	Stage & Severity[†]	Tight Junction Protein Alterations[#]	Methods
Errede et al.[113,c]	**C57BL/6 Mice**	• Brain (*Cortex*)	[‡]Early-mild: T-L/HL-PS [‡]Early-severe: HL-PL/FL-PS	Worsened disruption & loss of **CLDN5** reactivity in cortical & subcortical vessels from diseased animals with severe disability vs. those with mild disability or healthy controls. Disruption & loss of **CLDN5** reactivity in cortical vessels near demyelination. Disruption & loss of **OCLN** reactivity in cortical vessels from animals with severe disability, but not mild disability, vs. healthy controls.	IHC-IF
Paul et al.[109,b]	**C57BL/6 Mice**	• Spine (*Thoraco-lumbar*)	Early: T-L/HL-W	Disruption and loss of **CLDN5** reactivity in inflamed venules of diseased animals. Also, ↓ **CLDN5** density at tight junctions vs. diseased animals at pre-onset (9 *dpi*).	IHC-IF
Welser et al.[114,d]	**C57BL/6 Mice**	• Brain (*Medulla Oblongata*)	Early: HL-PS	↔ **CLDN5+** per CD31+ area vs. diseased animals sacrificed on the same day as induction.	IHC-IF
Alt et al.[125,c]	**C57BL/6 Mice**	• Brain MVs	[‡]12 *dpi*: T-L (*~Onset-Early*)	↓ ***Cldn11*** & ↓ ***Ocln*** mRNA in isolated BMVs.	MA
Sohet et al.[64,a,c,e]	**C57BL/6 Mice**	• Spine	[‡]4 *dpo*: *NP* (*~Early*)	Loss of **LSR** reactivity in vessels within inflamed areas vs. adjacent non-inflamed areas. Also, ↓ **LSR** intensity per vessel within inflamed areas vs. adjacent non-inflamed areas.	IHC-IF
Mora et al.[124,c,e]	**C57BL/6 Mice**	• Spine MVs	[‡]13 *dpi*: *NP* (*~Early*)	↓ ***Cldn5*** mRNA in isolated spine MVs.	qPCR
Chapouly et al.[122,c]	**C57BL/6 Mice**	• Spine (*Lumbar*)	[‡]15-18 *dpi*: HL-PPS/-PL (*~Early-Peak*)	Disruption & loss of **CLDN5** reactivity in vessels with fibrinogen deposition or near VEGFA reactivity. Also, mean pixel intensity of **CLDN5** negatively correlates with the mean pixel intensities of VEGFA or TYMP, but not GFAP, in diseased mice.	IHC-IF

Note: [†]Where possible, the disease stage & clinical scores are provided. Otherwise, original author-reported staging marked by a double dagger (‡), with estimated staging marked by a tilde (~). [#]Unless otherwise noted, comparisons are with respect to a healthy control animal. Increases are marked by an upwards arrow (↑), decreases by a downwards arrow (↓), and no change by a left-right arrow (↔).

[a]Comparisons with naïve animals were not performed. [b]Although naïve wild-type animals were included, no comparisons for claudin-5 density were performed. [c]Disease course graphs were not provided. [d]Micrographs were not provided. [e]Clinical scores were not provided.

MV: Microvessel. dpi: Days post-induction. dpo: Days post-onset. CS: Clinical score. T-L: Tail limpness. HL-W: Hind limb weakness. HL-PL: Hind limb paralysis. HL-PS: Hind limb paresis. FL-PS: Forelimb paresis. NP: Not provided. HL-PPS: Hind limb paraparesis. CLDN5: Claudin-5. OCLN: Occludin. VEGFA: Vascular endothelial growth factor A. CD31: Cluster of differentiation 31. CLDN11: Claudin-11. LSR: Lipolysis-stimulated lipoprotein receptor. TYMP: Thymidine phosphorylase. GFAP: Glial fibrillary acidic protein. IHC-IF: Immunofluorescent-based immunohistochemistry. WB: Western blotting. MA: Microarray analysis. qPCR: Quantitative polymerase chain reaction.

Peak-Late

Study	Strain	Origin	Stage & Severity[†]	Tight Junction Protein Alterations[#]	Methods
Wang et al.[117,a]	**C57BL/6 Mice**	• Brain & Spine (*Lumbar*)	Peak: CS 2.5[‡]	Disruption & loss of **CLDN5** reactivity in in brain & spinal cord vessels.	IHC-IE, IHC-IF
Bittner et al.[118]	**C57BL/6 Mice**	• Brain MVs	Peak: HL-PL	↔ ***Cldn5*** & ↔ ***Ocln*** mRNA in isolated BMVs from one set of experiments. However, ↔ ***Cldn5*** & ↓ ***Ocln*** mRNA from a different set of experiments.	qPCR
Li et al.[116]	**C57BL/6 Mice**	• Spine	Peak: HL-W/-PL	Disruption & loss of **CLDN5** & **OCLN** reactivity in vessels.	IHC-IF, IHC-IE
Welser et al.[114,b]	**C57BL/6 Mice**	• Brain (*Medulla Oblongata*)	Peak: HL-PL	↓ **CLDN5+** per CD31+ area vs. diseased animals sacrificed on the same day as induction.	IHC-IF
Uchida et al.[40]	**C57BL/6 Mice**	• Brain & Spine	Peak: HL-PL	Disruption & loss of **CLDN11** reactivity in brain & spinal cord vessels. Also, ↓ **CLDN11+** per GLUT1+ intensity for both.	IHC-IF
Niu et al.[115,c,d]	**C57BL/6 Mice**	• Spine	[‡]Peak: *NP*	Loss of **OCLN** reactivity in vessels.	IHC-IF
Argaw et al.[112]	**C57BL/6 Mice**	• Spine (*Ventro-lateral lumbar*)	Late: HL-W/-PL	Disruption & loss of **CLDN5** or **OCLN** reactivity in vessels with fibrinogen or albumin leakage.	IHC-IF
Errede et al.[113]	**C57BL/6 Mice**	• Brain (*Cortex*)	[‡]Late-mild: T-L/HL-PS [‡]Late-severe: HL-PL/FL-PS	Worsened disruption & loss of **CLDN5** & **OCLN** reactivity in cortical vessels from animals with severe disability vs. those with mild disability.	IHC-IF

Note: [†]Where possible, the disease stage & clinical scores are provided. Otherwise, original author-reported staging marked by a double dagger (‡), with estimated staging marked by a tilde (~). [#]Unless otherwise noted, comparisons are between the diseased animal vs. a healthy control. Increases are marked by an upwards arrow (↑), decreases by a downwards arrow (↓), and no change by a left-right arrow (↔).

[a]Scoring rubric was not provided. [b]Micrographs were not provided. [c]Clinical scores were not provided. [d]Disease course graphs were not provided. [e]Although staging for the brain IHC-IF data was not explicitly defined in either study, analysis of claudin-5 and occludin in the spine of knockout animals or bone marrow chimera animals were stated as 40 *dpi*. [f]Staging information was not provided.

MV: Microvessel. CS: Clinical score. HL-PL: Hind limb paralysis. HL-W: Hind limb weakness. NP: Not provided. T-L: Tail limpness. HL-PS: Hind limb paresis. FL-PS: Forelimb paresis. CLDN5: Claudin-5. OCLN: Occludin. CD31: Cluster of differentiation 31. CLDN11: Claudin-11. GLUT1: Glucose transporter 1. FOV: Field of view. IHC-IE: Immunoenzyme-based immunohistochemistry. IHC-IF: Immunofluorescent-based immunohistochemistry. qPCR: Quantitative polymerase chain reaction.

Peak-Late

Study	Strain	Origin	Stage & Severity[†]	Tight Junction Protein Alterations[#]	Methods
Paul et al.[110,c,d]	**C57BL/6 Mice**	• Spine (*Thoraco-lumbar*)	Late: *NP*	Disruption & loss of **CLDN5** reactivity in the venules, but not the capillaries. Also, ↓ **CLDN5** density in the venules, but not the capillaries.	IHC-IF
Bénardais et al.[120]	**C57BL/6 Mice**	• Spine	Late: HL-A/-PS	↓ **CLDN5+** vessels per FOV in vehicle-treated diseased animals vs. healthy controls.	IHC-IE
Eilam et al.[121]	**C57BL/6 Mice**	• Brain (*Cortex*)	Late: HL-PL/FL-PL	Disruption & loss of **CLDN5** reactivity in vessels. Also, ↓ **CLDN5** mean optical density.	IHC-IF
Zhang et al.[119]	**C57BL/6 Mice**	• Spine (*Lumbar*)	Late: HL-PL/FL-PL	Loss of **CLDN5** reactivity in vessels. Also, ↓ **CLDN5** fluorescence intensity.	IHC-IF
Ferrara et al.[126,e]	**C57BL/6 Mice**	• Brain (*Cortex*)	Unclear: HL-PS (*Likely Late*)	Disruption & loss of **CLDN5** & **OCLN** reactivity in vessels.	IHC-IF
Girolamo et al.[127,d,e]	**C57BL/6 Mice**	• Brain (*Cortex*)	Unclear: HL-PS/FL-PS (*Likely Late*)	Disruption & loss of **CLDN5** & **OCLN** reactivity in vessels.	IHC-IF
Becker et al.[123,c,f]	**C57BL/6 Mice**	• Spine	*NP*	Disruption & loss of **CLDN5** reactivity in vessels.	IHC-IF

Note: [†]Where possible, the disease stage & clinical scores are provided. Otherwise, original author-reported staging marked by a double dagger (‡), with estimated staging marked by a tilde (~). [#]Unless otherwise noted, comparisons are between the diseased animal vs. a healthy control. Increases are marked by an upwards arrow (↑), decreases by a downwards arrow (↓), and no change by a left-right arrow (↔).

[c]Clinical scores were not provided. [d]Disease course graphs were not provided. [e]Although staging for the brain IHC-IF data was not explicitly defined in either study, analysis of claudin-5 and occludin in the spine of knockout animals or bone marrow chimera animals were stated as 40 *dpi*. [f]Staging information was not provided.

CS: Clinical score. HL-PL: Hind limb paralysis. NP: Not provided. HL-PS: Hind limb paresis. FL-PS: Forelimb paresis. HL-A: Hind limb ataxia. FL-PL: Forelimb paralysis. CLDN5: Claudin-5. OCLN: Occludin. CD31: Cluster of differentiation 31. CLDN11: Claudin-11. FOV: Field of view. IHC-IF: Immunofluorescent-based immunohistochemistry.

Table E.2. Non-CNS-EC-specific Alterations in MOG_{35-55}-induced EAE Models (Base Disease).

CNS Homogenate-specific Analyses

Study	Strain/Genotype	Origin	Stage & Severity[†]	Tight Junction Protein Alterations[#]	Methods
Beard et al.[34]	**C57BL/6 Mice**	• Brain	Pre-onset: No CS (8 *dpi*[‡])	↓ Total **CLDN5** protein.	WB
Wang et al.[290,a]	**C57BL/6 Mice**	• Brain	Peak: CS 5[‡]	↓ Total **CLDN5** & ↓ total **OCLN** protein.	WB
Wang et al.[291]	**C57BL/6 Mice**	• Brain	Peak: HL-PL/FL-PL	↓ Total **CLDN5** & ↓ total **OCLN** protein.	WB
Lengfeld et al.[74]	**C57BL/6 Mice**	• Spinal Cord	[‡]CS 1 ~ Early: T-L [‡]CS 3 ~ Peak: HL-PL	↓ Total **CLDN5** & ↓ total **OCLN** protein, with a greater loss in animals with worsened disability.	WB
Wang et al.[117,b]	**C57BL/6 Mice**	• Spinal Cord	Peak: CS 2.5[‡]	↓ ***Cldn5*** mRNA & ↓ total **CLDN5** protein.	qPCR, WB
Choi et al.[292]	**C57BL/6 Mice**	• Spinal Cord	Peak: PPS	↓ ***Cldn3*** & ↓ ***Cldn5*** mRNA.	qPCR
Liu et al.[293]	**C57BL/6 Mice**	• Spinal Cord	Peak: HL-PL/FL-W	↓ Total **OCLN** protein.	WB

Note: [†]Where possible, the disease stage & clinical scores are listed. When partial information was available, estimated staging is demarked by a tilde (~), while author-reported information is demarked by a double dagger (‡). When neither staging, nor clinical scores were provided for tight junction analyses, but were available for associated data sets, estimated staging is in parentheses. [#]Unless otherwise noted, comparisons are between the diseased animal and healthy control. Increases are demarked by an upwards arrow (↑), decreases by a downwards arrow (↓), and no change by a left-right arrow (↔).

[a]The grading rubric was based off the sum of disability for tail and individual limbs, complicating direct assignment of disease severity to clinical score. [b]Clinical scores were not provided.

CS: Clinical score. dpi: Days post-induction. HL-PL: Hind limb paralysis. FL-PL: Forelimb paralysis. T-L: Tail limpness. PPS: Paraparesis. FL-W: Forelimb weakness. CLDN5: Claudin-5. OCLN: Occludin. CLDN3: Claudin-3. WB: Western blotting. qPCR: Quantitative polymerase chain reaction.

CNS Homogenate-specific Analyses

Study	Strain/Genotype	Origin	Stage & Severity[†]	Tight Junction Protein Alterations[#]	Methods
Niu et al.[115,b,c]	**C57BL/6 Mice**	• Spinal Cord	[‡]Peak: *NP*	↓ ***Ocln*** mRNA.	qPCR
Horng et al.[294,c]	**C57BL/6 Mice**	• Spinal Cord	[‡]18-21 dpi ~ Peak: HL-W/-PL	↓ Total **CLDN1** & ↓ total **CLDN4** protein, with degradation products detected for both.	WB
Kebir et al.[295c,d]	**C57BL/6 Mice**	• Spinal Cord	Unclear: Grade 4[‡] (*Likely Peak*)	↓ Total **OCLN** protein.	WB
Souza et al.[296]	**C57BL/6 Mice**	• Spinal Cord	Late: HL-W	↓ Total **CLDN4** & ↓ total **OCLN** protein.	WB
Zhang et al.[119]	**C57BL/6 Mice**	• Spinal Cord	Late: HL-PL/FL-PL	↓ Total **CLDN5** & ↓ total **OCLN** protein.	WB
Kim et al.[297,e,f]	**C57BL/6 Mice**	• *Unclear* (Brain or Spine)	*Insufficient Information*	↓ Total **OCLN** protein, but ↔ total **CLDN5** protein.	WB

Note: [†]Where possible, the disease stage & clinical scores are listed. When partial information was available, estimated staging is demarked by a tilde (~), while author-reported information is demarked by a double dagger (‡). When neither staging, nor clinical scores were provided for tight junction analyses, but were available for associated data sets, estimated staging is in parentheses. [#]Unless otherwise noted, comparisons are between the diseased animal and healthy control. Increases are demarked by an upwards arrow (↑), decreases by a downwards arrow (↓), and no change by a left-right arrow (↔).

[b]Clinical scores were not provided. [c]Disease course graphs were not provided. [d]The grading rubric was not provided. [e]The tissue homogenate analyzed was not explicitly defined. [f]No staging was provided.

NP: Not provided. dpi: Days post-induction. HL-W: Hind limb weakness. HL-PL: Hind limb paralysis. FL-PL: Forelimb paralysis. OCLN: Occludin. CLDN1: Claudin-1. CLDN4: Claudin-4. CLDN5: Claudin-5. qPCR: Quantitative polymerase chain reaction. WB: Western blotting.

Non-CNS Homogenate-specific Analyses

Study	Strain/Genotype	Origin	Stage & Severity[†]	Tight Junction Protein Alterations[#]	Methods
Horng et al.[294,b,c]	**C57BL/6 Mice**	• SC Astrocytes	[‡]21 dpi ~ Peak: *NP*	**CLDN4** reactivity detected at the glia limitans of diseased mice.	IHC-IF
Shrestha et al.[298,c]	**C57BL/6 Mice**	• CP Epithelium	[‡]6 dpi ~ Pre-onset: No CS [‡]9 dpi ~ Onset: No CS/T-L [‡]15 dpi ~ Early: HL-W/PL	Disruption & loss of **CLDN2** reactivity following onset of disease, but not pre-onset. Also, ↓ total **CLDN2+** area per nuclei.	IHC-IF
			[‡]15 dpi ~ Early: HL-W/PL	Disruption & loss of **CLDN3** reactivity.	IHC-IF
Uchida et al.[40]	**C57BL/6 Mice**	• CP Epithelium	Peak: HL-PL	No apparent alteration of **CLDN3** & **CLDN11** reactivity.	IHC-IF
		•CP Homogenate	Peak: HL-PL	↔ Total **CLDN3** & ↔ total **CLDN11** protein.	WB
		• BA & SCA Epithelium	Peak: HL-PL	Disruption & loss of **CLDN11** reactivity in both tissues.	IHC-IF
Paul et al.[111,b,c]	**C57BL/6 Mice**	• Peripheral Blood Leukocytes	[‡]8 dpi ~ Pre-onset: No CS	**CLDN5** reactivity detected in extravasated leukocytes by venules of diseased mice.	IHC-IF
			[‡]9 dpi ~ Pre-onset: No CS	**CLDN5** reactivity & total **CLDN5** protein detected in isolated PBLs of diseased mice.	IHC-IF, FC, WB
			[‡]8 dpi ~ Pre-onset: No CS [‡]13 dpi ~ Early: *NP*	↑ ***Cldn5*** mRNA in isolated PBLs of diseased mice at 8 *dpi* vs. healthy controls , with subsequent ↓ ***Cldn5*** mRNA at 13 *dpi* vs 8 *dpi*.	qPCR

Note: [†]Where possible, the disease stage & clinical scores are listed. When partial information was available, estimated staging is demarked by a tilde (~), while author-reported information is demarked by a double dagger (‡). When neither staging, nor clinical scores were provided for tight junction analyses, but were available for associated data sets, estimated staging is in parentheses. [#]Unless otherwise noted, comparisons are between the diseased animal and healthy control. Increases are demarked by an upwards arrow (↑), decreases by a downwards arrow (↓), and no change by a left-right arrow (↔).

[b]Clinical scores were not provided. [c]Disease course graphs were not provided.

SC: Spinal cord. CP: Choroid plexus. BA: Brain arachnoid. SCA: Spinal cord arachnoid. dpi: days post-induction. NP: Not provided. CS: Clinical score. T-L: Tail limpness. HL-W: Hind limb weakness. HL-PL: Hind limb paralysis. CLDN4: Claudin-4. CLDN2: Claudin-2. CLDN3: Claudin-3. CLDN11: Claudin-11. CLDN5: Claudin-5. IHC-IF: Immunofluorescent-based immunohistochemistry. WB: Western blotting. FC: Flow cytometry. qPCR: Quantitative polymerase chain reaction.

Table E.3. CNS-EC-specific Alterations in MOG_{35-55}-induced EAE Models (Therapeutic Interventions).

Study	Strain/Genotype	Origin	Intervention(s)	Stage & Severity[†]	Tight Junction Protein Alterations[#]	Methods
Argaw et al.[128]	**C57BL/6 Mice**	• Spine (*Lumbar*)	• AC Signaling Inhibition (*Cavtratin post-onset → early*)	Peak-VEH: HL-PL Peak-TX: T-L/HL-W	Rescue of **CLDN5** reactivity in vessels & fibrinogen leakage. Also, ↑ **CLDN5+** area per FOV.	IHC-IF
Chapouly et al.[122]	**C57BL/6 Mice**	• Spine (*Lumbar*)	• AC Signaling Inhibition (*Cavtratin, 2DLR, or both post-onset → early*)	Peak-VEH: HL-PL/FL-PL Peak-CAV: T-L/HL-W Peak-2LDR: T-L/HL-W Peak-Dual: T-L/HL-W	Rescue of **CLDN5** reactivity in vessels & fibrinogen leakage for all treatment groups. Additionally, ↑ **CLDN5+** area per FOV for all treatment groups, with the greatest increase in the dual treatment group.	IHC-IF
Niu et al.[115,a]	**C57BL/6 Mice**	• Spine	• Nrf2 Activation (*NGN pre-induction → peak*)	‡Peak: *NP*	Rescue of **OCLN** reactivity in vessels.	IHC-IF
Li et al.[116]	**C57BL/6 Mice**	• Spine	• Nrf2 Activation (*SFN post-onset → peak*)	Peak-VEH: HL-W/-PL Peak-TX: T-L	Rescue of **CLDN5** & **OCLN** reactivity in vessels.	IHC-IF, IHC-IE
Bénardais et al.[120]	**C57BL/6 Mice**	• Spine	• Nrf2 Activation (*DMF post-induction → late*)	Late-VEH: Mod. PPS Late-TX: AT/Mild PPS	No rescue of **CLDN5** reactivity in vessels. Also, ↔ number of **CLDN5+** vessels per FOV.	IHC-IE
Hou et al.[130]	**C57BL/6 Mice**	• Spine (*Lumbar*)	• Immunomodulatory (*Minocycline, MSC-IFN-β, or both post-onset → late*)	Late-VEH: HL-PL Late-Mino: T-L/HL-PL Late-MSC: T-L/HL-PL Late-Dual: No CS/T-L	Rescue of **OCLN** reactivity in all treatment groups. Also, ↑ **OCLN** intensity for all treatment groups, with the greatest increase in the dual treatment group.	IHC-IF
Eilam et al.[121]	**C57BL/6 Mice**	• Brain (*Cortex*)	• Immunomodulatory (*GA early → peak*)	Late-VEH: HL-PL/FL-PL Late-TX: T-L	Rescue of **CLDN5** reactivity in vessels. Also, ↑ **CLDN5** mean optical density.	IHC-IF
Zhang et al.[119]	**C57BL/6 Mice**	• Spine (*Lumbar*)	• NF-κB Inhibition (*TMP or IKK-16 post-onset → late*)	Late-VEH: HL-PL/FL-PL Late-TMP: T-L/HL-PL Late-IKK-16: T-L/HL-PL	Rescue of **CLDN5** reactivity in vessels for both treatment groups. Also, ↑ **CLDN5** intensity for both treatment groups.	IHC-IF
Bittner et al.[118,b]	**C57BL/6 Mice**	• Brain MVs	• Glutamate Blocker (*Riluzole – unclear → peak*)	Peak-VEH: Mild PPS Peak-TX: HL-W/-PL	↑ ***Ocln*** mRNA in isolated BMVs, but ↔ ***Cldn5*** mRNA when compared by treatment or disease.	qPCR

Note: [†]Where possible, the disease stage & respective clinical scores are provided. Otherwise, author-reported staging marked by a double dagger (‡). [#]Unless otherwise noted, comparisons are with respect to the control group. Increases are marked by an upwards arrow (↑), decreases by a downwards arrow (↓), and no change by a left-right arrow (↔).

[a]Clinical scores were not provided. [b]Two separate interventions were performed – one post-induction, the other post-onset. However, the treatment group analyzed was not explicitly defined.

MV: Microvessels. AC: Astrocyte. 2DLR: 2-deoxy-L-ribose. Nrf2: Nuclear factor erythroid 2–related factor 2. NGN: Naringenin. SFN: Sulforaphane. DMF: Dimethyl fumarate. MSC-IFN-β: Interferon beta-expressing mesenchymal stem cells. GA: Glatiramer acetate. NF-κB: Nuclear factor kappa beta. TMP: Tetramethylpyrazine. VEH: Vehicle group. TX: Treatment group. CAV: Cavtratin. Combo: Dual treatment group. Mino: Minocycline. HL-PL: Hind limb paralysis. T-L: Tail limpness. FL-PL: Forelimb paralysis. HL-W: Hind limb weakness. Mod: Moderate. PPS: Paraparesis. AT: Ataxia. CS: Clinical score. CLDN5: Claudin-5. FOV: Field of view. OCLN: Occludin. IHC-IF: Immunofluorescence-based immunohistochemistry. IHC-IF: Immunoenzyme-based Immunohistochemistry. qPCR: Quantitative polymerase chain reaction.

Table E.4. Non-CNS-EC-specific Alterations in MOG_{35-55}-induced EAE Models (Therapeutic Interventions).

CNS Homogenate-specific Analyses

Study	Strain/Genotype	Origin	Intervention(s)	Stage & Severity†	Tight Junction Protein Alterations#	Methods
Beard et al.[34]	**C57BL/6 Mice**	• Brain	• IR Agonist (DMAQ-B1 *24 hours prior*)	Pre-onset-VEH: *NP* Pre-onset-TX: *NP*	↑ Total **CLDN5** protein.	WB
Wang et al.[290]	**C57BL/6 Mice**	• Brain	• I_2R Antagonist (IDZ *post-induction → early*)	Peak-VEH: CS 5 Peak-TX: CS 2	↑ Total **CLDN5** protein, but ↔ total **OCLN** protein.	WB
Wang et al.[291]	**C57BL/6 Mice**	• Brain	• Anti-oxidant/-inflammatory (RSV *post-induction → peak*)	Peak-VEH: HL-PL/FL-PL Peak-LOW: HL-PL/FL-PL Peak-MED: HL-PL (full) Peak-HIGH: HL-PL (partial)	↑ Total **CLDN5** & ↑ total **OCLN** protein for the medium and high dosage treatment groups, but not the low dosage treatment group.	WB
Choi et al.[292]	**C57BL/6 Mice**	• Spinal Cord	• Immunomodulatory (HBPDS *post-onset → peak*)	Peak-VEH: PPS Peak-TX T-PL	↑ ***Cldn3*** mRNA, but ↔ ***Cldn5*** mRNA.	qPCR
Liu et al.[293]	**C57BL/6 Mice**	• Spinal Cord	• Mesenchymal Stem Cells (Single injection *post-onset*)	Peak-VEH: HL-PL Peak-MSC: HL-W	↑ Total **CLDN5** protein.	WB

Note: †Where possible, the disease stage & clinical scores are listed. When partial information was available, estimated staging is demarked by a tilde (~), while author-reported information is demarked by a double dagger (‡). When neither staging, nor clinical scores were provided for tight junction analyses, but were available for associated data sets, estimated staging is in parentheses. #Unless otherwise noted, comparisons are between the treatment group and control group. Increases are demarked by an upwards arrow (↑), decreases by a downwards arrow (↓), and no change by a left-right arrow (↔).

IR: Insulin receptor. DMAQ-B1: Demethylasterriquinone B1. I_2R: Imidazoline I_2 receptor. IDZ: Idazoxan. RSV: Resveratrol. HBPDS: Hyungbangpaedok-San. VEH: Vehicle group. TX: Treatment group. LOW: Low dosage. MED: Medium dosage. HIGH: High dosage. MSC: Mesenchymal stem cells. NP: Not provided. CS: Clinical score. HL-PL: Hind limb paralysis. FL-PL: Forelimb paralysis. PPS: Paraparesis. T-PL: Tail paralysis. HL-W: Hind limb weakness. NP: Not provided. T-W: Tail-weakness. T-L: Tail limpness. CLDN5: Claudin-5. OCLN: Occludin. CLDN4: Claudin-4. WB: Western blotting. qPCR: Quantitative polymerase chain reaction.

CNS Homogenate-specific Analyses

Study	Strain/Genotype	Origin	Intervention(s)	Stage & Severity[†]	Tight Junction Protein Alterations[#]	Methods
Niu et al.[115,a,b]	**C57BL/6 Mice**	• Spinal Cord	• Nrf2 activation (NGN pre-induction → peak)	[‡]Peak-VEH: *NP* [‡]Peak-TX: *NP*	↑ ***Ocln*** mRNA.	qPCR
Souza et al.[296]	**C57BL/6 Mice**	• Spinal Cord	• Strength or Endurance Train. (*Pre-induction* → *~onset*)	Late-CTL: HL-W Late-STR: T-W Late-END: No CS/T-W	↑ **CLDN4** & ↑ total **OCLN** protein with either physical exercise strategy.	WB
Zhang et al.[119]	**C57BL/6 Mice**	• Spinal Cord	• NF-κB Inhibition (TMP or IKK-16 *early* → *late*)	Late-VEH: HL-PL/FL-PL Late-TMP: T-L/HL-PL Late-IKK: T-L/HL-PL	↑ Total **CLDN5** & ↑ total **OCLN** protein for either treatment group vs. vehicle.	WB
Giacoppo et al.[299,c]	**C57BL/6 Mice**	• Brain	• Nrf2 Activation (GRA *pre-induction* → *unclear*)	*Insufficient information*	↑ Total **CLDN1,** ↑ total **CLDN3**, & ↑ total **CLDN5** protein.	WB
Kim et al.[297]	**C57BL/6 Mice**	• *Unclear* (Brain/Spine)	• PAR1 Antagonists (VOR or KC *post-induction* →*unclear*)	*Insufficient Information*	↑ Total **OCLN** protein for either treatment group vs. vehicle. However, ↔ total **CLDN5** protein when compared by disease or treatment.	WB

Note: [†]Where possible, the disease stage & clinical scores are listed. When partial information was available, estimated staging is demarked by a tilde (~), while author-reported information is demarked by a double dagger (‡). When neither staging, nor clinical scores were provided for tight junction analyses, but were available for associated data sets, estimated staging is in parentheses. [#]Unless otherwise noted, comparisons are between the treatment group and control group. Increases are demarked by an upwards arrow (↑), decreases by a downwards arrow (↓), and no change by a left-right arrow (↔).

[c]The staging in the Methods section contradicts the staging in the figure legend.

Nrf2: nuclear factor erythroid 2–related factor 2. NGN: Naringenin. NF-κB: Nuclear factor kappa B. TMP: Tetramethylpyrazine. GRA: Glucoraphanin. PAR1: Protease-activated receptor-1. VOR: Vorapaxar (SCH-530348). KC: KC-A0590. NP: Not provided. VEH: Vehicle group. TX: Treatment group. CTL: Control group. STR: Strength group. END: Endurance group. CS: Clinical score. HL-W: Hind limb weakness. T-W: Tail-weakness. HL-PL: Hind limb paralysis. FL-PL: Forelimb paralysis. OCLN: Occludin. CLDN4: Claudin-4. CLDN5: Claudin-5. CLDN1: Claudin-1. qPCR: Quantitative polymerase chain reaction. WB: Western blotting.

Table E.5. CNS-EC-specific Alterations in MOG_{35-55}-induced EAE Models (Genetic Manipulations).

Non-Claudin-involved Genetic Manipulations

Study	Strain/Genotype	Origin	Manipulation(s)	Stage & Severity†	Tight Junction Protein Alterations#	Method
Göbel et al.[132,a]	**C57BL/6 Mice** • *B1R*$^{-/-}$	• Brain MVs	• *B1R*-KO	Peak-WT: PPS Peak-KO: T-L	↑ ***Ocln*** mRNA, but ↔ ***Cldn5*** mRNA, in isolated BMVs.	qPCR
Wang et al.[117,b]	**C57BL/6 Mice** • *Irgm1*$^{-/-}$	• Brain & Spine (*Lumbar*)	• *Irgm1*-KO	Peak-WT: CS 2.5 Peak-KO: CS 1.0	Rescue of **CLDN5** reactivity in vessels.	IHC-IE, IHC-IF
Bittner et al.[118,c]	**C57BL/6 Mice** • *Kcnk2*$^{-/-}$	• Spine	• *Knck2*-KO	Unclear: *Likely Peak*	No rescue of **OCLN** reactivity in vessels. Also, ↔ **OCLN** intensity.	IHC-IF
		• BMVs	• *Knck2*-KO	Peak-WT: HL-PL Peak-KO: PPS	↔ ***Cldn5*** & ↔ ***Ocln*** mRNA in isolated BMVS from diseased *Kcnk2*-KO mice vs. diseased wild-type mice, naïve *Kcnk2*-KO mice, or naïve wild-type mice.	qPCR
Ferrara et al.[126,d]	**C57BL/6 Mice** • *NG2*$^{-/-}$	• Brain (*Cortex*)	• *NG2*-KO	Unclear: *Likely Late*	Rescue of **CLDN5** & **OCLN** reactivity in vessels.	IHC-IF
			• BM chimeras (W→W, K→W, W→K, K→K)	Late-WW: HL-PL Late-KW: HL-PS/-A Late-WK: HL-PL Late-KK: HL-PS/-A	Worsened disruption & loss of **CLDN5** & **OCLN** reactivity in wild-type recipients vs. *NG2*-KO recipients, regardless of donor genotype.	IHC-IF
		• Spine	• *NG2*-KO	Late-WT: HL-PS Late-KO: T-L	Rescue of **CLDN5** & **OCLN** reactivity in vessels of diseased *NG2*-KO animals vs. healthy *NG2*-KO animals.	IHC-IF
Girolamo et al.[127,e]	**C57BL/6 Mice** • *NG2*$^{-/-}$	• Brain (*Cortex*)	• *NG2*-KO	Unclear: *Likely Peak* WT: HL-PS/TPL KO: T-L/FL-PS	Rescue of **CLDN5** & **OCLN** reactivity in vessels.	IHC-IF
Wouters et al.[133,f]	**C57BL/6 Mice** • *LXRα*$^{-/-}$	• Brain	• *LXRα*-KO	Late-WT: HL-PL Late-KO: T-PL/HL-PPS	↓ **CLDN5+** area fraction.	IHC-IF
Becker et al.[123,g]	**C57BL/6 Mice** • *Asm*$^{-/-}$	• Spine	• *Asm*-KO	*NP*	Rescue of **CLDN5** reactivity in vessels.	IHC-IF

Note: †Where possible, the disease stage & clinical scores are provided. Otherwise, original author-reported staging marked by a double dagger (‡), with estimated staging marked by a tilde (~). #Unless otherwise noted, comparisons are with respect to a genotype control or wild-type animal. Increases are marked by an upwards arrow (↑), decreases by a downwards arrow (↓), and no change by a left-right arrow (↔).

[a]Although naïve animals were included, no statistical comparisons were performed. [b]No scoring rubric was provided. [c]Staging for the IHC-IF data was not explicitly defined, but related qPCR experiments were performed at peak. [d]Staging for the brain IHC-IF data was not explicitly defined, but related IHC-IF experiments were stated as 40 *dpi*. [e]Staging for the brain IHC-IF data was not explicitly defined, but related permeability experiments were stated as 20 *dpi*. [f]Micrographs were not provided. [g]Neither clinical score, nor staging were provided.

B1R: Bradykinin B1 receptor. Irgm1: Immunity-related GTPase family M protein 1. Knck2: Potassium channel subfamily K member 2. NG2: Neural/glial antigen 2. LXRα: Liver X receptor alpha. Asm: Acid sphingomyelinase. MV: Microvessel. KO: Knockout. BM: Bone marrow. WW: Wild-type BM into wild-type recipients. KW: Knockout BM into wild-type recipients. KW: Knockout BM into wild-type recipients. KK: Knockout BM into knockout recipients. WT: Wild-type. NP: Not provided. PPS: Paraparesis. T-L: Tail limpness. HL-PL: Hind limb paralysis. HL-PS: Hind limb paresis. HL-A: Hind limb ataxia. T-PL: Tail paralysis. TPL: Tetraplegia. OCLN: Occludin. CLDN5: Claudin-5. qPCR: Quantitative polymerase chain reaction. IHC-IF: Immunofluorescent-based immunohistochemistry.

Non-Claudin-involved Genetic Manipulations

Study	Strain/Genotype	Origin	Manipulation(s)	Stage & Severity[†]	Tight Junction Protein Alterations[#]	Method
Ni et al.[134]	**C57BL/6 Mice** • *IFNγR*$^{-/-}$ • *IFNγR*$^{-/-}$ *x Tie2-IFNγR*	• Brain (*Cerebellum*)	• *IFNγR*-KO • *IFNγR*-EC-only	Peak-WT: T-L/HL-PS Peak-KO: HL-PS Peak-EC-only: HL-PL	Loss of **CLDN5** reactivity in vessels for *IFNγR*-KO mice vs. wild-type mice. Also, ↓ **CLDN5+** per Tie2+ intensity. Rescue of **CLDN5** reactivity in vessels for *IFNγR*-EC-only mice vs. *IFNγR*-KO mice. Also, ↑ **CLDN5+** per Tie2+ intensity.	IHC-IF
Ouyang et al.[135,a]	**C57BL/6 Mice** •*Tie2-Cre x LR*$^{fl/fl}$	• SCMVs	• *LR*-EC^{KO}	Peak-WT: HL-uPL/-bPL Peak-KO: T-L/HL-uPL	↑ ***Ocln*** mRNA, but ↔ ***Cldn1***, ↔ ***Cldn2***, ↔ ***Cldn3***, & ↔ ***Cldn5*** mRNA, in isolated SCMVs.	qPCR
Welser et al.[114,b]	**C57BL/6 Mice** • *Tie2-Cre x Itgb4*$^{fl/fl}$	• Brain (*Medulla Oblongata*)	• *Itgb4*-EC^{KO}	Early-WT: HL-PS Early-KO: HL-PS	↔ **CLDN5+** per CD31+ area.	IHC-IF
				Peak-WT: HL-PL Peak-KO: QPL	Disruption & loss of **CLDN5** reactivity in vessels. Also, ↓ **CLDN5+** per CD31+ area.	IHC-IF
Paul et al.[109,c]	**C57BL/6 Mice** • *Gfap-Cre x Ccl2*$^{fl/fl}$ • *Tie2-Cre x Ccl2*$^{fl/fl}$	• Spine (*Thoraco-lumbar*)	• *Ccl2*-EC^{KO} • *Ccl2*-AC^{KO}	‡9 dpi-WT: No CS ‡9 dpi-EC^{KO}: No CS	↑ **CLDN5** density in venules at tight junctions of *Ccl2*-EC^{KO} mice at both time points vs wild-type mice. Also, ↔ **CLDN5** density between time points for *Ccl2*-EC^{KO} mice.	IHC-IF
				‡16 dpi-WT: T-L/HL-W ‡16 dpi-EC^{KO}: No CS	↓ **CLDN5** density in venules at tight junctions of *Ccl2*-EC^{KO} mice at 9 *dpi* vs *Ccl2*-AC^{KO} mice. However, ↑ **CLDN5** density vs. *Ccl2*-AC^{KO} mice at 16 *dpi*.	
				‡9 dpi-AC^{KO}: No CS ‡16 dpi-AC^{KO}: No CS/T-L	↑ **CLDN5** density in venules of *Ccl2*-AC^{KO} mice at both time points vs. wild-type mice. Also, ↓ **CLDN5** density between time points for *Ccl2*-AC^{KO} mice.	
Argaw et al.[128]	**C57BL/6 Mice** • *Gfap-Cre x Vegfa*$^{fl/fl}$	• Spine	• *Vegfa*-AC^{KO}	Peak-WT: HL-W/-PL Peak-KO: LT	Rescue of **CLDN5** reactivity, plus fibrinogen deposition, in vessels. Also, rescue of **CLDN5**+ area per FOV.	IHC-IF
Brambilla et al.[136,d]	**C57BL/6 Mice** • *Gfap-IκBα-dn*	• Spine (*Thoracic*)	• NF-κB inhibition (AC-specific)	Late (x2)-WT: T-L/HL-PL Late (x2)-DN: T-W/-L	No rescue of **CLDN5** optical density in *GFAP-IκBα-dn* mice vs. wild-type mice at either two analyzed time points (both post-peak).	IHC-IE

Note: [†]Where possible, the disease stage & respective clinical scores are provided. Otherwise, author-reported staging marked by a double dagger (‡). [#]Unless otherwise noted, comparisons are with respect to a genotype control or wild-type animal. Increases are marked by an upwards arrow (↑), decreases by a downwards arrow (↓), and no change by a left-right arrow (↔).

[a]Although naïve animals were included, no statistical comparisons by disease were performed. [b]Micrographs were only provided for the peak stage. [c]Onset of disease was delayed in *Ccl2*-KO mice, complicating direct comparison of animals by stage. [d]The two time points were approximately 1- and 3-weeks post-peak.

IFNγR: Interferon gamma receptor. Tie2: Tyrosine kinase with Ig and EGF homology domains 2. Cre: Cyclic recombinase. LR: Leptin receptor. fl: Floxed allele. Itgb4: Integrin subunit beta 4. Gfap: Glial fibrillary acidic protein. Ccl2: Chemokine (C-C motif) ligand 2. Vegfa: Vascular endothelial growth factor A. IκBα-dn: Dominant-negative mutant of inhibitor of nuclear factor kappa B. SCMV: Spinal cord microvessel. KO: Knockout. EC-only: Endothelial cell-restricted expression. EC^{KO}: Endothelial-restricted knockout. AC^{KO}: Astrocyte-restricted knockout. NF-κB: Nuclear factor kappa B. AC: astrocyte. WT: Wild-type or genotype control. dpi: Days posts-induction. x2: Two time points. DN: Dominant-negative mutant. T-L: Tail limpness. HL-PS: Hind limb paresis. HL-PL: Hind limb paralysis. HL-uPL: Hind limb unilateral paralysis. HL-bPL: Hind limb bilateral paralysis. QPL: Quadriplegia. CS: Clinical score. HL-W: Hind limb weakness. T-W: Tail weakness. CLDN5: Claudin-5. Ocln: Occludin. CLDN1: Claudin-1. CLDN2: Claudin-2. CLDN3: Claudin-3. CD31: Cluster of differentiation 31. FOV: Field of view. IHC-IF: Immunofluorescent-based immunohistochemistry. qPCR: Quantitative polymerase chain reaction. IHC-IE: Immunoenzyme-based immunohistochemistry.

Claudin-involved Genetic Manipulations

Study	Strain/Genotype	Origin	Manipulation(s)	Stage & Severity[†]	Phenotype or Tight Junction Protein Alterations[#]	Method
Pfeiffer et al.[45,a]	**C57BL/6 Mice** • *Tie2-tTA x [TRE]-Cldn1*	--	• *Cldn1*-EC^{KI}	Induction → Late	↔ Day of onset & ↔ peak CS, but rescue of chronic CS.	--
		• Brain	• *Cldn1*-EC^{KI}	Late-CTL: HL-PPS/-PL Late-EC^{KI}: T-L	↔ Number of CD45+ inflammatory cuffs, but ↓ % of cuffs with Hoechst or fibronectin leakage.	IHC-IF
Paul et al.[111]	**C57BL/6 Mice** • *Tie2-eGFP-Cldn5*$^{+/-}$	• Spine (*Thoraco-Lumbar*)	• *eGFP-Cldn5*- EC^{KI}	Pre-onset: No CS (9 dpi[‡])	Disruption of **eGFP-CLDN5** reactivity in inflamed venules near dual DRAQ5+/**eGFP-CLDN5+** inflammatory cuffs.	IHC-IF
Lutz et al.[137]	**C57BL/6 Mice** • *Tie2-eGFP-Cldn5*$^{+/-}$ • *Tie2-eGFP-Cldn5*$^{+/-}$ *x Cav1*$^{-/-}$	• Spine (*Lumbar*)	• *eGFP-Cldn5*- EC^{KI}	Pre-onset: No CS Early: T-PL Peak: HL-W/-PL	↑ % of **eGFP-CLDN5+** tight junctions in venules with static or dynamic protrusions in all diseased groups. ↑ % of **eGFP-CLDN5+** tight junctions in venules with gaps or tortuosity in the early & peak diseased groups only. Disruption & loss of **eGFP-CLDN5** reactivity in areas with fibrinogen leakage in all diseased groups, with worsened alterations in areas with greater leakage.	IV-2PM
			• *eGFP-Cldn5*- EC^{KI} & *Cav1*-KO	Pre-onset: No CS	↔ % of **EGFP-CLDN5+** tight junctions in venules with protrusions, gaps, or tortuosity in *eGFP-Cldn5*-EC^{KI} x *Cav1*-KO mice vs. *eGFP-Cldn5*-EC^{KI} mice.	IV-2PM
Castro-Dias et al.[48,b]	**C57BL/6 Mice** • *Cldn12*$^{LacZ/LacZ}$ • *Cldn12*$^{LacZ/+}$	--	• *Cldn12*-KO	Induction → Late	↔ Day of onset & ↔ overall disease severity.	--
		• Brain	• *Cldn12*-KO	[‡]CS 2: HL-PL	No apparent difference in leakage of fibronectin or IgG.	IHC-IF
		• Brain (*Cortex & Cerebellum*)	• *Cldn12-LacZ*	[‡]CS 0: No CS [‡]CS 2: HL-PL	No apparent difference in LacZ activity in the cortex or cerebellum of diseased *Cldn12-LacZ* animals at CS 2 vs. those at CS 0.	X-Gal

Note: [†]Where possible, the disease stage and respective clinical score are provided. Otherwise, author-reported staging marked by a double dagger (‡). [#]Unless otherwise noted, comparisons are with respect to the genotype control or wild-type animal. Increases are marked by an upwards arrow (↑), decreases by a downwards arrow (↓), and no change by a left-right arrow (↔).

[a]Only ~30% of Tie2+ vessels exhibited detectable claudin-1 expression before induction. [b]Staging information was not provided.

Tie2: Tyrosine kinase with Ig and EGF homology domains 2. tTA: Tetracycline transactivator. TRE: Tetracycline-responsive promoter element. CLDN1: Claudin-1. CLDN3: Claudin-3. eGFP: Enhanced green fluorescent protein. CLDN5: Claudin-5. CAV1: Caveolin-1. CLDN12: Claudin-12. LacZ: β-galactosidase reporter gene replacing the encoding exon of *Cldn12*. EC^{KI}: Endothelial-specific knockout. KO: Knockout. CTL: Genotype control. CS: Clinical score. HL-PPS: Hind limb paraparesis. HL-PL: Hind limb paralysis. T-L: Tail limpness. NS: No score. T-PL: Tail paralysis. HL-W: Hind limb weakness. CD45: Cluster of differentiation 45. DRAQ5: Deep red anthraquinone 5. IHC-IF: Immunofluorescent-based immunohistochemistry. IV-2PM: Intravital two-photon microscopy. X-Gal: 5-bromo-4-chloro-3-indolyl β-d-galactopyranoside.

Table E.6. Non-CNS-EC-specific Alterations in MOG_{35-55}-induced EAE Models (Genetic Manipulations).

Non-Claudin-involved Genetic Manipulations (CNS Homogenates)

Study	Strain/Genotype	Origin	Manipulation(s)	Stage & Severity[†]	Tight Junction Protein Alterations[#]	Method
Wang et al.[117,a]	**C57BL/6 Mice** • *Igrm1*$^{-/-}$	• Spinal Cord	• *Igrm1*-KO	Peak-WT: CS 2.5[‡] Peak-KO: CS 1.0[‡]	↑ ***Cldn5*** mRNA & ↑ total **CLDN5** protein.	qPCR, WB
Zheng et al.[300]	**C57BL/6 Mice** • *ApoE*$^{-/-}$	• Brain	• *ApoE*-KO	Late-WT: T-LT Late-KO: T-F	↓ ***Cldn5*** & ↓ ***Ocln*** mRNA vs. diseased wild-type, healthy *ApoE*-KO, or healthy wild-type animals.	qPCR
					↓ Total **CLDN5** protein & ↓ total **OCLN** protein vs. diseased wild-type, healthy *ApoE*-KO, or healthy wild-type animals.	WB
Lengfeld et al.[74,b]	**C57BL/6 Mice** • *Cdh5-tTA x [TRE]-Axin-IRES-eGFP*	• Spinal Cord	• *Axin*-EC^{KI}	[‡]Peak-CTL: LT/HL-PS [‡]Peak-EC: HL-PS	↔ Total **CLDN5** & ↔ total **OCLN** protein.	WB
Mora et al.[124]	**C57BL/6** • *Cdh5-Cre x Dhh*$^{fl/fl}$	• Spinal Cord	• *Dhh*-EC^{KO}	Late-CTL: HL-PL Late-KO: HL-W/-PL	↑ Total **CLDN4** protein.	WB

Note: [†]Where possible, the disease stage & clinical scores are listed. When partial information was available, estimated staging is demarked by a tilde (~), while author-reported information is demarked by a double dagger (‡). When neither staging, nor clinical scores were provided for tight junction analyses, but were available for associated data sets, estimated staging is in parentheses. [#]Unless otherwise noted, comparisons are between the genetically manipulated animal and the wild-type or genotype control. Increases are demarked by an upwards arrow (↑), decreases by a downwards arrow (↓), and no change by a left-right arrow (↔).

[a]The scoring rubric was not provided. [b]When the animals that died are included, there was a significant increase in disability for *Axin*-EC^{KI} mice. However, when these mice are excluded, there was no difference.

Irgm1: Immunity-related GTPase M protein 1. ApoE: Apolipoprotein E. Cdh5: Cadherin-5. tTA: Tetracycline-controlled transactivator. TRE: Tetracycline-responsive promotor element. IRES: internal ribosome entry site. eGFP: Enhanced green fluorescent protein. Cre: Cyclic recombinase. Dhh: Desert hedgehog. fl: Flanked by loxP. KO: Knockout. EC^{KI}: Endothelial-restricted knockin. EC^{KO}: Endothelial-restricted KO. WT: Wild-type. CTL: Genotype control. CLDN5: Claudin-5. OCLN: Occludin. CLDN4: Claudin-4. qPCR: Quantitative polymerase chain reaction. WB: Western blotting.

Claudin-involved Genetic Manipulations

Study	Strain/Genotype	Origin	Manipulation(s)	Stage & Severity[†]	Phenotype & Tight Junction Protein Alterations[#]	Method
Kooij et al.[285]	**C57BL/6 Mice** • *Cldn3*$^{-/-}$	--	• *Cldn3*-KO	Induction → Late	Earlier onset, worsened peak disability, & worsened chronic disability.	--
Castro-Dias et al.[47]	**C57BL/6 Mice** • *Cldn3*$^{-/-}$	--	• *Cldn3*-KO	Induction → Late	No difference in onset or overall disease severity.	--
Horng et al.[294]	**C57BL/6 Mice** • *Gfap-Cre x Cldn4*$^{fl/fl}$	--	• *Cldn4*-AC^{KO}	Induction → Peak	Worsened peak disability, total average disability, and mortality.	--
		• Spine	• *Cldn4*-AC^{KO}	Peak-CTL: HL-W/-PL Peak-KO: HL-PL/FL-PL	Worsened CD4+ infiltration, fibrinogen & IgG leakage, & demyelination.	IHC-IF
		• Spinal Astrocytes	• *Cldn4*-AC^{KO}	Unclear: *NP* (*Likely Peak*)	**CLDN1** reactivity in astrocytes from spinal cord lesions of diseased *Cldn4*-AC^{KO} mice.	IHC-IF

Note: [†]Where possible, the disease stage & clinical scores are listed. When partial information was available, estimated staging is demarked by a tilde (~), while author-reported information is demarked by a double dagger (‡). When neither staging, nor clinical scores were provided for tight junction analyses, but were available for associated data sets, estimated staging is in parentheses. [#]Unless otherwise noted, comparisons are between the genetically manipulated animal and the wild-type or genotype control. Increases are demarked by an upwards arrow (↑), decreases by a downwards arrow (↓), and no change by a left-right arrow (↔).

[a]The *Cldn3*-KO mice were independently generated, rather than two publications characterizing the same line.

CLDN3: Claudin-3. GFAP: Glial fibrillary acidic protein. Cre: Cyclic recombinase. CLDN4: Claudin-4. fl: flanked by loxP. CTL: Genotype control. HL-W: Hind limb weakness. HL-PL: Hind limb paralysis. FL-PL: Forelimb paralysis. NP: Not provided. CD4: Cluster of differentiation 4. CLDN1: Claudin-1. IHC-IF: Immunofluorescent-based immunohistochemistry.

Claudin-involved Genetic Manipulations

Study	Strain/Genotype	Origin	Manipulation(s)	Stage & Severity[†]	Phenotype & Tight Junction Protein Alterations[#]	Method
Paul et al.[111,a]	**C57BL/6 Mice** • *Tie2-eGFP-Cldn5*$^{+/-}$ • *CD45.1/CD45.2*	• PBLs	• *eGFP-Cldn5*-EC^{KI}	‡9 dpi ~ Pre-onset: No CS	**eGFP-CLDN5** reactivity in extravasated leukocytes near venules of diseased *eGFP-Cldn5*-EC^{KI} mice.	IHC-IF
				‡8 dpi ~ Pre-onset: No CS	**eGFP-CLDN5** in PBLs isolated from diseased *eGFP-Cldn5*-EC^{KI} mice	FC
			• BM Chimeras *CD45.1/CD45.2* → *eGFP-Cldn5*-EC^{KI}	‡9 dpi ~ Pre-onset: No CS	**eGFP-CLDN5** detected in extravasated leukocytes near **eGFP-CLDN5+** venules in diseased chimeric mice.	IHC-IF
				‡8 dpi ~ Pre-onset: No CS	**eGFP-CLDN5** in PBLs isolated from diseased chimeric mice.	FC
		• BP-EVs	• *eGFP-Cldn5*-EC^{KI}	‡8 dpi ~ Pre-onset: No CS	**eGFP-CLDN5+** in blood plasma-derived EVs from diseased *eGFP-Cldn5*-EC^{KI} mice.	FC

Note: [†]Where possible, the disease stage & clinical scores are listed. When partial information was available, estimated staging is demarked by a tilde (~), while author-reported information is demarked by a double dagger (‡). When neither staging, nor clinical scores were provided for tight junction analyses, but were available for associated data sets, estimated staging is in parentheses. [#]Unless otherwise noted, comparisons are between the genetically manipulated animal and the wild-type or genotype control. Increases are demarked by an upwards arrow (↑), decreases by a downwards arrow (↓), and no change by a left-right arrow (↔).

[a]No disease course graph was provided.

Tie2: Tyrosine kinase with Ig and EGF homology domains 2. eGFP: Enhanced green fluorescent protein. CLDN5: Claudin-5. CD45.1: Cluster of differentiation 45.1 allele. CD45.2: Cluster of differentiation 45.2 allele. PBL: Peripheral blood leukocyte. BP-EV: Blood plasma-derived extracellular vesicle. EC^{KI}: Endothelial-restricted knockin. BM: Bone marrow. dpi: Days post-induction. CS: Clinical score. IHC-IF: Immunofluorescent-based immunohistochemistry. FC: Flow cytometry.

Table E.7. CNS-EC-specific Alterations in MBP-induced EAE Models.

Study	Strain/Genotype	Origin	Intervention(s)	Stage & Severity[†]	Tight Junction Protein Alterations[#]	Method
Morgan et al.[140]	**Lewis Rats**	• Spine (*Lumbar*)	--	Peak: HL-PL	Disruption & loss of **CLDN5** & **OCLN** reactivity in vessels with Hoechst+ inflammatory cuffs.	IHC-IF
Ninkovic et al.[141,a]	**CBA/H Mice** • *iNOS*$^{-/-}$	• Brain (*Forebrain*)	--	Late: HL-W	Loss of **OCLN** reactivity.	IHC-IE
			• NO Synthase Inhibition (AG *post-induction* → *late*) • *iNOS*-KO	Late-WT/VH: HL-W Late-WT/TX: HL-W Late-KO/VH: T-L/HL-W Late-KO/TX: T-L	Comparable loss of **OCLN** reactivity in vehicle-treated wild-type or *iNOS*-KO mice vs. healthy wild-type or *iNOS*-KO mice. Rescue of **OCLN** reactivity in agmatine-treated diseased wild-type & *iNOS-KO* mice vs. respective vehicle-treated diseased counterparts or healthy counterparts.	IHC-IE

Note: [†]Where possible, the disease stage and respective clinical score are provided. Otherwise, author-reported staging marked by a double dagger (‡). [#]Unless otherwise noted, comparisons are made for the diseased animal vs. a healthy control, the treatment group vs. the control group, or the genetically manipulated animal vs. the wild-type control. Increases are marked by an upwards arrow (↑), decreases by a downwards arrow (↓), and no change by a left-right arrow (↔).

[a]Agmatine has multiple putative mechanisms of action.

iNOS: Inducible nitric oxide synthase. AG: Agmatine. KO: Knockout. WT: Wild-type. VH: Vehicle group. TX: Treatment group. HL-PL: Hind limb paralysis. HL-W: Hind limb weakness. T-L: Tail limpness. CLDN5: Claudin-5. OCLN: Occludin. IHC-IF: Immunofluorescent-based immunohistochemistry. IHC-IE: Immunoenzyme-based immunohistochemistry.

Table E.8. Non-CNS-EC-specific Alterations in MBP-induced EAE Models.

Study	Strain/Genotype	Origin	Stage & Severity[†]	Tight Junction Protein Alterations[#]	Method
Morgan et al.[140,a]	**Lewis Rats**	• SCH	Peak: HL-PL	↔ Total **CLDN5** protein.	WB
				↑ **OCLN** protein dephosphorylation. ↑ **OCLN** protein in TX100-soluble fractions.	IP-WB
			Pre-onset: No CS Onset-Early: T-L → HL-W Peak: HL-PL Late (x3): T-L → No CS	↑ **OCLN** protein dephosphorylation at all stages.	IP-WB

Note: [†]Where possible, the disease stage & clinical scores are listed. When partial information was available, estimated staging is demarked by a tilde (~), while author-reported information is demarked by a double dagger (‡). When neither staging, nor clinical scores were provided for tight junction analyses, but were available for associated data sets, estimated staging is in parentheses. [#]Unless otherwise noted, comparisons are between the diseased animal and healthy control. Increases are demarked by an upwards arrow (↑), decreases by a downwards arrow (↓), and no change by a left-right arrow (↔).

[a]Increased electrophoretic mobility of higher molecular weight occludin bands was interpreted as dephosphorylation rather than the usage of an anti-phospho-OCLN antibody..

SCH: Spinal cord homogenate. x3: Three time points. HL-PL: Hind limb paralysis. CS: Clinical score. T-L: Tail limpness. HL-W: Hind limb weakness. CLDN5: Claudin-5. OCLN: Occludin. WB: Western blotting. IP-WB: Immunoprecipitation WB.

Table E.9. CNS-EC-specific Alterations in MOG_{1-125}-induced EAE Models.

Study	Strain/Genotype	Origin	Intervention(s)	Stage & Severity[†]	Tight Junction Protein Alterations[#]	Method
Adzemovic et al.[139,b]	**DA Rats** • *Eae18b*	• Spine	• EAE Resistance	Early-WT: No CS/T-L Early-EAE18b: No CS/T-L	Rescue of **OCLN** reactivity in vessels of diseased *Eae18b* animals vs. wild-type. Also, ↑ number of **OCLN+** vessels per tissue cross section.	IHC-IE

Note: [†]Where possible, the disease stage and respective clinical score are provided. Otherwise, author-reported staging marked by a double dagger (‡). [#]Unless otherwise noted, comparisons are made for the diseased animal vs. a healthy control, the treatment group vs. the control group, or the genetically manipulated animal vs. the wild-type control. Increases are marked by an upwards arrow (↑), decreases by a downwards arrow (↓), and no change by a left-right arrow (↔).

[a]The Eae18 locus, which contains C-C motif chemokine ligands (CCLs) 1, 2, 7, 11, and 12, was introduced into the EAE-susceptible DA strain by breeding with the EAE-resistant PVG.av1 rat strain.

WT: Wild-type. CS: Clinical score. HL-PL: Hind limb paralysis. HL-W: Hind limb weakness. T-L: Tail limpness. HL-PS: Hind limb paresis. CLDN5: Claudin-5. OCLN: Occludin. FOV: Field of view. CD31: Cluster of differentiation 31. IHC-IF: Immunofluorescent-based immunohistochemistry. IHC-IE: Immunoenzyme-based immunohistochemistry.

Table E.10. Non-CNS-EC-specific Alterations in MOG_{1-125}-induced EAE Models.

Study	Strain/Genotype	Origin	Stage & Severity[†]	Tight Junction Protein Alterations[#]	Method
Becanovics et al.[301]	**Various Rats**	• gDNA	--	A polymorphism in the ***Cldn4*** gene (K191E) segregates with susceptibility to EAE.	DNA-Seq
		• Thymus, Spleen, Lymph node, Spine, Brain	Onset:CS > 0.	↑ ***Cldn4*** mRNA in spleen, thymus, spine and brain homogenates, but not lymph node homogenate, in strains resistant to EAE vs. susceptible to EAE.	qPCR
Fairless et al.[302]	**BN Rats**	• Optic nerve head	Pre-onset: No CS. Onset: CS > 0.	Disruption of **OCLN** reactivity in vessels at both stages.	IHC-IF

Note: [†]Where possible, the disease stage & clinical scores are listed. When partial information was available, estimated staging is demarked by a tilde (~), while author-reported information is demarked by a double dagger (‡). When neither staging, nor clinical scores were provided for tight junction analyses, but were available for associated data sets, estimated staging is in parentheses. [#]Unless otherwise noted, comparisons are between the diseased animal and healthy control. Increases are demarked by an upwards arrow (↑), decreases by a downwards arrow (↓), and no change by a left-right arrow (↔).

gDNA: Genomic DNA. CS: Clinical score. CLDN4: Claudin-4. OCLN: Occludin. DNA-Seq: DNA sequencing. qPCR: Quantitative polymerase chain reaction. IHC-IF: Immunofluorescent-based immunohistochemistry.

Table E.11. Non-CNS-EC-specific Alterations in OSP/CLDN11-induced EAE Models.

Study	Strain/Genotype	Origin	Stage & Severity[†]	Tight Junction Protein Alterations[#]	Method
Stevens et al.[303,a]	**SJL Mice**	• SC Myelin	[‡]Peak: *NP*	Disruption & loss of **CLDN11** reactivity in demyelinated areas with Cresyl Violet+ infiltrates.	IHC-IE

Note: [†]Where possible, the disease stage & clinical scores are listed. When partial information was available, estimated staging is demarked by a tilde (~), while author-reported information is demarked by a double dagger (‡). When neither staging, nor clinical scores were provided for tight junction analyses, but were available for associated data sets, estimated staging is in parentheses. [#]Unless otherwise noted, comparisons are between the diseased animal and healthy control. Increases are demarked by an upwards arrow (↑), decreases by a downwards arrow (↓), and no change by a left-right arrow (↔).

[a]Claudin-11 (previously named OSP) is expressed by oligodendrocytes as a component of the myelin sheath, hence its usages as a demyelination marker rather than a vascular marker here.

SC: Spinal cord. NP: Not provided. CLDN11: Claudin-11. IHC-IE: Immunoenzyme-based immunohistochemistry.

Table E.12. CNS-EC-specific Alterations in $PLP_{139-159}$-induced EAE Models.

Study	Strain/Genotype	Origin	Intervention(s)	Stage & Severity†	Tight Junction Protein Alterations#	Method
Halder et al.[142]	**SJL/L Mice**	• Spine (*Lumbar*)	--	Peak: HL-PL	Disruption & loss of **OCLN** reactivity in vessels. Also, ↓ **OCLN** signal per FOV.	IHC-IF
			• CMH (10% O_2) (*Post-induction → peak*)	Peak-Norm: HL-PL Peak-CMH: T-L	Rescue of **OCLN** reactivity in vessels. Also, ↑ **OCLN** signal per FOV.	IHC-IF
Halder et al.[143,a]	**SJL/L Mice**	• Spine (*Lumbar*)	--	Peak: HL-PL Late: HL-PS	Disruption & loss of **OCLN** reactivity in vessels at both stages.	IHC-IF
				Peak: HL-PL	↓ Proportion of **OCLN**+ per CD31+ vessels per FOV.	
			• CMH (10% O_2) (*Post-onset → late*)	Peak-Norm: HL-PL Peak-CMH: HL-PL Late (x3)-Norm: HL-PS Late (x3)-CMH: T-L	Rescue of **OCLN** reactivity in vessels at a late stage (1-week post-peak), but not at peak.	IHC-IF
					↑ Proportion of **OCLN+** per CD31+ vessels per FOV at the late stage (1-, 2-, & 3-weeks post-peak), but not at peak.	
Lanz et al.[144,b]	**SJL Mice**	• Spine	• PKCβ Inhibition (ENZ *unclear → unclear*)	Unclear – *Likely Late*	Rescue of **CLDN5** reactivity in vessels.	IHC-IF

Note: †Where possible, the disease stage and respective clinical score are provided. Otherwise, author-reported staging marked by a double dagger (‡). #Unless otherwise noted, comparisons are made for the diseased animal vs. a healthy control, the treatment group vs. the control group, or the genetically manipulated animal vs. the wild-type control. Increases are marked by an upwards arrow (↑), decreases by a downwards arrow (↓), and no change by a left-right arrow (↔).

[a]Statistical comparisons between diseased animals at the late-stage time points and healthy controls were not provided. [b]Neither clinical scores, nor staging information were provided for the IHC-IF data. For other data sets, treatment was initiated at peak disability and continued through an unspecified late stage.

CMH: Chronic mild hypoxia. O_2: Oxygen. PKCβ: Protein kinase C-beta type. ENZ: Enzastaurin (LY-317615). WT: Wild-type. Norm: Normoxia. x3: Three time points analyzed. HL-PL: Hind limb paralysis. T-L: Tail limpness. HL-PS: Hind limb paresis. OCLN: Occludin. CLDN5: Claudin-5. FOV: Field of view. CD31: Cluster of differentiation 31. IHC-IF: Immunofluorescent-based immunohistochemistry. IHC-IE: Immunoenzyme-based immunohistochemistry.

Table E.13. CNS-EC-specific Alterations in CNS Homogenate-induced EAE Models.

Syngeneic Homogenates

Study	Strain/Genotype	Origin	Intervention(s)	Stage & Severity[†]	Tight Junction Protein Alterations[#]	Method
Wolburg et al.[44,a]	**SJL/N Mice**	• Brain	--	Paraplegic[‡]	Loss of **CLDN1** & **CLDN3** reactivity, but not **CLDN5** or **OCLN** reactivity, in vessels near CD45+ inflammatory cuffs.	IHC-IF
Huang et al.[145]	**SD Rats**	• Brain (*Cerebellum*)	--	[‡]CS 1:T-L [‡]CS 4:HL-PL/FL-PL	Worsened disruption & loss of **CLDN5** reactivity in rats with more severe disability vs. those with milder disability.	IHC-IF
			• K_v1 blocker (ImKTx88 *post-induction* or *post-onset* → *peak*)	Peak-VEH:HL-PL Peak-TX-PI:No CS/T-L Peak-TX-PO:T-L/HL-W	Rescue of **CLDN5** reactivity for either treatment group.	IHC-IF

Note: [†]Where possible, the disease stage and respective clinical score are provided. Otherwise, author-reported staging marked by a double dagger (‡). [#]Unless otherwise noted, comparisons are with respect to healthy or vehicle controls. Increases are marked by an upwards arrow (↑), decreases by a downwards arrow (↓), and no change by a left-right arrow (↔).

[a]Although claudin-5 & occludin reactivity was detected in inflamed vessels, the vessels exhibited tortuous morphology. The authors stated that this confounded assessment about subcellular localization.

KV1: Voltage-gated potassium channel. CS: Clinical score. VEH: Vehicle group. TX: Treatment group. PI: Post-induction. PO: Post-onset. T-L: Tail limpness. HL-PL: Hind limb paralysis. FL-PL: Forelimb paralysis. HL-W: Hind limb weakness. CLDN1: Claudin-1. CLDN3: Claudin-3. CD45: Cluster of differentiation 45. CLDN5: Claudin-5. OCLN: Occludin. IHC-IF: Immunofluorescent-based immunohistochemistry.

Guinea Pig Homogenates

Study	Strain/Genotype	Origin	Intervention(s)	Stage & Severity[†]	Tight Junction Protein Alterations[#]	Method
Shou et al.[146]	**Wistar Rats**	• Brain	--	Onset: T-L Peak: FL-PL Late: HL-W	Loss of **CLDN5** reactivity in vessels at all stages. Also, ↓ **CLDN5** AOD between onset and peak, with modest ↑ **CLDN5** AOD at remission.	IHC-IF
Yang et al.[147,b]	**Lewis Rats**	• Brain	--	‡Peak: HL-PL/PPL	Loss of **CLDN5** & **OCLN** reactivity. Also, ↓ **CLDN5** & ↓ **OCLN** IOD.	IHC-IE
			• Immunomodulatory (TIIA *post-onset* → *early*)	Peak-VEH: HL-PL/PPL Peak-LOW: HL-W/-PL Peak-HIGH: T-L/HL-W	Rescue of **CLDN5** & **OCLN** reactivity for both treatment groups. Additionally, ↑ **CLDN5** & ↑ **OCLN** IOD for both treatment groups, with a greater increase at the higher dosage.	IHC-IE
Grygorowicz et al.[148,c]	**Lewis Rats**	• BMVs (*GM*)	--	Pre-onset (x4): No CS Peak: HL-PL	↓ Total **CLDN5** protein in isolated BMVs at four time points pre-onset, and at peak disability.	WB
				Pre-onset (x2): No CS Peak: HL-PL	Disruption & loss of **CLDN5** reactivity in isolated BMVs at two times points pre-onset, but no apparent alteration at peak disability.	IHC-IF
			• P2X7R antagonist (BBG *post-induction* → *pre-onset*)	Pre-onset-VEH: No CS Pre-onset-TX: No CS	↑ Total **CLDN5** protein in isolated BMVs from the treatment group vs. the vehicle group or healthy controls.	WB
				‡12 dpi-VEH: HL-PL ‡12 dpi-TX: > No CS.	↑ Total **CLDN5** protein in isolated BMVs from the treatment group vs. the vehicle group, but not healthy controls.	WB
Viñuela-Berni et al.[149,d]	**Lewis Rats**	• BMVs, SCMVs	--	Peak: HL-PL/-A	↓ Total **CLDN5** in isolated BMVs & SCMVs.	WB
			• AVPR antagonist (CO *pre-induction* → *peak*)	Peak-VEH: HL-PL/-A Peak-TX: No CS/L-T	Intermediate rescue of total **CLDN5** protein.	WB

Note: [†]Where possible, the disease stage and respective clinical score are provided. Otherwise, author-reported staging marked by a double dagger (‡). [#]Unless otherwise noted, comparisons are with respect to healthy or vehicle controls. Increases are marked by an upwards arrow (↑), decreases by a downwards arrow (↓), and no change by a left-right arrow (↔).

[b]The drug was considered at two dosages. [c]Onset of disease was delayed in the treatment group, complicating direct comparison of groups. [d]There was no significant difference between the treatment group and the vehicle group or healthy controls, but there was a significant difference between the vehicle group and healthy controls.

BMV: Brain microvessel. GM: Grey Matter. SCMV: spinal cord microvessel. TIIA: Tanshinone IIA. P2X7R: Purinergic Receptor P2X 7. BBG: Brilliant Blue G. AVPR: Arginine vasopressin receptor. CO: Conivaptan. CS: Clinical score. VEH: Vehicle group. LOW: Low dosage. HIGH: High dosage. TX: Treatment group. x4: Four time points. x2: Two time points. T-L: Tail limpness. FL-PL: Forelimb paralysis. HL-W: Hind limb weakness. HL-PL: Hind limb paralysis. PPL: Paraplegia. HL-A: Hind limb ataxia. CLDN5: Claudin-5. AOD: Average optical density (OD). OCLN: Occludin. IOD: Integrated OD. IHC-IF: Immunofluorescent-based immunohistochemistry (IHC). IHC-IE: Immunoenzyme-based IHC. WB: Western blotting.

Table E.14. Non-CNS-EC-specific Alterations in CNS Homogenate-induced EAE Models.

Syngeneic Homogenates

Study	Strain/Genotype	Origin	Intervention(s)	Stage & Severity†	Tight Junction Protein Alterations#	Method
Wolburg et al.[304,a,b]	**SJL/N Mice**	• CP Epithelium	--	*Insufficient Information*	Disruption & loss of **CLDN1**, **CLDN2**, & **CLDN11** reactivity, but not **OCLN** reactivity.	IHC-IF
Huang et al.[145,c]	**SD Rats**	• BH	--	Unclear:HL-PL *(Likely Peak)*	↓ ***Cldn5*** & ↓ ***Ocln*** mRNA. Also, ↓ Total **CLDN5** & ↓ total **OCLN** protein.	qPCR, WB
			• K_v1 Blocker (ImKTx88 *post-induction* or *post-onset* → *unclear*)	Unclear – *Likely Peak* VEH:HL-PL TX-PI:T-L TX-PO:T-L	↑ ***Cldn5*** & ↑ ***Ocln*** mRNA for either intervention strategy vs. vehicle ↑ Total **CLDN5** & total ↑ **OCLN** protein for either intervention strategy vs. vehicle.	qPCR

Note: †Where possible, the disease stage & clinical scores are listed. When partial information was available, estimated staging is demarked by a tilde (~), while author-reported information is demarked by a double dagger (‡). When neither staging, nor clinical scores were provided for tight junction analyses, but were available for associated data sets, estimated staging is in parentheses. #Unless otherwise noted, comparisons are between the diseased animal and healthy control, or treatment group and vehicle. Increases are demarked by an upwards arrow (↑), decreases by a downwards arrow (↓), and no change by a left-right arrow (↔).

[a]Staging information was not provided. [b]Clinical scores were not provided. [c]Neither the staging, nor the clinical scores were explicitly defined. However, for associated data sets, the staging was defined as peak.

CP: Choroid plexus. BH: Brain homogenate. K_v1: Voltage-gated potassium channel subfamily A. VEH: Vehicle group. TX: Treatment group. PI: Post-induction. PO: Post-onset. HL-PL: Hind limb paralysis. T-L: Tail limpness. CLDN1: Claudin-1. CLDN2: Claudin-2. CLDN11: Claudin-11. OCLN: Occludin. CLDN5: Claudin-5. IHC-IF: Immunofluorescence-based immunohistochemistry. qPCR: Quantitative polymerase chain reaction. WB: Western blotting.

Guinea Pig Homogenates

Study	Strain/Genotype	Origin	Intervention(s)	Stage & Severity[†]	Tight Junction Protein Alterations[#]	Method
Huang et al.[305]	**Lewis Rats**	• BH (*Cerebellum*) • SCH (*Lumbar*)	--	Pre-onset (x2):No CS Onset:HL-W/PL Peak:HL-PL/FL-PL	↓ Total **OCLN** protein in BH & SCH at all stages vs. animals sacrificed at 0 dpi.	WB
Huang et al.[306]	**Lewis Rats**	• BH (*Cerebellum*) • SCH (*Lumbar*)	--	Peak:HL-PL	↓ Total **OCLN** protein in BH & SCH.	WB
			• ROCK Inhibitor (FSD *post-induction* → *peak*)	Peak-VEH:HL-PL Peak-TX:HL-W	↑ Total **OCLN** protein in BH & SCH.	WB
Yang et al.[147]	**Lewis Rats**	• BH	--	Peak:HL-PL/PPL	↓ Total **CLDN5** & ↓ total **OCLN** protein.	WB
			• Anti-Inflamm./Immunomod. (TIIA *post-induction* → *peak*)	Peak-VEH:HL-PL/PPL Peak-LOW:HL-W/-PL Peak-HIGH:T-L/HL-W	↑ Total **CLDN5** & ↑ total **OCLN** protein for either dosage vs. vehicle.	WB

Note: [†]Where possible, the disease stage & clinical scores are listed. When partial information was available, estimated staging is demarked by a tilde (~), while author-reported information is demarked by a double dagger (‡). When neither staging, nor clinical scores were provided for tight junction analyses, but were available for associated data sets, estimated staging is in parentheses. [#]Unless otherwise noted, comparisons are between the diseased animal and healthy control, or treatment group and vehicle. Increases are demarked by an upwards arrow (↑), decreases by a downwards arrow (↓), and no change by a left-right arrow (↔).

BH: Brain homogenate. SCH: Spinal cord homogenate. ROCK: Rho-associated kinase. TIIA: Tanshinone IIA. x2: Two time points. VEH: Vehicle group. TX: Treatment group. LOW: Low dosage. HIGH: High dosage. CS: Clinical score. HL-W: Hind limb weakness. HL-PL: Hind limb paralysis. FL-PL: Forelimb paralysis. PPL: Paraplegia. T-L: Tail limpness. OCLN: Occludin. CLDN5: Claudin-5. dpi: Days post-induction. WB: Western blotting.

Table E.15. CNS-EC-specific Alterations in Transgenic EAE Models.

TCR-1640 Model[a]

Study	Strain/Genotype	Origin	Stage[†]	Tight Junction Protein Alterations[#]	Method
Alvarez et al.[9]	**SJL/J Mice** • *TCR-1640*	• Brain (*Cerebellum*)	Pre-onset: 30 & 35 dpn[‡]	**OCLN** & **CLDN3** reactivity detected in vessels at 35 dpn. Also, ↔ **OCLN**, ↔ **CLDN3**, & ↔ **CLDN5** pixel intensity between 30 and 35 dpn.	IHC-IF
			Pre-onset: 45, 50, & 55 dpn[‡]	Disruption of **OCLN** & **CLDN3** reactivity in vessels near astrogliosis & fibrinogen deposition. Additionally, ↓ **OCLN** pixel intensity at 45-55 dpn vs. 30-35 dpn, but ↔ **CLDN3** & ↔ **CLDN5** pixel intensity at same time points.	IHC-IF

Note: [†]Where possible, the disease stage and respective clinical score are provided. Otherwise, author-reported staging marked by a double dagger (‡). [#]Increases are marked by an upwards arrow (↑), decreases by a downwards arrow (↓), and no change by a left-right arrow (↔).

[a]In this model, astrogliosis and barrier dysfunction is observed ~45 *dpn* onwards, while onset of disability is generally ~65 dpn. In females, the disease generally follows a relapse-remission course. However, in males, the disease generally follows a primary-progressive course.

TCR-1640: T cell receptor reactive to residues 92-106 of myelin oligodendrocyte glycoprotein. dpn: Days post-natal. OCLN: Occludin. CLDN3: Claudin-3. CLDN5: Claudin-5. IHC-IF: Immunofluorescent-based immunohistochemistry.

APPENDIX F

Summary Tables for Studies with Other Animal Models of CNS-IDDs

Table F.1. CNS-EC-specific Alterations in Experimental NMOSD Models.

Intracortical Injection of Patient-derived Recombinant AQP4 Antibody & Complement[a]

Study	Strain/Genotype	Origin	Intervention	Staging[†]	Tight Junction Protein Alterations[#]	Method
Winkler et al.[20,b,c]	**Lewis Rats**	• Brain (*Cortex*)	--	10, 24 *hpi*, & 3 *dpi*	Loss of **OCLN** reactivity in lesional vessels at 10 & 24 *hpi* vs. control Ab-injected animals, with recovery of **OCLN** reactivity by 3 dpi.	IHC-IF
				10 *hpi*	No apparent alteration of **CLDN3** & **CLDN5** reactivity detected in lesional vessels vs. control Ab-injected animals.	
				6, 10, 24 *hpi*, 3 & 6 *dpi*	↓ Proportion of **OCLN+** lesional vessels over the first 24 hpi, with partial and complete recovery at 3 & 6 dpi, respectively. However, ↔ proportion of **CLDN3+** or **CLDN5+** lesional vessels over the same timeframe.	
			• Immune cell Depletion (*Antiserum pre-induction*)	6 *hpi*	↑ Proportion of **OCLN+** lesional vessels from immune cell-depleted animals vs. control serum-injected animals. However, ↔ proportion of **CLDN3+** or **CLDN5+** lesional vessels with respect to disease or intervention.	IHC-IF

Note: [#]Increases are marked by an upwards arrow (↑), decreases by a downwards arrow (↓), and no change by a left-right arrow (↔).

[a]In this model, barrier dysfunction, neutrophil infiltration, and astrocyte loss occurred by 6 *hpi*. Barrier function was restored by 24 *hpi*, but astrocyte loss and neutrophil infiltration persisted over 3 *dpi*. [b]Micrographs were not provided for every time point measured, nor were micrographs were provided for the intervention experiments. [c]Injection of an anti-PMN antiserum depleted multiple immune cell types by ~90%, including neutrophils, T cells, and B cells.

AQP4: Aquaporin-4. hpi: Hours post-injection. OCLN: Occludin. CLDN3: Claudin-3. CLDN5: Claudin-5. IHC-IF: Immunofluorescent-based immunohistochemistry.

Table F.2. CNS-EC-specific Alterations in TMEV Models.

***Peptide-induced Fatal Syndrome*[a]**

Study	Strain/Genotype	Origin	Intervention	Stage	Tight Junction Protein Alterations[#]	Method
Suidan et al.[159,b]	**C57BL/6 Mice** • *Prf1*$^{-/-}$	BMVs	--	0, 4, 12, & 24 *hpp*	↔ Total **CLDN5** over first 12 *hpp*, but increase at 24 *hpp*, in VP2-injected wild-type animals. ↓ **Total OCLN** over first 12 *hpp*, with recovery at 24 *hpp* in VP2-injected wild-type animals.	WB
			• *Prf1*-KO	24 *hpp*	↔ Total **CLDN5** & ↔ total **OCLN** in VP2-injected *Prf1*-KO animals vs. E7-injected counterparts.	WB
Suidan et al.[163]	**C57BL/6 Mice**	BMVs	• Peptide-based NRP-1 inhibitor (-0.5, +3, +6, & +9 *hpp)*	12 *hpp*	↑ Total **OCLN** in NRP-1-treated VP2-injected animals vs. vehicle-treated counterparts.	WB
Johnson et al.[161]	**C57BL/6 Mice**	Brain	• No immune cell depletion (Rat serum days 5-7 post-infection)	24 *hpp*	Disruption & loss of **CLDN5** and **OCLN** reactivity in vessels near FITC-albumin leakage in non-depleted VP2-injected mice vs. E7-injected counterparts.	IHC-IF
			• Neutrophil depletion (anti-Ly6G days 5-7 post-infection)	24 *hpp*	No rescue in **CLDN5** and **OCLN** reactivity in vessels near FITC-albumin leakage in neutrophil-depleted VP2-injected mice vs. non-depleted counterparts.	IHC-IF
			• CD8+ T cell depletion (anti-GR-1 days 5-7 post-infection)	24 *hpp*	Rescue of **CLDN5** & **OCLN** reactivity, plus FITC-albumin leakage, in CD8-depleted VP2-injected animals vs. non-depleted counterparts.	IHC-IF
Johnson et al.[164]	**C57BL/6 Mice** • *Prf1*$^{-/-}$	Brain	• *Prf1*-KO mice restored with *Prf1*-competent CD8+ T cells	24 *hpp*	Disruption & loss of **CLDN5** and **OCLN** reactivity in vessels with FITC-albumin leakage in VP2-injected animals vs. E7-injected counterparts.	IHC-IF
Willenbring et al.[162]	**C57BL/6 Mice** • *Prf1*$^{+/-}$ or *Prf1*$^{-/-}$	Brain	• *Prf1*-KO (hemi- or homozygous)	12 *hpp*	Disruption & loss of **CLDN5** reactivity in vessels, plus severity of fibrinogen leakage, increases with the number of *Prf1* alleles in VP2-injected animals vs. respective E7-injected counterparts.	IHC-IF

Note: No studies that characterized members of the claudin, TAMP, or angulin families using the classic TMEV model were found. [#]Increases are marked by an upwards arrow (↑), decreases by a downwards arrow (↓), and no change by a left-right arrow (↔).

[a]In this model, detectable astrogliosis and barrier dysfunction is observed by 4 *hpi*, peaking at ~12 *hpi* for both. [b]Statistics were not enumerated for the WB experiments using wild-type mice.

Prf1: Perforin. BMVs: Brain microvessels. KO: Knockout. NRP-1: Neurpilin-1. Ly6G: Lymphocyte antigen 6 complex, locus G. CD8: Cluster of differentiation 8. GR-1: Granulocyte receptor-1. hpp: Hours post-injection of the VP2 or E7 peptides. CLDN5: Claudin-5. VP2: Peptide encoding the immunodominant epitope of the VP2 capsid protein ($VP2_{121-130}$). OCLN: occludin. E7: Control peptide. FITC: Fluorescein isothiocyanate. WB: Western blotting. IHC-IF: Immunofluorescent-based immunohistochemistry.

Table F.3. CNS-EC-specific Alterations in Cuprizone Models.

Study	Strain/Genotype	Origin	Intervention	Stage	Tight Junction Protein Alteration[#]	Method
Berghoff et al.[172,a]	**C57BL/6 mice**	• Brain (*Corpus Callosum*)	--	5 weeks of feeding	Disruption & loss of **OCLN** reactivity in vessels. Also, ↓ **OCLN+** area fraction.	IHC-IF
		• Brain (*Cortex*)	--	5 weeks of feeding	No apparent alteration of **OCLN** reactivity in vessels. Also, ↔ **OCLN+** area fraction.	IHC-IF

Note: [#]Comparisons are between cuprizone-fed mice and control chow-fed mice. Increases are marked by an upwards arrow (↑), decreases by a downwards arrow (↓), and no change by a left-right arrow (↔).

[a]5 weeks of feeding was chosen by the authors as it corresponded to peak demyelination and barrier dysfunction in the corpus callosum, but not for the cortex.

OCLN: Occludin. IHC-IF: Immunofluorescent-based immunohistochemistry.

Table F.4. Non-CNS-EC-specific Alterations in Cuprizone Models.

Study	Strain/Genotype	Origin	Manipulation(s)	Stage	Tight Junction Protein Alterations[#]	Method
Berghoff et al.[172]	**C57BL/6 mice** • *Cxcr3*$^{-/-}$	• BH (*Corpus Callosum*)	--	5 days of feeding	↓ ***Cldn5*** & ↓ ***Ocln*** mRNA in homogenate.	qPCR
			• *Cxcr3*-KO	5 days of feeding	Rescue of ***Cldn5*** & ***Ocln*** mRNA in homogenate from cuprizone-fed *Cxcr3*-KO mice vs. cuprizone-fed wild-type mice.	qPCR
			--	5 weeks of feeding	↓ ***Cldn5*** & ↓ ***Ocln*** mRNA in homogenate.	qPCR
					↓ Total **CLDN5** protein in homogenate.	WB
		• BH (*Cortex*)	--	5 days of feeding	↓ ***Cldn5*** & ↓ ***Ocln*** mRNA in homogenate.	qPCR
				5 weeks of feeding	↔ Total **CLDN5** protein in homogenate.	WB
Shelestak et al.[174]	**C57BL/6 mice**	• BH (*Corpus Callosum*)	--	3 days of feeding	↓ Total **OCLN** protein in homogenate.	WB

Note: [#]Unless otherwise noted, comparisons are between cuprizone-fed mice and control chow-fed mice. Increases are demarked by an upwards arrow (↑), decreases by a downwards arrow (↓), and no change by a left-right arrow (↔).

CXCR3: C-X-C Motif Chemokine Receptor 3. BH: Brain homogenate. KO: Knockout. CLDN5: Claudin-5. OCLN: Occludin. qPCR: Quantitative polymerase chain reaction. WB: Western blotting.

APPENDIX G

Reagents, Primers, Antibodies, & Software Used in These Studies.

Table G.1. List of Reagents Used in These Studies.

Purpose	Reagent	Manufacturer	Catalogue
Active EAE Induction	MOG_{35-55}/CFA Emulsion PTX	Hooke Laboratories	EK-2110
Barrier Function (*in vivo*)	Sodium Fluorescein Salt	Sigma-Aldrich	F6377
	Boric Acid	Sigma-Aldrich	B6768
	Trichloroacetic Acid	Sigma-Aldrich	T6399
Immunohistochemistry	*Lycopersicon Esculentum* (Tomato) Lectin, DyLight 649	Vector Laboratories	DL-1178-1
	Paraformaldehyde	Sigma-Aldrich	P6148
	Triton X-100	Acros Organics	327371000
	Bovine Serum Albumin	Sigma-Aldrich	A1470
	Vectashield Antifade Mounting Medium	Vector Laboratories	H-1000-10
	PFTE Printed Slides	Electron Microscopy Services	63419-14
BBB-EC Isolation	Gibco™ HBSS, no calcium, no magnesium, no phenol red	ThermoFisher Scientific	14175095
	HEPES	Fisher Bioreagents	BP310-100
	Bovine Serum Albumin	Sigma-Aldrich	A1470
	Gibco™ DMEM, high glucose, HEPES, no phenol red	ThermoFisher Scientific	21063029
	Collagenase/Dispase	Sigma-Aldrich	11097113001
	DNAse	Spectrum	D348910MG
	Complete Endothelial Cell Medium with Kit	Cellbiologics	M1168-Kit
	Gibco™ Puromycin Dihydrochloride	ThermoFisher Scientific	A1113803
	R&D Systems™ Cultrex Rat Collagen I, Lower Viscosity	R&D Systems	3443-100-01

Purpose	Reagent	Manufacturer	Catalogue
T Cell Activation	C57BL/6 MOG_{35-55} Spleen & Lymph Node Cells	Hooke Laboratories	CF-1003
	RPMI 1640	Gibco	11875085
	HEPES	Fisher Bioreagents	BP310-100
	Gibco™ Fetal Bovine Serum, One Shot™	ThermoFisher Scientific	A3160401
	L-Glutamine–Penicillin–Streptomycin solution (100X)	Sigma-Aldrich	G6784
	Gibco™ MEM Non-Essential Amino Acids Solution (100X)	ThermoFisher Scientific	11140050
	Gibco™ Sodium Pyruvate (100 mM)	ThermoFisher Scientific	11360070
	2-Mercaptoethanol	Alfa Aesar	A1589030
	MOG_{35-55} Peptide in TC Media (100X)	Hooke Laboratories	DS-0111
	Recombinant Mouse IL-12 p70	BioLegend	577002
	Ultra-Leaf Purified anti-mouse IFN-γ	BioLegend	505847
Conditioned Media	C8-D1A Mouse Astrocyte Line	ATCC	CRL-2541
	Gibco™ DMEM, High Glucose, L-Glutamine, Phenol Red	ThermoFisher Scientific	11965092
	Fetal Bovine Serum	Atlanta Biologicals	S11150
	Gibco™ Penicillin-Streptomycin (100X)	ThermoFisher Scientific	15140122
	Naïve C57BL/6 Spleen Cells & Lymph Node Cells	Hooke Laboratories	CF-1203
	Neutrophil Isolation Kit, mouse	Miltenyi Biotec	130-097-658
RNA Isolation & Analysis	RNAzol RT	Molecular Research Center	RN 190
	4-Bromoanisole (BAN)	Molecular Research Center	BN 191
	iScript cDNA Synthesis Kit	Bio-Rad	1708891
	SsoAdvanced Universal SYBR Green Supermix	Bio-Rad	1725271

Purpose	Reagent	Manufacturer	Catalogue
TAT-Cre-mediated Recombination	TAT-Cre Recombinase Protein	Sigma-Aldrich	SCR508
	TAT-HA2 Fusion Peptide	AnaSpec	AS-64876
	Complete Endothelial Cell Medium	Cellbiologics	M1168
	Live Cell Imaging Solution	ThermoFisher Scientific	A14291DJ
	Paraformaldehyde	Sigma-Aldrich	P6148
	Triton X-100	Acros Organics	327371000
	Bovine Serum Albumin	Sigma-Aldrich	A1470
	Tween-20	ThermoFisher Scientific	BP337-100
Barrier Function (Cell Culture)	Sodium Fluorescein Salt	Sigma-Aldrich	F6377
	Boric Acid	Sigma-Aldrich	B6768
	Trichloroacetic Acid	Sigma-Aldrich	T6399
	6.5 mm Transwell® with 0.4 µm Pore Polyester Membrane Insert	Corning	3470
	8W10E+ PET Array	Applied Biophysics	8W10E+
	R&D Systems™ Cultrex Rat Collagen I, Lower Viscosity	R&D Systems	3443-100-01
	Type IV Collagen, Lyophilized, Human	Advanced BioMatrix	5022
	R&D Systems™ Mouse Decorin Recombinant Protein	R&D Systems	1060-DE
Tamoxifen-induced Recombination *in vivo*	Tamoxifen (Free base)	Sigma-Aldrich	T5648
	Corn Oil	Thermo Scientific Chemicals	405435000

Purpose	Reagent	Manufacturer	Catalogue
Genomic DNA Isolation & Analysis	Dextran from *Leuconostoc spp.* (M_r ~70,000)	Sigma-Aldrich	31390
	Fetal Bovine Serum	Atlanta Biologicals	S11150
	Phire Hot Start II PCR Master Mix	ThermoFisher Scientific	F125S
	UltraPure™ Agarose	ThermoFisher Scientific	16500-100
	Promega Molecular Grade Ethidium Bromide Solution	ThermoFisher Scientific	H5041
	GeneRuler 50 bp DNA Ladder	ThermoFisher Scientific	SM0373
In-Cell Western	96-well Flat Clear Bottom Black Polystyrene TC-treated Microplates	Corning	3904
	Type IV Collagen, Lyophilized, Human	Advanced BioMatrix	5022
	Odyssey Blocking Buffer (TBS)	LI-COR	927-50000
	Paraformaldehyde	Sigma-Aldrich	P6148
	Triton X-100	Acros Organics	327371000
	Bovine Serum Albumin	Sigma-Aldrich	A1470
	Tween-20	ThermoFisher Scientific	BP337-100
	Methylprednisolone	Tocris	4819/50
	Demethylasterriquinone B1	Tocris	1819
	CellTag™ 700 Stain	LI-COR	926-41090

Table G.2. List of Primers Used in These Studies.

Purpose	Gene Name	Gene Symbol	PrimePCR Assay ID	Sequence (5' to 3')	Size (bp)
qPCR	Claudin-5	*Cldn5*	qMmuCED0001017	--	--
	Decorin	*Dcn*	qMmuCID0039628	--	--
	Beta Actin	*Actb*	qMmuCED0027505	--	--
Recombination of Floxed Alleles	Biglycan	*Bgn*	--	GAG CCA GGA GGA GTT TGA TG CTC AGT CCA GTC GGT GTC CT	Wild-type: 978 Floxed: 1195 Excised: 414

Table G.3. List of Antibodies Used in These Studies.

Antibody	Figure	Manufacturer	Catalogue	RRID
Decorin-AF488	2.5, 2.6	A kind gift from Dr. David E. Birk (Clone: LF-113)		
Claudin-5-AF488	2.15	ThermoFisher Scientific	352588	AB_2532189
Claudin-5	2.31	ThermoFisher Scientific	35-2500	AB_2533200
Donkey anti-Mouse IgG-IRDye® 800CW	2.31	LI-COR	926-32212	AB_621847

Table G.4. List of Software Used in These Studies.

Software	Version	Manufacturer
ECIS	1.2.215.0	Applied Biophysics
Image Studio Lite	5.2	LI-COR
Prism	9.2.0	GraphPad

APPENDIX H

Clinical Scoring Rubric According to Hooke Labs

Table H. EAE Scoring Rubric for Mice at Onset & Peak Disease.

Score	Clinical observations
0.0	No obvious changes in motor function compared to non-immunized mice. When picked up by base of tail, the tail has tension and is erect. Hind legs are usually spread apart. When the mouse is walking, there is no gait or head tilting.
0.5	Tip of tail is limp. When picked up by base of tail, the tail has tension except for the tip. Muscle straining is felt in the tail, while the tail continues to move.
1.0	Limp tail. When picked up by base of tail, instead of being erect, the whole tail drapes over finger. Hind legs are usually spread apart. No signs of tail movement are observed.
1.5	Limp tail and hind leg inhibition. When picked up by base of tail, the whole tail drapes over finger. When the mouse is dropped on a wire rack, at least one hind leg falls through consistently. Walking is very slightly wobbly.
2.0	Limp tail and weakness of hind legs. When picked up by base of tail, the legs are not spread apart, but held closer together. When the mouse is observed walking, it has a clearly apparent wobbly walk. One foot may have toes dragging, but the other leg has no apparent inhibitions of movement. - OR - Mouse appears to be at score 0.0, but there are obvious signs of head tilting when the walk is observed. The balance is poor.
2.5	Limp tail and dragging of hind legs. Both hind legs have some movement, but both are dragging at the feet (mouse trips on hind feet). - OR - No movement in one leg/completely dragging one leg, but movement in the other leg. - OR - EAE severity appears mild when picked up (as score 0.0-1.5), but there is a strong head tilt that causes the mouse to occasionally fall over.

Score	Clinical observations
3.0	Limp tail and complete paralysis of hind legs (most common). - OR - Limp tail and almost complete paralysis of hind legs. One or both hind legs are able to paddle, but neither hind leg is able to move forward of the hind hip. - OR - Limp tail with paralysis of one front and one hind leg. - OR - ALL of: Severe head tilting, Walking only along the edges of the cage, Pushing against the cage wall, Spinning when picked up by base of tail.
3.5	Limp tail and complete paralysis of hind legs. In addition to: Mouse is moving around the cage, but when placed on its side, is unable to right itself. Hind legs are together on one side of body. - OR - Mouse is moving around the cage, but the hind quarters are flat like a pancake, giving the appearance of a hump in the front quarters of the mouse.
4.0	Limp tail, complete hind leg and partial front leg paralysis. Mouse is minimally moving around the cage but appears alert and feeding. Often euthanasia is recommended after the mouse scores 4.0 for 2 days. However, with daily s.c. fluids most C57BL/6 mice may recover to 3.5 or 3.0, while SJL mice may fully recover even if they reach score 4.0 at the peak of disease. When the mouse is euthanized because of severe paralysis, a score of 5.0 is entered for that mouse for the rest of the experiment.
4.5	Complete hind and partial front leg paralysis, no movement around the cage. Mouse is not alert. Mouse has minimal movement in the front legs. The mouse barely responds to contact. Euthanasia is recommended. When the mouse is euthanized because of severe paralysis, a score of 5.0 is entered for that mouse for the rest of the experiment.

Score	Clinical observations
5.0	Mouse is spontaneously rolling in the cage (euthanasia is recommended). - OR - Mouse is found dead due to paralysis. - OR - Mouse is euthanized due to severe paralysis.
	Table reproduced with permission by Hooke Laboratories Inc., https://hookelabs.com

APPENDIX I

Brain-related RNA-Seq Data Sets for Alpha Integrin Isoform Expression

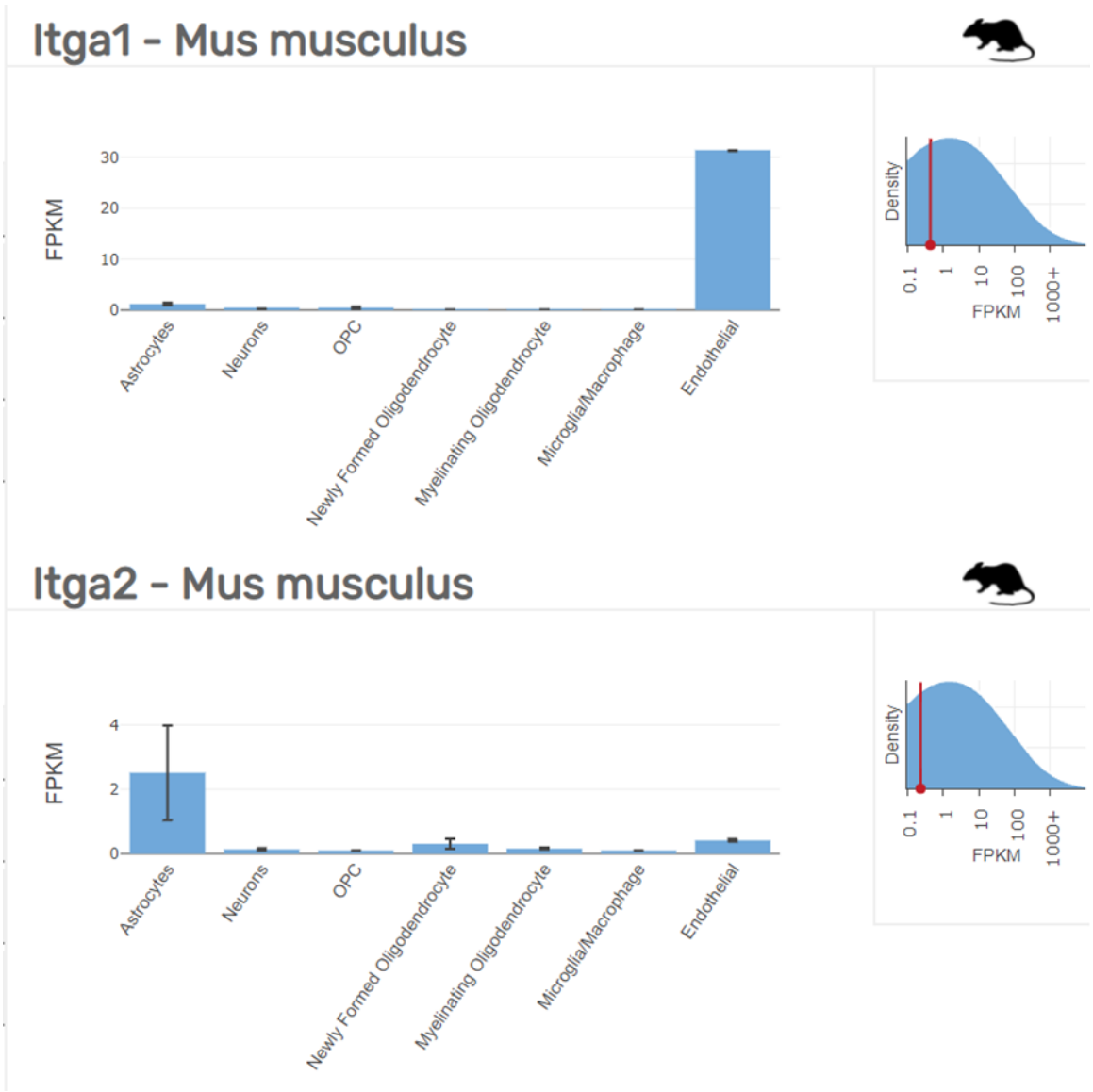

Figure I.1. Integrin Expression in Cells Isolated from the Mouse Cortex.

A publicly available bulk RNA-Seq data set[31] for various cell types isolated from the cortex of mice was queried for the expression of *Itga1* (*upper*) and *Itga2* (*lower*) through its web portal (http://www.brainrnaseq.org/). FPKM: Fragments per kilobase million. OPC: Oligodendrocyte precursor cell.

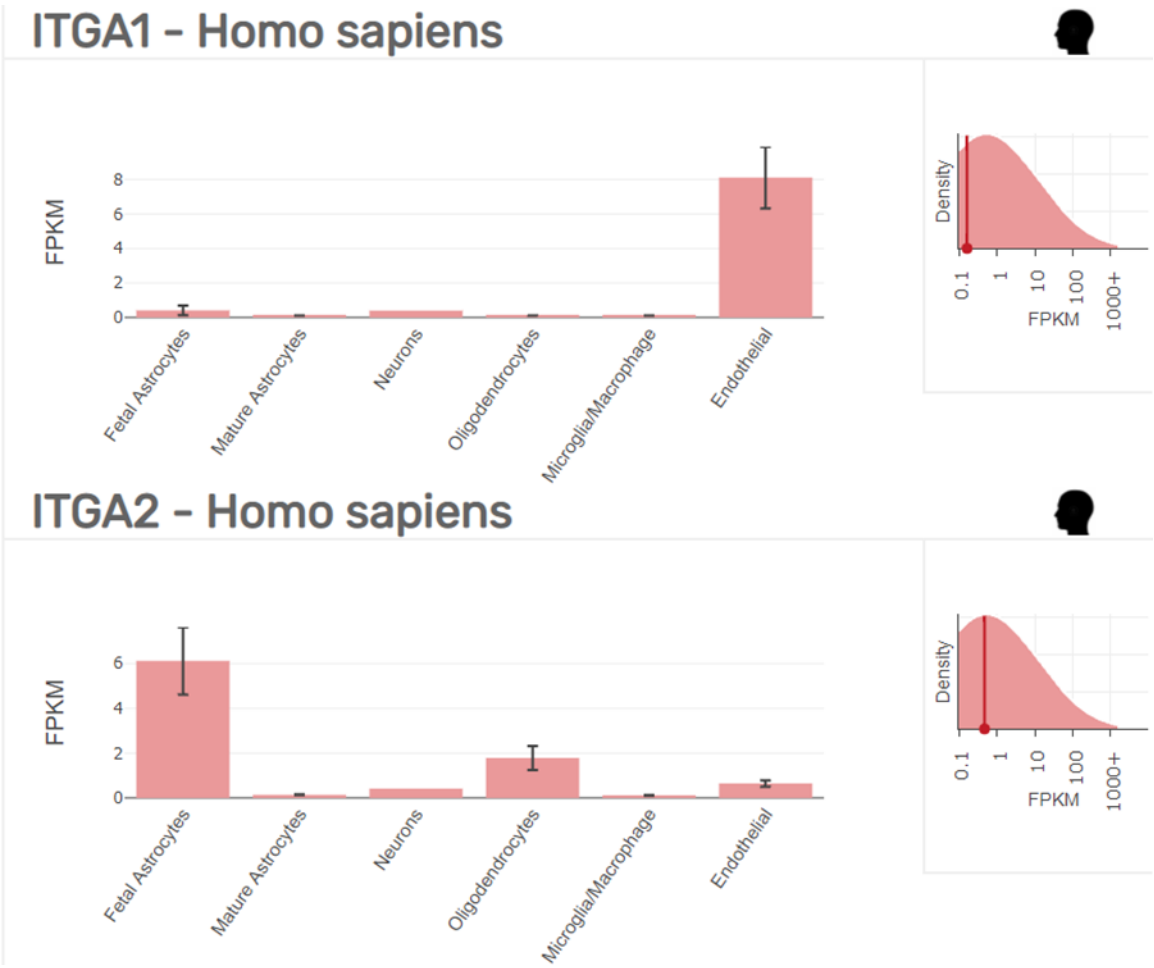

Figure I.2. Integrin Expression in Cells Isolated from the Human Cortex.

A publicly available bulk RNA-Seq data set[32] for various cell types isolated from the cortex of human patients was queried for the expression of *Itga1* (*upper*) and *Itga2* (*lower*) through its web portal (http://www.brainrnaseq.org/). FPKM: Fragments per kilobase million.

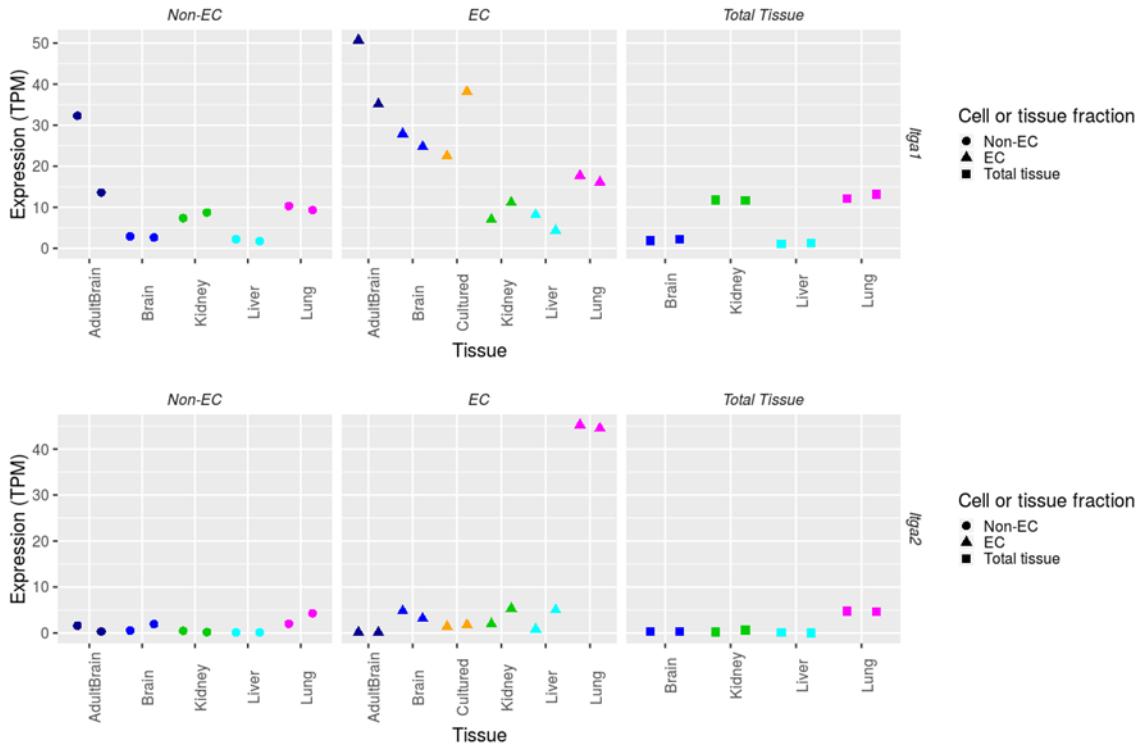

Figure I.3. Integrin Expression Across Mouse Endothelial Cell Types.

A publicly available bulk RNA-Seq data set[33] for brain and peripheral endothelial cell types isolated from *Tie2-GFP* mice was queried for the expression of *Itga1* (*upper*) and *Itga2* (*lower*) through its web portal (https://markfsabbagh.shinyapps.io/vectrdb/). Non-EC: GFP-negative cells. EC: GFP-positive cells. TPM: Transcripts per million. Brain: Cells derived from one-week-old animals. Cultured: Cultured primary mouse BBB-ECs.

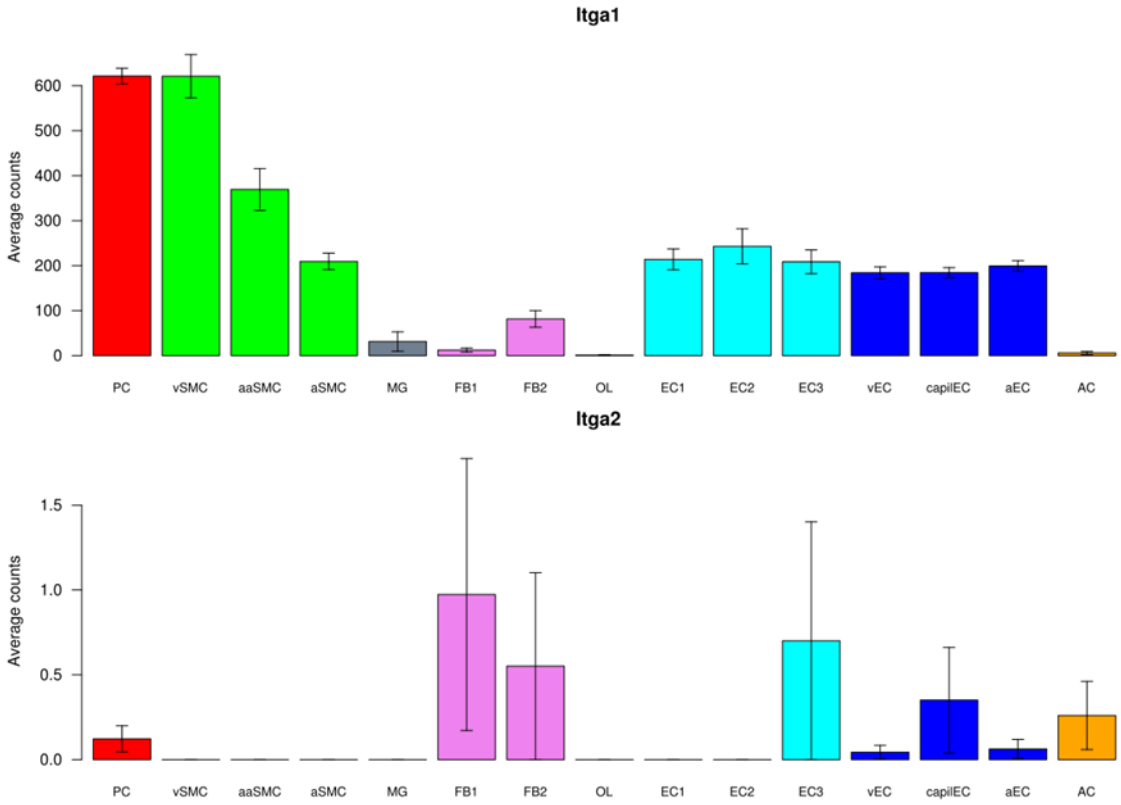

Figure I.4. Integrin Expression in Cells Isolated from the Mouse Brain.

A publicly available single-cell RNA-Seq data set[34] for CNS cell types isolated from fluorescent reporter mice was queried for the expression of *Itga1* (*upper*) and *Itga2* (*lower*) through its web portal (http://betsholtzlab.org/VascularSingleCells/database.html). PC: Pericyte. vSMC: Vascular smooth muscle cell. aaSMC: Arteriolar smooth muscle cell. aSMC: Arterial smooth muscle cell. MG: Microglia. FB: Fibroblast-like. OL: Oligodendrocyte. EC: Endothelial cell. vEC: Venous endothelial cell. capilEC: Capillary endothelial cell. aEC: Arterial endothelial cells. AC: Astrocyte.

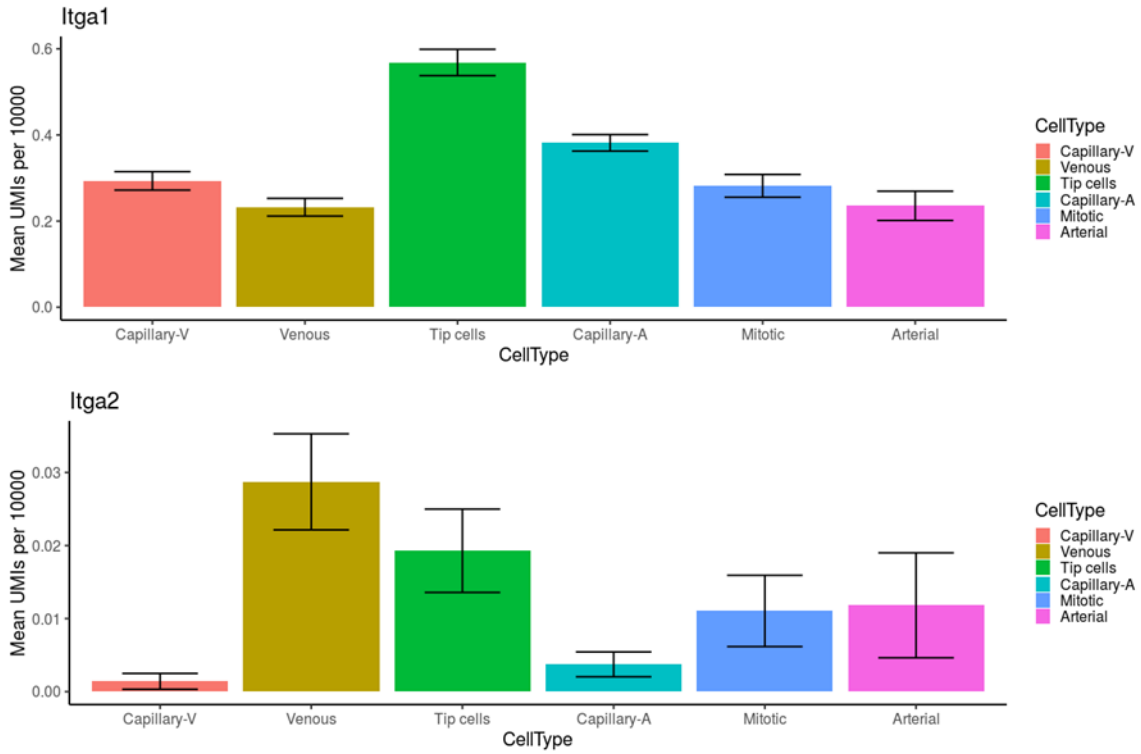

Figure I.5. Integrin Expression in Across Mouse Brain Endothelial Cell Types.

A publicly available single-cell RNA-Seq data set[33] for brain endothelial cell types isolated from *Tie2-GFP* mice was queried for the expression of *Itga1* (*upper*) and *Itga2* (*lower*) through its web portal (https://markfsabbagh.shinyapps.io/vectrdb/). UMI: Unique molecular identifier. Capillary-V: Capillary (venous-side). Capillary-A: Capillary (arterial-side).

APPENDIX J

AKT2 Maintains Brain Endothelial Claudin-5 Expression and Selective Activation of IR/AKT2/FOXO1-signaling Reverses Barrier Dysfunction

Citation: Beard, R. S., Jr, **Hoettels, B. A.**, Meegan, J. E., Wertz, T. S., Cha, B. J., Yang, X., Oxford, J. T., Wu, M. H., & Yuan, S. Y. (2020). AKT2 maintains brain endothelial claudin-5 expression and selective activation of IR/AKT2/FOXO1-signaling reverses barrier dysfunction. Journal of cerebral blood flow and metabolism: official journal of the International Society of Cerebral Blood Flow and Metabolism, 40(2), 374–391. https://doi.org/10.1177/0271678X18817512

Abstract

Inflammation-induced blood–brain barrier (BBB) dysfunction and microvascular leakage are associated with a host of neurological disorders. The tight junction protein claudin-5 (CLDN5) is a crucial protein necessary for BBB integrity and maintenance. CLDN5 is negatively regulated by the transcriptional repressor FOXO1, whose activity increases during impaired insulin/AKT signaling. Owing to an incomplete understanding of the mechanisms that regulate CLDN5 expression in BBB maintenance and dysfunction, therapeutic interventions remain underdeveloped. Here, we show a novel isoform-specific function for AKT2 in maintenance of BBB integrity. We identified that AKT2 during homeostasis specifically regulates CLDN5-dependent barrier integrity in brain microvascular endothelial cells (BMVECs) and that intervention with a selective insulin-receptor (IR) agonist, demethylasterriquinone B1 (DMAQ-B1), rescued IL-1β-induced AKT2 inactivation, FOXO1 nuclear accumulation, and loss of CLDN5-dependent barrier integrity. Moreover, DMAQ-B1 attenuated preclinical CLDN5-dependent BBB dysfunction in mice subjected to experimental autoimmune encephalomyelitis. Taken together, the data suggest a regulatory role for IR/AKT2/FOXO1-signaling in CLDN5 expression and BBB integrity during neuroinflammation.

Introduction

Blood–brain barrier (BBB) dysfunction is a pathological hallmark in inflammation-associated diseases of the central nervous system (CNS), including multiple sclerosis, stroke, dementia, traumatic brain injuries, encephalopathies, and brain metastases.[1–4] Under homeostasis, local cues promote BBB maintenance by fostering highly restrictive brain endothelial cell–cell contacts.[5–7] During an aberrant inflammatory response, however, BBB dysfunction can be triggered by mediators from circulation or the CNS, which act upon endothelial cells (ECs) to reduce their cell–cell adhesive forces. Loss of this adhesion results in barrier hyperpermeability, leading to edema, poor nutrient exchange, neuronal toxicity, and CNS dysfunction.[8,9]

This compromise in BBB integrity is a direct result of inflammatory-mediated disruption of the adherens and tight junction complexes at endothelial cell–cell contacts.[10,11] Although the establishment of the BBB interface requires the involvement of various junctional proteins, the tight junction protein claudin-5 (CLDN5) is known to play an indispensable role in restricting small molecule flux through paracellular passageways.[12–14] *In vitro* BBB models have demonstrated that CLDN5 is a common target of inflammatory mediators such as interleukin-1β (IL-1β),15 homocysteine,[16,17] and tumor necrosis factor alpha,[18] while multiple animal models of CNS diseases have shown loss of CLDN5 is a common phenomenon associated with BBB dysfunction.[16,18–23]

Maturation of endothelial tight junctions produced by high levels of CLDN5 is known to require AKT-dependent inactivation and dissociation of the transcription factor FOXO1 from a silencer region within the Cldn5 promoter.[13,15] Under certain proinflammatory conditions, FOXO1 can re-occupy this silencer, resulting in CLDN5

downregulation and endothelial barrier dysfunction.[15,24,25] Moreover, we have shown *in vitro* that siRNA-mediated knockdown of FoxO1 prevents loss of CLDN5 during IL-1β-mediated barrier dysfunction,[15] suggesting that targeting FOXO1 inactivation directly or through upstream regulators, such as AKT, could be an effective means for therapeutic preservation of CLDN5 during inflammation.

Given the complexity and extensiveness of the AKT signaling network, it is not surprising that the outcome of AKT signaling on endothelial barrier maintenance appears to be highly context-dependent. This convolution is, in part, due to AKT isoforms that can have both overlapping and distinct functions,[26] of which both AKT1 and AKT2 have been shown to have unique regulatory roles in vascular endothelium. While much remains undetermined about these isoform-specific functions, AKT1 is known to be involved in the proinflammatory-mediated loss of endothelial barrier integrity, while its deficiency protects against endothelial hyperpermeability in a λ-carrageenan-induced edema model.[27] By way of contrast, AKT2 is known to distinctly regulate endothelial insulin signaling,[28] but it remains largely unknown whether AKT2 is involved in any modulation of barrier integrity.

The role of vascular insulin signaling in endothelial barrier maintenance is even more complicated, as some groups have shown insulin-mediated barrier enhancement, while others have shown negligible effects.[29–31] Although vascular insulin signaling canonically acts through the insulin receptor (IR), insulin is well-known to be cross-reactive with the insulin-like growth factor 1 receptor (IGF1R) and vice versa with insulin-like growth factors (IGFs) cross-reacting with the IR. Despite a high degree of homology between these two receptors, knockout studies have demonstrated that these pathways

mediate very distinct cellular and physiological processes. Namely, the IGF1R primarily mediates mitogenic pathways, while the IR regulates metabolic effects. Due to insulin's receptor promiscuity and conflicting information regarding the effects of insulin on BBB integrity, identifying selective agonists would undoubtedly aid in clarifying the role for IR-specific signaling in endothelial barrier modulation.

Given that FOXO1 inactivation is a known metabolic target for IR signaling,[32] we explored a novel role for IR/AKT/FOXO1-signaling to regulate CLDN5-dependent BBB integrity. First, we establish a pathophysiological relevance for studying this pathway by analyzing brain microvessels isolated from mice with neuroinflammation-induced BBB disruption and demonstrate increased FOXO1 concurrent with decreased CLDN5. We next show that AKT-mediated regulation of CLDN5 and brain microvascular endothelial cell (BMVEC) integrity is distinct to the AKT2 isoform. Furthermore, the selective IR agonist demethylasterriquinone B1 (DMAQ-B1), unlike insulin or IGF-1, preferentially induces IR signaling, decreases FOXO1 nuclear accumulation, upregulates CLDN5, and enhances barrier function in cultured BMVECs. Finally, and most importantly, we demonstrate that DMAQ-B1-dependent IR/AKT2/FOXO1-signaling reverses inflammation-mediated CLDN5 loss and BBB dysfunction. The results from these experiments establish that selective activation of the IR can reverse the aberrant loss of BBB integrity during inflammation. We suggest targeting the IR/AKT2/FOXO1/CLDN5-axis as a potential therapy in CNS diseases associated with BBB dysfunction.

Materials and Methods

Reagents and Supplies

A complete list of reagents and supplies including purchasing information can be found in Supplementary Tables 1 and 2.

Animal Use

Mice used in these studies were C57BL/6 J purchased from Jackson Laboratory. Animals were maintained under a 12-h light/dark schedule with food and water ad libitum. All animal use was approved by the Institutional Animal Care and Use Committees at the University of South Florida and Boise State University and was performed in accordance with the Guide for the Care and Use of Laboratory Animals. All experiments have been reported in compliance with the ARRIVE guidelines.

Experimental Autoimmune Encephalomyelitis and DMAQ-B1 Pharmacotherapy

Ten-week-old male mice were immunized with experimental autoimmune encephalomyelitis (EAE)-inducing kits per the manufacturer's instructions (Hooke Labs, MA) and standardized protocols.[33,34] All analyses and treatments were performed during the preclinical stage at seven to eight days post-induction (d.p.i.), which is a time frame well-established for the onset of EAE-induced BBB dysfunction.[35] For pharmacologic studies, EAE mice (7 d.p.i.) or controls were randomly assigned to receive a single dose of DMAQ-B1 (5 mg/kg) or vehicle (0.5% methylcellulose).[36] Methylcellulose and DMAQ-B1 were prepared fresh daily and administered via oral-gavage with a stainless-steel curved gavage needle (18 G, 5 cm length, 2.4 mm tip; Kent Scientific). Mice were monitored for signs of distress or hypoglycemia for 24 h. Pilot studies revealed that a single-dose of 5 mg/kg did not result in any hypoglycemic episodes.

Analyses of BBB Integrity

As previously described with minor modifications, Evans blue (EB) extravasation assays were used to determine EAE-induced BBB dysfunction.[37,38] Briefly, for EB leakage studies in Figure 1(a), animals (n = 3; EAE – 7 d.p.i.) were injected I.P. with 100 μL of 2% EB in PBS, or PBS alone as a 'no EB' control for autofluorescence, 24 h prior to Lactated Ringer's (LR) flushes via transcardial perfusion and perfusion fixation with 4% paraformaldehyde (PFA). Brains were excised and sectioned into 1 mm slices from rostral to caudal using a coronal Adult Mouse Brain Slicer (Zivic Instruments). Slices were arranged and imaged at 700 and 800 nm with a near-infrared imaging system (Odyssey CLx; LI-COR Biosciences). For EB leakage studies in Figure 7(e) and (f) (n = 5–6), blood was collected via cardiac puncture and brains were removed after LR flushes and divided into right and left halves. The right half was post-fixed for 24 h in 4% PFA and a sagittal image was obtained with the Odyssey CLx, as shown in Figure 1(a). The left half was homogenized in 1 mL of PBS. EB from the homogenates and plasma was extracted into formamide (2 mL at 60 °C for 24 h) and supernatants (5000 × g for 30 min) were compared against an EB standard curve. As an indicator of BBB protein leakage, brain/serum EB concentrations were normalized per brain weight (mg), and values are represented as fold change from control.

In an additional set of experiments (Figure 7(g)), sodium fluorescein extravasation assays were used as an indicator of small solute (376 Da; Stokes' radius ≈ 0.45 nm) leakage.[16,39] Mice (n = 3; EAE – 8 d.p.i) were injected I.P. with 5 μL/g of 10% sodium fluorescein in saline solution. After 2 h, blood was collected by cardiac puncture, the remaining blood in the cerebrovasculature was flushed with LR, and brains were rapidly

excised. Diluted blood-serum (1:10 in PBS) and supernatants (12,000 × g for 15 min at 4°C) from brain homogenates (6 strokes with loose-fitting Dounce homogenizer) were diluted 1:10 in 20% trichloroacetic acid (TCA). After incubation at 4°C for 24 h, supernatants (12,000 × g for 15 min) were removed and diluted with equal volumes of borate buffer (0.05 M, pH 10). Fluorescence (ex. 480 nm, em. 538 nm) from sample supernatants containing solubilized sodium fluorescein in 10% TCA and 0.025 M borate buffer was quantified, brain/serum sodium fluorescein concentration values were normalized per brain weight (mg), and values are represented as fold change from control.

Microvessel Isolation and Characterization

Microvessel isolations were performed as previously described.[40] Whole brains were excised, meninges and pial vessels were carefully removed, and the remaining tissue was homogenized (six strokes with a loose-fitting Dounce homogenizer) in phenol-free DMEM + 2% FBS (DMEM-S). Homogenates were then mixed 1:1 with 36% dextran (~70 kDa; Sigma), and centrifuged for 10 min at 10,000 × g. Pellets were resuspended in DMEM-S and sieved through a 70 μm strainer to retain large vessels and allow microvessels to pass through. To reduce RBC contamination, microvessel pellets were layered over Percoll and centrifuged at 1700 × g for 10 min. The microvessel enriched pellet was rinsed twice with DMEM and used for further analyses.

For immunostaining and confocal fluorescence microscopy experiments, isolated microvessels from three mice were pooled (n = 27; 9 pools of 3), fixed with 4% PFA and permeabilized with 10% donkey serum containing 0.05% Triton X-100. Microvessels were immunostained per standard protocols with appropriate primary and secondary antibodies in microfuge tubes with end-over-end rotation (see Supplementary Table 2). Stained

vessels were adhered to slides via cytocentrifugation (Cytospin, Thermo Shandon), then mounted in Vectashield containing DAPI to coverslips. Confocal micrographs were taken with an Olympus FLUOVIEW FV1000 confocal laser scanning microscope (Olympus), and image stacks were analyzed and processed with Imaris (Bitplane). For Figure 1(b) to ((f),f), Imaris 'Surface' rendering (thresholding) was used to define regions showing positive fluorescence intensity and then the average intensity per voxel in those regions, or volumes of interest (VOI), was determined. For Figure 1(d), nuclei were defined by thresholding and FOXO1 intensities only within these nuclear VOIs were measured.

For Western blotting, microvessels were isolated as above, except that mice were perfused (transcardial) with PBS containing protease and phosphatase inhibitors before excising the brain. Microvessel pellets from three mice were pooled (n = 9; 3 pools of 3), resuspended in ice-cold RIPA with protease and phosphatase inhibitors, homogenized (20 strokes with tight-fitting Dounce homogenizer) and incubated on ice for 20 min. Samples were centrifuged at 12,000 × g for 10 min at 4°C, supernatants were collected, protein concentrations were determined by BCA assay, and sample protein was normalized in Laemmli sample buffer.

Primary BMVEC Isolation

As we have previously described,[15] primary BMVECs were obtained from isolated microvessels (described above) of C57BL/6 J pups between P7 and P10 (~10 pups for a confluent 25 cm^2 monolayer). The resultant microvessel pellets were resuspended in HBSS with collagenase/dispase, DNase I, and Na-tosyl-L-lysine chloromethyl ketone (TLCK) for 40 min at 37°C. BMVECs were pelleted, washed with DMEM-S, seeded at confluence, and grown on collagen type IV-coated plates in endothelial growth medium (Cell

Biologics) at 37°C with 5% CO2 in a humidified incubator. Unless otherwise stated in figure legends, only initially plated cells (P0) or cells passaged once (P1) at a 1:1 ratio were used in these experiments. Additionally, before use in experiments, BMVECs were grown for two to seven days post-confluence (P.C.) to allow for proper maturation of tight junctions.

BMVEC Barrier Function Assays

Endothelial cell barrier functional assays were conducted as we have previously demonstrated.[15] *For solute permeability and transwell transendothelial electrical resistance (TEER) assays,* BMVEC monolayers were grown seven days P.C. in collagen type IV-coated, 0.4 μm PTFE transwell inserts prior to inflammatory injury and/or treatment with pharmacologic and molecular interventions. Before adding sodium fluorescein (0.5 mg/mL) to the luminal chamber, stable measurements of TEER ($\Omega \times cm^2$) were obtained with a Millicell-ERS voltohmmeter (EMD Millipore). Then, 30 min after luminal addition of sodium fluorescein, samples were collected from both the upper (luminal) and lower (abluminal) chambers for fluorescence analyses. Sodium fluorescein concentrations were determined using a standard curve and the sodium fluorescein permeability coefficient (Ps) was calculated as follows: PS = [A]/t×1/A×V/[L] where [A] is the abluminal concentration; t is the time in seconds; A is the area of the membrane in cm2; V is the volume of the abluminal chamber; and [L] is the luminal concentration. *For electric cell-substrate impedance (ECIS)-based TEER assays,* an indicator of cell-cell adhesive barrier resistance, the barrier function of cultured BMVEC monolayers was determined by measuring real-time TEER using an ECIS sensor (ECIS Zθ, Applied

BioPhysics). ECIS tracings are presented as normalized TEER, and peak changes are quantified for statistical analyses.

Gene Silencing

Introduction of siRNA duplexes was achieved using a Nucleofector® Kit from Amaxa Biosystems (MD, USA), as we have previously described.[15] BMVECs (1×10^6) were resuspended in 100 μL of transfection solution, mixed to final concentration of 2 μM siRNA, and transfected with program T-011 on the Nucleofector IIb™ device. Cells were plated onto collagen type IV-coated ECIS arrays, transwell inserts and/or culture flasks.

BMVEC Immunocytochemistry

Tight junction proteins were immunostained in BMVEC monolayers per standard immunohistochemistry (ICC) protocols and as we have shown before.[15,41,42] BMVECs were grown to 48 h P.C. on glass coverslips and treated with various doses of DMAQ-B1 for 6 h. Cell monolayers were fixed with 4% PFA, permeabilized with 0.05% Triton X-100, blocked with 2% BSA in PBS, and probed with anti-CLDN5 (AF 488) and anti-ZO-1 (AF 594) primary conjugated antibodies overnight at 4°C. Coverslips were mounted with Vectashield containing DAPI, confocal micrographs were obtained with Olympus FLUOVIEW FV1000 confocal laser-scanning microscope, and images were analyzed and processed with Imaris (Bitplane). For Figure 5, ZO-1+ areas at endothelial cell–cell borders were defined by thresholding with Surface rendering in Imaris software. Then the total CLDN5 intensity in these ZO-1+ areas was measured and divided by ZO-1+ areas to provide average CLDN5. For representative 3D images, a 3D-colocalization channel (yellow) was used to highlight the increased density of CLDN5 in tight junction complexes.

Sandwich FLISAs

Three separate sandwich fluorescent-linked immunosorbent assays (FLISAs) were used per standard protocols and adapted for detection with the Odyssey CLx. Briefly, microtiter plates were coated with capture antibodies (5 µg/mL) in carbonate/bicarbonate buffer (pH 9.6) overnight at 4°C, and blocked at RT for 1 h. Protein concentrations of BMVEC lysates were normalized (BCA assay) and incubated in capture antibody-coated wells for 90 min at 37°C. Plates were washed with TBS + 0.05% Tween-20 (TBST) and then incubated with detection antibodies for 2 h at RT. Plates were either imaged immediately on Odyssey CLx (IRDye® 800CW-conjugated primary antibodies) or incubated with IRDye® 800CW-conjugated secondary antibody for 1 h at RT before imaging. As an indicator of IR and IGFR1 activity, a sandwich FLISA was developed to determine tyrosine phosphorylation on insulin receptor substrate 1 (IRS-1). A mouse anti-IRS-1 antibody was used as the capture antibody, and a primary rabbit anti-phosphotyrosine followed by a secondary IRDye® 800CW-conjugated donkey anti-rabbit was used as the detection antibody. In order to identify the isoform-specificity of AKT activation loop phosphorylation at T308 (pT308 on AKT), isoform-specific rabbit monoclonal antibodies against either AKT1 or AKT2 were used as capture antibodies and an IRDye® 800CW-conjugated rabbit anti-pAKT(T308) was used as the detection antibody. An IRDye® 800CW Labeling Kit (LI-COR Biosciences) was used for primary conjugation to the rabbit anti-pAKT(T308), as per the manufacturer's instructions.

High-Salt Nuclear Extraction

Nuclear isolation and protein extraction was performed as previously described.[15] Following treatments, BMVECs were collected into non-nuclear extraction buffer (Buffer A: 10 mM HEPES, 1.5 mM MgCl2, 10 mM KCl, 0.5 mM DTT, 0.05% NP40, pH 7.9) with protease and phosphatase inhibitors. Nuclei were pelleted and washed. Pellets were resuspended in Buffer B (5 mM HEPES, 1.5 mM MgCl2, 0.2 mM EDTA, 0.5 mM DTT, 26% glycerol (v/v), 300 mM NaCl, pH 7.9). Samples were homogenized (20 strokes tight-fitting Dounce homogenizer), incubated on ice for 30 min, centrifuged at 24,000 × g for 20 min at 4°C, and the supernatant was collected as nuclear extract. Protein from nuclear extract was quantified (BCA assay) and normalized in Laemmli sample buffer.

mRNA and Protein Analyses

For real-time quantitative PCR (qPCR) assays, mRNA was isolated from BMVEC monolayers with RNAzol® following manufacturer's procedures. RNA was normalized, and reverse transcription was completed with iScript™ cDNA Synthesis Kit according to the manufacturer's procedures. Quantification cycle (Cq) values were determined with quantitative real-time PCR in accordance with the PrimePCR™ assay. The $2^{-\Delta\Delta Cq}$ method was used as a relative quantification strategy with the results presented as the fold change of target gene expression in a target sample relative to a control sample, normalized to β-actin as the reference gene. For Western blotting, two-color near-infrared immunoblotting was completed per standardized protocols and imaged with an Odyssey CLx scanner.

Statistical Analyses

All statistical analyses were performed with Prism (Version 7.0 e; Graphpad Software, Inc.). α was set at 0.05 a priori for statistical significance. No specific blinding was performed in these studies. A detailed list of statistical analyses is provided in Supplementary Table 3.

Results

Endothelial FOXO1 is Activated and CLDN5 is Downregulated During Neuroinflammation

EAE-induced BBB dysfunction precedes the onset of CNS damage, demyelination, and paralysis.[43] Accordingly, CLDN5 loss from BBB has also been reported during EAE.[20,35,45] Using this model, we analyzed EB leakage to confirm neuroinflammatory-mediated BBB dysfunction (Figure 1(a)). Given the knowledge, albeit primarily based on cell culture studies, that CLDN5 is regulated by FOXO1-mediated transcriptional repression,[13,15,25] we then sought out evidence for this mechanism in microvessels isolated from mice with EAE-induced BBB dysfunction. As hypothesized, microvessels from EAE mice have significantly total and nuclear-localized FOXO1 (^{t}FOXO1 and ^{n}FOXO1, respectively) staining (Figure 1(b) to (d)). At BBB tight junctions, ZO-1 expression remained unchanged and served as a volume of interest (VOI) to analyze changes in CLDN5 density (Figure 1(b), (e) and (f)). Expressional changes were also confirmed by immunoblotting microvessel homogenates (Figure 1(g) and (h)).

BMVEC Regulation of CLDN5 by AKT is Isoform-Specific

Next, we investigated AKT isoform-specific regulation of CLDN5-dependent BMVEC barrier function. We tested several conditions where CLDN5 expression is known

to change and evaluated relative differences in the most likely AKT isoforms to be involved in CLDN5 regulation, AKT1 and AKT2 (Figure 2). BBB endothelial cells are known to lose their barrier properties in culture, especially with subsequent passaging. Here we demonstrate by immunoblotting BMVEC lysates that CLDN5 and AKT2, but not AKT1, are significantly decreased after passaging freshly isolated BMVECs (P0) (Figure 2(a)). Knowing that BMVEC CLDN5 expression levels continue to incrementally increase for several days after confluence, we compared the daily changes in expression levels of *Akt1*, *Akt2*, and *Cldn5* in BMVEC monolayers relative to the levels in subconfluent BMVECs (Figure 2(b)). While relative mRNA for all of these genes increased after confluence (1 day P.C.), only *Akt2* and *Cldn5* continued over the following days. To determine the direct isoform-specific effect of AKT on CLDN5, we silenced *Akt1* and *Akt2* with siRNA and evaluated CLDN5 expression and TEER. Knockdown efficiency was ∼50% for both AKT1 and AKT2. However, immunoblotting the same lysates for CLDN5 revealed that only knockdown of AKT2 had any detectable effect on CLDN5 expression (Figure 2(c) and ((d)). Simultaneously, the effects of *Akt1* and *Akt2* silencing on BMVEC monolayers revealed that loss of AKT2 causes significant barrier dysfunction (Figure 2(e)). Interestingly, AKT1 knockdown produced a nominal increase in barrier integrity, which is consistent with the findings that suggest AKT1 activation may be involved in hyperpermeability.[27]

We previously reported that exposing BMVECs to elevated IL-1β for 1.5 h causes AKT inactivation (decreased pT308 on AKT), FOXO1 activation (increased pT24 on FOXO1, nuclear accumulation, and occupancy on *Cldn5* silencer), and CLDN5 loss (decreased mRNA and protein) sustained for at least 24 h.[15] Here, we found that exposing

BMVECs to IL-1β for 24 h also leads to loss of AKT2 expression, but not AKT1 (Figure 2(f)). Since we have shown in this work that nuclear accumulation of FOXO1 and downregulation of CLDN5 are present in brain microvessels of EAE mice (Figure 1), we immunoblotted those same lysates for expression levels of AKT1 and AKT2 (Figure 2(g)). As with IL-1β-mediated loss of AKT2, microvessels from EAE mice have decreased AKT2 with no loss of AKT1.

Selective Activation of IR Signaling in BMVECs Enhances Barrier Integrity

While the role of AKT1 in endothelial cells has been well-studied, the only known function in endothelium for which AKT2 may be the predominant mediator is insulin signaling. Although the insulin signaling pathway is well-known to regulate FOXO transcription factors,[46] there is a scarcity of knowledge regarding insulin signaling in the regulation of CLDN5-dependent BBB integrity. This lack of information is likely because of multiple confounders that make it difficult to study insulin-receptor signaling, such as receptor promiscuity and overlapping functions of insulin and IGFs, heterogeneous IR and IGFR expression, heterodimerization of the IR and IGFR subunits, insulin resistance, and multiple intracellular targets. Thus, in these studies, we used the IR-selective agonist DMAQ-B1 and compared it to insulin- and IGF-signaling in BMVECs. Since IRS-1 can be a common substrate for both IR and IGFR tyrosine kinases[47] and may be upstream of AKT2/FOXO1-signaling,[46] we used sandwich FLISAs to identify the EC50 of insulin (Figure 3(a)), IGF-1 (Figure 3(b)), and DMAQ-B1 (Figure 3(c)), on tyrosine phosphorylation of IRS-1. The EC_{50} for insulin and IGF-1 was within the physiological response ranges,[48] and the EC_{50} for DMAQ-B1 was similar to previous reports.[36]

As one of several small-molecule IR agonists that have been tested for their utility as oral anti-diabetics, DMAQ-B1 was discovered to preferentially trigger IR-dependent activation of PI3K/AKT signaling at low concentrations, without activating the IGF1R or its canonical downstream ERK1/2 pathway.53 Using the EC_{50} for pIRS-1, we found that treating BMVECs with insulin [2 nM], IGF-1 [20 nM], and DMAQ-B1 [5 μM] all led to a similar increase in active AKT; however, only insulin and IGF-1 increased ERK activity (Figure 3(d)). Interestingly, even though all three agonists induced comparable phosphorylation of IRS-1 and AKT phosphorylation, only DMAQ-B1 led to decreased nuclear localization of FOXO1, upregulation of CLDN5, and enhancement of BMVEC barrier function (Figure 3(e) to ((h)). To confirm that the presence of DMAQ-B1 had no confounding impact on BMVEC proliferation or viability in our cell culture studies, a stain-based cell cycle assay (DAPI) and a stain-based viability assay (calcein AM and propidium iodide) were conducted on BMVEC monolayers (P3; two days P.C.) following 6 h of incubation with DMAQ-B1 [5 μM] or a vehicle control and no differences were observed in either cell cycle distribution or ratio of viable to nonviable cells (Figure S1).

DMAQ-B1 Promotes AKT2/FOXO1-Signaling and Increases Cldn5 mRNA Upregulation

Further analyses of DMAQ-B1 revealed that DMAQ-B1 dose-dependently promotes AKT2-specific activation (pT308 on AKT2; Figure 4(a) and ((b)), FOXO1 inactivation (decreased nuclear accumulation; Figure 4(c)), and transcriptional-mediated upregulation of *Cldn5* (qRT-PCR/mRNA – Figure 4(d); ICC/protein – Figure 5; and WB/protein – Figure S2). Compared to vehicle (0 μM), treating BMVECs with 2.5, 5, and 10 μM of DMAQ-B1 increased total active AKT (pT308) after 45 min. However, sandwich

FLISAs revealed that DMAQ-B1 [10 μM] significantly increased pT308 on AKT2, but not AKT1 (Figure 4(b)). Additionally, we found that *Cldn5* mRNA is increased concurrently with decreased ^{n}FOXO1 following 45 min of treatment with DMAQ-B1. DMAQ-B1 also dose-dependently increased CLDN5 protein levels after 6 h (WB – Figure S1; ICC – Figure 5). Confocal analysis of fixed BMVECs demonstrated that increased CLDN5 levels were indeed localized to the EC–EC tight junctions demarcated by ZO-1, which was unchanged with DMAQ-B1 treatment. Furthermore, 3D rendering of a CLDN5 at ZO-1 colocalization channel highlights how upregulation of CLDN5 does not just increase its turnover, but significantly increases its density at EC–EC junctions (Figure 5).

DMAQ-B1-Mediated BMVEC Barrier Enhancement is Dependent upon CLDN5 Upregulation

Using three separate techniques to measure BMVEC barrier function, we found in all cases that DMAQ-B1 dose-dependently increases ECIS-TEER (Figure 6(a)), transwell-fluorescein permeability (Figure 6(b)), and transwell-TEER (Figure 6(c)). To determine a causal role for CLDN5 in DMAQ-B1-mediated BMVEC barrier enhancement, we silenced Cldn5 with siRNA (Figure 6(d)) and analyzed TEER (Figure 6(e)) or transwell permeability assays (Figure 6(f)). Efficiency of CLDN5 knockdown was determined by immunoblotting 24 h after transfection (Figure 6(d)). Cldn5-silenced monolayers abrogated the barrier-enhancing effects of DMAQ-B1 [5 μM; 6 h] compared to controls (Figure 6(e) and ((f)).

DMAQ-B1 Reverses Inflammation-Induced BMVEC Barrier Disruption *in vitro* and *in vivo*

Given that inflammation is well known to mediate insulin resistance,[49,71] we sought to determine if DMAQ-B1 could attenuate inflammation-mediated BMVEC barrier dysfunction in vitro and in vivo. We first found that DMAQ-B1 can attenuate IL-1β-mediated AKT activation, FOXO1 inactivation, and CLDN5 downregulation (Figure 7(a)). Next, we treated IL-1β-stimulated [100 ng/mL] BMVECs on ECIS after 1 h with DMAQ-B1 and followed TEER tracings for an additional 5 h. DMAQ-B1 [5 μM] not only increased baseline TEER, but also increased TEER of IL-1β-treated BMVECs (Figure 7(b) and ((c)). Additionally, IL-1β-mediated sodium fluorescein hyperpermeability was rescued with co-treatment of DMAQ-B1 (Figure 7(d)). Since we have observed significant BBB dysfunction eight days post-induction of EAE mice, 24 h prior (7 d.p.i.) we gave one single dose of DMAQ-B1 [5 mg/kg; via oral gavage] to both control and EAE mice. Both EB and sodium fluorescein extravasation assays revealed significantly less leakage from brain microvessels in EAE mice treated with DMAQ-B1 compared to those untreated (Fig. 7(f) to (g)). Concomitantly, EAE-induced loss of CLDN5 was abrogated with DMAQ-B1 (Figure 7(h)).

Discussion

The key finding presented in this study is that isoform-specific activation of AKT2 by the selective IR agonist, DMAQ-B1, rescued loss of CLDN5-dependent BBB integrity. We applied a step-wise approach to demonstrate the involvement of the AKT2/FOXO1-signaling pathway in maintaining high CLDN5 expression, and determined the potential of DMAQ-B1 to reverse diminished CLDN5 levels. First, we detected significant nuclear

accumulation of FOXO1 and loss of CLDN5 in microvessels isolated from mice with EAE-induced BBB dysfunction. Second, by determining the correlation of AKT2 and CLDN5 expression and conducting AKT2-specific knockdown experiments, we identified the importance of AKT2 in maintaining high levels of CLDN5. Third, by evaluating the canonical IR/AKT2/FOXO1 signaling pathway, we determined the novel capacity of DMAQ-B1 to reduce FOXO1 nuclear accumulation, increase CLDN5 density at tight junctions, and strengthen barrier function of primary BMVEC monolayers. Fourth, siRNA-mediated silencing of BMVEC *Cldn5* confirmed that CLDN5 is necessary for enhanced barrier function induced by DMAQ-B1. Lastly, DMAQ-B1 reversed BMVEC barrier dysfunction in vitro and in vivo following inflammatory challenge.

Contemporaneous with inflammation-induced microvascular leakage, a quantitative loss of CLDN5 from the BBB has been reported in multiple neurological diseases, which at least in part suggests that CLDN5 is transcriptionally downregulated. Hence, preventing or reversing this downregulation is key to therapeutic preservation of BBB integrity. FOXO1-mediated transcriptional repression of *Cldn5* was first identified in cell culture studies for its role in AJ-dependent upregulation of CLDN5 following endothelial confluency,[13] and Morini *et al.*[25] recently extended their findings to include that FOXO1 also recruits a polycomb repressor complex to the same *Cldn5* silencer occupied by FOXO1 in subconfluent endothelial cells. We recapitulate this data as a proof-of-principle for our culture model, but also demonstrate that *Cldn5* mRNA levels continue to increase beyond endothelial confluency. Elevated levels of FOXO1, along with the loss of CLDN5, were also observed in an acrolein-induced lung injury model.[24] Our results here extend our previous in vitro findings to an in vivo model of neuroinflammatory-mediated

CNS injury. In this model, BBB dysfunction precedes EAE-induced paralysis, and CLDN5 downregulation concomitant with BBB dysfunction has been reported multiple times.[20,35,45] However, the precise onset and regulatory mechanisms governing CLDN5 downregulation during EAE was not well-resolved, and to the best of our knowledge, this is the first report of EAE-induced FOXO1 activation in brain microvessels associated with a loss of CLDN5-dependent BBB integrity.

Most literature devoted to FOXO1 in endothelial cells has been focused on angiogenesis and postnatal neovascularization.[31,50–53] However, the role of FOXO1 in highly mature endothelial cells, such as those of the BBB, remains unclear. Our studies, therefore, were intentionally conducted on adult mice in vivo (> 90 d.p.n.), and mature BMVEC monolayers. In addition to our previous FOXO1 knockdown studies,[15] we found enhanced barrier properties of BMVEC monolayers with no signs of overgrowth or apparent problems. Similarly, Park et al.[54] demonstrated inactive FOXO1 in the blood–retinal barrier (BRB) of adult mice, which was reactivated in diabetic retinopathy leading to loss of BRB integrity.[54] Our finding of inflammation-mediated FOXO1 activation and diminished endothelial cell–cell integrity is in line with this finding, as well as another *in vivo* study demonstrating the atheroprotective effects of endothelial-specific FOXO1 depletion from aortic endothelial cells.[55] Interestingly, this study also reported that upregulation of ICAM-1 and increased monocyte-endothelial adhesion is dependent on FOXO1 activation. Taken as a whole, it would appear that FOXO1 lies dormant in mature endothelium, especially at the BBB, yet serves as an inflammatory response element that may couple leukocyte transmigration with disassembly of endothelial cell–cell junctional complexes.

FOXO1 inactivation by AKT is a canonical target of insulin signaling in endothelial cells, which is well-known to be impaired during inflammation.[56] Nevertheless, tightly controlled insulin therapy to maintain normoglycemia has been shown to counteract inflammation-mediated endothelial dysfunction,[57–59] suggesting that at least some level of IR activation is intact. A role for insulin-signaling in BBB function remains controversial, as some have shown insulin-mediated barrier enhancement and others have shown no effect.[29–31,60–63] Our results demonstrate that exposing BMVECs to physiologically relevant concentrations of insulin and IGF-1 produced equal levels of IRS-1 phosphorylation compared with DMAQ-B1, but unlike DMAQ-B1-mediated IR agonism they did not reduce nuclear accumulation of FOXO1, alter CLDN5 expression, or enhance BMVEC barrier function. How then do we explain the barrier-enhancing effects of DMAQ-B1, given that all three agonists produced equal levels of not just IRS-1, but AKT phosphorylation too? AKT is well-known to simultaneously both proangiogenic and antiangiogenic, which may be related to isoform-specificity. Thus, one plausible explanation is that insulin and IGF-1 trigger IRS-1 and AKT1 phosphorylation through the IGF1R or hybrid IR/IGF1R receptors,[63] whereas DMAQ-B1 is selective for IR agonism that is known to result in phosphorylation of AKT2. This is additionally supported by our finding that insulin and IGF-1 uniquely trigger the canonical IGF1R target, ERK1/2, which is also known for its proangiogenic and hyperpermeability-inducing roles in microvessels. Indeed, we did find a nominal decrease in barrier function following IGF-1, but we did not observe the same for insulin. This discrepancy may be due to insulin promiscuity counterbalancing both the positive and negative effects on barrier regulation.

While certain aspects of endothelial AKT remain poorly elucidated, there is consensus that specificity of these isozymes is highly context-dependent owing to factors such as tissue distribution, cellular localization, temporal regulation, and different signaling pathways.[64–67] Based upon gene ablation studies, only AKT1 and AKT2 appear to have physiological relevance in endothelial cells, although their roles appear to be markedly different with minor functional compensations. For example, deletion of endothelial Akt1 in Akt2$^{-/-}$ mice displays either impaired proliferation and aberrant angiogenesis if excised during development,[65] or loss of mural cell coverage and organ failure if deleted in adult mice.[68] Conversely, AKT2 function is known to promote cell cycle exit through p21 binding[69] and is the primary isoform responsible for endothelial IR-signaling,[28,65] which is consistent with our work supporting an isoform-specific role of AKT2-activity to maintain barrier function of highly quiescent BBB endothelial cells.

It is well-known that the BBB requires additional establishment and maintenance of TJ proteins to maintain the highly restrictive paracellular clefts of BBB endothelial cells. Our observation of passaging-induced loss of AKT2 and CLDN5 may partially explain why elevated TJ protein expression and BMVEC integrity are diminished in cultured ECs.[70,71] It is also well-described that TJ expression continues to increase following monolayer formation of brain endothelial cells, and a major step in endothelial barrier formation requires AKT1-dependent inactivation of FOXO1 and increased *Cldn5* transcriptional upregulation.[13,25] Consistently, peripheral vessels of *Akt1*-null mice have baseline vascular leakage.[66] Until now, a role for AKT2 in endothelial barrier regulation had not been established. Recently, however, Zhang *et al.* showed Akt2 upregulation was a target of β-catenin/Tcf transcriptional regulation,[72] which is known to be necessary for

development and maintenance of the BBB.[38,73–76] Additionally, Frisa *et al.* have demonstrated in aortic endothelial cells an AKT1-to-AKT2 switch model which was Notch-induced and dependent upon AKT2 upregulation, inhibition of GSK-3β phosphorylation, and FOXO1 inactivation. Our work agrees with all these observations, suggesting that AKT1 drives initial barrier development and that AKT2 expression regulates barrier maintenance. Interestingly, it was recently shown in brain endothelial cells that inhibition of GSK-3β increases the half-life of Cldn5 protein.[77] Thus, coupled with our findings, this places AKT2 upstream of both maximal transcriptional regulation and protein stabilization of CLDN5.

Significant progress has been made in the past decade to understand the contributions of isoform-specific AKT activity during various diseases.[78] In accordance with AKT-mediated regulation of FOXO1, reports defining a role of AKT isoforms in vascular disease are largely limited to aberrant vascular remodeling and macrovascular disease.[79] Consistent with the angiogenic role of endothelial AKT1, several reports have described pro-inflammatory roles for AKT1 in endothelial cells. Though global AKT1 deletion was shown to increase baseline vascular permeability, AKT1-deficient mice are resistant to acute histamine- and λ-carrageenan-induced microvascular leakage, as well as infiltration of neutrophils and monocytes.[27,65] Much less is known about the contribution of AKT activity to BBB function and neuroinflammatory disease, especially as it pertains to isoform-specificity. Several reports show that loss of BBB integrity involves impairment of AKT signaling[80–82]; however, to the best of our ability, we were unable to find any reports describing a role for AKT2 in BBB endothelial cells. Here, we have identified a novel isoform-specific role for AKT2 in the maintenance of CLDN5-dependent endothelial

barrier integrity, which is impaired following inflammatory insult. In similar samples used to obtain our results of brain endothelial cell FOXO1 activation by IL-1β in vitro,[15] and EAE in vivo, we identified a significant decrease in expression of AKT2 concomitant with CLDN5, but no changes in AKT1. Similarly, inflammation-mediated changes in AKT2 expression have been reported in other insulin-sensitive tissues, such as the liver and muscles.[83] We never observed complete loss of AKT2 in the inflammatory models employed here and our results show that activating the remaining AKT2 with DMAQ-B1 to promote restoration of CLDN5 is still possible.

Given the complexity of insulin signaling during inflammation, and the mixed results pertaining to insulin therapy for endothelial dysfunction, we were unsure if DMAQ-B1 could attenuate or reverse inflammatory-mediated BBB integrity. Coupled with our *in vitro* findings, however, a model of sepsis-induced insulin resistance and brain injury was attenuated with metformin administration. While this rescue was associated with increased global AKT phosphorylation and diminished edema, the cellular origin of this AKT-dependent neuroprotective effect was not addressed as only whole tissue homogenates were analyzed.[84] Therefore, we chose the primary focus of our culminating *in vivo* work to be whether DMAQ-B1 could rescue CLDN5 expression and CLDN5-dependent barrier integrity. For the underlying intracellular signaling mechanisms, we tested the IR/AKT2/FOXO1/CLDN5 pathway in endothelial monolayers and while it would have been ideal to quantitatively measure the signaling activity of these proteins *in vivo* or within intact microvessels, such experiments were hindered by several technical limitations. In particular, the abundance of AKT2 and FOXO1 expressed within brain microvessels is very low and there exist no commercially available pAKT2 isoform-specific antibodies,

thereby making it challenging to quantitatively compare the levels of their expression or isoform-specific AKT2 activity under basal and EAE conditions following administration of DMAQ-B1. Nevertheless, the profound rescue in BBB integrity we observed following DMAQ-B1 treatment, suggests that during neuroinflammation the AKT2/FOXO1/CLDN5 signaling axis remains responsive to pharmacologic intervention and, therefore, might be a viable therapeutic strategy for restoration of BBB function.

In summary, our current findings define a regulatory role for IR/AKT2/FOXO1-mediated regulation of CLDN5 which can be selectively triggered by the IR agonist, DMAQ-B1, to restore submaximal CLDN5 expression and barrier integrity back to the BBB during neuroinflammation.

Acknowledgments

We thank the Advanced Microscopy and Cell Imaging core at University of South Florida and the Biomolecular Research Center at Boise State University. We acknowledge Jonathan Overstreet, Kristina Chapman, Desiree Self and Ofeira Faapouli for their technical support with animal experiments and endothelial cell isolations and Laura Bond for statistical support.

Funding

The author(s) disclosed receipt of the following financial support for the research, authorship, and/or publication of this article: This work was supported by funding from the National Institutes of Health grants GM097270 (S.Y.Y.), HL070752 (S.Y.Y.), HL126646 (S.Y.Y.), HL120954 (M.H.W.), GM109095 (J.T.O.), and a Veterans Administration Merit Review BX000799 (M.H.W.). R.S.B.J. was supported by career development funding from

the National Institutes of Health (GM109095 and GM103408) and the American Heart Association (16POST27060005 and 17SDG33660381).

Declaration of Conflicting Interests

The author(s) declared no potential conflicts of interest with respect to the research, authorship, and/or publication of this article.

Authors' Contributions

RSBJ performed, analyzed and interpreted most of the experiments. BAH participated in cell culture, gene silencing, and Western blotting experiments. JEM participated in cell culture, mRNA isolation and RT-PCR. TSW participated in animal maintenance and microvessel isolations. BJC assisted with confocal imaging and analyses. JTO contributed to the design and analyses of sandwich FLISAs. XY and MHW contributed to the design and data analyses of in vivo experiments. SYY initiated, directed and sponsored the work through all levels of development. All the authors discussed the results and approved the manuscript.

References

1. Hawkins BT and Davis TP. The blood-brain barrier/neurovascular unit in health and disease. *Pharmacol Rev* 2005; 57: 173–85.

2. Muldoon LL, Alvarez JI, Begley DJ, et al. Immunologic privilege in the central nervous system and the blood-brain barrier. *J Cereb Blood Flow Metab* 2013; 33: 13–21.

3. Rosenberg GA. Neurological diseases in relation to the blood-brain barrier. *J Cereb Blood Flow Metab* 2012; 32: 1139–1151.

4. Sweeney MD, Sagare AP and Zlokovic BV. Blood-brain barrier breakdown in Alzheimer disease and other neuro- degenerative disorders. *Nat Rev Neurol* 2018; 14: 133–150.

5. Armulik A, Genove G, Mae M, et al. Pericytes regulate the blood-brain barrier. *Nature* 2010; 468: 557–561.

6. Abbott NJ, Ronnback L and Hansson E. Astrocyte-endothelial interactions at the blood-brain barrier. *Nat Rev Neurosci* 2006; 7: 41–53.

7. Thomsen MS, Routhe LJ and Moos T. The vascular basement membrane in the healthy and pathological brain. *J Cereb Blood Flow Metab* 2017; 37: 3300–3317.

8. Obermeier B, Daneman R and Ransohoff RM. Development, maintenance and disruption of the blood- brain barrier. *Nat Med* 2013; 19: 1584–1596.

9. Liebner S, Dijkhuizen RM, Reiss Y, et al. Functional morphology of the blood-brain barrier in health and disease. *Acta Neuropathol* 2018; 135: 311–336.

10. Yuan SY and Rigor RR. *Regulation of endothelial barrier function*. San Rafael (CA): Morgan & Claypool Life Sciences, 2010.

11. Luissint AC, Artus C, Glacial F, et al. Tight junctions at the blood brain barrier: physiological architecture and disease-associated dysregulation. *Fluids Barriers CNS* 2012; 9: 23.

12. Morita K, Sasaki H, Furuse M, et al. Endothelial claudin: claudin-5/TMVCF constitutes tight junction strands in endothelial cells. *J Cell Biol* 1999; 147: 185–194.

13. Taddei A, Giampietro C, Conti A, et al. Endothelial adherens junctions control tight junctions by VE- cadherin-mediated upregulation of claudin-5. *Nat Cell Biol* 2008; 10: 923–934.

14. Nitta T, Hata M, Gotoh S, et al. Size-selective loosening of the blood-brain barrier in claudin-5-deficient mice. *J Cell Biol* 2003; 161: 653–660.

15. Beard RS Jr, Haines RJ, Wu KY, et al. Non-muscle Mlck is required for beta-catenin- and FoxO1-dependent downregulation of Cldn5 in IL-1beta-mediated barrier dysfunction in brain endothelial cells. *J Cell Sci* 2014; 127: 1840–1853.

16. Beard RS Jr, Reynolds JJ and Bearden SE. Hyperhomocysteinemia increases permeability of the blood-brain barrier by NMDA receptor-dependent regulation of adherens and tight junctions. *Blood* 2011; 118: 2007–2014.

17. Beard RS Jr, Reynolds JJ and Bearden SE. Metabotropic glutamate receptor 5 mediates phosphorylation of vascular endothelial cadherin and nuclear localization of beta-catenin in response to homocysteine. *Vascul Pharmacol* 2012; 56: 159–167.

18. Aveleira CA, Lin CM, Abcouwer SF, et al. TNF-alpha signals through PKCzeta/NF-kappaB to alter the tight junction complex and increase retinal endothelial cell permeability. *Diabetes* 2010; 59: 2872–2882.

19. McColl BW, Rothwell NJ and Allan SM. Systemic inflammation alters the kinetics of cerebrovascular tight junction disruption after experimental stroke in mice. *J Neurosci* 2008; 28: 9451–9462.

20. Argaw AT, Gurfein BT, Zhang Y, et al. VEGF-mediated disruption of endothelial CLN-5 promotes blood-brain barrier breakdown. *Proc Natl Acad Sci U S A* 2009; 106: 1977–1982.

21. D'Agnillo F, Williams MC, Moayeri M, et al. Anthrax lethal toxin downregulates claudin-5 expression in human endothelial tight junctions. *PLoS One* 2013; 8: e62576.

22. Ma X, Zhang H, Pan Q, et al. Hypoxia/Aglycemia-induced endothelial barrier dysfunction and tight junction protein downregulation can be ameliorated by citicoline. *PLoS One* 2013; 8: e82604.

23. Greene C, Kealy J, Humphries MM, et al. Dose-dependent expression of claudin-5 is a modifying factor in schizophrenia. *Mol Psychiatry* 2017; 1–11.

24. Jang AS, Concel VJ, Bein K, et al. Endothelial dysfunction and claudin 5 regulation during acrolein-induced lung injury. *Am J Respir Cell Mol Biol* 2011; 44: 483–490.

25. Morini MF, Giampietro C, Corada M, et al. VE-cadherin-mediated epigenetic regulation of endothelial gene expression. *Circ Res* 2018; 122: 231–245.

26. Konishi H, Kuroda S, Tanaka M, et al. Molecular cloning and characterization of a new member of the RAC protein kinase family: association of the pleckstrin homology domain of three types of RAC protein kinase with protein kinase C subspecies and beta gamma subunits of G proteins. *Biochem Biophys Res Commun* 1995; 216: 526–534.

27. Di Lorenzo A, Fernandez-Hernando C, Cirino G, et al. Akt1 is critical for acute inflammation and histamine- mediated vascular leakage. *Proc Natl Acad Sci U S A* 2009; 106: 14552–14557.

28. Rask-Madsen C, Li Q, Freund B, et al. Loss of insulin signaling in vascular endothelial cells accelerates atherosclerosis in apolipoprotein E null mice. *Cell Metab* 2010; 11: 379–389.

29. Hasselbalch SG, Knudsen GM, Videbaek C, et al. No effect of insulin on glucose blood-brain barrier transport and cerebral metabolism in humans. *Diabetes* 1999; 48: 1915–1921.

30. Kondo T, Hafezi-Moghadam A, Thomas K, et al. Mice lacking insulin or insulin-like growth factor 1 receptors in vascular endothelial cells maintain normal blood-brain barrier. *Biochem Biophys Res Commun* 2004; 317: 315–320.

31. Liu H, Liu X, Jia L, et al. Insulin therapy restores impaired function and expression of P-glycoprotein in blood-brain barrier of experimental diabetes. *Biochem Pharmacol* 2008; 75: 1649–1658.

32. Cai W, Sakaguchi M, Kleinridders A, et al. Domain- dependent effects of insulin and IGF-1 receptors on signalling and gene expression. *Nat Commun* 2017; 8: 14892.

33. Wilhelm K, Happel K, Eelen G, et al. FOXO1 couples metabolic activity and growth state in the vascular endothelium. *Nature* 2016; 529: 216–220.

34. Mendel I, Kerlero de Rosbo N and Ben-Nun A. A myelin oligodendrocyte glycoprotein peptide induces typical chronic experimental autoimmune encephalomyelitis in H-2b mice: fine specificity and T cell receptor V beta expression of encephalitogenic T cells. *Eur J Immunol* 1995; 25: 1951–1959.

35. Thakker P, Leach MW, Kuang W, et al. IL-23 is critical in the induction but not in the effector phase of experimental autoimmune encephalomyelitis. *J Immunol* 2007; 178: 2589–2598.

36. Lutz SE, Smith JR, Kim DH, et al. Caveolin1 is required for Th1 cell infiltration, but not tight junction remodeling, at the blood-brain barrier in autoimmune neuroinflammation. *Cell Rep* 2017; 21: 2104–2117.

37. Zhang B, Salituro G, Szalkowski D, et al. Discovery of a small molecule insulin mimetic with antidiabetic activity in mice. *Science* 1999; 284: 974–977.

38. Beard RS Jr, Yang X, Meegan JE, et al. Palmitoyl acyltransferase DHHC21 mediates endothelial dysfunction in systemic inflammatory response syndrome. *Nat Commun* 2016; 7: 12823.

39. Zhou Y, Wang Y, Tischfield M, et al. Canonical WNT signaling components in vascular development and barrier formation. *J Clin Invest* 2014; 124: 3825–3846.

40. Gulati A, Nath C, Shanker K, et al. Fluorescein spectrophotofluorometry: a sensitive quantitative method for evaluating the blood brain barrier. *Pharmacol Res Commun* 1982; 14: 649–661.

41. Bell RD, Winkler EA, Sagare AP, et al. Pericytes control key neurovascular functions and neuronal phenotype in the adult brain and during brain aging. *Neuron* 2010 68: 409–427.

42. Rigor RR, Beard RS Jr, Litovka OP, et al. Interleukin-1beta-induced barrier dysfunction is signaled through PKC-theta in human brain microvascular endothelium. *Am J Physiol Cell Physiol* 2012; 302: C1513–C1522.

43. Mayo JN, Beard RS Jr, Price TO, et al. Nitrative stress in cerebral endothelium is mediated by mGluR5 in hyperhomocysteinemia. *J Cereb Blood Flow Metab* 2012; 32: 825–834.

44. Roukos V, Pegoraro G, Voss TC, et al. Cell cycle staging of individual cells by fluorescence microscopy. *Nat Protoc* 2015; 10: 334–348.

45. Aube B, Levesque SA, Pare A, et al. Neutrophils mediate blood-spinal cord barrier disruption in demyelinating neuroinflammatory diseases. *J Immunol* 2014; 193: 2438–2454.

46. Paul D, Cowan AE, Ge S, et al. Novel 3D analysis of Claudin-5 reveals significant endothelial heterogeneity among CNS microvessels. *Microvasc Res* 2013; 86: 1–10.

47. Cheng Z, Guo S, Copps K, et al. Foxo1 integrates insulin signaling with mitochondrial function in the liver. *Nat Med* 2009; 15: 1307–1311.

48. Kleinridders A. Deciphering brain insulin receptor and insulin-like growth factor 1 receptor signalling. *J Neuroendocrinol* 2016; 28: 1–13.

49. Mastick CC, Kato H, Roberts CT Jr, et al. Insulin and insulin-like growth factor-I receptors similarly stimulate deoxyribonucleic acid synthesis despite differences in cellular protein tyrosine phosphorylation. *Endocrinology* 1994; 135: 214–222.

50. de Luca C and Olefsky JM. Inflammation and insulin resistance. *FEBS Lett* 2008; 582: 97–105.

51. Potente M, Urbich C, Sasaki K, et al. Involvement of Foxo transcription factors in angiogenesis and postnatal neovascularization. *J Clin Invest* 2005; 115: 2382–2392.

52. Dharaneeswaran H, Abid MR, Yuan L, et al. FOXO1- mediated activation of Akt plays a critical role in vascular homeostasis. *Circ Res* 2014; 115: 238–251.

53. Nwadozi E, Roudier E, Rullman E, et al. Endothelial FoxO proteins impair insulin sensitivity and restrain muscle angiogenesis in response to a high-fat diet. *FASEB J* 2016; 30: 3039–3052.

54. Paik JH, Kollipara R, Chu G, et al. FoxOs are lineage- restricted redundant tumor suppressors and regulate endothelial cell homeostasis. *Cell* 2007; 128: 309–323.

55. Park DY, Lee J, Kim J, et al. Plastic roles of pericytes in the blood-retinal barrier. *Nat Commun* 2017; 8: 15296.

56. Tsuchiya K, Tanaka J, Shuiqing Y, et al. FoxOs integrate pleiotropic actions of insulin in vascular endothelium to protect mice from atherosclerosis. *Cell Metab* 2012; 15: 372–381.

57. Shoelson SE, Lee J and Goldfine AB. Inflammation and insulin resistance. *J Clin Invest* 2006; 116: 1793–1801.

58. Franklin VL, Khan F, Kennedy G, et al. Intensive insulin therapy improves endothelial function and microvascular reactivity in young people with type 1 diabetes. *Diabetologia* 2008; 51: 353–360.

59. Tian J, Wang J, Li Y, et al. Endothelial function in patients with newly diagnosed type 2 diabetes receiving early intensive insulin therapy. *Am J Hypertens* 2012; 25: 1242–1248.

60. Zhang WF, Zhu XX, Hu DH, et al. Intensive insulin treatment attenuates burn-initiated acute lung injury in rats: role of the protective endothelium. *J Burn Care Res* 2011; 32: e51–e58.

61. Woods SC, Seeley RJ, Baskin DG, et al. Insulin and the blood-brain barrier. *Curr Pharm Des* 2003; 9: 795–800.

62. Hoheisel D, Nitz T, Franke H, et al. Hydrocortisone reinforces the blood-brain barrier properties in a serum free cell culture system. *Biochem Biophys Res Commun* 1998; 244: 312–316.

63. Ito S, Yanai M, Yamaguchi S, et al. Regulation of tight-junction integrity by insulin in an in vitro model of human blood-brain barrier. *J Pharm Sci* 2017; 106: 2599–2605.

64. Nitert MD, Chisalita SI, Olsson K, et al. IGF-I/insulin hybrid receptors in human endothelial cells. *Mol Cell Endocrinol* 2005; 229: 31–37.

65. Ackah E, Yu J, Zoellner S, et al. Akt1/protein kinase Balpha is critical for ischemic and VEGF-mediated angiogenesis. *J Clin Invest* 2005; 115: 2119–2127.

66. Lee MY, Luciano AK, Ackah E, et al. Endothelial Akt1 mediates angiogenesis by phosphorylating multiple angiogenic substrates. *Proc Natl Acad Sci U S A* 2014; 111: 12865–12870.

67. Chen J, Somanath PR, Razorenova O, et al. Akt1 regulates pathological angiogenesis, vascular maturation and permeability in vivo. Nat Med 2005; 11: 1188–1196.

68. Somanath PR, Chen J and Byzova TV. Akt1 is necessary for the vascular maturation and angiogenesis during cutaneous wound healing. Angiogenesis 2008; 11: 277–288.

69. Kerr BA, West XZ, Kim YW, et al. Stability and function of adult vasculature is sustained by Akt/Jagged1 signalling axis in endothelium. *Nat Commun* 2016; 7: 10960.

70. Heron-Milhavet L, Franckhauser C, Rana V, et al. Only Akt1 is required for proliferation, while Akt2 promotes cell cycle exit through p21 binding. *Mol Cell Biol* 2006; 26: 8267–8280.

71. Liebner S, Kniesel U, Kalbacher H, et al. Correlation of tight junction morphology with the expression of tight junction proteins in blood-brain barrier endothelial cells. *Eur J Cell Biol* 2000; 79: 707–717.

72. Deli MA, Abraham CS, Kataoka Y, et al. Permeability studies on in vitro blood-brain barrier models: physiology, pathology, and pharmacology. *Cell Mol Neurobiol* 2005; 25: 59–127.

73. Zhang J, Huang K, Shi Z, et al. High beta-catenin/Tcf-4 activity confers glioma progression via direct regulation of AKT2 gene expression. *Neuro Oncol* 2011; 13: 600–609.

74. Tran KA, Zhang X, Predescu D, et al. Endothelial beta-catenin signaling is required for maintaining adult blood-brain barrier integrity and central nervous system homeostasis. *Circulation* 2016; 133: 177–186.

75. Liebner S, Corada M, Bangsow T, et al. Wnt/beta-catenin signaling controls development of the blood-brain barrier. *J Cell Biol* 2008; 183: 409–417.

76. Daneman R, Agalliu D, Zhou L, et al. Wnt/beta-catenin signaling is required for CNS, but not non-CNS, angiogenesis. *Proc Natl Acad Sci U S A* 2009; 106: 641–646.

77. Engelhardt B and Liebner S. Novel insights into the development and maintenance of the blood-brain barrier. *Cell Tissue Res* 2014; 355: 687–699.

78. Ramirez SH, Fan S, Dykstra H, et al. Inhibition of glycogen synthase kinase 3beta promotes tight junction stability in brain endothelial cells by half-life extension of occludin and claudin-5. *PLoS One* 2013; 8: e55972.

79. Hers I, Vincent EE and Tavare JM. Akt signalling in health and disease. *Cell Signal*. 2011; 23: 1515–27.

80. Yu H, Littlewood T and Bennett M. Akt isoforms in vascular disease. *Vascul Pharmacol* 2015; 71: 57–64.

81. Wang ZG, Cheng Y, Yu XC, et al. bFGF protects against blood-brain barrier damage through junction protein regulation via PI3K-Akt-Rac1 pathway following traumatic brain injury. *Mol Neurobiol* 2016; 53: 7298–7311.

82. Wu F, Chen Z, Tang C, et al. Acid fibroblast growth factor preserves blood-brain barrier integrity by activating the PI3K-Akt-Rac1 pathway and inhibiting RhoA following traumatic brain injury. *Am J Transl Res* 2017; 9: 910–925.

83. Li L, McBride DW, Doycheva D, et al. G-CSF attenuates neuroinflammation and stabilizes the blood-brain barrier via the PI3K/Akt/GSK-3beta signaling pathway following neonatal hypoxia-ischemia in rats. *Exp Neurol* 2015; 272: 135–144.

84. Kim YB, Peroni OD, Franke TF, et al. Divergent regulation of Akt1 and Akt2 isoforms in insulin target tissues of obese Zucker rats. *Diabetes* 2000; 49: 847–856.

85. Tang G, Yang H, Chen J, et al. Metformin ameliorates sepsis-induced brain injury by inhibiting apoptosis, oxidative stress and neuroinflammation via the PI3K/Akt signaling pathway. *Oncotarget* 2017; 8: 97977–97989.

Figures

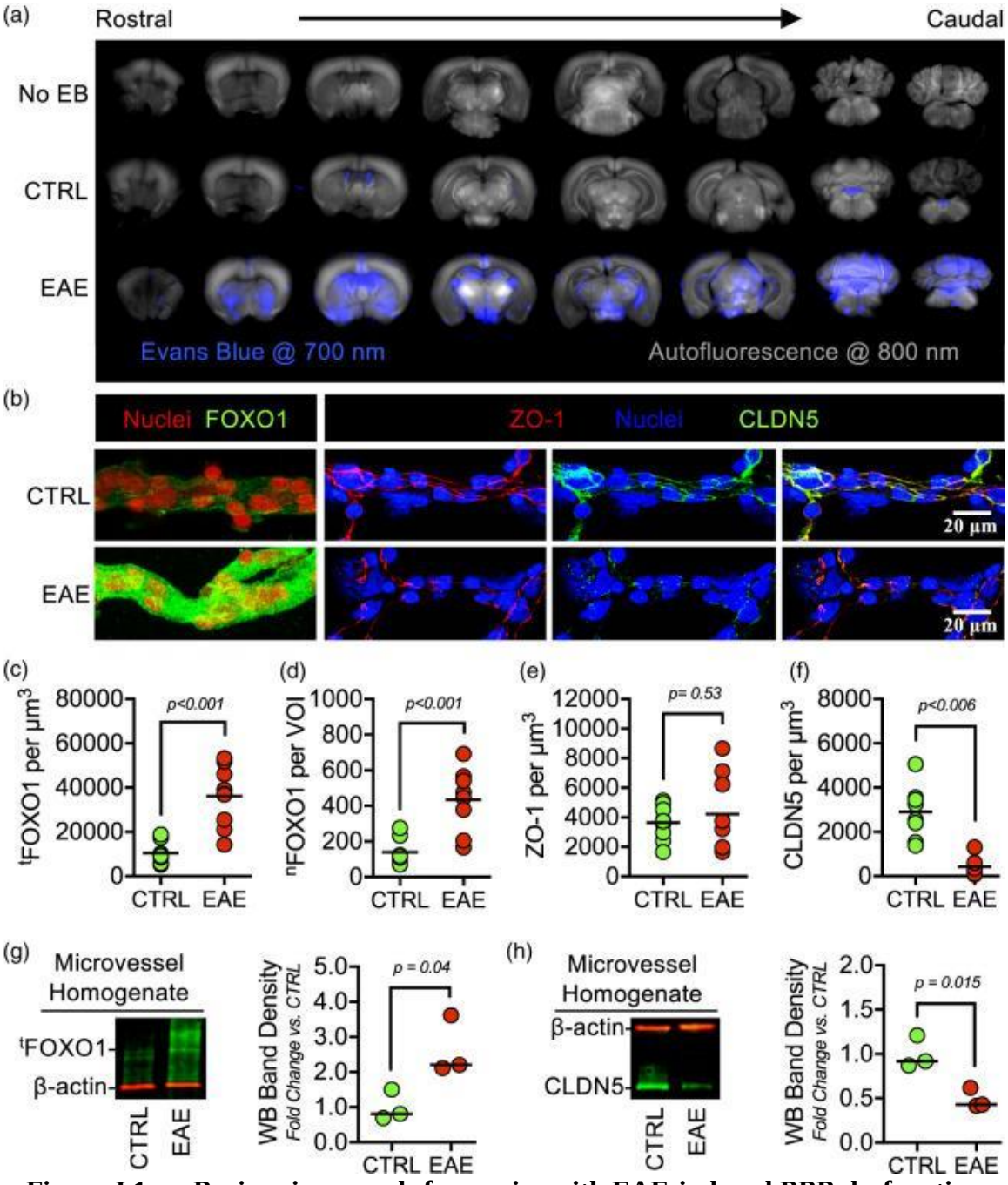

Figure J.1. Brain microvessels from mice with EAE-induced BBB dysfunction have increased nuclear FOXO1 and decreased tight junctional expression of CLDN5.

EAE or mock-EAE (Ctrl) were induced per standard protocols and analyzed for BBB dysfunction eight days post-induction (d.p.i.). (a) Proof-of-principle that EAE mice 8 d.p.i. have BBB dysfunction. Qualitative plasma protein leakage into the mouse brains

was determined by imaging Evans blue (EB) extravasation. Representative images of 1 mm coronal brain slices (olfactory bulbs not included) showing EB leakage captured at 700 nm (pseudo-colored blue) and brain autofluorescence at 800 nm (pseudo-colored grayscale) with a near-infrared imaging scanner. (b) Representative confocal micrographs of isolated brain microvessels (those ≤ 30 μm in diameter) immunostained for either FOXO1, ZO-1, and/or CLDN5, then counterstained with DAPI to demarcate nuclei. In total, 27 mice per group were used and microvessel pellets were pooled together from 3 mice each for a total of 9 pools per group. (c–f) Imaris 3D visualization software was used to analyze confocal micrographs and quantify: (c) total FOXO1 (tFOXO1) density; (d) nuclear-localized FOXO1 (nFOXO1) per uniform spherical volume of interest (VOI) centered within each nucleus; and 3D density of ZO-1 (e) and CLDN5 (f) at endothelial cell–cell contacts. Data are represented as aligned dot plots, where each dot represents a microvessel pool. **(g–h)** Representative Western blots and densitometry analysis for ^{t}FOXO1 **(g)** and CLDN5 **(h)**. In total, nine mice per group were used and microvessel pellets were pooled together from three mice each for a total of three pools per group. Data are represented as scatter dot plots overlaid with mean fold change compared to control group plus corresponding p-value reported above each comparison.

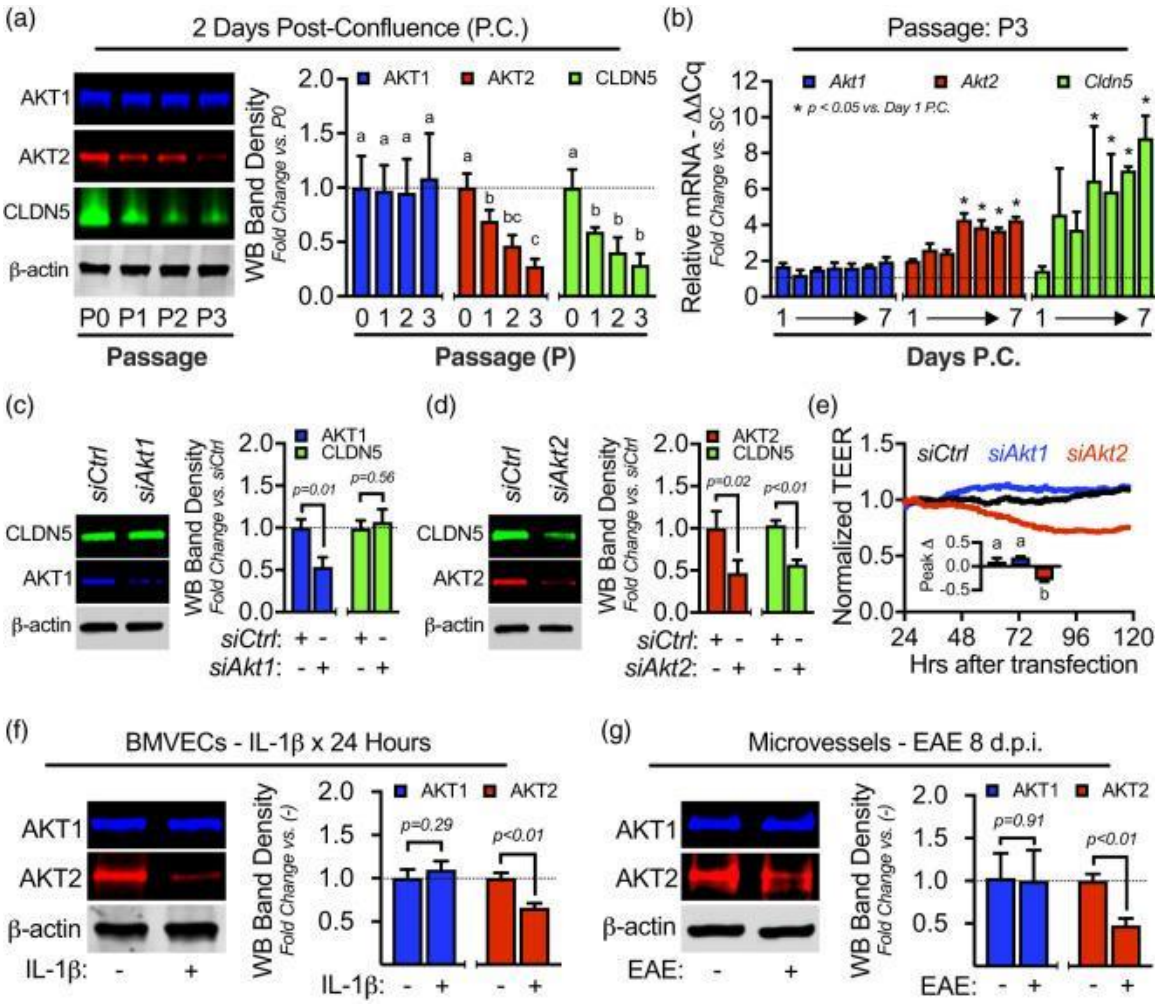

Figure J.2. The AKT2 isoform is distinctly correlated with primary BMVEC barrier integrity and changes in CLDN5 expression.

(a) Freshly isolated BMVECs were seeded at confluence in cultureware (P0). Additional cells were passaged three times (P1–P3). BMVECs from each passage were allowed to mature for two days post-confluence (P.C.). Lysates were collected and expression levels of AKT1, AKT2, and CLDN5 were determined by Western blotting. Bar graphs are divided into individual datasets for each protein target and represent the mean ± S.D. Groups with the same symbol within each individual dataset are not significant from each other ($p \geq 0.05$). **(b)** Conversely, total mRNA from P3 BMVECs was collected from sub-confluent (SC) cells and confluent monolayers each day through seven days P.C. Relative mRNA expression (ΔΔCq; fold change relative to SC samples normalized to β-actin as the reference gene) for *Akt1*, *Akt2*, and *Cldn5* was determined by qRT-PCR. Bar graphs are divided into individual datasets for each mRNA target and represent the mean ± S.D. Asterisks indicate $p < 0.05$ versus 1 day P.C. for each target mRNA. **(c–e)** AKT1 and AKT2 were silenced in BMVECs by siRNA (*siAkt1* or *siAkt2*). Confirmation of knockdown and the effect on CLDN5 expression was determined by Western blotting **(c–d)**. Bar graphs are divided into individual datasets for each protein target and are represented as mean fold change compared to the *siCtrl* group plus corresponding *p*-value

reported above each comparison. **(e)** Representative ECIS tracings demonstrating the impact of AKT1 or AKT2 knockdown on BMVEC barrier integrity from 24 to 120 h post-transfection. At least three independent experiments for each transfection were performed with cells from three separate BMVEC isolations. Each tracing was normalized to the first time point and the peak change in TEER was determined. Embedded bar graphs represent mean normalized peak change ± S.D. and groups with the same symbol are not significant from each other ($p \geq 0.05$). (f–g) Comparison of inflammatory-mediated changes in AKT isoform expression levels in vitro and in vivo. (f) In vitro, mature BMVECs (P1; 7 days P.C.) were stimulated with IL-1β [100 ng/mL] or vehicle control (−) for 24 h and expression levels of AKT1 and AKT2 were compared by Western blotting. Bar graphs are divided into individual datasets for each protein target and are represented as mean fold change compared to the control group plus corresponding *p*-value reported above each comparison. **(g)** In vivo, EAE was induced in mice and compared to mock controls. After 8 d.p.i., brain microvessels were isolated from both groups and AKT1-2 expression was determined by Western blotting. Bar graphs are divided into individual datasets for each protein target and are represented as mean fold change compared to the control group plus corresponding *p*-value reported above each comparison.

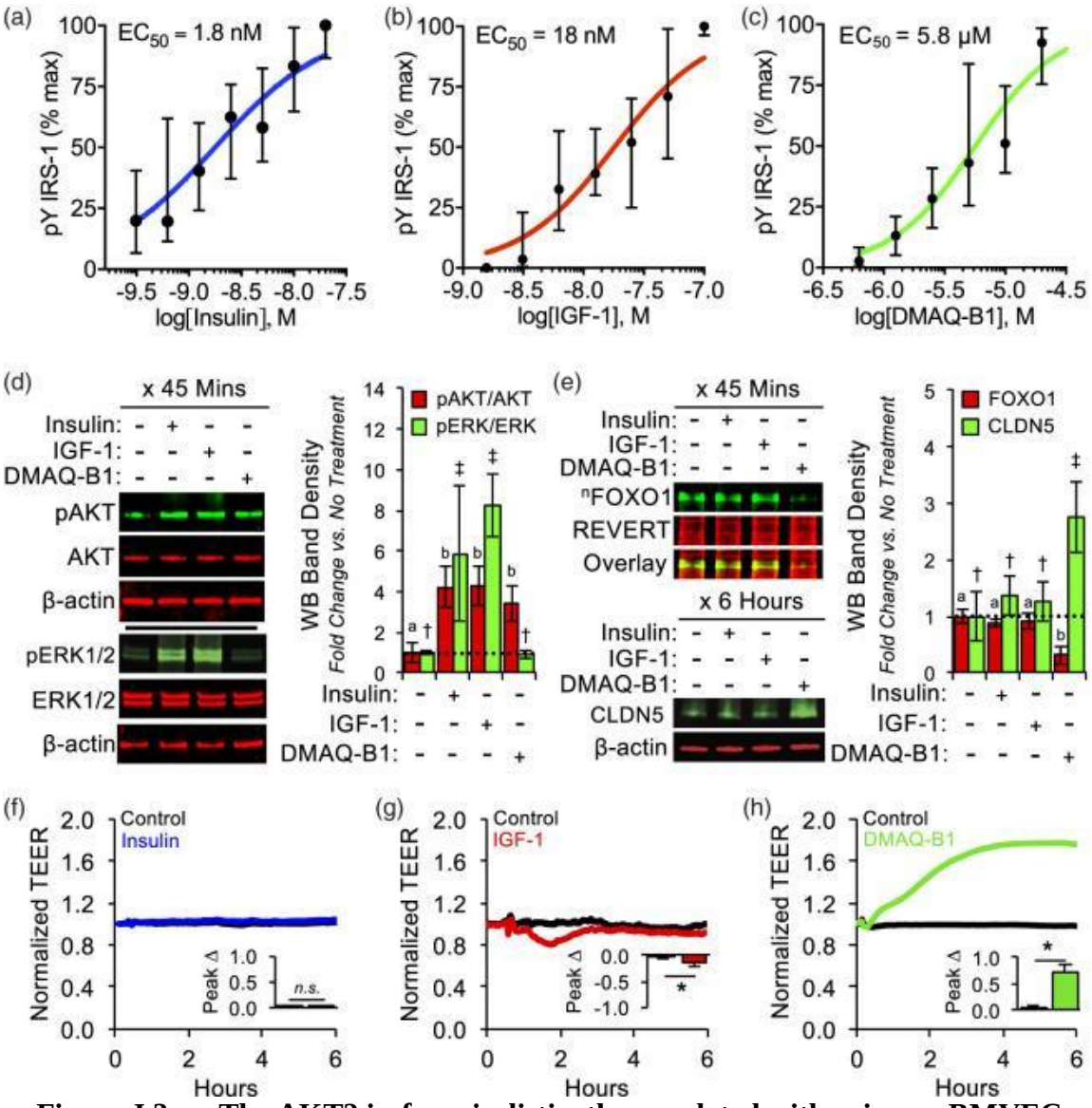

Figure J.3. The AKT2 isoform is distinctly correlated with primary BMVEC barrier integrity and changes in CLDN5 expression.

BMVECs were allowed to mature for 48 h P.C. and then treated with varying concentrations of insulin, IGF-1, or DMAQ-B1. (a–c) After 45 min, cell lysates were analyzed with a sandwich FLISA (capture Ab = anti-IRS-1, detection Ab = anti-pY) to determine total tyrosine phosphorylation on IRS-1 (pY IRS-1). Dots represent median percentage of maximal dose-response ± IQR and EC50 values were obtained from dose-response curves. (d–e) Representative Western blots and densitometry analyses for active AKT (pT308), active Erk1/2 (pT202/pY204), and nFOXO1 (blotting nuclear lysates for FOXO1) were determined after treating BMVECs for 45 min with insulin [2 nM], IGF-1 [20 nM], or DMAQ-B1 [5 µM]. Subsequent changes in CLDN5 expression 6 hours after treatment were also determined by Western blotting and densitometry (e). Data for each protein target are represented as mean fold change compared to the no treatment group ± S.D. Within each individual protein target dataset, groups with the same symbol

are not significant from each other ($p \geq 0.05$). Target proteins were not compared against each other. (f–h) Changes in BMVEC barrier resistance to insulin, IGF-1, or DMAQ-B1 were evaluated for 6 h after treatment. At least three independent ECIS experiments were performed with cells from three separate BMVEC isolations. Each tracing was normalized to its baseline and peak change in TEER was determined. Representative tracings for treatment groups are depicted by colored lines and untreated controls are depicted by black lines. Embedded bar graphs represent mean normalized peak changes in TEER ± S.D. Asterisks indicate $p < 0.05$ versus untreated controls and n.s. indicates no significance.

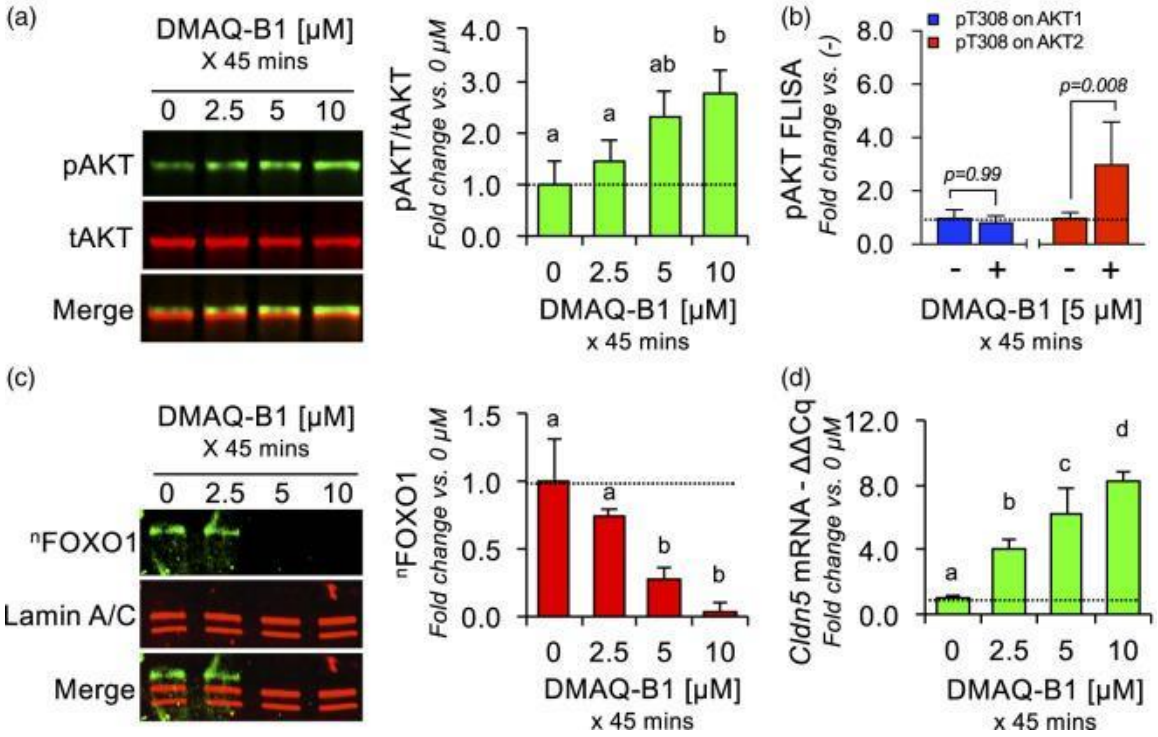

Figure J.4. DMAQ-B1 dose-dependently increases AKT2 activity, decreases FOXO1 nuclear accumulation, and upregulates *Cldn5* mRNA.

(a–d) BMVECs (P3; two days P.C.) were treated with DMAQ-B1 [0, 2.5, 5, or 10 μM] for 45 min and lysates were analyzed for AKT2 activity, nFOXO1 levels, and Cldn5 mRNA levels. (a) AKT activity was determined by Western blotting for pT308 on AKT (pAKT; not isoform-specific) and normalizing against total AKT (tAKT; not isoform-specific). Data are represented as mean fold change compared to the no treatment group ± S.D. Groups with the same symbol are not significant from each other ($p \geq 0.05$). (b) AKT isoform-specific phosphorylation in response to DMAQ-B1 was determined by FLISAs using AKT1- or AKT2-specific antibodies as capture antibodies and pT308-AKT as the detection antibody. Bar graphs are divided into individual datasets for each protein target and are represented as mean fold change compared to the vehicle control (−) group ± S.D. and corresponding p-values reported above each comparison. (c) FOXO1 levels in BMVEC nuclear lysates were determined by Western blotting with lamin A/C used as a nuclear loading control. Data are represented as mean fold change compared to the vehicle control (0 μM) group ± S.D. Groups with the same symbol are not significant from each other ($p \geq 0.05$). (d) Relative Cldn5 mRNA was determined by qRT-PCR. Data are represented as mean fold change compared to the no treatment group ± S.D. Groups with the same symbol are not significant from each other ($p \geq 0.05$).

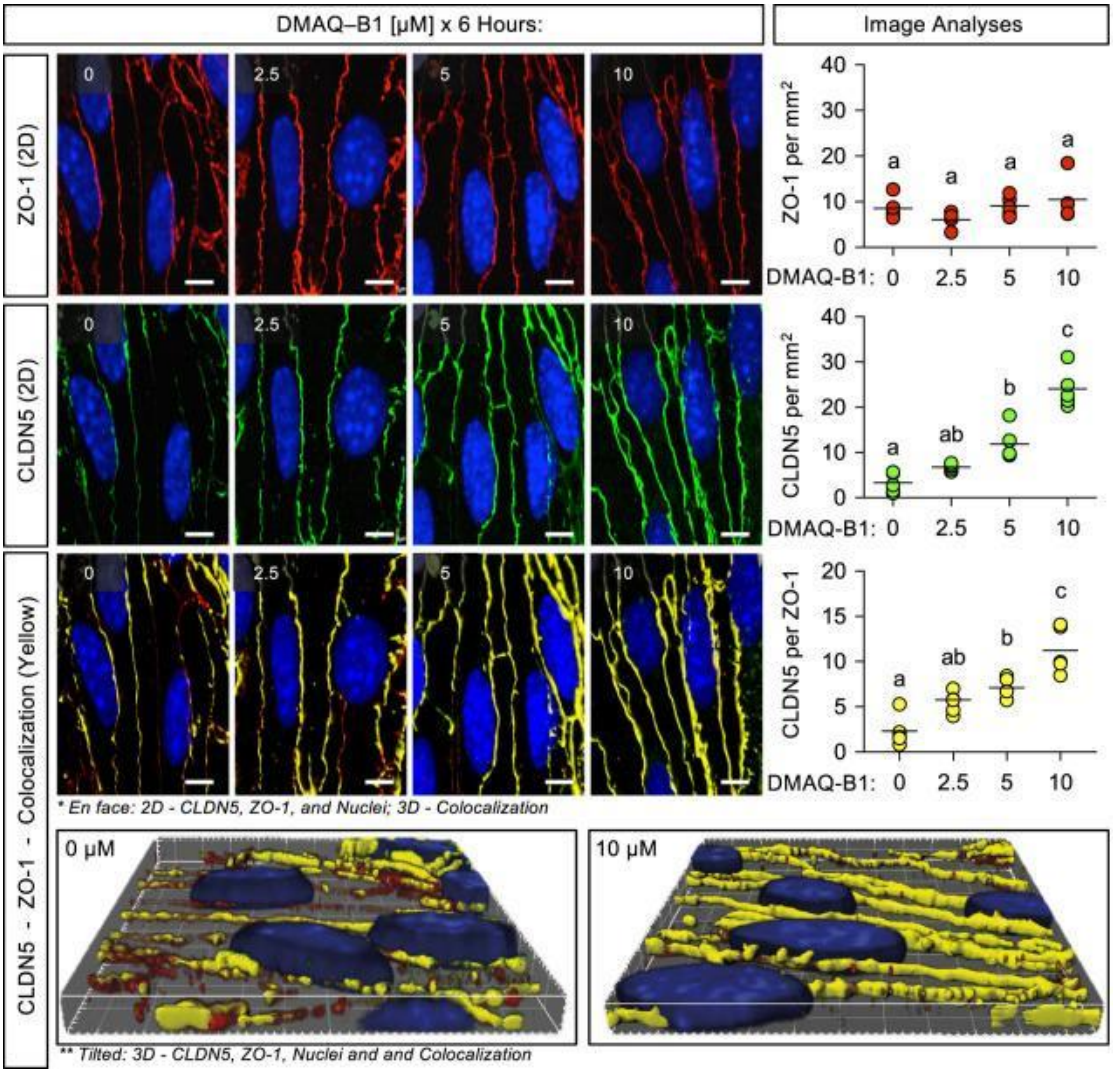

Figure J.5. DMAQ-B1-mediated upregulation of CLDN5 increases the density of CLDN5 protein at BMVEC tight junctions.

BMVECs (P3; two days P.C.) were grown on glass coverslips and treated with DMAQ-B1 [0, 2.5, 5, or 10 μM] for 6 h. BMVEC monolayers (n = 5) were fixed and immunostained for ZO-1 and CLDN5, then counterstained with DAPI to demarcate nuclei (Blue). Confocal micrographs were obtained and Imaris software was used for image analyses and 3D rendering. Representative 2D images of ZO-1 (Red) and CLDN5 (Green) and corresponding graphs of intensity analyses are displayed in the top two rows. ZO-1 at BMVEC cell–cell contacts was used to establish a VOI at tight junctions and a 3D colocalization channel (Yellow; ZO-1+ and CLDN5+ voxels) was established for visual evaluation of CLDN5 expression at BMVEC tight junctions. Representative 2D merged images with 3D rendering of the colocalization channel displayed en face, and graph of CLDN5 intensity per VOI are displayed in the third row. The last row is the same 3D image area as those shown for 0 and 10 μM DMAQ-B1, but expanded and tilted to enhance visual representation. All graphs are represented as aligned dot plots overlaid

with mean value (black line) and groups with the same symbol within each plot are not significant from each other ($p \geq 0.05$).

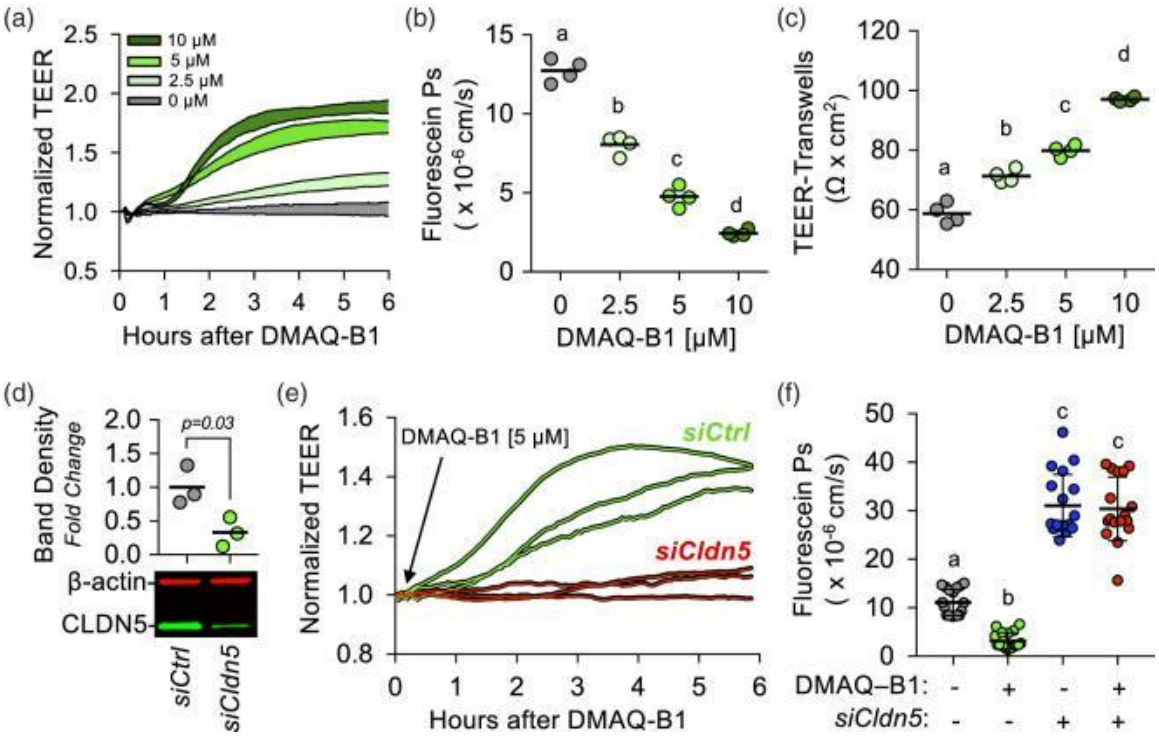

Figure J.6. CLDN5 upregulation is necessary for DMAQ-B1-mediated BMVEC barrier enhancement.

(a–c) DMAQ-B1 dose-dependently enhances BMVEC barrier function. (a) Representative ECIS tracings in response to DMAQ-B1 [0, 2.5, 5, or 10 µM]. At least three independent experiments for each treatment were performed with cells from three separate BMVEC isolations. Each tracing was normalized to the first time point and the filled area for each group represents mean change in TEER ± S.D. Alternatively, after 6 h of treating BMVEC monolayers grown in transwell inserts (P3; two days P.C.) with DMAQ-B1, sodium fluorescein permeability coefficients (Ps) were obtained (b) and transwell-TEER was measured (c). Data are represented as scatter dot plots overlaid with mean value (black line) and groups with the same symbol within each plot are not significant from each other ($p \geq 0.05$). (d–f) The effects of CLDN5 knockdown on DMAQ-B1-mediated BMVEC barrier enhancement were determined with ECIS and transwell permeability assays. (d) Knockdown efficiency of CLDN5 in BMVECs as verified by Western blotting. Data are represented as scatter dot plots overlaid with mean value (black line) plus corresponding p-value reported above. (e) Representative spaghetti plots of individual ECIS tracings of BMVECs transfected with siCldn5 or siCtrl and then treated 24 h later with DMAQ-B1 [5 µM]. Each tracing was normalized to the first time point. (f) The effects of CLDN5 knockdown on BMVEC monolayer permeability to sodium fluorescein with or without DMAQ-B1 were measured. DMAQ-B1 [5 µM] was applied to BMVEC monolayers for 6 h, and permeability was calculated based on sodium fluorescein transendothelial diffusion rate. Data are represented as scatter dot plots overlaid with mean ± S.D. lines. Groups with the same symbol are not significant from each other ($p \geq 0.05$).

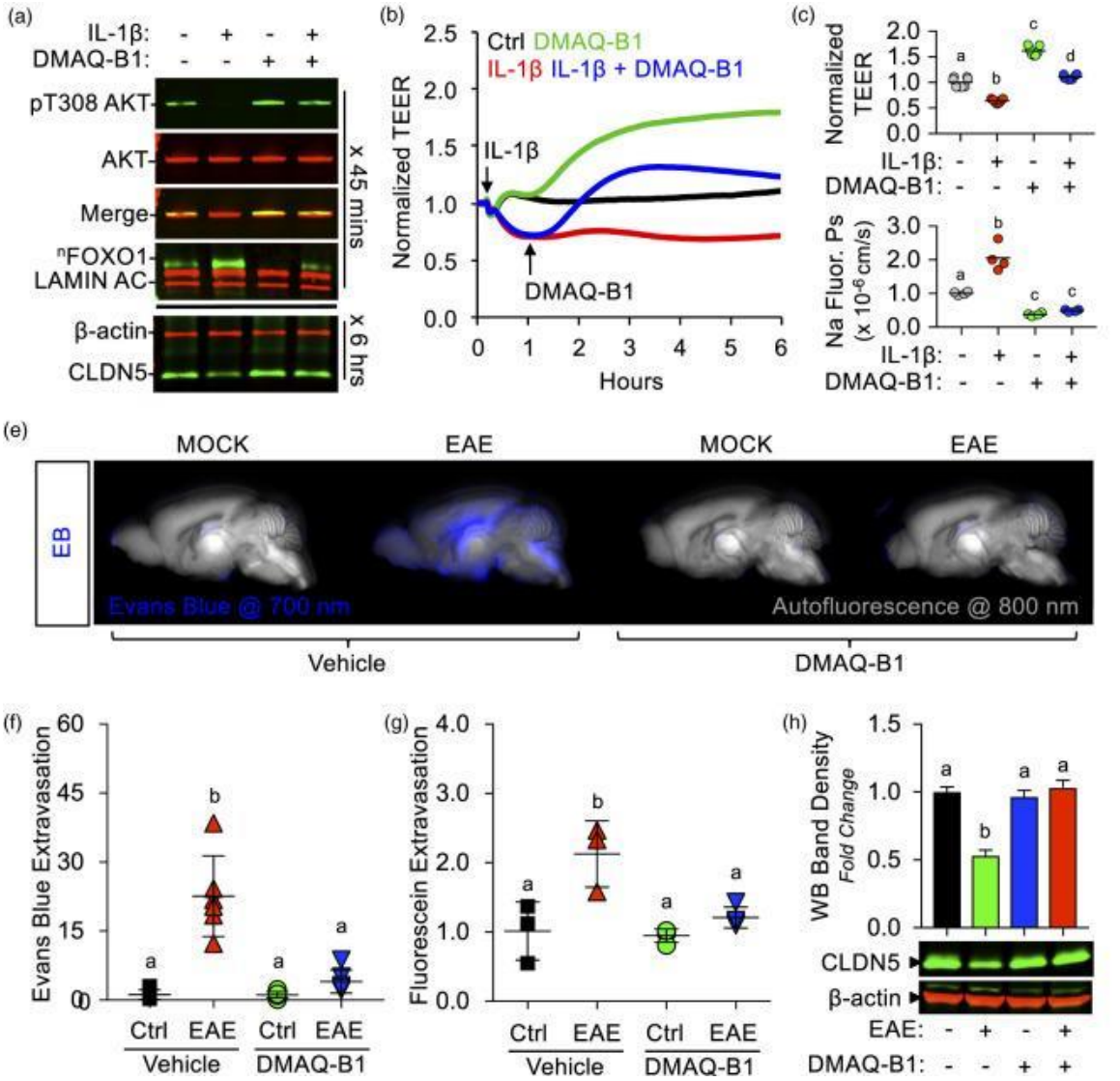

Figure J.7. DMAQ-B1 reverses inflammation-mediated brain endothelial barrier dysfunction *in vitro* and *in vivo*.

(a-d) BMVEC monolayers (P3; two days P.C.) were divided into four groups: (1) vehicle control (Ctrl), (2) IL-1β [100 ng/mL], (3) DMAQ-B1 [5 μM], or (4) DMAQ-B1 + IL-1β. (a) The ability of DMAQ-B1 to attenuate IL-1β-mediated AKT inactivation, FOXO1 nuclear accumulation, and CLDN5 downregulation was determined by Western blotting. Representative Western blots from three independent experiments are shown (b–d) The ability of DMAQ-B1 to reverse IL-1β-mediated BMVEC barrier dysfunction was tested with ECIS-TEER measurements or transwell permeability assays. DMAQ-B1 was added 1 h after IL-1β challenge. (b) Representative normalized ECIS tracings, (c) normalized peak TEER changes, and (d) sodium fluorescein permeability coefficients. All values were obtained from at least 3 independent experiments. Data for (c) and (d) are represented as scatter dot plots overlaid with mean value (black line) and groups with the same symbol within each plot are not significant from each other ($p \geq 0.05$). (e–h) EAE or mock-EAE (Ctrl) were induced and analyzed 8 d.p.i. for BBB dysfunction and CLDN5

expression changes. 24 h prior to harvest (7 d.p.i.), mice from each group were split into two additional groups that received DMAQ-B1 [5 mg/kg] or vehicle (0.5% methylcellulose) via oral gavage. In total, 8–10 mice per group were used and harvested brains were split by hemisphere to allow for simultaneous determination of BBB dysfunction and CLDN5 expression. (e–g) Plasma protein and solute leakage into the mouse brains were determined by EB ($n = 5–6$) and sodium fluorescein ($n = 3–4$) extravasation assays. (e) Representative images from EB extravasation assay showing plasma protein leakage into the right hemisphere. Images were captured at 700 nm (pseudo-colored blue) and brain autofluorescence at 800 nm (pseudo-colored grayscale). Quantitative results from EB (f) and sodium fluorescein (g) permeability assays. (h) CLDN5 expression from left hemisphere brain homogenates was determined by Western blotting. All in vivo values were normalized to the vehicle-treated group subjected to mock EAE (Ctrl) and graphs are represented as dot plots or bar graphs overlaid with mean ± S.D. lines. Groups with the same symbol within each graph are not significant from each other ($p \geq 0.05$).

Supplementary Methods

Cell-cycle Analysis and Viability Assay

Imaging-based cell-cycle analysis was performed as described elsewhere with some minor modifications.[44] Briefly, after DMAQ-B1 treatments, BMVEC monolayers from four independent isolations were fixed, stained with DAPI and imaged (n = 20; 5 micrographs per isolation and treatment group) with an EVOS FL Imaging System (ThermoFisher Scientific). To determine the total number of BMVECs within each monolayer and generate cell-cycle histograms, micrographs were processed with ImageJ (NIH; Version: 2.0.0.rc-65/1.51s) and image analysis–based quantification of integrated nuclear (DAPI) intensity was performed. Relative frequency (%) distributions of nuclear areas were created with Prism (Version 7.0e; Graphpad Software, Inc.) to generate cell cycle profiles, and cell cycle phases (G1/G0, S, and G2/M) were identified by applying visually selected cutoffs. To assess whether DMAQ-B1 may affect BMVEC viability, BMVEC monolayers (P3; 2 days P.C.) were incubated with either a vehicle control, DMAQ-B1 [5 μM], or doxorubicin [0.4 μM] (as a positive control) for 6 hours (n = 15; 5 micrographs per isolation and treatment group), then a commercial live/dead viability/cytotoxicity kit was used according to manufacturer's instructions. Fluorescent micrographs were acquired with an EVOS FL Imaging System using light cubes appropriate for the kit (GFP for calcein AM and RFP for propidium iodide) and the number of positive cells for each stain were tabulated to calculate the ratio of viable to nonviable cells for each group.

Supplementary Tables

Table J.1. Reagents used in these studies.

Reagents	Company	Catalog Number
Amaxa® Cell Line Nucleofector® Kit V	Lonza	VCA-1003
Boric Acid	Sigma	B6768
cOmplete™ protease/phosphatase inhibitor	Sigma	5892970001
Collagen Type IV	Advanced BioMatrix	5022
Dextran ~70 kD	Sigma	31390
DNAse I	ThermoFisher	EN0521
DMAQ-B1	Tocris	LM22B 10
DMEM	Gibco	31053028
Donkey serum	Sigma	D9663
Doxorubicin	Sigma	D1515
EAE Induction Kit	Hooke Labs	EK-2110
Endothelial Growth Medium	Cell Biologics	M116
Evans blue	Sigma	E2129

Reagents	Company	Catalog Number
Formamide	Sigma	F9037
Laemmli sample buffer	LI-COR	928-40004
LIVE/DEAD viability/cytotoxicity kit, for mammalian cells	ThermoFisher	L3224
Nα-Tosyl-L-lysine chloromethyl ketone hydrochloride	Sigma	90182
Paraformaldehyde	Sigma	P6148
Percoll	Sigma	GE17-0891
RIPA lysis buffer	Sigma	20-188
siControl	SCBT	sc-37007
siAkt1	SCBT	sc-29196
siAkt2	SCBT	sc-38910
siCldn5	SCBT	sc-43045
Sodium fluorescein	Sigma	F6377
Trichloroacetic acid	Sigma	T6399
Vectashield with DAPI	Vector Laboratories	H-1200

Table J.2. Antibodies used in these studies.

Antibody	Fig.	Company	Catalog #
α-catenin	S2A	SCBT	sc-7894
β-actin	1G,H; 2A,C,D,F,G; 3D; 6D; 7A,H; S2A	LI-COR	926-42214
β-catenin	S2A	CST	2677
δ-catenin	S2A	SCBT	sc-81793
γ-catenin	S2A	SCBT	sc-514115
AKT	3D; 4A; 7A	CST	2966
AKT1	2A,C,F,G; 4B	CST	3063
AKT2	2A,D,F,G; 4B	CST	2938
Claudin-3	S2A	ThermoFisher	34-1700
Claudin-5	1B,H; 2A,C,D,F,G; 6D; 7A,H; S2A	Invitrogen	35-2500
Claudin-5 (AF 488)	5	ThermoFisher	352588
Claudin-12	S2A	Invitrogen	38-8200
ERK 1/2	3D	CellSciences	CPE201
FoxO1	1B,G; 3E; 4C; 7A	EMD Millipore	05-1075
Lamin A/C	4C; 7A	CST	4777
Occludin	S2A	Invitrogen	33-1500
pAKT(T308)	3D; 4A,B; 7A	CST	4056
pERK 1/2	3D	CST	4695
IRS-1	3A,B,C	CST	2382
Phosphotyrosine (pY)	3A,B,C	Millipore-Sigma	05-321

Antibody	Fig.	Company	Catalog #
VE-Cadherin	S2A	SCBT	sc-52751
ZO-1	1B; S2A	Invitrogen	40-2200
ZO-1 (AF 594)	5	ThermoFisher	339194

Table J.3. Statistical Analyses used in these studies.

Fig. #	Summary Statistics	Statistical Test	Post-Hoc Test
Fig. 1C-F	Aligned dot plots - mean - no error bars	Unpaired t-test	N/A
Fig. 1G,H	Scattered dot plots – normalized mean - no error bars	Unpaired t-test	N/A
Fig. 2A	Bar graphs – normalized mean for each protein ± S.D.	One-way ANOVA	Tukey's
Fig. 2B	Bar graphs – normalized mean for each mRNA ± S.D.	One-way ANOVA	Dunnett's
Fig. 2C,D	Bar graphs – normalized mean for each protein ± S.D.	Unpaired t-test	N/A
Fig. 2E	Representative ECIS tracings – normalized mean – bar graphs of normalized mean peak changes in TEER ± S.D.	One-way ANOVA	Tukey's
Fig. 2F,G	Bar graphs – normalized mean ± S.D.	Unpaired t-test	N/A
Fig. 3A-C	Dose-response curves - median ± IQR	Variable slope	N/A
Fig. 3D,E	Bar graphs – normalized mean ± S.D.	One-way ANOVA	Tukey's
Fig. 3F-H	Representative ECIS tracings – normalized mean – bar graphs of normalized mean peak changes in TEER ± S.D.	Unpaired t-test	N/A
Fig. 4A	Bar graphs – normalized mean ± S.D.	One-way ANOVA	Tukey's
Fig. 4B	Bar graphs – normalized mean for each protein ± S.D.	Unpaired t-test	N/A
Fig. 4C,D	Bar graphs – normalized mean ± S.D. One-way	One-way ANOVA	Tukey's
Fig. 5	Aligned dot plots - mean - no error bars	One-way ANOVA	Tukey's

Fig. #	Summary Statistics	Statistical Test	Post-Hoc Test
Fig. 6B-C	Scattered dot plots - mean - no error bars	One-way ANOVA	Tukey's
Fig. 6D	Scattered dot plots - normalized mean - no error bars	Unpaired t-test	N/A
Fig. 6F	Scattered dot plots - normalized mean ± S.D.	One-way ANOVA	Tukey's
Fig. 7C,D	Scattered dot plots – normalized mean - no error bars	One-way ANOVA	Tukey's
Fig. 7F,G	Scattered dot plots - normalized mean ± S.D.	One-way ANOVA	Tukey's
Fig. 7H	Bar graphs - normalized mean ± S.D.	One-way ANOVA	Tukey's
Fig. S1A	Scattered dot plot – normalized mean ± S.D.	Unpaired t-test	N/A
Fig. S1D	Scattered dot plot – normalized mean ± S.D.	One-way ANOVA	Tukey's
Fig. S2B	Bar graphs – normalized mean ± S.D.	One-way ANOVA	Tukey's

Supplemental Figures

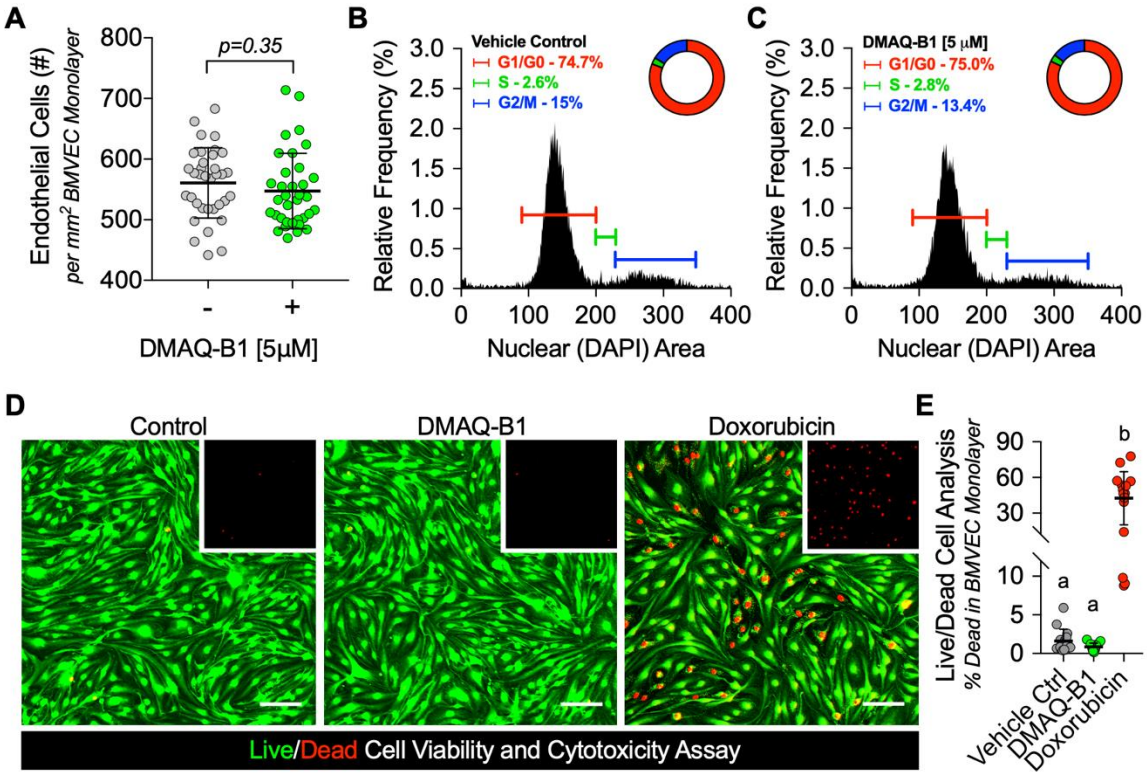

Figure J.8. DMAQ-B1 does not alter BMVEC proliferation, viability, or cytotoxicity.

BMVEC monolayers (P3; 2 days P.C.) were treated with DMAQ-B1 [5 μM] for 6 hours and two different assays were used to determine the effect of DMAQ-B1 on BMVEC proliferation, viability, and cytotoxicity. (A-C) Following DMAQ-B1 treatment, BMVEC monolayers from four independent isolations and experiments were stained with DAPI and fluorescence micrographs (n = 20) were used to: (A) determine the total number of endothelial cells within each imaged monolayer, which are presented as scatter dot plots overlaid with mean ± S.D. lines plus corresponding p-value reported above; or, (B,C) generate cell-cycle histograms to determine the percentage of BMVECs in G1/G0, S, or G2/M phases which are provided as percentages and as 'parts of a whole' in donut charts. (D,E) In a separate set of experiments (n = 3), the number of viable ('live') and non-viable ('dead') cells in each BMVEC monolayer was determined by using a live/dead cell viability and cytotoxicity assay. Doxorubicin – [0.4 μM] for the same time frame – was used as a positive control for cell death and/or cytotoxicity. (D) Representative fluorescence micrographs of BMVEC monolayers with live cells (green) and dead cells (red), and insets displaying only the red channel. Scale bars = 0.1 mm. (E) Quantification of the percentage of non-viable, or 'dead' cells, within each BMVEC monolayer. Percentages are presented as scatter dot plots overlaid with mean ± S.D. lines and groups with the same symbol are not significant from each other ($p \geq 0.05$).

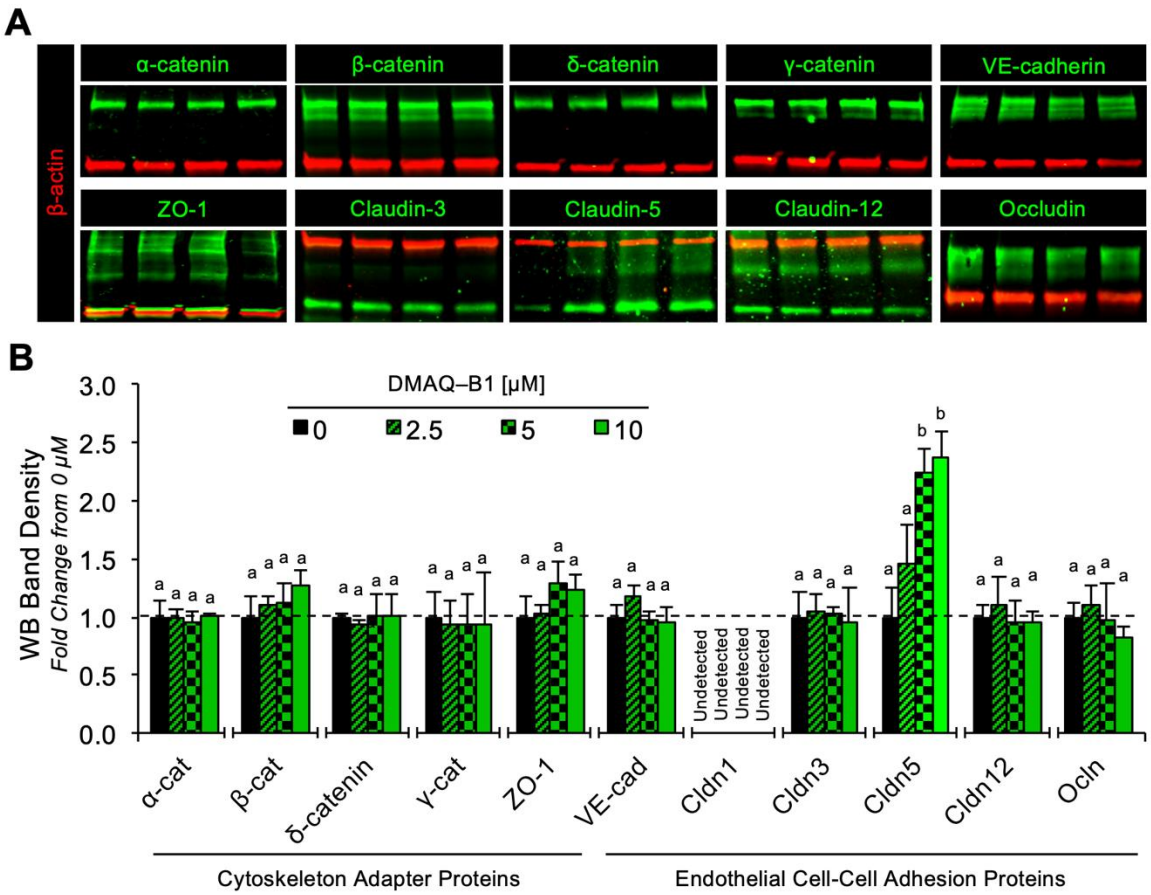

Figure J.9. Compared with other common adherens and tight junctional proteins DMAQ-B1 uniquely upregulates CLDN5.

(A-B) BMVECs (P3; 2 days P.C.) were treated with DMAQ-B1 [0, 2.5, 5, or 10 μM] for 6 hours and adherens and tight junction proteins (adherens junction proteins = α-, β-, δ-, γ-catenin and VE-cadherin; tight junction proteins = ZO-1, claudin-1, -3, -5, -12, and occludin) expression levels were determined by two-color near- infrared western blotting for each protein (pseudo-colored green) and β-actin (pseudo-colored red). Representative western blots are provided **(A)**, and densitometry results **(B)** are reported as normalized fold changes compared to vehicle control (0 μM) treated BMVECs. Bar graphs are divided into individual data sets for each protein target and represent the mean ± S.D. Groups with the same symbol within each individual target protein data set are not significant from each other ($p \geq 0.05$).